

**TRANSPORT, PHASE FORMATION AND
STATISTICAL PHYSICS IN DISORDERED SYSTEMS**

**THESIS SUBMITTED FOR THE DEGREE OF
DOCTOR OF PHILOSOPHY (SCIENCE)
OF THE
UNIVERSITY OF CALCUTTA**

**TANUSRI SAHA
SATYENDRANATH BOSE NATIONAL CENTRE
FOR BASIC SCIENCES, CALCUTTA
NOVEMBER, 1994**

ACKNOWLEDGEMENTS

First of all I express my gratitude to Prof. Abhijit Mookerjee for introducing and inspiring me in the fascinating field of disordered systems . His kind help and constant guidance has made this work possible. His deep involvement in the work was a source of motivation to me.

I am grateful to Prof. C. K. Majumdar , Director S. N. Bose National Centre For Basic Sciences for giving me the opportunity to work in this centre. I am grateful to Prof. B. K. Chakrabarty (Saha Institute Of Nuclear Physics, Calcutta) for many useful discussion and collaborative work on Quantum transport . I also express my gratitude to Dr. G. P. Das (Bhabha Atomic Research Centre , Bombay) for useful discussion regarding LMTO . I would like to thank Prof. F. Ducastelle (ONERA, Paris) , Prof. J. Kudrnovský (Technical University, Vienna) and Prof. R. Haydock (Materials Research Institute , Oregon) whom I met during my visit to I.C.T.P for many useful discussions which helped me a lot in the improvement of my thesis work.

I would specially like to thank my collogue Mr. Indra Dasgupta with whose collaboration a major portion of my research work has been carried out. I also thank my other colleagues Ms. Chaitali Basu , Mr. Sushil Manna and Mr. Abhijit Dutta for creating a stimulating environment. I wish to thank the members and staffs of the S. N. Bose Centre for their co-operation during the course of my research work . My sincerest thank goes to the computer centres of ICTP , Trieste and VECC , Calcutta .

I would like to thank Department of Science and Technology , India for the financial assistance during the course of my Ph.D. work.

Finally I express my sincere and heartiest gratitude to my parents for sharing my dream and providing me inspiration.

PUBLICATIONS *

1. **Is There A Delocalisation Transition In a Two-dimensional Model For Quantum Percolation ?**
Indra Dasgupta , Tanusri Saha , Abhijit Mookerjee and B. K. Chakrabarti
Mod. Phys. Lett. **B6** , 817 (1992).
2. **Quantum Percolation and breakdown . Absence of the delocalisation transition in two dimensions.**
Abhijit Mookerjee , Bikas K. Chakrabarti , Indra Dasgupta and Tanusri Saha
Physica **A186** 258 (1992)
3. *** Scaling of resistance in two dimensional tight binding Anderson Model**
Indra Dasgupta , Tanusri Saha and Abhijit Mookerjee
J. Phys. Condensed Matter **4**, 7865 (1992).
4. ***Analysis of Stochastic Resonances in two dimensional Quantum Percolation Model.**
Indra Dasgupta , Tanusri Saha and Abhijit Mookerjee
Phys. Rev. **B47** 3097 (1993).
5. *** A New Mechanism Of Transport In Quantum Percolation Model**
Indra Dasgupta , Tanusri Saha and Abhijit Mookerjee
Solid.State Physics Symposium **D. A. E.** (1992)
6. **Fine Structure Of Anderson Transition**
Indra Dasgupta , Tanusri Saha and Abhijit Mookerjee
Solid State Physics Symposium **D. A. E.** (1993)
7. *** A Study of annealed and quenched averaging of the thermodynamic potential in a disordered system : an augmented space approach.**
Tanusri Saha and Abhijit Mookerjee
J. Phys. Condens Matter **6**, 1529 (1994).
8. **Stochastic Resonances and the Mobility Edge in the three dimensional tight binding Anderson Model .**
Indra Dasgupta , Tanusri Saha and Abhijit Mookerjee
Phys. Rev. **B** (1994) (*in press*).
9. *** An Augmented Space recursive Technique for the calculation of electronic structure of random binary alloys.**
Tanusri Saha , Indra Dasgupta and Abhijit Mookerjee
J. Phys. Condens. Matter **6** L245 (1994).
10. **An Augmented Space Recursive Method for the study of short range ordering effects in binary alloys**

Tanusri Saha , Indra Dasgupta and Abhijit Mookerjee
Phys. Rev. B 1994 (*in press*).

11. * **An Augmented Space Recursive Technique for the analysis of alloy phase stability in random binary alloys.**
Indra Dasgupta , Tanusri Saha and Abhijit Mookerjee
Phys. Rev. B (1994) (*accepted for publication*)
12. **Electronic Structure Of ordered and disordered transition metal aluminides**
I. Dasgupta, T. Saha , A. Mookerjee and G. P. Das
I. C. T.P. preprint IC/94/241 (1994)
13. **An Augmented Space Recursive Technique for the calculation of electronic structure of random binary alloys (II).**
Tanusri Saha , Indra Dasgupta and Abhijit Mookerjee
Phys. Rev. B 1994 (*submitted*)
14. **Quantum Percolation (Review Article)**
Abhijit Mookerjee , Indra Dasgupta and Tanusri Saha
Int. J. Mod. Phys. 1994 (*submitted*)
15. * **Effect of lattice relaxation on electronic structure of disordered non-isochoric alloys : augmented space recursive approach**
Tanusri Saha and Abhijit Mookerjee (*submitted*)
16. * **Phase-segregation in PdRh system .**
Tanusri Saha and Abhijit Mookerjee (*submitted*)

¹The thesis is based on publications marked by *

Contents

1	INTRODUCTORY REMARKS	1
2	QUANTUM MECHANICAL TRANSPORT THROUGH DISORDERED MEDIA	5
2.1	INTRODUCTION	5
2.2	MODELS STUDIED	8
2.2.1	The Anderson Model	8
2.2.2	The Quantum Percolation Model	9
2.3	PREVIOUS NUMERICAL ATTEMPTS	10
2.3.1	Scaling in the Two-dimensional Anderson Model	10
2.3.2	Stochastic Resonances In Disordered Systems	11
2.4	METHODOLOGY USED IN PRESENT WORK	12
2.4.1	Determination Of The Transmittance and Wavefunction In Random Media	12
2.4.2	Block Spin Analogy and Scaling In Two-dimensional Anderson Model	17
2.4.3	Detection Of Stochastic Resonances and Multifractal Analysis in Two-dimensional Quantum Percolation Model	20
2.5	RESULTS AND DISCUSSION	23
2.5.1	Scaling Of Resistance In The Two Dimensional Anderson Model	23
2.5.2	Study Of Stochastic Resonances In The Two Dimensional Quantum Percolation Model	30
2.6	SUMMARY	40
3	AUGMENTED SPACE RECURSIVE APPROACH FOR CONFIGURATION AVERAGING IN DISORDERED ALLOYS	41
3.1	INTRODUCTION	41
3.2	METHODOLOGY	43
3.2.1	Description of Electronic Structure	43
3.2.2	Configuration Averaging	47
3.3	SYMMETRY REDUCTION OF AUGMENTED SPACE RECURSION	63
3.3.1	Real Space Recursion Invoking Symmetry	63
3.3.2	Augmented Space Recursion Invoking Symmetry	68
3.4	COMPUTATIONAL DETAILS	71
3.4.1	Charge Self Consistency	71

3.4.2	The MultiSpin Coding Technique	74
3.5	APPLICATIONS	75
3.5.1	AgPd Alloys : A Test Case	75
3.5.2	CuPd Alloys	78
3.6	LATTICE RELAXATION	80
3.6.1	Approaches for the study of Lattice Relaxation	81
3.6.2	Application to Cu-rich CuPd and CuBe alloys	86
3.7	SUMMARY	92
4	STUDY OF PHASE FORMATION AND PHASE TRANSITIONS IN BI-NARY ALLOY SYSTEM	93
4.1	INTRODUCTION.	93
4.2	THE FREE ENERGY MODEL	94
4.3	ENERGY CALCULATION : MODEL IN TERMS OF EFFECTIVE CLUSTER INTERACTIONS	95
4.3.1	Previous Approaches	95
4.3.2	Present Approach	101
4.3.3	Comparison With Previous Approaches	107
4.3.4	Phase Stability in PdV Alloys	110
4.4	ENTROPY CONTRIBUTION : THE BRAGG-WILLIAMS MODEL	120
4.4.1	Phase-separation And Calculation Of The Instability Temperatures In Pd-Rh Alloys	121
4.5	SUMMARY.	130
5	CONFIGURATION AVERAGING OF THERMODYNAMIC POTENTIAL IN DISORDERED ALLOYS	131
5.1	INTRODUCTION.	131
5.2	THE AUGMENTED SPACE FORMALISM AND FERMION FIELD THEORY. 132	
5.2.1	Calculation Of The Quenched Averaged Thermodynamic Potential And Scattering Diagrams	133
5.2.2	Summation Of The Perturbation Series For The Thermodynamic Potential	138
5.2.3	Annealed Averaging Of The Thermodynamic Potential	145
5.3	SUMMARY.	153

List of Figures

2.1	The chain formed out of vector recursion process (reproduced from the ref. (Godin and Haydock ,1988))	15
2.2	(a) Partition of the lattice into blocks (b) An isolated block , renormalization of the block to a single scatter and the renormalized lattice (c) The single-site scatterer with ordered leads	19
2.3	Figure showing the connected cluster ($q = 0.3$) characterized by a backbone and dangling bonds	21
2.4	The distribution of scattering elements for four successive steps in the block renormalization	24
2.5	The averaged logarithm of the resistance vs the logarithm of the size for $\delta = 0.5$	25
2.6	The averaged logarithm of the resistance vs the logarithm of the size for $\delta =$ (a) 6.25×10^{-4} , (b) 0.5 , (c) 5.0 and (d) 12.5	27
2.7	Variation in the disorder parameter with the slope α	28
2.8	Resistance vs the logarithm of the size (a) for $\delta = 5.0 \times 10^{-4}$ (b) for $\delta = 0.037$.	29
2.9	Plot of transmittance vs energy for a square lattice of size (a) 20×20 (b) 30×30 at $q = 0.3$	31
2.10	Resolved plot of transmittance vs energy for size 30×30 in the neighbourhood of a resonance	32
2.11	(a) Wavefunction squared amplitude vs site co-ordinates (b) contour diagram of the wavefunction squared amplitude over the sample for resonating state ($q = 0.3$, $E = -0.651$)	33
2.12	Plot of the directionality averaged probability density $I(r)$ vs r measured in units of lattice distance a , from the site with maximum probability along with the best linear fit for the resonating state shown in Figure. 2.11	34
2.13	(a) Wavefunction squared amplitude vs site co-ordinates (b) contour diagram of the wavefunction squared amplitude over the sample for the localized state ($q = 0.3$, $E = 0.5$)	35
2.14	Plot of $\tau(Q)$ vs Q for the localized states (solid line) and the resonating states (dashed line)	36
2.15	Plot of $f(\alpha)$ vs α for the localized states (solid line) and the resonating states (dashed line)	38
2.16	The singularity spectrum of (a) the localized state and (b) the resonating state at various system sizes : 20×20 (solid line) , 30×30 (dotted line) , 40×40 (dashed line)	39

- 3.1 (a)-(c) Density of states for square, simple cubic and fcc lattice described by tight binding Hamiltonian (on-site term $e = 0$. and transfer term $V = -1.0$) obtained by recursion on symmetry reduced maps (d) density of states for fcc based Ag metal described by LMTO Hamiltonian on symmetry reduced map . . . 66
- 3.2 (a) Density of states for a model 50-50 alloy based on square lattice described by tight binding Hamiltonian (on-site terms $e_A = 2.0$, $e_B = -2.0$ and transfer term $V = -1.0$) obtained by recursion on symmetry reduced map . (b) density of states for fcc based 50-50 AgPd alloy described by LMTO Hamiltonian obtained by recursion on symmetry reduced map 70
- 3.3 The total(solid) and partial densities of states on Ag(dotted) and Pd(dashed) in Ag_xPd_{1-x} alloys for (a) $x=1.0$ (b) 0.75 (c) 0.5 (d) 0.25 (e) 0.0 as obtained in TB-LMTO-ASR calculation . The vertical lines show the position of the Fermi level. 76
- 3.4 The XPS density of states for Ag_xPd_{1-x} alloys (Hüfner *et. al.* , 1973). 77
- 3.5 The total and partial densities of states on Cu and Pd sites in Cu_xPd_{1-x} alloys for (a) $x=1.0$ (b) 0.5 (c) 0.25 (d) 0.0 as obtained in (i) TB-LMTO-ASR calculation and (ii) LMTO-CPA calculation . Solid lines represent total densities of states , dotted(dashed) and dashed(long-dashed) lines represent partial densities of states in Cu and Pd for figures (i) ((ii)). Vertical lines mark the positions of Fermi-levels. 79
- 3.6 Structure of a tetrahedron fcc cluster for various possible occupations of vertices by A and B atoms 85
- 3.7 The local densities of states on Pd site in (i) $Cu_{95}Pd_5$ and (ii) $Cu_{75}Pd_{25}$ alloys. The solid one represents result without lattice relaxation and the dashed one with lattice relaxation effect. The vertical lines show the position of the Fermi Energy. 87
- 3.8 The local densities of states on Cu site in (i) $Cu_{95}Pd_5$ and (ii) $Cu_{75}Pd_{25}$ alloys. The solid one represents result without lattice relaxation and the dashed one with lattice relaxation effect. The vertical lines show the position of the Fermi Energy. 88
- 3.9 (a) Cu and (b) Pd LDOS's obtained from the valence-band photoelectron spectra in $Cu_{75}Pd_{25}$ of Wright *et. al.*(1987) . Results of relaxed TB-LMTO-ASR calculation are also shown by plotting data in the same scale as that of experiment for comparison . Fermi energy has been adjusted at 0 eV. 90
- 3.10 (i) The local densities of states on Cu site in $Cu_{90}Be_{10}$ alloys. The solid one represents result without lattice relaxation and the dashed one with lattice relaxation effect. The vertical lines show the position of the Fermi Energy. (ii) Same as (i) but for local densities of states on Be site 91
- 4.1 Density of states vs Energy for Pd_xV_{1-x} alloys. (a) $x=0.0$ (b) $x=0.25$ (c) $x=0.5$ (d) $x=0.75$ (e) $x=1.0$. The vertical lines mark the positions of the Fermi energies. 111

4.2	The nearest neighbour pair interaction V_1 vs band filling for $\text{Pd}_x\text{V}_{1-x}$ alloys : from top to bottom $x=0.25$, $x = 0.5$ and $x = 0.75$. Vertical lines mark the band filling in the three different concentrations.	112
4.3	The nearest neighbour pair interaction V_1 vs energy for $\text{Pd}_x\text{V}_{1-x}$ alloys : from top to bottom $x=0.25$, $x = 0.5$ and $x = 0.75$.Vertical lines mark the Fermi energies.	113
4.4	The number of states per atom as functions of energy for the three alloys mentioned in Figure. 4.2-4.3. The vertical lines mark the Fermi energies.	114
4.5	The n^{th} neighbour pair interactions vs band filling for $x=0.5$, from top to bottom $n=2$, $n = 3$ and $n = 4$. Vertical lines mark the band filling in the three different concentrations.	115
4.6	The superstructures (a) L1_2 , (b) DO_{22} , (c) L1_0 and (d) A_2B_2 . Two unit cells have been represented for L1_0 and L1_2 for a comparison.	118
4.7	The antiphase boundary energies for $x =$ (a) 0.25 (b) 0.5 and (c) 0.75 Vertical lines mark the band filling in the three different concentrations.	119
4.8	The nearest neighbour pair interaction V_1 vs energy for $\text{Pd}_x\text{Rh}_{1-x}$ alloys : from top to bottom $x=0.75$, $x = 0.5$ and $x = 0.25$. Vertical lines mark the Fermi energies.	122
4.9	V_n as a function of n for the $\text{Pd}_{50}\text{Rh}_{50}$ alloy	123
4.10	$V(\mathbf{h})$ surface for the $\text{Pd}_{50}\text{Rh}_{50}$ alloy at $h_3 = 0$ plane.	127
4.11	Spinodal curve for PdRh alloys . The points indicate calculated points while the solid line is the cubic spline fit through points.	129
5.1	The first order scattering diagram for the thermodynamic potential. Full lines indicate electron propagators, the dashed lines indicate the disorder propagators and the dotted line the interaction W_{ij}	136
5.2	Two second order scattering diagrams for the thermodynamic potential.	137
5.3	The scattering diagram obtained by opening up one of the closed electron loops in the diagram for thermodynamic potential in Figure 5.1. This belongs to the scattering diagram set for the averaged electron propagator.	139
5.4	The scattering diagrams obtained by opening up one of the closed electron loops in the second order scattering diagrams for the thermodynamic potential in Figure 5.2	141
5.5	Irreducible scattering diagrams for the self-energy for the averaged electron propagator	143
5.6	A scattering diagram for correlated scattering from two sites .Such diagrams are neglected in the single site coherent potential approximation	144
5.7	(a) A scattering vertex in augmented space. (b) A new scattering diagram for the annealed average. Note that for annealed average electron propagators renormalize the disorder propagator.	146
5.8	Scattering diagrams which arise in annealed averaging of the thermodynamic potential but not its quenched average.	147

5.9	Scattering diagrams for an <i>annealed</i> propagator obtained by opening up one of the electron loops in the scattering diagrams shown in Figure 5.8	149
-----	---	-----

List of Tables

3.1	Comparison in system size and time taken in recursion for square , face centered cubic and simple cubic lattices decribed by model tight-binding Hamiltonian with only s-orbital invoking and not invoking symmetry for fixed number of shells (N_{sh}) and fixed number of recursion steps (M). N_f and N_r are the number of sites in the full and symmetry reduced maps. τ_f and τ_r are the corresponing CPU times in seconds on a HP 9000/300 machine	65
3.2	Comparison in system size and time taken in recursion for face centered cubic lattices decribed by LMTO Hamiltonian with s-p-d orbital invoking and not invoking symmetry for fixed number of shell and fixed recursion step. Time quoted are CPU time in minutes in a HP 9000/300 machine . All table headings have the same meaning as in Table 3.1	65
3.3	Comparison in system size and time taken in augmented space recursion for a model 50-50 alloy system described by tight-binding s-orbital Hamiltonian (on-site term for components A and B ; $\epsilon_A = 2.0$, $\epsilon_B = -2.0$ and non-random off-diagonal term $V = -1.0$.) in a square lattice , invoking and not invoking symmetry for fixed number of shell and fixed recursion step. Time quoted are CPU time in seconds on a HP 9000/300 machine . All table headings have the same meaning as in Tables 3.1 and 3.2.	69
3.4	Comparison in system size and time taken in augmented space recursion for the fcc based AgPd alloy system at 50-50 concentration described by TB-LMTO Hamiltonian , invoking and not invoking symmetry for fixed number of shell and fixed recursion step. Time quoted are CPU time in minutes in a HP 9000/300 machine . All table headings have the same meaning as in Tables 3.1-3.3.	69
3.5	Peak positions and relative peak heights of Pd local desity of states (relaxed calculation) in the $Cu_{75}Pd_{25}$ alloy . Values quoted for LMTO-CPA and LMTO-recursion are taken from figures of Bose <i>et. al.</i> (1992) and the results for LAPW-supercell are taken from Lu <i>et. al</i> (1992). Peak I , Peak II , Peak III denote the positions of three sucessive peaks in LDOS of Pd positioned from higher to lower energy .Peak positions are measured in Ryd from Fermi levels . ρ_I , ρ_{II} , ρ_{III} denote density of states at corresponding positions	89

3.6	Peak positions and relative peak heights of Pd local density of states (relaxed calculation) in the $\text{Cu}_{95}\text{Pd}_5$ alloy . Values quoted for LMTO-CPA and KKR-Green function method are taken from figures of Kudrnovský and Drachal (1989) . Peak I , Peak II , Peak III denote the positions of three successive peaks in LDOS of Pd positioned from higher to lower energy .Peak positions are measured in Ryd from Fermi levels . ρ_I , ρ_{II} , ρ_{III} denote density of states at corresponding positions	89
4.1	Effective Pair Potentials in mRyd/atom for various distances between the pairs for a 50-50 PdV alloy. TBLMTO-DCA values are taken from (Wolverton <i>et. al.</i> ,1993a) and KKR-GPM from (Turchi <i>et. al.</i> ,1988).	111
4.2	Antiphase boundary energies in mRy/atom-spin for PdV at different atomic compositions. The antiphase boundary energies for the KKR-GPM has been taken from Figure. 1 of (Turchi <i>et. al.</i> , 1988) while the value for TBLMTO-DCA has been calculated from pair interactions quoted in table 3 of (Wolverton <i>et. al.</i> ,1993a)	117
4.3	Ordering energies in mRy/atom for PdV at different atomic compositions. . . .	117
4.4	Effective Pair Potentials in mRyd/atom for various distances between the pairs for a 50-50 PdPh alloy. TBLMTO-DCA values are taken from (Wolverton <i>et. al.</i> , 1993b) and KKR-GPM from (Turchi <i>et. al.</i> ,1988) . In order to make our and KKR-GPM result comparable to that of TB-LMTO-ASR , effective pair interactions have been multiplied by factor of 1/4 as in table 4.1.	123

Chapter 1

INTRODUCTORY REMARKS

Ever since the enunciation of the Bloch's theorem in 1928, considerable successful effort has gone into the understanding of the electronic properties of crystalline solids with periodic potential. However most solids around us are disordered. Deviation from crystallinity seems the rule rather than exception.

Any deviation in a crystal from a perfectly periodic lattice arrangements of atoms is an imperfection. Examples of common point imperfections are chemical impurities, vacant lattice sites and extra atoms not in regular lattice positions. The crystal surface is a planer imperfection where lattice periodicity is broken in a direction normal to the surface. Real crystals are always imperfect in some respect. Many important properties are controlled as much by imperfections as by the nature of the host crystal, which may act as a vehicle or solvent or matrix for the imperfections. The conductivity of some semiconductors are due to trace amounts of chemical impurities. The colour of many crystals arise from the imperfections. The luminiscence of crystals is always connected with the presence of impurities. The mechanical and plastic properties are usually controlled by defects.

The nature of the common point imperfections are fairly well understood for many solids. The bulk of the recent work is concerned with disordered solids with high concentration of such imperfections. Concerted and extensive effort began into the study of these disordered solids only in the late sixties. Disordered solids encompass a rather extensive class. Broadly speaking they can be grouped into following classes:

- (1) Compositionally disordered solids like random alloys, both substitutional (CuZn, CuPd, CuAu, FeTi, NiPt etc) and interstitial (PdH).
- (2) Structurally disordered solids as in the case of amorphous materials like amorphous Si, amorphous Se and the glasses.
- (3) Magnetic alloys with compositionál disorder (AuFe, CuFe, FeNi etc) and structural disorder like metallic glasses.

- (4) Amorphous alloys α -Au_xSi_{1-x} , La_{1-x}Sr_xVO₃ and doped semiconductors like Si:P with associated localization effects.
- (5) Polymers.

The kind of problems one encounters when one turn to random systems are also multifarious . Some of them are :

- (1) The understanding and description of the nature of disorder-driven localization of the electrons in random systems.
- (2) The theoretical understanding of various electronic properties like density of states , photo-emission , optical properties and electron related magnetic properties.
- (3) The understanding of disorder linked transitions like compositional order-disorder transitions.

In the present thesis we have made an attempt to address some of these problems related to disordered materials. Chapter 2 is concerned with transport of electrons through random media . Since Anderson's suggestion in 1958 that sufficient disorder can localize electronic states , the physics of quantum transport has received immense interest . Though exponential localization in presence of weakest amount of disorder is an accepted fact in one dimension , the situation is not settled for two dimensions. Analytic work on quantum transmittance in two dimension has proven to be difficult and many results apply only to limiting cases . The vector recursion technique (Godin and Haydock , 1988) provides a stable and accurate method for numerical determination of transmittance and hence conductance via the Landauer formula (Imry, 1986) of disordered system at $T = 0^\circ \text{K}$. We have applied this methodology in conjunction with coarse-graining technique of real space renormalization procedure to study the scaling behaviour of resistance in a two-dimensional tight-binding Anderson model with on-site disorder . Same vector recursion method has also been used for detecting probabilistically exceptional stochastic resonances in the localized regime, exhibiting high transmittance value in a two-dimensional Quantum Percolation model characterized by random occupancy of bonds with a given probability. Multifractal analysis has been applied for characterising internal geometric structure of these resonating states . While in real materials , the situation is complicated by the fact that electron-electron interaction masks the localization effect due to disorder , these simple tight-binding models help in understanding the effect of disorder in quantum transport in absence of correlation effect.

In Chapter 3 , we propose and demonstrate practical implementation of the augmented space recursion method for obtaining configuration averaged quantities related to electronic structure of disordered alloy systems . While in recent years , there have been attempts (Stocks *et. al.* , 1977; Kudrnovský and Drchal , 1990) at calculating the electronic structure of disordered alloys

from first-principles, most of the works are based on mean-field approaches like the coherent potential approximation (CPA) in conjunction with first-principle electronic structure methods like the KKR, LMTO. Though these CPA-based first principle methods give reasonable descriptions of disordered alloy systems in many cases it is expected to fail in describing effects involving multisite scattering like clustering, local lattice distortion, short-range ordering etc

The augmented space recursion method based on augmented space theorem (Mookerjee, 1973) for general configuration averaging and the recursion method (Haydock *et. al.*, 1972), provides a theory extending beyond the CPA and is capable of handling effects arising from multisite correlations. A first principle application of this methodology within the framework of TB-LMTO method (Andersen and Jepsen, 1984) of electronic structure calculation has been made to alloy systems like AgPd, CuPd, CuBe.

Knowledge of electronic structure also provides us with the information of phase formation and stability of substitutional alloy systems. It requires accurate approximations of the configurational energy on one hand and the use of approximate statistical model on the other

Models are often formulated (Gonis *et. al.*, 1987) to represent configurational energy in terms of effective pair interactions. The problem of stability analysis thus reduces to obtaining ground states of the three-dimensional Ising model whose interaction parameters are obtained by first-principle electronic structure calculations. An alternative viewpoint of phase formation is the instability of the disordered solid solution phase with respect to static concentration wave perturbations corresponding to particular superstructure formation, indicated by minima in the Fourier transform of the effective pair interaction. An augmented space recursive approach in conjunction with the TB-LMTO method has been made in Chapter 4 for the first principle study of phase stability and phase transition in PdV alloys where a number of ordered super-structures are present at various concentrations and PdRh alloys which is a well-known phase-segregating system throughout the concentration range.

For disordered systems, the major issue is the concept of configurational averaging. The question is whether or not the average of the physical quantity will be observed with a probability unity in the thermodynamic limit of infinite extension. If it is so then the quantity will be called self-averaging. The situation encountered in magnetic alloys with quenched disorder is that the partition function is not self-averaging but its logarithm is. Thus, depending upon whether one is concerned with static or dynamic aspect of disorder, the configuration averaging of thermodynamic potential has to be carried out differently (Ducastelle, 1991). Chapter 5 deals with a diagrammatic calculation based on the fermionic field theoretic approach of augmented space formalism for obtaining averaged thermodynamic potential in quenched random system along with its difference with usual annealed case.

In all our calculations (leaving the analytic calculation of the fifth chapter) we have made use of the recursion procedure. Randomness destroys periodicity and for a disordered system the Bloch wavevector \vec{k} no longer remains a good quantum number. This is reflected in the smearing out of the van Hove singularities in the density of states. As a result application of \vec{k} -space techniques demands introduction of some artificial periodicity via the mean field the-

ories like coherent potential approximation . On the other hand the recursion method based on real space technique has the power of exploring the true environmental effect . The recursion processes define a hierarchy of environments with the relative influence of environments explicitly displayed in the local properties one is interested in . Since the successively more distant environments have lesser effects on local properties , the recursion process is dominated by environments close to the local site and finite sized cluster calculations with terminators appended give reasonably accurate results . Furthermore , the numerical accuracy and stability of the recursion method has been studied elaborately and can be controlled efficiently.

In all subsequent chapters we have started with an introduction defining the motivation , a brief discussion of previous works wherever possible , a presentation of our formalism and results and we have ended with a summary of the content.

Chapter 2

QUANTUM MECHANICAL TRANSPORT THROUGH DISORDERED MEDIA *

2.1 INTRODUCTION.

Electrons interacting with lattice imperfections get scattered . The scattering manifests itself as electrical resistance of the sample arising out of energy conserving momentum randomization. At finite temperatures , in addition to such elastic scatterings one also has phonon assisted inelastic scatterings . In the present work we will consider the zero-temperature case, so that only elastic scatterings are responsible for momentum randomization . Parametrizing the degree of elastic scattering by the elastic mean free path length l_e , which is the mean distance travelled by a conduction electron between two successive collisions , two asymptotic limits can be identified , one the weak scattering limit i.e. , $k_F l_e \gg 1$ (k_F is the Fermi wavevector) and the opposite dirty limit, i.e., $k_F l_e \approx 1$. In the weak scattering limit , the interactions are more or less adequately accounted for by the Boltzmann equation which describes transition between the states of the perfect crystal induced by the interactions giving rise to the Boltzmann residual resistivity at $T = 0^\circ$ K. On the other hand in the dirty limit of strong scattering , quantum effects become predominantly important. An important consequence of these quantum phenomena is coherent backscattering (Khmelnitskii,1984). As a general wave phenomenon , what this effect states is that as long as all the scatterings are elastic and we have time reversal invariance, the incident and back-scattered waves (those with scattering angle $\Theta = \pi$) are always coherent and should therefore exhibit constructive interference . As a result scattering in the backward direction is twice as probable as in the other directions leading to

¹ * The contents of this chapter has been published in J.Phys.Condens.Matter 4 7865 (1992) and Phys. Rev. B47 3097 (1993)

a diminished diffusion constant. For strong enough scattering correction to diffusion constant is correspondingly large. When the correction becomes equal in magnitude to the classical diffusion constant the electron gets localized.

This fascinating phenomenon of electron localization caused by quantum interference effects was first pointed out by Anderson (1958). He demonstrated that for a single band tight-binding Hamiltonian on a three dimensional lattice having band-width B and a rectangular distribution of width W of the site diagonal matrix elements of the potential all states are localized for

$$\frac{W}{B} > \left(\frac{W}{B}\right)_{critical}$$

Since then it has become increasingly clear that the presence of quenched disorder in an otherwise crystalline system brings about an entirely new behaviour of electrons. This manifests itself in effects like negative magnetoresistance, non additive and non self-averaging nature of quantum resistances etc. The work we present in this chapter focuses on this strong disorder regime with its associated quantum effects.

As is well known, an impurity may produce a bound state with the wavefunction falling off exponentially away from the impurity site. This picture of localized impurity level is adequate when concentration of impurity atoms is low but the natural question one can ask is what happens when the impurities instead of being almost isolated are close to one another. In this situation, there is sufficient admixture between localized orbitals bound by deep but statistically probable fluctuations in the random potential. If the potential be of sufficiently random nature then the states that are nearly degenerate in energy are in general very far apart in space while the orbitals that are close to each other in space are in general very different in energy

Thus because of statistical repulsion of levels in space and energy the admixture of localized states cannot produce in general an extended state composed of linear combinations of infinitely many localized states. This argument is valid for strong enough disorder irrespective of the dimensionality of the system.

The real impetus to the theory of quantum transport in disordered systems came from the work of Thouless (1974) who gave the first ever microscopic definition of conductance G for a finite sample of size L :

$$G = (e^2/\pi\hbar) (\delta E/\Delta E)$$

where ΔE is the level spacing at the Fermi level and δE is the level shift at the Fermi level due to a change of the boundary conditions from symmetric to antisymmetric ones. $e^2/\pi\hbar$ sets the scale of the conductance. This formed the basis of the one parameter scaling theory of localization. Based on the ansatz that the conductance is the only relevant variable, Abrahams *et. al.* (1979) proposed that

$$\beta = \frac{\partial \log g}{\partial \log L}$$

is an analytic function of the dimensionless conductance g given by

$$g = \left(\frac{\pi \hbar}{e^2} \right) G$$

alone and that the zero of the β function is an unstable fixed point characterized by conductance g_c . Thus for $g > g_c$ the conductance scales to the metallic regime, whereas for $g < g_c$ it scales to the insulating regime. An important consequence is that for dimensions $D = 1$ and $D = 2$, there is no truly metallic regime, while in $D = 3$ the conductance vanishes at the mobility edge continuously. In other words, localization of electronic states arising out of statistical repulsion of levels in space and energy, holds good for $D = 1$ and 2 for arbitrary amount of disorder.

The microscopic basis of the scaling theory and critical behaviour is a subject of continuing debate. The experimental results are complicated by the fact that the electron-electron interactions are to be distangled from the localization aspects. By this time it is now more or less universally accepted that in an one-dimensional crystal even the weakest amount of disorder changes the nature of the electronic wave function from an extended Bloch state to an exponentially decaying one and in three dimensions, beyond a critical value of disorder, there exists a sharp mobility edge separating the localized states from the extended ones while the situation for two dimension is not settled. In general, the analytic solution of the problem proves to be difficult, nor are analytic attempts free from controversy. It is for this reason there has been considerable emphasis on numerical studies. The numerical studies on two-dimensional disordered systems have led to controversy. Some of them suggesting the presence of a weak localization regime for small enough disorder while others suggesting all states to be exponentially localized as in an one-dimensional disordered systems. However most of the numerical methods that have been used either assumes exponential localization *a priori* or involves numerically unstable procedures like divergent recursions and matrix inversions. This motivates us to examine the problem of localization in two dimensional disordered systems using the numerically stable vector recursion technique which is applicable for any geometry of the system without any *a priori* assumption of exponential localization.

Another interesting feature of transport through random media is the presence of sharp reproducible structures in conductance measurements in small devices and in tunneling junctions at low temperatures. These structures have been interpreted in terms of resonant tunneling via probabilistically exceptional states in localized regimes. The conductance of a macroscopic system in strongly localized regime obey's Mott's law of variable-range hopping (Mott, 1968) and can be described successfully using percolation theory. Obviously this picture breaks down when the sample length L is reduced so that it becomes comparable to the correlation radius of the critical network. It has been proposed that in that case the conduction proceeds via variable range hopping along isolated chains. Finally when the sample length becomes of the order of most probable hopping length R_0 , inelastic processes are no longer important and the conduction is expected to occur via resonant tunneling. Theoretical understanding of such

resonant tunneling in strongly localized structure has been put forward by Azbel (1983) .An alternative viewpoint was proposed by Pendry (1987).

Azbel's theoretical interpretation of resonating states was based on the assumption of exponential localization of electronic states . For exponentially localized states with centre of localization situated nearer one of the metallic contacts attached with two sides or corners of the sample , intuition tells that an electron jumping into the state from that particular side will nearly always escape back to that side because the localized state overlaps most with the contact on that side. Electrons incident from the opposite end will find it difficult to tunnel into the state because of the relatively small overlap with contact on that side. Thus the transmission coefficient will always be small , unless the state is localized near the centre of the disordered material. This simple minded argument of identifying states near the centre of the system as dominating the transport properties has been criticised by Pendry on the ground that *far from either metallic contacts , they are very long-lived and contribute to the conductivity over a restricted range of energies* . Pendry proposed an altogether new mechanism of transport in the localized regime. Such states are a necklace of quasi-extended states with approximately equal energy stretching from one side of the disordered sample to the other. The band-width is determined by the overlap integrals between individual states so that such a *necklace state* will serve as an effective contributor to transport process having a wider band-width for communication than the Azbel states. These resonating states carry little probabilistic weight but dominate the statistics. The measurements carried out on series of multi-channel rectangular metal-oxide-semiconductor field effect transistors at temperature below 0.1° K do indicate that conduction occur via resonant tunneling through channels that contain more than one localized state (Popovic *et. al.* 1991). Numerical studies for resonating states in localized regime have been carried out . Most of them seem to support Azbel's idea. The remainder portion of our work on study of transmittance in disordered medium will be devoted in detecting and identifying the nature of such resonating states.

2.2 MODELS STUDIED

2.2.1 The Anderson Model

In his paper entitled *The absence of diffusion in certain random lattices* Anderson (1958) considered a simple model for a random system in which the electron has an energy ϵ_i at lattice sites i , spread with equal probability in the range $-W/2 \leq \epsilon_i \leq W/2$. The excitation propagates by hopping from site i to site j , for which the amplitude is V_{ij} . The model called the Anderson model , has the Hamiltonian

$$H = \sum_i \epsilon_i a_i^\dagger a_i + \sum_{ij} V_{ij} a_i^\dagger a_j$$

where a_i^\dagger and a_i are creation and annihilation operators for the electron at the site i . The

hopping (or overlap) term is generally assumed to connect only the nearest neighbours with amplitude V , so that the electron kinetic energy spread or bandwidth is $B = 2ZV$ where Z is the number of nearest neighbours. For $W = 0$ all the sites have the same zero energy, and the model describes a perfect crystalline solid in the tight-binding approximation. For small W electrons are weakly scattered by the random local energy fluctuations and diffuse rather than propagating ballistically. It was believed prior to Anderson's work that as W increases, an electron in the random system continues to diffuse but more and more slowly. Anderson showed that this is not true and that as W/B exceeds a certain critical amount, there is a qualitative change in the nature of the electronic states. They become spatially localized or non-diffusive.

There are a number of features which have been left out in this model.

- (i) The hopping term V_{ij} also may have distribution of random values.
- (ii) There are often many orbitals at each site.
- (iii) The fundamental and the most important fact missing is that interaction between electrons. This introduces new effects like Mott transition (Mott, 1974) even for a system without disorder.

In spite of all these, disorder is described in a particularly simple way in the Anderson model. It gives the qualitative understanding of the effect of disorder taken alone. Furthermore the model is applicable to wave propagation in general. This includes acoustical as well as optical wave propagation. The latter is in a sense ideal in that it is free from the interaction effect, the most fundamental point left out in Anderson model.

2.2.2 The Quantum Percolation Model

The well studied classical percolation model (Stauffer, 1979) deals with clusters (groups of neighbouring occupied sites or bonds) that are formed on a lattice whose every site or bond is occupied (unoccupied) randomly with probability p ($q=1-p$) and the phenomena of percolation near the concentration p_c (q_c) where for the first time a cluster is formed connecting two ends of the lattice. The singularities in the percolation model occur in the properties of the physical clusters, rather than in quantities related to the thermodynamic properties. Though it is a model of much utility in describing many physical situations ranging from dilute magnets to polymer gelation, it fails in cases like low temperature electrical transport properties of granular metal film, propagation of sound waves through random distribution of pipes etc. The understanding of these phenomena needs the inclusion of quantum effects. The quantum percolation model introduced by Kirkpatrick and Eggarter (1972) can be thought as the quantum version of the classical model of occupied and missing links. In particular, it is a variant of Anderson model where the hopping term becomes random, taking values 0 and V with

probability q and $1-q$, keeping the on-site term independent of lattice occupancy. This model gives an understanding of interplay between the geometry and quantum effects.

Switching on quantum effects on the classical model of percolation theory, introduces a number of differences compared to classical case. In the classical case, the backbone of the infinite cluster (obtained by removing all the dead ends, namely the dangling bonds), plays the central role for transmission. Whereas in the quantum-mechanical case the whole cluster is relevant since wavelets are reflected from the dangling bonds and may coherently interfere. It should also be emphasized that in the quantum-mechanical problem the energy of the incoming electron is an additional parameter and the transmission occurs only within the energy band or window.

2.3 PREVIOUS NUMERICAL ATTEMPTS

2.3.1 Scaling in the Two-dimensional Anderson Model

- (i) **Picard and Sharma (1981)** – Picard and Sharma studied the problem of electron localization in two-dimensional Anderson model by investigating the behaviour of a characteristic length l_{max} , defined as the inverse of the smallest Lyapunov characteristic exponent of random transfer matrix products on strips. It represents the largest possible localization length for an eigenvector if it exists at a given energy. Their study indicates that the states are exponentially localized for disorder greater than a critical value and below the critical disorder the states are *singular*, decaying to zero with a power law. However these conclusions have been criticized on the ground that the system size used were small.
- (ii) **McKinnon and Kramer (1981)** – The methodology employed by McKinnon and Kramer is based on the slice recursion technique. In this method one calculates the properties of a long chain with finite cross-section (width M for a 2D strip and $M \times M$ for a 3D block) and studies how the properties of the chain scale with M . In practice the localization length is calculated for the strip and then the characteristic length scale for the sample of infinite cross-section which is identified as the 2D localization length is obtained by assuming a scaling law in analogy with the critical phenomena.

With this method McKinnon and Kramer concluded that 2D systems display behaviour similar to 1D system with universal exponential localization and a smooth variation of the localization length in agreement with the scaling theory of localization.

However the methodology of slice recursion technique has several points that need further consideration. Firstly as far as the scaling of the electronic state is concerned the work Pastawski *et al.* (1983) (discussed below) reveal that a strip and a true two-dimensional block are expected to behave differently. In particular with the increase of strip width, the exponential localization begins to break down in the weak disorder regime. They find that the proportion of non-exponentially localized states increases as the width of

the system increases. The second point is concerned with the numerical stability of the method itself. Godin and Haydock (1988) noted that by defining recursion in terms of slices, the method introduces an instability compared to 1D case. Quantities such as Green function contain polynomials or ratio of polynomials in energy whose orders are comparable to the number of basis states. Many numbers of greatly differing magnitudes are added together creating errors that accumulate rapidly.

- (iii) *Pastawski et. al. (1983)* – Pastwaski et. al. calculated the matrix continued fraction expansion coefficients of diagonal element of self-energy Δ and looked for the convergence of continued fraction coefficients. They interpreted the convergence length ℓ as measure of localization length. This is identical to the criteria that for state to be extended self-energy has to be non-real for which the continued fraction expansion donot converge. Their method involved the study of the statistical distribution of localization lengths among different configurations. The exponential localization length is defined through the assumption that the norm of the difference between successive convergents decreases exponentially, namely $\|\Delta_{oo}^{(N)} - \Delta_{oo}^{(N-1)}\| \sim \exp(-N/\lambda)$ with λ the localization length equal to the convergent length ℓ for exponential localization. Study on strip geometry indicate that the number of systems for which exponential fit is good decreases as the width of the strip increases. In other words the convergence procedure of using exponential fit becomes invalid suggesting the breakdown of exponential localization. According to the authors this suggests the setting of weak localization in accordance with the result of Picard and Sharma (1981).

2.3.2 Stochastic Resonances In Disordered Systems

- (i) *Basu et. al. (1991)* - Basu et. al. have used the transfer matrix formalism (Liu and Chao, 1986) for detection and study of resonating states in one-dimensional tight-binding Anderson model. The transfer matrix relates the wavefunction at the n-th site to that at (n+1) th site, so that the transmitted wave is given by $\psi_N(E) = t_N \psi_0(E)$, where $t_N(E)$ carries information about the relative amplitude and phase of the transmitted wave for a sample of length N. The authors then have used that set $\{ T_N(E) = |t_N(E)|^2 \}$ as a set of measurements on a collection of chains of varying length $\{ N \}$. They have supplemented their study with multifractal analysis. Their study indicated that the resonating states detected by them are quasi-extended like states as proposed by Pendry. This method has the advantage of being exponentially fast when one keeps on adding length elements at the end of the original chain but has the disadvantage of being limited to one dimension only.
- (ii) *Zhang and Sheng (1991)* - Zhang and Sheng employing the recursive Green function methodology predicted the presence of stochastic resonances in two-dimensional site quantum percolation model. They calculated the conductance of a sample of size $L \times L$ by connecting perfectly conducting two dimensional leads at two sides of the sample and

imposing the hard wall boundary condition along the transverse direction in order to fix the number of propagating channels. The conductance related to transmission and reflection matrices via Landauer formula (Imry , 1986) was obtained by expressing transmission and reflection matrices in terms of retarded Green function $G_{ij}(n,n')$ with source at n' of the channel j and receiver at n of channel i . The same recursive Green function method of calculating $G_{ij}(n,n')$ is also used to probe the wavefunctions of the resonating states with the additional knowledge of eigenfunction projection along transverse direction in the pure lead. Plot of average probability density as a function of distance from the centre of a resonating wavefunction where the probability density is maximum, seemed to support Azbel's idea. However since the determination of average probability density involves directional averaging there remains high probability of necklace like nature of wavefunction with non-isotropic character to be washed out. This fact is indicated in our study. The same methodology has also been used by Xue and Lee (1988) to demonstrate that two-dimensional Anderson model sustain Azbel like resonances.

2.4 METHODOLOGY USED IN PRESENT WORK

2.4.1 Determination Of The Transmittance and Wavefunction In Random Media

The methodology to be employed for determining transmittance and wavefunction of electronic states , the chief ingredients for understanding wave propagation in disordered system is the vector recursion or block recursion technique (Godin and Haydock , 1988). The vector recursion technique is a generalization of the scalar recursion (Haydock , 1980) and the related Lanczos methods. The high accuracy and stability which can be achieved using this family of methods is well understood (Haydock, 1989) .

Our system is a two-dimensional lattice with $2N$ sites. We shall describe the system by a tight-binding Hamiltonian of the type described below.

$$H_{sample} = \sum_i \epsilon_i |i\rangle \langle i| + \sum_i \sum_{j \in N_i} V_{ij} |i\rangle \langle j|$$

The tight-binding basis orbitals $\{|i\rangle\}$ is labelled by the sites on the lattice. N_i are the neighbours of i on the lattice. For the description of usual Anderson model with rectangular distribution of on-site random potential and non random off-diagonal term we have $V_{ij} = V$ if i, j are nearest neighbours and 0 if not.

The on-site probability distribution given by

$$p(\epsilon_i) = \begin{cases} \frac{1}{W}, & \text{for } -W/2 \leq \epsilon_i \leq W/2 ; \\ 0 & \text{otherwise.} \end{cases}$$

The model of quantum percolation is a variant of this and can be described by a Hamiltonian given by

$$H_{sample} = \sum_i \epsilon |i\rangle \langle i| + \sum_i \sum_{j \in N_i} V_{ij} |i\rangle \langle j|$$

The diagonal non-random term ϵ sets the zero of the energy scale. The nearest neighbour off-diagonal terms V_{ij} randomly take value V if the bond exists and 0 if the bond is broken. The probability density of V_{ij} is independent of the particular bond and is given by

$$p(V_{ij}) = (1 - q)\delta(V_{ij} - 1) + q\delta(V_{ij})$$

q being the probability of a bond not to exist between two sites labelled by i and j , that is a broken bond.

The opposite sides of the lattice are coupled via matrix elements to orbitals at the ends of periodic, semi-infinite one dimensional leads. We will describe the methodology for the case of two lead, attached to opposite corners of the lattice. An immediate generalization for the multi-lead case will be indicated. The lead basis states have constant nearest-neighbour hopping V' , which is adjusted to have lead band-width comparable to or larger than that of the two dimensional sample. Incident waves can thus be reflected or transmitted by the sample through the leads. Expressed in tight-binding form, the lead Hamiltonian are thus given by

$$H_{in} = \sum_{i=0}^{-\infty} V' (|i\rangle \langle i+1| + |i+1\rangle \langle i|)$$

$$H_{out} = \sum_{i=2N+1}^{\infty} V' (|i\rangle \langle i+1| + |i+1\rangle \langle i|)$$

Determination Of Transmittance and Conductance.

Transmittance for the above mentioned two dimensional system coupled with leads can be calculated as follows. Let $|i_1\rangle$ and $|i_{2N}\rangle$ be two site orbitals located at opposite ends of the lattice and $|u_1\rangle$ denote $2N \times 2$ matrix whose two columns are the vectors which represent $|i_1\rangle$ and $|i_{2N}\rangle$ respectively. The first step is to generate from this a set of $2N \times 2$ matrices $\{|u_1\rangle, |u_2\rangle, \dots, |u_N\rangle\}$ which satisfy the recurrence relation

$$H|u_n\rangle = |u_{n-1}\rangle B_n^\dagger + |u_n\rangle A_n + |u_{n+1}\rangle B_{n+1} \quad (2.1)$$

where B_n^\dagger , A_n and B_{n+1} are two by two matrices and $|u_0\rangle$ is taken to be $|0\rangle$. The matrix inner product is defined as $\{u|v\}_{\mu\nu} = \sum u_\mu v_\nu$ and the orthogonality as $\{u|v\}_{\mu\nu} = I$. It can be easily shown that demanding the orthogonality of matrix basis sets $\{|u\rangle\}$ gives $A_n = \{u_n|H|u_n\rangle$

while B_{n+1} and $|u_{n+1}\rangle$ may be unravelled by using the Gram-Schmidt procedure to ensure that the column vectors of the matrix $|u_{n+1}\rangle B_{n+1}^\dagger$ are themselves orthogonal to one another. The process is repeated by applying H to $|u_{n+1}\rangle$ and so on.

The columns of $|u_n\rangle$ are vectors which form a new basis in which the Hamiltonian is block tri-diagonal, that is, the transformed Hamiltonian matrix can be divided into 2×2 blocks, only the diagonal and subdiagonal blocks are non-zero.

We now wish to find solutions of the time-dependent Schrödinger equation $H\psi = E\psi$ and from them the scattering matrix for the disordered region. The solutions to the Schrödinger equation in the leads are Bloch waves of the form $\sum \exp(\pm in\theta)|n\rangle$ where $\cos(\theta) = E/2V'$. Now in the input lead there will be an incoming wave of the form $\sum \exp(+in\theta)|n\rangle$ and a reflected wave of the form $\sum r \exp(-in\theta)|n\rangle$. In the output lead there will be a transmitted wave $\sum t \exp(-in\theta)|n\rangle^2$, r and t being reflection and transmission coefficients for wave incident with energy E. The problem, then is to solve the Schrödinger equation in the disordered region with these boundary conditions. The solution of the Schrödinger equation ψ can be specified by $\{\psi_n\}$, the projection of ψ on the basis orbitals $\psi = \sum_n \psi_n |u_n\rangle$. The boundary condition can be represented in terms of ψ_n as

$$\psi_0 = \begin{pmatrix} 1 + r \\ t \end{pmatrix}$$

$$\psi_1 = \begin{pmatrix} \exp(i\theta) + r \exp(-i\theta) \\ t \exp(-i\theta) \end{pmatrix}$$

Each ψ_n can be written as

$$\psi_n = X_n \psi_0 + Y_n \psi_1$$

where X_n and Y_n are 2×2 matrices. By operating with the Hamiltonian on the ψ_n with the Schrödinger equation, we find a three-term recurrence relation for the X_n and Y_n identical to equation (2.1) with EI replacing H and also satisfying the boundary condition $X_0 = I$, $X_1 = 0$ and $Y_0 = 0$, $Y_1 = 1$.

Since the vector recursion is basically a change of basis, the rank of the transformed Hamiltonian remains unchanged. The number of new basis sets is therefore N since we have clumped the old basis sets two by two. This introduces additional boundary conditions which can be expressed in terms of X_{N+1} and Y_{N+1} as

²The process of vector recursion converts the lattice into an one-dimensional chain, which is then folded to clump two sites of the chain together in order to define the basis set $\{|u_n\rangle\}$. For a chain with folded configuration (Figure. 2.1) both the reflected and the transmitted wave move in opposite direction to that of the incident wave.

$$X_{N+1}\psi_0 + Y_{N+1}\psi_1 = 0$$

The above equation gives two linear equations which can be solved for t and r in terms of X_{N+1} , Y_{N+1} and $\exp(\pm i\theta)$. If we now interchange the incoming and outgoing leads, we get a similar pair of equations for r' and t' , the transmission and reflection co-efficients for waves incident from lead 2. Time reversal symmetry demands that t must be same for waves of the same energy incident from either lead so that $t = t'$. Solving these equations for scattering S-matrix for the disordered region one have

$$S = -(X_{N+1} + Y_{N+1}\exp(-i\theta))^{-1}(X_{N+1} + Y_{N+1}\exp(i\theta)) = \begin{pmatrix} r & t \\ t & r' \end{pmatrix} \quad (2.2)$$

Generalization of this methodology for the multi-lead case with M number of incoming leads and M number of outgoing leads is now a trivial task. The representation of new vector basis states formed out of repeatative application of recurrence relation are now matrices of sizes $2N \times 2M$ with the first member chosen as $|u_1\rangle = (|i_1\rangle, |i_2\rangle, \dots, |i_M\rangle, |o_1\rangle, |o_2\rangle, \dots, |o_M\rangle)$, where $|i_k\rangle$ and $|o_k\rangle$ are the position at which the incoming and outgoing leads attach to the system. The $2M \times 2M$ matrices A_n and B_n are the block tridiagonal representations of the Hamiltonian in the new basis. The termination of the new basis sets occur after $\nu = N/M$ steps with the scattering S-matrix given by

$$S = \begin{pmatrix} r_{11} & r_{12} & \dots & r_{1M} & t'_{2M,1} & \dots & t'_{2M,M} \\ \vdots & \vdots & \dots & \vdots & \vdots & \dots & \vdots \\ r_{M,1} & r_{M,2} & \dots & r_{M,M} & t'_{M+1,1} & \dots & t'_{M+1,M} \\ t_{M+1,1} & t_{M+1,2} & \dots & t_{M+1,M} & r'_{M,1} & \dots & r'_{M,M} \\ \vdots & \vdots & \dots & \vdots & \vdots & \dots & \vdots \\ t_{2M,1} & t_{2M,2} & \dots & t_{2M,M} & r'_{11} & \dots & r'_{1M} \end{pmatrix} \quad (2.3)$$

We denote the reflection coefficient of the wavelet coming in from i -th incoming lead and reflected into the j -th incoming lead by $r_{ij}(E)$ and transmission coefficient of the same wavelet transmitted into the j' -th outgoing lead as $t_{ij'}$. $\{r'_{ij}, t'_{ij}\}$ denote reflection and transmission coefficients with interchanged incoming and outgoing leads. The reflectance into the i -th incoming lead is thus given by $R_i(E) = \sum_{j \in I} |r_{ij}(E)|^2$ and similarly the transmittance the i -th outgoing lead is given by $T_i(E) = \sum_{j \in O} |t_{ij}(E)|^2$ Here I and O denotes the sets of incoming and outgoing leads. The Landauer formula (Imry, 1986) then gives the zero-temperature conductance as

$$G = \left(\frac{e^2}{\pi \hbar} \right) \left[\frac{\sum_i T_i(E) \sum_i 1/v_i}{\sum_i R_i(E) \sum_i 1/v_i} \right]_{E=\mu}$$

where v_i is the velocity of the electrons carrying current in the i -th lead and μ is the chemical potential of the system. In our case all the leads are equivalent so that $v_i = v_F$, the Fermi velocity of the system. The above equation then reduces to

$$G = \left(\frac{e^2}{\pi \hbar} \right) \frac{MT(\mu)}{R(\mu)} \quad (2.4)$$

$T(E) = \sum_i T_i(E)$ and $R(E) = \sum_i R_i(E)$ are the total transmittance and reflectance. The resistance $\rho = 1/G$ is given by

$$\rho = \frac{\pi \hbar}{e^2} \frac{R(\mu)}{MT(\mu)}$$

Determination Of Wavefunction.

Wavefunction or eigenstate at a given energy E is the solution of the Schrödinger equation ψ specified in terms of projection $\{\psi_n\}$ of ψ on basis orbitals $|u_n\rangle$

$$\psi = \sum \psi_n |u_n\rangle$$

The knowledge about the total wavefunction of the system involves information about the probability amplitude at each site of the two dimensional lattice. Once the reflection and transmission co-efficient at the particular eigen energy are known, the probability amplitude ψ_n at n -th new vector basis $|u_n\rangle$ can be obtained utilising the relation

$$\psi_n = X_n \psi_0 + Y_n \psi_1$$

Now each component on the n -th new vector basis is a linear combination of the original tight-binding basis vectors so that $|u_n^i\rangle = \sum_i C_n^i(i)|i\rangle$ where $C_n^i(i)$ denotes the co-efficient of linear combination and $|u_n^i\rangle$ denotes i -th column of the n -th member of new basis sets $\{|u_n\rangle\}$

If ψ_n^i denotes the i -th row of the projection amplitude then the wavefunction amplitude at the i -th lattice site will be given by $\sum_n \sum_i \psi_n^i C_n^i(i)$.

2.4.2 Block Spin Analogy and Scaling In Two-dimensional Anderson Model

The methodology we employed for obtaining the scaling properties of resistance in a two-dimensional Anderson model closely resembles the real space renormalisation idea in the sense that it involves coarse graining but not followed by rescaling at each iteration step. We shall divide the two dimensional square lattice into rectangular blocks $M_1 \times M_2$ in size as shown in Figure. 2.2(a). For an isolated block as shown in Figure. 2.2(b), the bonds attaching it to the rest of the system appear as input and output leads into the block. The input leads bring in electronic wave from the rest of the system into the block, the blocks then scatters the wave

the output leads take the wave away from the block and it re-enters back into the rest of the system. The vector recursion technique gives the scattering S-matrix which describes the scattering characteristic of the block in terms of its reflectance, transmittance or resistance. For energy conserving system with no inelastic scattering these three quantities are dependent. The crucial step is to obtain an equivalent single-site scatterer of the same resistance as that of the block. This single site scatterer is characterized by an effective Hamiltonian with diagonal disorder $\hat{\epsilon}$. Since we are interested only in the resistance as a physically observable quantity and not in the detailed wavefunction characteristic within the system, this equivalence is justified. In analogy with the block spin idea where we replace a block of spins by a single effective spin and effective coupling such that the free energy remains invariant, here we replace a block of scatterers by a single effective scatterer with an effective diagonal Hamiltonian term $\hat{\epsilon}$, such that the resistances of the block and scatterer remains invariant.

To obtain $\hat{\epsilon}$ we proceed as follows: to the effective single-site scatterer we attach two semi-infinite, perfectly conducting leads (Figure. 2.2(c)) in exact analogy to the vector recursion procedure described earlier. In this simple problem, the vector recursion equations can be solved by hand to obtain

$$\begin{aligned}
 A_1 &= \begin{pmatrix} \hat{\epsilon} & V' \\ V' & 0 \end{pmatrix} \\
 B_1 &= \begin{pmatrix} V' & 0 \\ 0 & V' \end{pmatrix} \\
 B_2^\dagger X_2 &= \begin{pmatrix} -V' & 0 \\ 0 & -V' \end{pmatrix} \\
 B_2^\dagger Y_2 &= \begin{pmatrix} E - \hat{\epsilon} & -V' \\ -V' & E \end{pmatrix} \tag{2.5}
 \end{aligned}$$

so that the S-matrix is given by

$$S = -\{B_2^\dagger X_2 + B_2^\dagger Y_2 \exp(-i\theta)\}^{-1} \{B_2^\dagger X_2 + B_2^\dagger Y_2 \exp(i\theta)\}^{-1}$$

The various symbols have already been introduced earlier. The reflection and transmission co-efficients are given by

$$r(E) = S_{11} = \frac{(E - \hat{\epsilon})V' \exp(-i\theta) + V' E \exp(-i\theta) - (E - \hat{\epsilon})E}{\Delta}$$

$$t(E) = S_{21} = \frac{(2iV'^2 \sin\theta)}{\Delta}$$

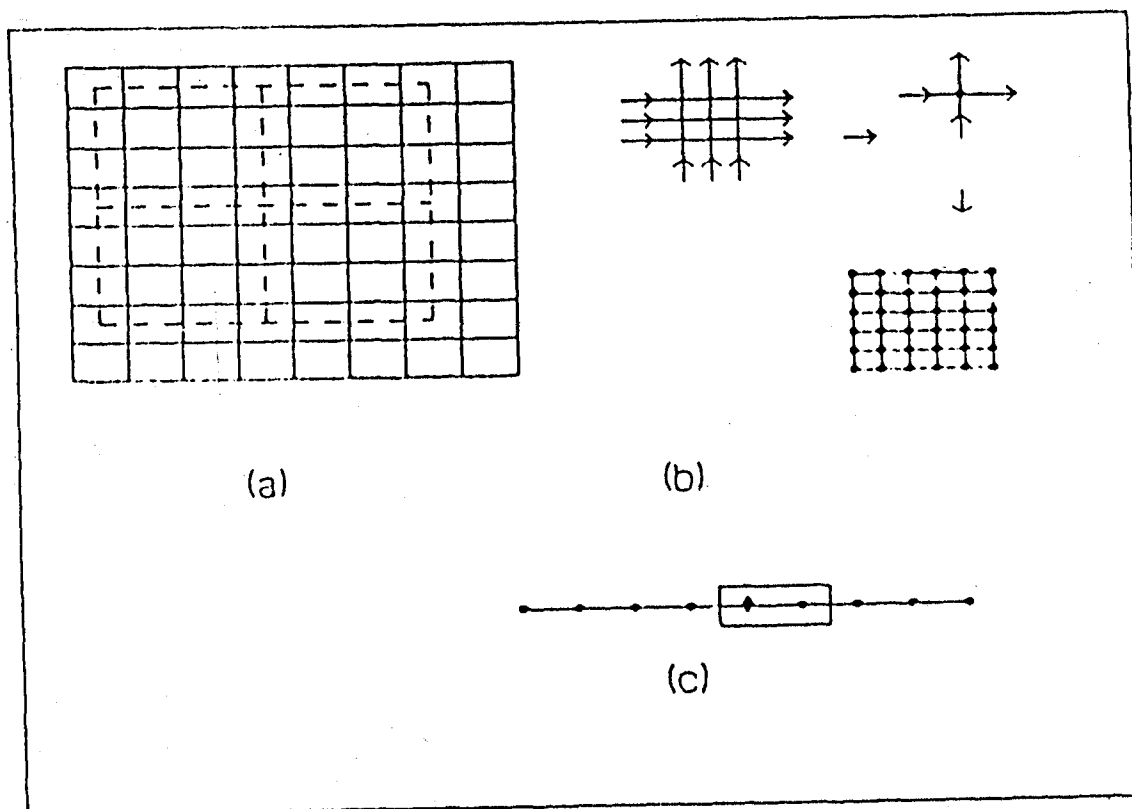


Figure 2.2: (a) Partition of the lattice into blocks (b) An isolated block , renormalization of the block to a single scatterer and the renormalized lattice (c) The single-site scatterer with ordered leads

with

$$\Delta = \det\{B_2^\dagger X_2 + B_2^\dagger Y_2 \exp(-i\theta)\}$$

Finally the relationship between the effective diagonal term $\hat{\epsilon}$ and resistance ρ defined in units of $\frac{e^2\pi}{h}$ is given by

$$\hat{\epsilon}_I = \sqrt{\rho(4V^2 - E^2)}$$

The newly defined effective Hamiltonian then takes the form

$$H_{eff} = \sum_I \hat{\epsilon}_I |I\rangle\langle I| + \sum_I \sum_J V |I\rangle\langle J|$$

Since the different blocks involve random Hamiltonian element, the new effective diagonal terms $\{\hat{\epsilon}_I\}$ are also random. The distribution of these $\hat{\epsilon}_I$ may be determined from the distribution of the block resistances. The above procedure may now be iterated by dividing the renormalised lattice into blocks and reducing these by an identical procedure, obtaining a second level set $\{\hat{\epsilon}'_I\}$. This will reduce the sample to a size $N/(M_1 M_2)^2$. At each stage of this procedure, the vector recursion will always involve a fixed size $M_1 \times M_2$ but will give information about systems of increasingly larger sizes.

2.4.3 Detection Of Stochastic Resonances and Multifractal Analysis in Two-dimensional Quantum Percolation Model

(i) Detection Of Stochastic Resonances.

We choose 2-dimensional quantum percolation Hamiltonian as the model system for present study on stochastic resonances. The model as already discussed is described by tight-binding Hamiltonian with random occupancy of nearest neighbour bonds. The underlying lattice structure (Figure. 2.3) suggests that we have indeed looked upon the problem of maze conduction quantum mechanically.

The conduction here is not mainly along a single path of favorable links, as expected classically. The percolation clusters are topologically complicated and provide many parallel multiply connected pathways for the current. Because of coherent backscattering from these paths one expects electronic states to be localized in two dimensional quantum percolation model and numerical studies reveal that it is indeed the case. We measure the transmittance of such a random maze using the vector recursion technique. The location of the stochastic resonances has to be carefully carried out. We first plot the transmittance vs energy for a small system with sufficiently fine energy mesh. We locate a transparent state. We next increase the systems size, refine the energy mesh and scan the neighbourhood of the state energy. If the state was a localized state with a localization domain larger than the original system size, the transmittance in the enlarged size becomes smaller. If not, we again increase the size and further

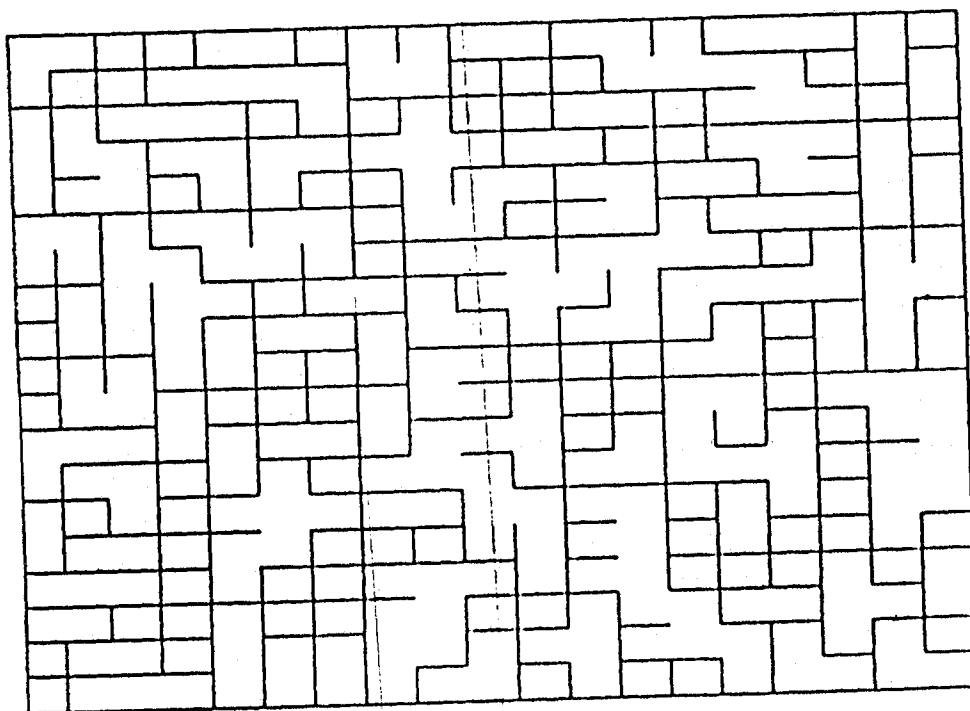


Figure 2.3: Figure showing the connected cluster ($q = 0.3$) characterized by a backbone and dangling bonds

refine the energy mesh and continue our search. There seems to exist a distinction between the high transmitting states arising out of finite size effect (states whose transmittance rapidly falls to zero with increase of system size) and the few probabilistically exceptional resonant states. The positions of the resonant states with transmittance nearly equal to unity remains almost fixed in energy scale with the increase of size. However the resonance widths rapidly decrease with increasing size so that we have to carefully search for them in suitably refined energy meshes. Once we have located a resonant state, the wavefunction corresponding to its energy is obtained by repeating the vector recursion with the known values of the reflection and transmission coefficients.

(ii) Multifractal Analysis.

Multifractal analysis provides a framework of studying the internal geometric structure of the wavefunction amplitudes.

Different moments of a set may scale in different ways and one may therefore describe the set in terms of a continuous set of scaling indices. The set is then called multi-fractal. This point of view suggests new ways of computing fractal properties of sets. It has been used to describe strange attractors , fully developed turbulence, diffusion-limited aggregation etc (Halsey *et. al.* 1986). We will use this approach of describing statistical properties of measures to investigate the internal structure of wavefunction amplitudes in a random tight-binding model, clearly differentiating between a localized state and a necklace state as suggested by Pendry.

The principal step in multifractal analysis is to obtain α - $f(\alpha)$ singularity spectrum . The α - $f(\alpha)$ singularity spectrum provides a mathematically precise and naturally intuitive description of multifractal measure in terms of interwoven sets with singularity strength α , whose Hausdroff dimension is $f(\alpha)$.

Determination of α - $f(\alpha)$ singularity spectrum is based on the box counting procedure . For our case we divide the system into N boxes of linear size L and choose the probability distribution of the wavefunction in the k-th box

$$P_k(L) = \frac{|\psi_k|^2}{\sum_k |\psi_k|^2}$$

as a suitable measure. The length L is so chosen that it encloses a single site. The local singularity strength α_k can then be defined as $P_k(L) \sim L^{\alpha_k}$. If we count the number of boxes $N(\alpha)$ where the probability P_k has singularity strength between α and $\alpha + d\alpha$, then $f(\alpha)$ can be defined as the fractal dimension of the set of boxes with singularity strength α given by $N(\alpha) \sim L^{-f(\alpha)}$ The *generalized dimensions* D_q which correspond to scaling exponents for the q-th moments of the measure provide an alternative description of the singularity measure. They are defined as

$$D_q = \frac{1}{q-1} \lim_{N \rightarrow \infty} \frac{\log \sum_k P_k^q(L)}{\log L}$$

$f(\alpha)$ and D_q are smooth functions of α and q . $f(\alpha)$ is simply related to $\tau(q) = (q - 1)D_q$

by a Legendre transformation. This relationship reflects the deep connection with the thermodynamic formalism of equilibrium statistical mechanics where $\tau(q)$ and q are conjugate thermodynamic variables of $f(\alpha)$ and α . In this case the D_q curves can be easily transformed into $f(\alpha)$ curves. Such an operation involves first smoothing the D_q curve and then Legendre transforming. This has the disadvantage of the fact that error bars from the smoothing procedure make the estimate of error bars from the data itself more difficult. A direct evaluation of $\alpha - f(\alpha)$ spectrum without restoring to the intermediate Legendre transform has been provided by Chhabra and Jensen (1989). This is done by constructing a one-parameter family of normalized measures $\mu(q)$ with

$$\mu_k(q, L) = \frac{\{P_k(L)\}^q}{\sum_k \{P_k(L)\}^q}$$

The parameter q provides a microscope for exploring different regions of the singular measure. For $q > 1$, $\mu(q)$ amplifies the more singular regions of the measure, for $q < 1$ it accentuates the less singular regions and for $q = 1$, $\mu(1)$ replicates the original measure. The Hausdorff dimension and the average singularity strength of the measure theoretic support $\mu(q)$ are then given by

$$f(q) = \lim_{N \rightarrow \infty} \frac{\sum_k \mu_k(q, L) \log \{\mu_k(q, L)\}}{\log L}$$

$$\alpha(q) = \lim_{N \rightarrow \infty} \frac{\sum_k \mu_k(q, L) \log \{P_k(L)\}}{\log L}$$

This provides a relationship between Hausdorff dimension f and average singularity strength α as implicit function of q .

2.5 RESULTS AND DISCUSSION

2.5.1 Scaling Of Resistance In The Two Dimensional Anderson Model

The present study of scaling of resistance in the two-dimensional Anderson model is based on determination of the Hamiltonian with effective single site scatterers. Figure 2.4 shows the distribution of the diagonal Hamiltonian elements of the effective single site scatterers at the end of the first four block renormalizations. Since the Hamiltonian elements of the individual blocks are random the effective scatterer elements $\{\hat{\epsilon}\}$ are themselves random. Their distribution is obtained by running the vector recursion upto 500 configurations of the block and obtaining the distribution as histograms. This distribution is used in the next iteration to generate the

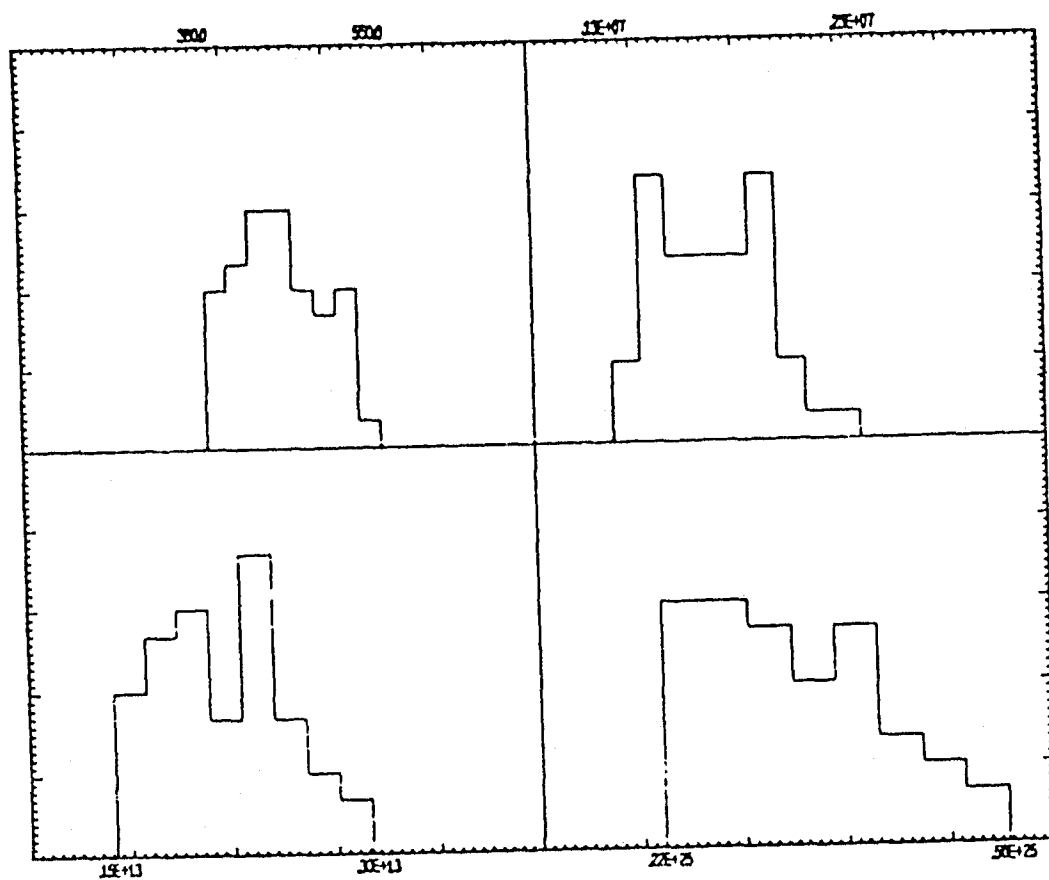


Figure 2.4: The distribution of scattering elements for four successive steps in the block renormalization

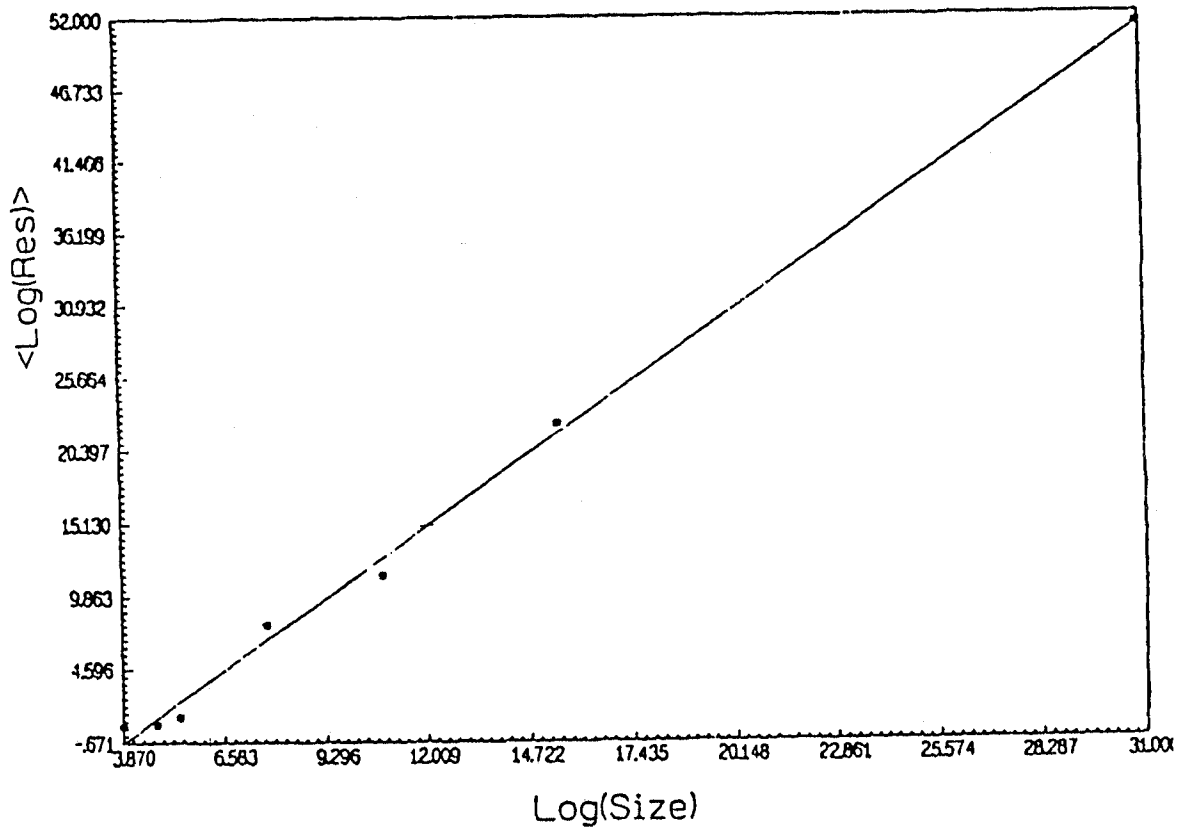


Figure 2.5: The averaged logarithm of the resistance vs the logarithm of the size for $\delta = 0.5$

effective Hamiltonians . Several features of the distributions may be commented upon. An examination of the relationship between the resistance and effective on-site term of the single scatterer indicate that $\hat{\epsilon}$ and $-\hat{\epsilon}$ both give the same resistance , making the distribution of $\{\hat{\epsilon}\}$ symmetric about the origin. In Figure. 2.4 we have shown only the positive part of $\hat{\epsilon}$ axis. It is to be noted that with each iteration a hole of increasing width opens up at the origin although at the starting point there was no hole at the center of the distribution. The initial uniform distribution centered at the origin shows that there is finite probability that ϵ takes the value in the neighbourhood of zero. The probability that a number of ϵ -values are simultaneously zero is very small. This probability becomes progressively smaller as we go on iterating the renormalization procedure. After each stage of renormalization which amounts to working with larger sizes , the width of the distribution of on-site term increases indicating the state under study to be localized with the resistance exhibiting non-ohmic behaviour of increment with system size. For the scaling calculations we have used blocks of sizes 48,120 and 224. Very small blocks are not used as the effect of quantum coherence which is the basic cause of localization may not effectively be demonstrated. Very large blocks also pose problems since their resistances become too large for numerical stability.

The strength of the disorder is measured by the quantity $\delta = W/B$ where B is the band width. We first study the case of a moderate disorder $\delta = 0.5$. Figure 2.5 shows the plot of $\langle \log \rho \rangle$ vs $\log(\text{size})$. The points are the numerical values . These correspond to blocks of sizes 48 , 48^2 , 48^4 and 48^8 , 112 and 112^2 , 224 and 224^2 .

The figure also shows the least square fitted straight line , appropriate for a power law dependence of ρ on size. Figure 2.6 shows a similar plot but for disorders varying from $\delta = 6.25 \times 10^{-4}$ to $\delta = 12.5$.

As expected the power α defined by $\rho(N) = \rho_0 N^\alpha$ is a function of disorder parameter δ and increases with the disorder strength. The curve $\delta = 0.0373\alpha^{0.579}$ is the best fit through the data points and its extrapolation to very low disorder is shown in Figure. 2.7.

In Figure. 2.8(a) we plot resistance vs $\log(N)$ for $\alpha = 1.796 \times 10^{-4}$ which corresponds to a disorder parameter $\delta = 5.0 \times 10^{-4}$. Throughout the size range quoted , the resistance variation at this low disorder is consistent with the logarithmic scaling . Similar plot for $\delta = 0.037$ ($\alpha = 1$) (Figure. 2.8(b)) show deviation from the logarithmic form. All the results quoted above are for energy $E = 0.5$, that is, energy near the band center.

The above study indicates that for states near the center of the band , the nature of localization appears to be of power law type which extrapolates to logarithmic behaviour for low enough disorder. Though such a power law behaviour is not in conformity with the scaling theory of localization which predicts universal exponential localization in 2D systems is supported by other analytic and numerical works. Analytic works (Haydock , 1981,1986) based on perturbative calculation using the recursion method suggest different regimes of exponential and power law localization , indicating a transition between weakly and strongly insulative states. This analytic result also seems to be confirmed by recent numerical work of Godin and Haydock (1991) which reports presence of weakly localized states near the band center and exponentially

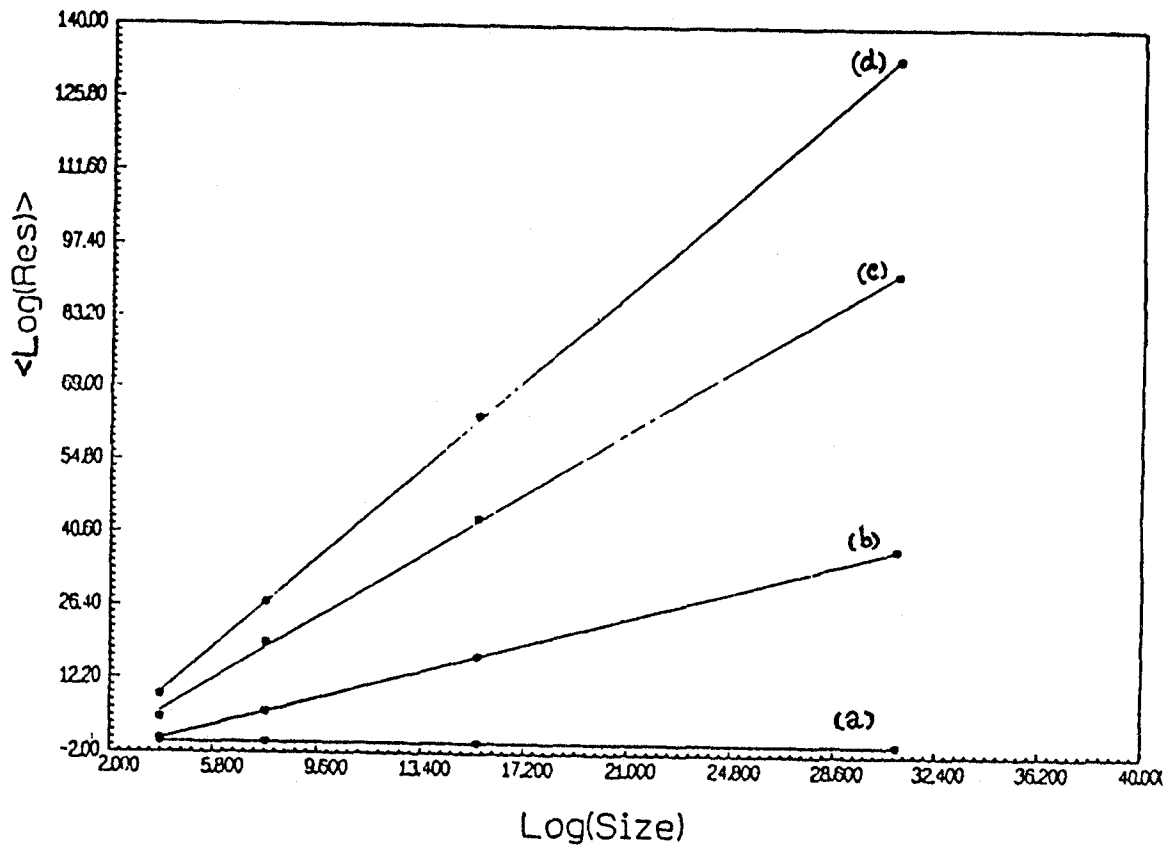


Figure 2.6: The averaged logarithm of the resistance vs the logarithm of the size for $\delta =$ (a) 6.25×10^{-4} , (b) 0.5, (c) 5.0 and (d) 12.5

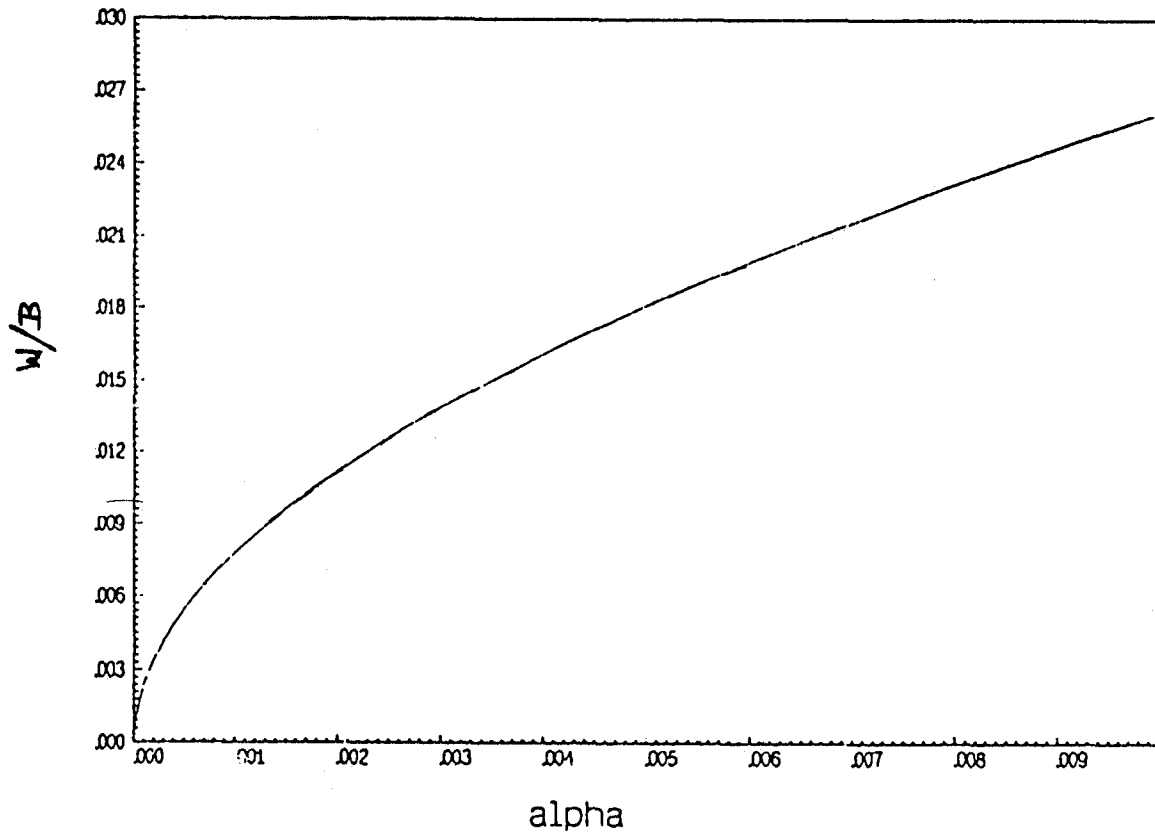


Figure 2.7: Variation in the disorder parameter with the slope α

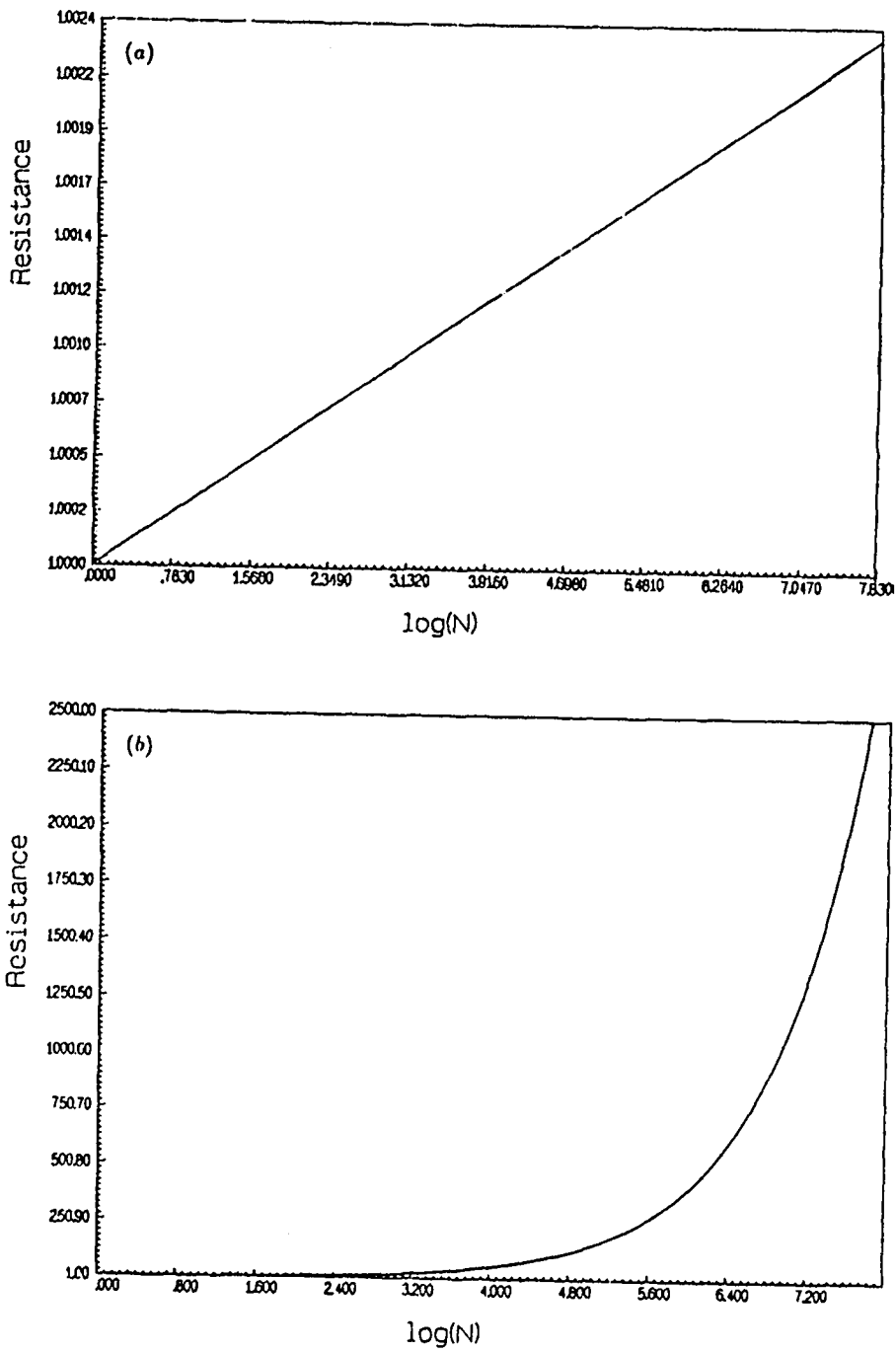


Figure 2.8: Resistance vs the logarithm of the size (a) for $\delta = 5.0 \times 10^{-4}$ (b) for $\delta = 0.037$

localized states near the band edge , in conformity with previous numerical studies of Picard and Sharma (1981) and that of Pastwaski *et. al* (1983) .

2.5.2 Study Of Stochastic Resonances In The Two Dimensional Quantum Percolation Model

For an infinite two-dimensional disordered system all states are expected to be localized with the critical threshold probability q_c (the probability below which states are extended) equal to 0. However, for a finite lattice one may have a threshold $q_0 > 0$ at which the localization length becomes of the order of system size length. For the present work, in order to assure that we belong to the localized regime of the spectrum, we have taken $q > q_0$. Information about q_0 has been obtained from work on finite sized scaling (Mookerjee *et. al.* , 1992). On the other hand, since we are well below the classical threshold q_0^c , which is 0.5 for two-dimensional bond percolation model ,there is always a system spanning cluster, characterized by a backbone and dangling bonds between the two leads. Figure 2.9(a) and 2.9(b) show the plot of transmittance versus energy for a square maze of sizes 20×20 and 30×30 respectively at bond breaking probability $q = 0.3$.

A comparison of the transmittance vs. energy plot for sizes 20×20 and 30×30 reveal that transparent states arising due to finite size effect in size 20×20 have fallen to zero in size 30×30 . These are attributed to localized states with localization domains larger than the system size. On the other hand , at some specific energies the transmittance remain close to 1 consistently both at size 20×20 and 30×30 , along with a small shift in position. We identify these states to be the stochastic resonances. Figure 2.10 shows a resolved plot of the transmittance vs energy near one such resonance for the size 30×30 .

Fig 2.11(a) and 2.11(b) are plots of the wavefunction squared amplitudes and its contour map for a square lattice of size 30×30 at a resonant energy $E = -0.651$. The figure clearly indicates that the wavefunction is not centrally localized. Rather it seems that the state is like a Pendry necklace state with more than one local minimum spaced evenly across the sample. They are more like quasi-extended or clumped states, distinct from the usual extended (Bloch) states. Obviously such states are of statistical origin, and one finds very few of them in an ensemble of several thousand.

It is also evident that the wavefunction squared amplitudes are far being isotropic. The wavefunction plot with directional averaging essentially misses this non-isotropic character , giving rise to an exponentially decaying nature from the region where it has its highest value. This is clearly shown in Figure. 2.12 , where we have plotted the logarithm of direction averaged probability density as a function of distance in order to compare our result with that of Zhang and Sheng (1991). The straight line fit, similar to Zhang and Sheng suggests the exponential decay. Zhang and Sheng's identification of resonances as Azbel resonances based on this decaying nature therefore seems to be an artifact of the directional averaging procedure.

To compare the resonating states with a localized state we have plotted in Figure 2.13(a) and

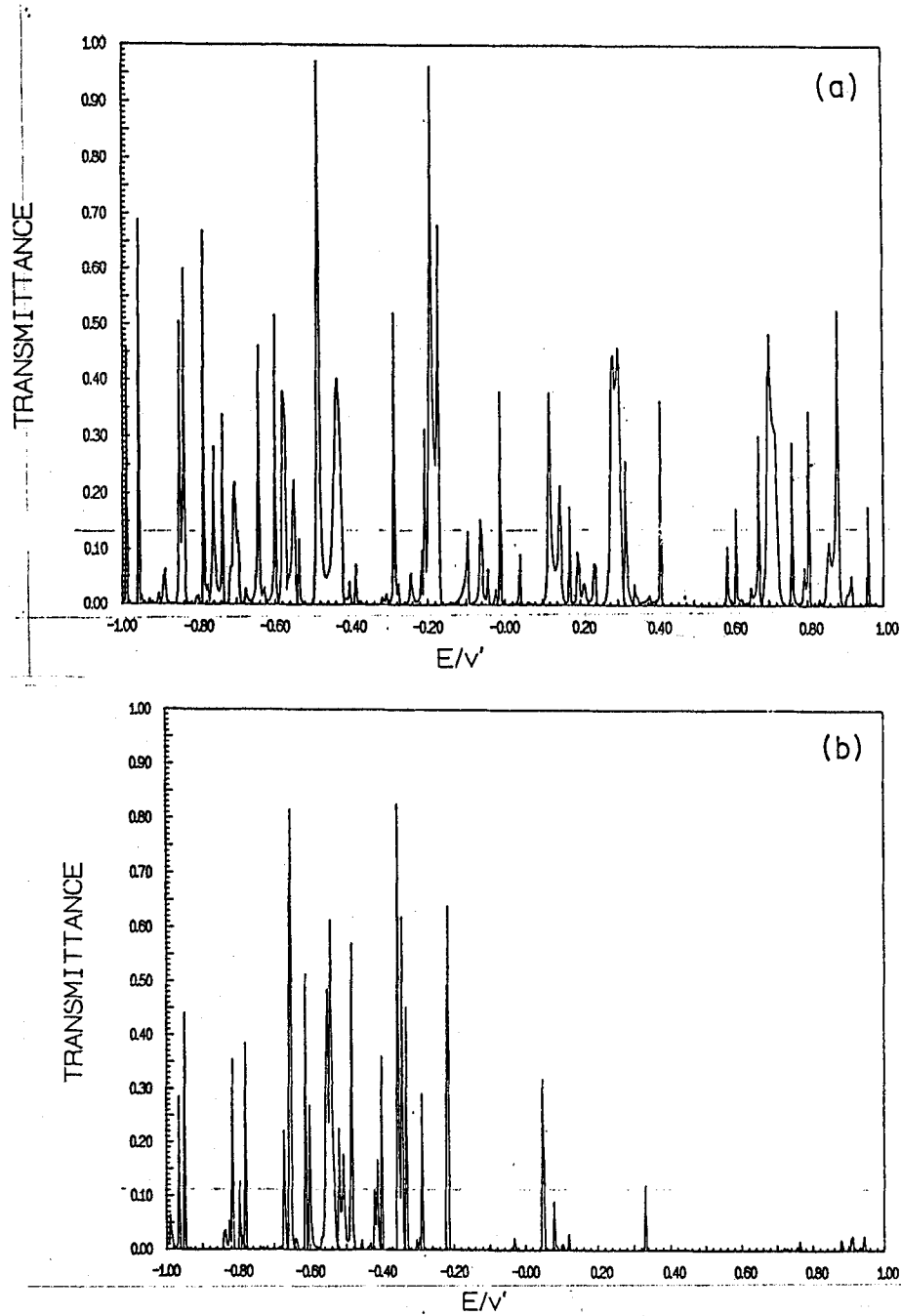


Figure 2.9: Plot of transmittance vs energy for a square lattice of size (a) 20×20 (b) 30×30 at $q = 0.3$

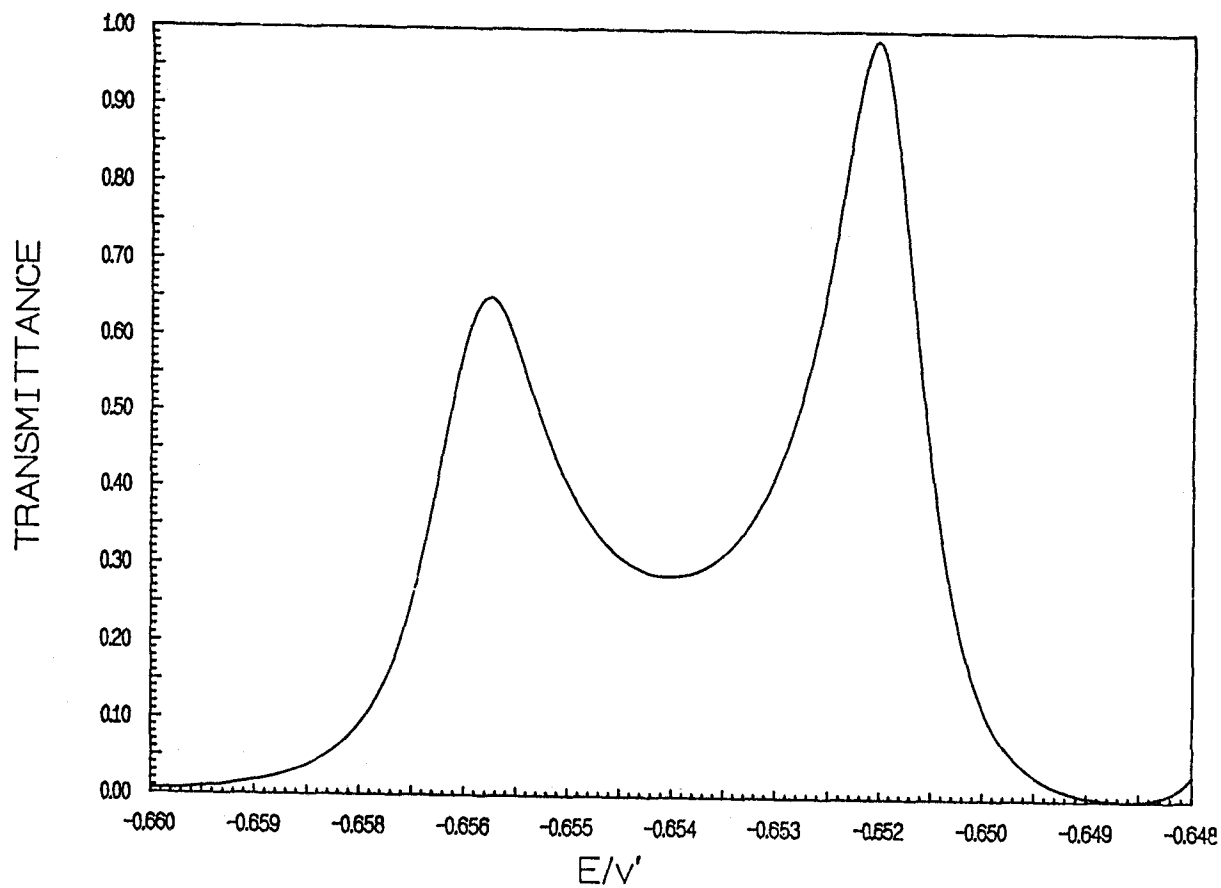


Figure 2.10: Resolved plot of transmittance vs energy for size 30 x 30 in the neighbourhood of a resonance

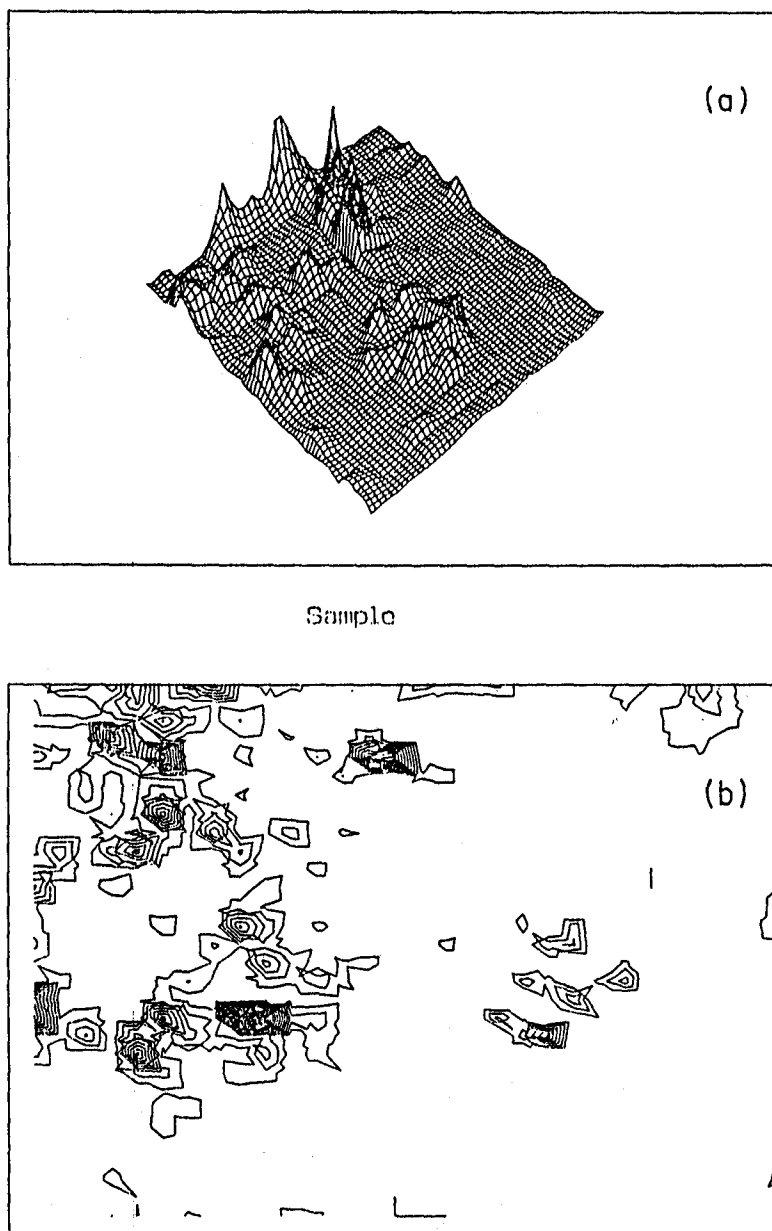


Figure 2.11: (a) Wavefunction squared amplitude vs site co-ordinates (b) contour diagram of the wavefunction squared amplitude over the sample for resonating state ($q = 0.3$, $E = -0.651$)

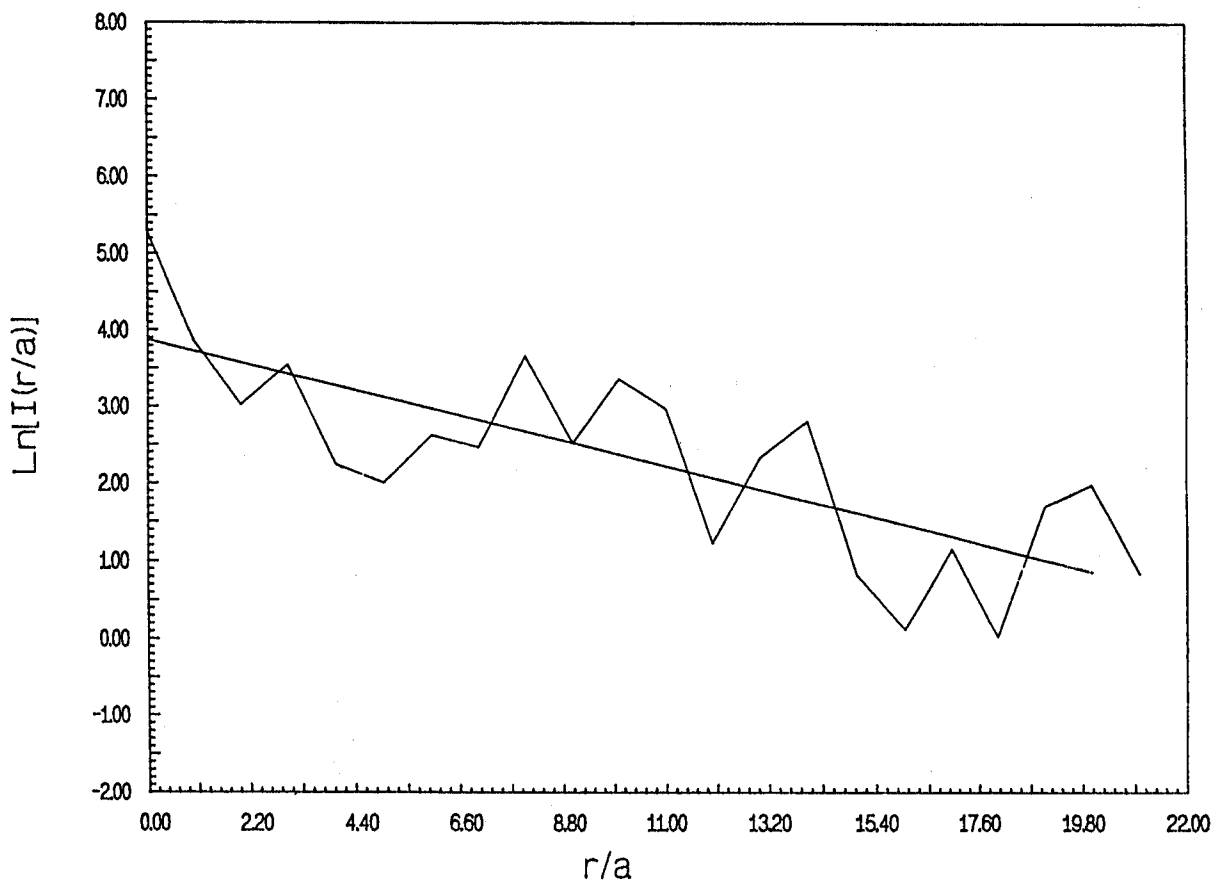


Figure 2.12: Plot of the directionality averaged probability density $I(r)$ vs r measured in units of lattice distance a , from the site with maximum probability along with the best linear fit for the resonating state shown in Figure 2.11

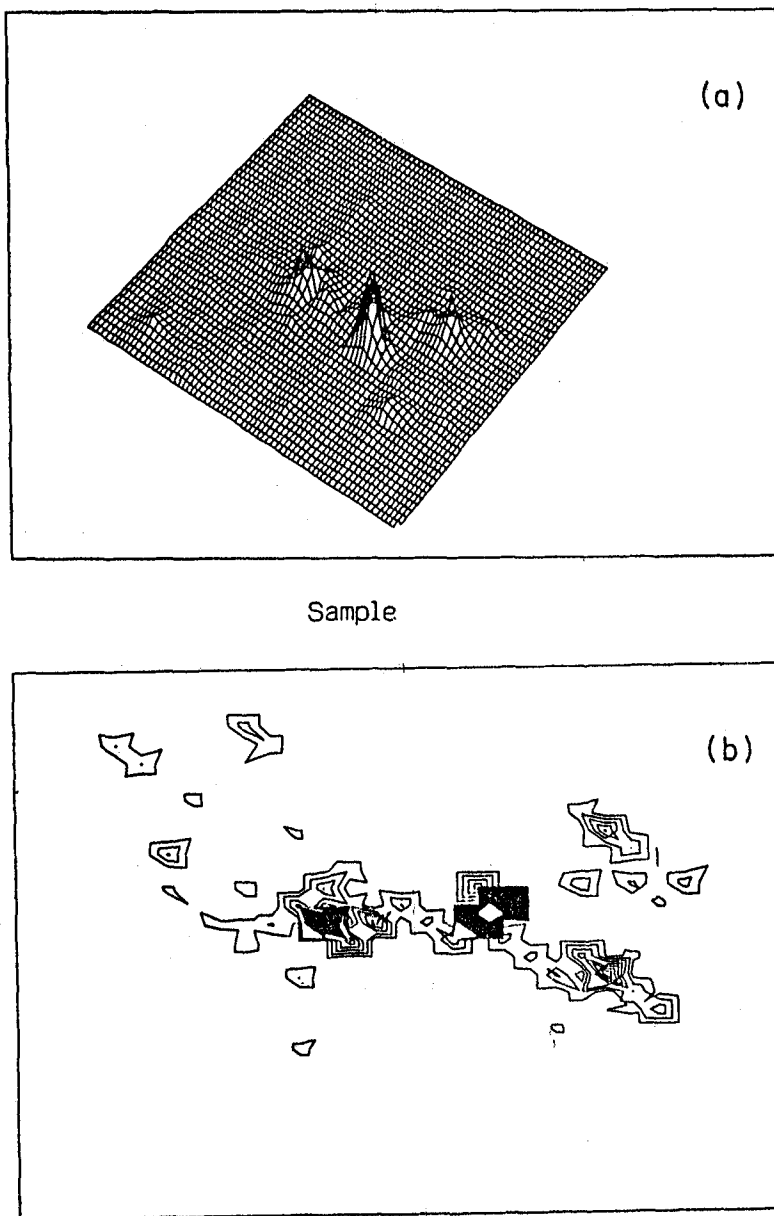


Figure 2.13: (a) Wavefunction squared amplitude vs site co-ordinates (b) contour diagram of the wavefunction squared amplitude over the sample for the localized state ($q = 0.3$, $E = 0.5$)

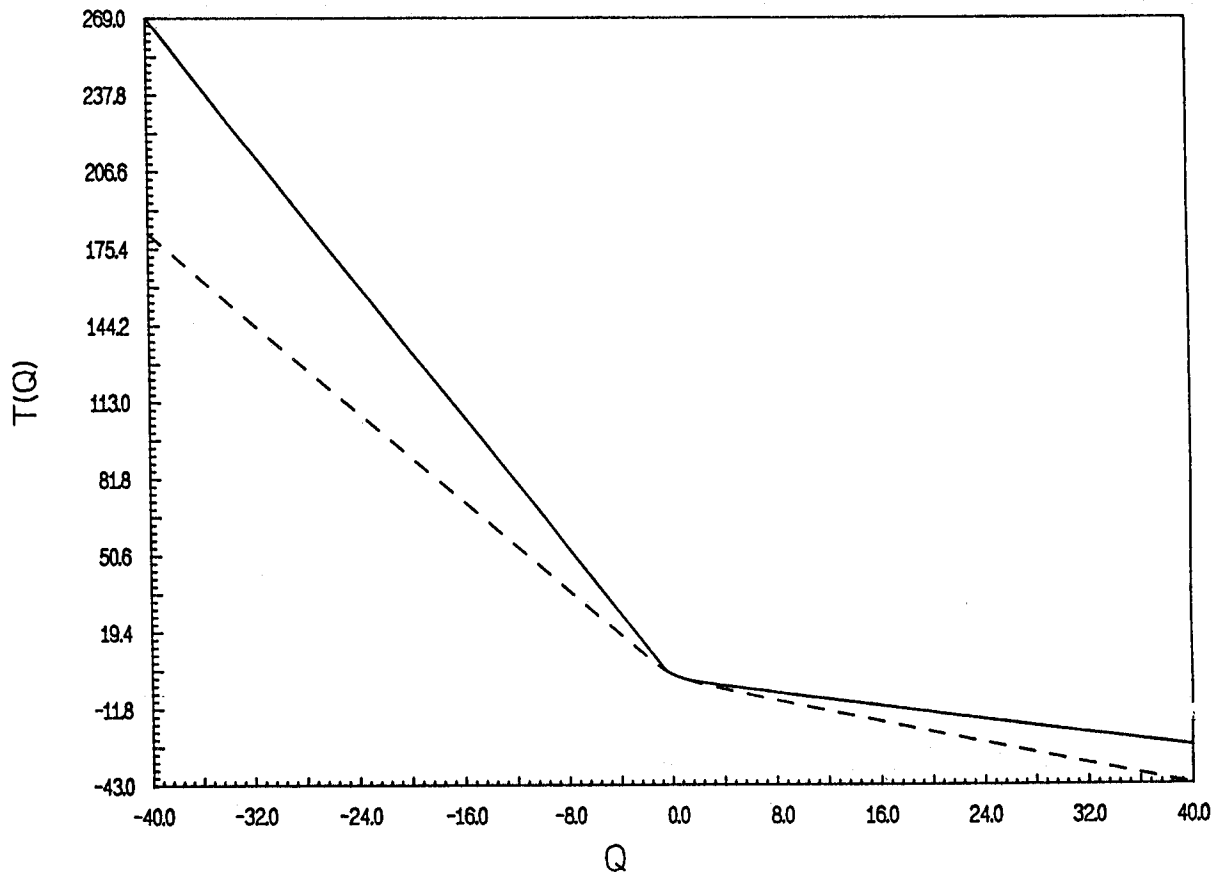


Figure 2.14: Plot of $\tau(Q)$ vs Q for the localized states (solid line) and the resonating states (dashed line)

(b) the wavefunction squared amplitudes and the contour map of a typical localized state ($T(E) \sim 10^{-20}$) for a lattice of size 30×30 and $E = 0.5$.

In order to confirm our conclusion we have carried out a multifractal analysis on the wavefunction which yield information about the internal structure of the resonating states, clearly differentiating between a exponentially localized state and *necklace* state. Figure 2.14 shows $\tau(Q)$ vs Q plot for the localized and resonant states.

A simple homogeneous fractal (a state having a typical power law behaviour with a single exponent) can be completely characterized by two of the moments, hence $\tau(Q)$ vs Q curve should be a straight line. The deviation from linear behaviour in Fig 2.14 suggests that the resonating as well as the localized state is a multifractal entity characterized by several powers. Physically the states with several singularities scale differently according to their mass exponents $\tau(Q)$, hence each subset of the measure is itself a fractal with its own fractal dimension and the entire state therefore does not possess self-similarity. The similarity dimension D_0 is almost 2 within our calculational inaccuracies. The most transparent information regarding the nature of the wavefunctions are obtained from the singularity spectrum ($f(\alpha)$ vs α) plots. A typical singularity spectrum for an extended state is a single point, characteristic of a single mass exponent. For an exponentially localized (fast-decaying) state we may assume that only a few boxes contribute significantly. From the defining equations it is easy to see that the spectrum will be clustered around the points $\alpha = 0, f(\alpha) = 0$ and $\alpha \rightarrow \infty, f(\alpha) = f(\alpha)_{max}$. However, if we take a finite sized system this clustering may not be evident. To characterize a localized state, therefore, we should study the way in which the singularity spectrum behaves as the size of the system increases.

Figure 2.15 is a plot of the singularity spectrum for the resonating and localized states for the largest size with Q values from -40 to 40 in steps of 0.8. The figure shows multifractal behaviour for both the localized and resonating states. It appears that the localized state may not be exponentially localized and that a number of boxes that contribute to the box counting seems to be much larger than in the case of typically exponentially localized states . However, the spectral width ($\alpha_{max} - \alpha_{min}$) for the localized state is much larger as compared to that for the resonating state. This result can be interpreted in the following way : large values of α indicate that probabilities whose scaling is characterized by α are themselves small. Hence in the case of localized states, boxes with low probability have non-zero contribution, suggesting the decaying nature of the localized states. However, for the resonating state the probability amplitude does not decay over large length scales. This supports the clumped nature of the resonating state, where, as a result of sufficient overlap between the individual localized states with centres of localization at different sites (beads of the necklace) the probability value cannot be very low. Large widths for the localized states were also observed in incommensurate chains by Thakur *et.al* (1989) .

Since our investigations are restricted to finite sample sizes, we have carried out, as discussed earlier, a study of the way in which the singularity spectrum behaves with sample size. Figure 2.16(a) and (b) show the singularity spectrum for different sample sizes for localized and

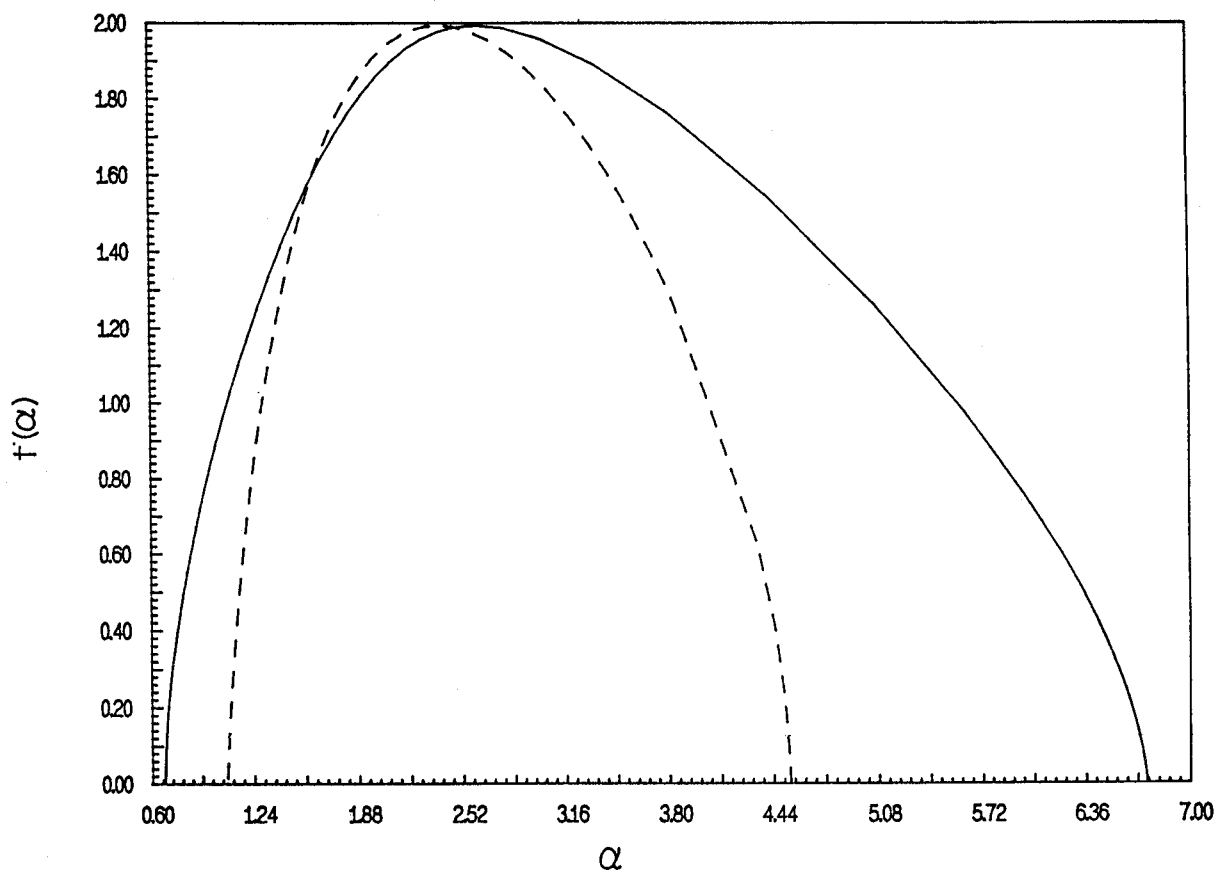


Figure 2.15: Plot of $f(\alpha)$ vs α for the localized states (solid line) and the resonating states (dashed line)

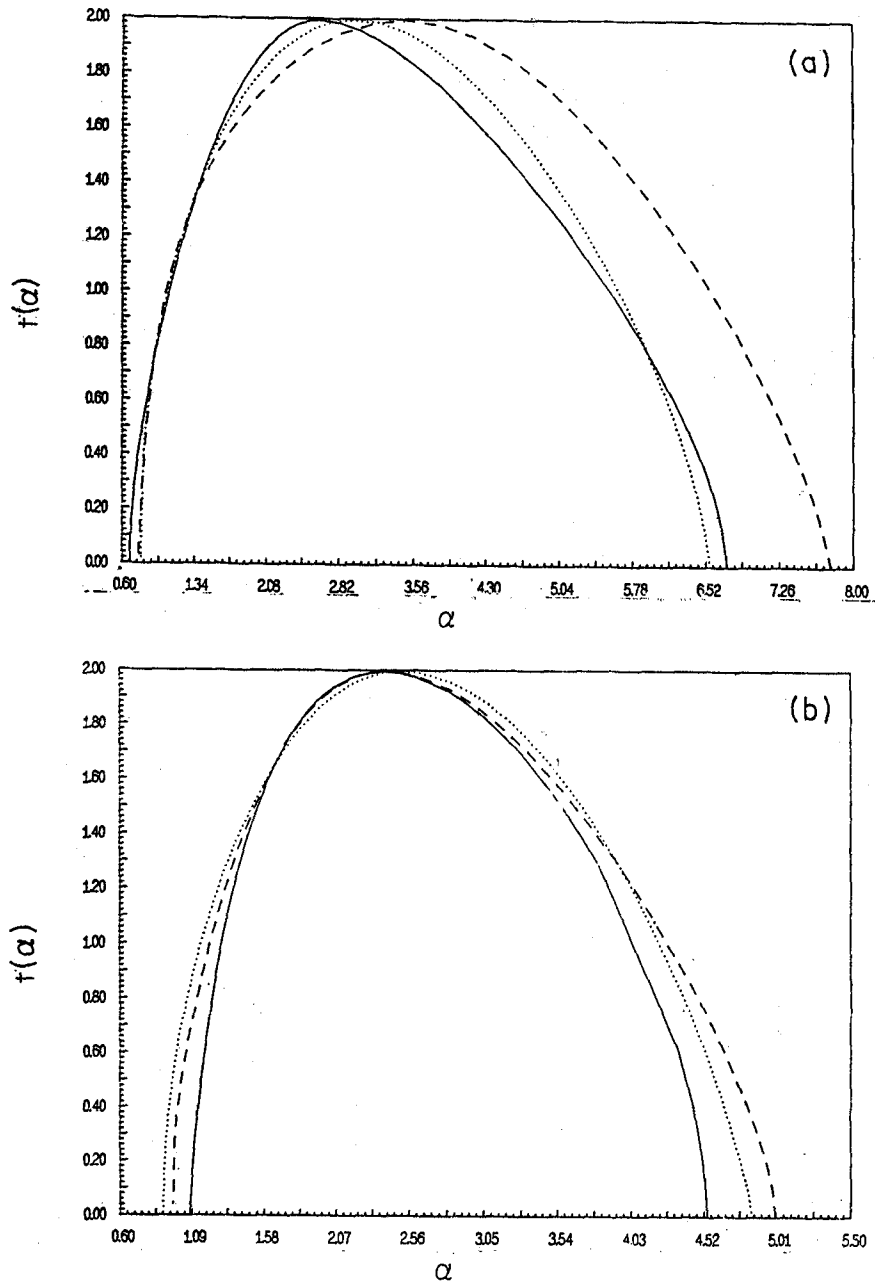


Figure 2.16: The singularity spectrum of (a) the localized state and (b) the resonating state at various system sizes : 20 x 20 (solid line) , 30 x 30 (dotted line) , 40 x 40 (dashed line)

resonating states respectively. The spectrum for the localized states has a very wide support, however the edges oscillate with size, as opposed to α_{max} diverging with system size. This is a sure indication that the localized state (at the band centre) has a slower than exponential decay. The spectrum for the resonant state has a much narrower support and the edges are almost identical.

2.6 SUMMARY

To summarize , our numerical study employing vector recursion method on 2-dimensional Anderson model indicate presence of power law localized states with power decreasing with decrease of disorder strength , for energies near the band centre of the spectrum . In 2-dimensional Quantum Percolation model with all states expected to be localized we identify presence of some probabilistically exceptional resonating states characterized by high transmittance value . The determination of wavefunction amplitudes corresponding to these states reveal that they are formed out of superposition of localized states with centres of localization close enough to each other . This *necklace* like nature of resonating states has been verified by multifractal analysis based on box counting procedure.

Chapter 3

AUGMENTED SPACE RECURSIVE APPROACH FOR CONFIGURATION AVERAGING IN DISORDERED ALLOYS *

3.1 INTRODUCTION.

In the modern world metallic alloys are used in a enormous variety of applications . The reasons for this ubiquitous use revolve around the possibility of modifying the properties – strength , ductility , corrosion , resistance , thermal and electrical properties to meet specific engineering requirements. Because most commercial alloys are complex multiphase mixtures , it is important to have an understanding of all of the possible alloy phases that can occur : pure metals , possible ordered intermetallic compounds and possible disordered solid solutions.

Considerable effort has been devoted to the theoretical study of the electronic structure of binary disordered alloys. Indeed these investigations present a two-fold interest : first , from the fundamental point of view , the understanding of the electronic structure of disordered systems has long remained a challenge ;and second, by their possible applications in metallurgy . The theory of electronic structure calculations in disordered alloys pose a challenge to theoretical physicists . Because of the lack of translational symmetry , Bloch's theorem and standard band structure method remain no longer applicable. As a result Bloch quantum number \vec{k} no longer remain a good quantum number and smearing out of van Hove singularities in electronic density of states occur. The situation is further complicated by the fact that in addition to an accurate electronic structure description of components , the electronic structure calculation

¹ * Part of this chapter has been published in J.Phys.Condens.Matter 6 L245 (1994)

in disordered alloy systems requires an appropriate averaging scheme for describing averaging over random disorder configurations.

In the last decade many calculations on disordered alloys, based on semi-empirical tight-binding Hamiltonians, have been reported. In spite of its encouraging success the electronic structure calculations based on the semi-empirical tight-binding Hamiltonians has some underlying approximations which are often unjustified (Pettifor, 1992). It calls the need for first-principle theories of disordered alloy systems. During the last few years it has become clear that density functional theory (DFT) in the local density approximation (LDA) (Kohn and Sham, 1965; Hohenberg and Kohn, 1964) provides a sound, *ab-initio* theoretical basis for calculating ground state properties of pure metals and ordered compounds. Consequently DFT-LDA provides a logical starting point for relevant disordered solid solution also. A number of electronic structure methods within the framework of DFT-LDA exists in literature. While Korringa-Kohn-Rostoker (KKR) method (Korringa, 1947; Kohn and Rostoker, 1954) and Augmented Plane Wave (APW) method (Slater, 1937) provides the most accurate electronic structure description of solid, their energy linearized version, linearized muffin-tin orbital (LMTO) method (Andersen and Jepsen, 1984) and linearized augmented plane wave (LAPW) method (Andersen, 1975) are also widely applied because of the better computer tractability compared to their parent methods. The successful theoretical tools for understanding the electronic properties of disordered alloys is based on these first-principle electronic structure techniques in conjunction with mean field approaches like single site coherent potential approximation (CPA) (Soven, 1967; Taylor, 1967) for describing configuration averaging, super-cell methods (Lu *et al.*, 1991a) with repeated cells whose sites are occupied by component atoms so as to model the random infinite alloy and direct configuration averaging over limited number of configurations (Bose *et al.*, 1992) to get an average picture. All of these methods have their own limitations and though applicable for a particular class of alloy systems may fail in other cases. It is therefore necessary to have a first-principle alloy theory which will be applicable to all possible alloy systems.

In the following sections we propose and implement a method of electronic structure description of random binary alloys within the framework of tight-binding LMTO based on augmented space formalism (ASF) introduced by Mookerjee (1973), coupled with the recursion method of Haydock, Heine and Kelly (1972). This method retains the Herglotz properties of the configuration averaged Green function². The coupling to the recursion method allows effects of quite large clusters to be taken into account. Since the recursion method is intrinsically a multi-site one, such a methodology will have wide applicability in treating features involving more than one site like the effect of clustering, short-range order, local lattice distortion *etc.*

Describing the random alloy Hamiltonian by a tight-binding one, disorder can be in on-site atomic levels as well as in off-diagonal transfer terms. In some alloys there is strong randomness both in the atomic levels and in the transfer integrals. It has been shown that for

²A complex function $f(z)$ is said to be Herglotz if (i) the singularities of $f(z)$ lie on the real z axis (ii) $\text{Im } f(z) \leq 0$ for $\text{Im } z > 0$, $\text{Im } f(z) \geq 0$ for $\text{Im } z < 0$ and (iii) $f(z) \sim 1/z$ as $z \rightarrow \infty$ on the real axis

such alloys the constituents come from the different rows of the periodic table, as a result there exists an appreciable amount of mismatch between atomic radii of the constituents. This non isochoricity in turn results in distortion of the lattice deviating from perfect lattice structure. The relaxation of ideal lattice has been verified by extended x-ray absorption fine structure (EXAFS) experiment (Weightman *et. al.*, 1987). Since lattice relaxation introduces a kind of positional disorder it essentially brings about disorder in structure matrix describing the geometry of the lattice, in addition to disorder in scattering properties of potential leading to complicated off-diagonal disorder. An application of augmented space recursive method to such non isochoric alloys with predominant lattice relaxation effect has been made in the subsequent section.

3.2 METHODOLOGY

3.2.1 Description of Electronic Structure

LMTO

The theory of electronic states in infinite crystals has for many years been of great value in the quest for a better understanding of the chemical and physical properties of solid state materials. Electrons at the microscopic level govern the behaviour of these materials and good description of many macroscopic properties are obtained in terms of stationary states of the electronic system. This is because of the well-known approximation of Born-Oppenheimer which states that nuclei and the electrons to a good approximation may be treated separately.

The electronic structure problem consists in finding the eigenstates for an infinite number of interacting fermions and immediately calls for further approximation. The most important of these is the one-electron approximation which describes each electron as an independent particle moving in the mean field of the other electrons plus the field of the nuclei. At present the most satisfactory foundation of the one electron picture is provided by the local approximation to the Hohenberg-Kohn-Sham density functional formalism (Kohn and Sham, 1965; Hohenberg and Kohn, 1964). The local-density approximation (LDA) leads to an effective one electron potential which is a function of local electron density. Since the density in turn depends on the solutions of the effective one electron Schrödinger equation one is forced to perform self-consistent electronic structure calculations.

The traditional methods in this context may be divided into those which express the wavefunctions as linear combinations of some fixed basis functions say plane waves or atomic orbitals and those like the cellular, APW and KKR methods (Callaway, 1964) which employ matching of partial waves. In the method of fixed basis sets by standard variation techniques one obtain a set of linear equation given by

$$(H - EO).a = 0 \quad (3.1)$$

in terms of the Hamiltonian H and overlap matrix O to determine the eigenvalues E and the expansion coefficients a , while the method of partial waves results in solving set of equations of the form,

$$M(E).b = 0 \quad (3.2)$$

In contrast to equation (3.1) which is polynomial in E , the secular equation (3.2) has a complicated non-linear energy dependence.

The partial wave methods do have advantages. Firstly, they provide solutions of arbitrary accuracy for a muffin-tin potential and for close packed systems, this makes them far more accurate than the traditional fixed basis methods. Secondly the information about the potential enters only via a few functions of energy. However it has the disadvantage of being computationally heavy, the one electron energies E_j must be found individually by tracing the roots of the determinant of M as a function of E .

The linear methods devised by Andersen (1975) are characterized by using fixed basis functions constructed from partial waves and their first energy derivatives obtained within the muffin tin approximation to the potential. These methods therefore lead to secular equations like (3.1) rather than (3.2). The linear methods thus combine the desirable features of the fixed basis and partial wave methods. In the LMTO (Andersen and Jepsen, 1984) an energy dependent basis set $\chi_{RL}(r)$ is derived from the energy dependent partial waves in the form of muffin-tin orbitals.

The set is constructed such that it is

- (a) appropriate to the one electron effective potential $V(r)$ of the solid
- (b) as complete as possible in the entire space
- (c) continuous and singly differentiable in all space

The transformation of this method for self-consistent calculations of the electronic structure of solids into a first-principles tight-binding method (TB-LMTO) is particularly useful due to localized nature of basis functions, extending the applicability of this methodology to disordered alloys both metallic and semiconductor or solid surfaces and interfaces. Literature for extensive description for this methodology exists (Andersen *et. al.*, 1985; Das, 1992) and we only cover the salient features.

In the present work, we use the atomic sphere approximation (ASA) where the sphere is divided into Wigner-Seitz (WS) cells which are then approximated by WS spheres of the same volume. In this approximation the information needed to set up the Hamiltonian can be divided into two independent parts. The first part is contained in the structure matrix which depends only on the structure and the positions of the atoms and not on the type of atoms occupying the sites. The second part of the information depends on the solution of the Schrödinger equation

inside each inequivalent WS sphere with appropriate boundary conditions . This second part yields the so-called potential parameters for each site.

Within the ASA , the LMTO basis functions have the following form:

$$\chi_{RL}^{\alpha}(r_R) = \phi_{RL}(r_R) + \sum_{R'L'} \dot{\phi}_{R'L'}^{\alpha}(r_{R'}) h_{R'L',RL}^{\alpha}$$

where L denotes collective angular momentum index (ℓm) . Atomic sites are given by the position vectors R with $r_R = r - R$. ϕ is a product of a spherical harmonic and the solution $\phi_{\nu RL}(|r_R|)$ to the radial wave equation inside the sphere centered at R for a certain energy $E_{\nu RL}$ which is in principle arbitrary but in the energy range of interest. The functions $\dot{\phi}^{\alpha}$ are the linear combinations of the ϕ 's and their energy derivatives $\dot{\phi}$. The actual choice of how the linear combination is made determines the basis *i. e.* the label α . The functions ϕ are normalized inside the spheres to which they are associated , ϕ and $\dot{\phi}$ are orthogonal and they vanish , by definition outside their own sphere. The matrix h^{α} is given by,

$$h^{\alpha} = C^{\alpha} - E_{\nu} + (\Delta^{\alpha})^{1/2} S^{\alpha} (\Delta^{\alpha})^{1/2}$$

where C^{α} and Δ^{α} are the diagonal potential matrices. They depend on the potential inside the spheres , the representation (α) chosen and on the sphere radii. The band center parameter C^{α} is given by.

$$C^{\alpha} = E_{\nu} - \frac{P^{\alpha}(E_{\nu})}{\dot{P}^{\alpha}(E_{\nu})}$$

and the band width parameter is given by

$$\sqrt{\Delta^{\alpha}} = 1/\dot{P}^{\alpha}(E_{\nu})$$

where $P^{\alpha}(E)$ and $\dot{P}^{\alpha}(E)$ are the potential function and its energy derivative appropriate to the representation α . The relationship between the potential function $P^{\alpha}(E)$, the representation matrix α and the logarithmic derivative D_l of the partial wave at sphere boundary is given by

$$\{P^{\alpha}(E)\}^{-1} = \left(2(2l+1) \frac{D_l + l + 1}{D_l(E) - 1}\right)^{-1} - \alpha$$

S^{α} is the structure constant matrix depending on the representation and the geometrical arrangement of the atomic sites. In terms of the canonical structure constant S^0 , S^{α} is given by

$$S^{\alpha} = S^0(1 - \alpha S^0)^{-1}$$

The representation is uniquely defined by the choice of the α matrix. All representation span the same Hilbert space, and there exists an exact transformation from one representation to another. Two particular representations are of interest the γ -representation and the tight-binding representation (TB), β . The former is used in the construction of sp^3 hybrids for which it is convenient due to the orthogonality of the basis function. In the TB representation on the other hand the basis functions are very localized. The γ -representation Hamiltonian correct to second order in energy ($E - E_\nu$) is given by

$$H^{(2)} = E_\nu + h^\gamma = C^\gamma + (\Delta^\gamma)^{1/2} S^\gamma (\Delta^\gamma)^{1/2}$$

where E_ν is the diagonal matrix containing the linearization energies. The overlap matrix in this representation is a unit, diagonal matrix and therefore this representation is also referred to as the *orthogonal representation*. The transformation from the γ to the β representation involves a scaling of the potential parameters C and Δ , calculation of the real space structure constants S^β . With the choice

$$\beta = \begin{cases} 0.3485 & \ell = 0(s) \\ 0.05303 & \ell = 1(p) \\ 0.010714 & \ell = 2(d) \end{cases} \quad (3.3)$$

the screened structure constants are found to be most localized with universal exponential decay in distance d measured in terms of WS radius w .

$$S_{ll'm}^\beta = A \exp(-\lambda_{ll'm}^\beta d/w)$$

for all the structures (f.c.c, b.c.c, h.c.p etc.). In this representation the TB orbitals are extremely compact, extending only to nearest neighbour shell. For recursion calculation which is the methodology to be employed in the present study, it is practical to work in an orthogonal representation. At the same time short range is essential. With LMTO's it is then most practical to work in γ -representation and to express h^γ as the power series in the two center first order TB Hamiltonians which is of the form same as γ -representation Hamiltonian with C^β , Δ^β and S^β replacing C^γ , Δ^γ and S^γ . This is given by

$$h^\gamma = h^\beta - h^\beta o^\beta h^\beta - \dots$$

where the matrix o^β is diagonal in RL representation and its value is determined by the overlap of ϕ and ϕ^α . The truncation of the series at various orders allows us to work on the orthogonal representation but express the Hamiltonian in terms of parameters of the TB representation. It has been found (Nowak *et. al.*, 1991) that in all practical calculations recursion with

$$H^{(1)} = E_\nu + h^\beta$$

accurate to first order in $(E - E_v)$ gives reasonable result. The second term $(\hbar \omega)$ is necessary for systems with wide bands specially for s-p states. We have made uses of both Hamiltonian $H^{(1)}$ and $H^{(1)} - \hbar \omega$ in our subsequent calculations.

3.2.2 Configuration Averaging

There are several approaches existing in literature for configuration averaging in disordered alloys with increasing degree of sophistication, such as the rigid band approximation (Mott and Jones, 1958), the virtual crystal approximation (Nordheim, 1931), the single site coherent potential approximation (Soven, 1967; Taylor, 1967) and cluster coherent potential approximations (Mookerjee, 1987; Razee *et. al.*, 1990; Datta *et. al.*, 1993).

In the rigid band approximation the shape of the density of states is taken to be same throughout the concentration range with only shift in the position of Fermi energy due to change in filling while in virtual crystal approximation the actual random alloy potential is replaced by an average, periodic potential which is taken as the concentration weighted arithmetic mean of the the constituent's potential. The rigid band approximation gives crude picture of the effect of change in electron to atom ratio on alloying while the virtual crystal approximation serves as the starting point of more sophisticated iterative self-consistent approxiamtions. We shall first give brief review of the existing methods which are capable of capturing features characteristic of disorder. Then we shall present the augmented space recursion method, the methodology to be applied in the present study.

Single Site Coherent Potential Approximation.

The single site coherent potential approximation (CPA) remains to date the main theoretical development in the study of the electronic structure of random systems. It maintains the analytic features of the exact Green function and interpolates correctly between several individual limiting cases of random binary alloys e. g. virtual crystal, atomic and dilute limits.

The CPA is a single site mean field theory which allows the self-consistent determination of a translationally invariant effective medium that replaces the configurational average of the disordered material. The medium is determined through the condition that scattering of an impurity atom of any of the atom species vanishes on the average.

We present a simple physical insight into the CPA within the frame work of parametrized tight-binding method.

A random Hamiltonian in the tight-binding basis can be represented as,

$$H = \sum_i \epsilon_i P_i + \sum_{ij} V_{ij} T_{ij}$$

where P_i and T_{ij} are projection and transfer operators respectively.

One defines an effective Hamiltonian

$$H^{eff} = \sum_i \Sigma_i(E) P_i + \sum_{ij} \Sigma_{ij}(|\bar{r}_i - \bar{r}_j|) T_{ij}$$

In the single site CPA the self-energy Σ_i is same for all the sites i . e. $\Sigma_i(E) = \Sigma_0(E)$ and $\Sigma_{ij} = V$. The idea is to find those $\Sigma_0(E)$ which will yield

$$\langle G \rangle = (zI - H^{eff})^{-1}$$

$\langle G \rangle$ indicates configuration average of the random Green function G . For determination of self energy Σ_0 in single site CPA one embeds an exact potential ϵ_i at the site i within the effective medium in such a way that it does not produce any extra scattering on the average.

Hamiltonian with an impurity atom embedded at site i in otherwise periodic solid with on-site potential Σ_0 is

$$H_{eff}^i = H_{eff} + (\epsilon_i - \Sigma_0) P_i = H_{eff} + h$$

The corresponding Green function is given by

$$G^i = G_{eff} + G_{eff} \underline{T} G_{eff}$$

where

$$\underline{T} = \sum_i t_i = \sum_i \frac{(\epsilon_i - \Sigma_0(E)) P_i}{I - (\epsilon_i - \Sigma_0(E)) G_{eff}}$$

The self-consistency condition demands that $\langle G^i \rangle = G_{eff}$ or $\langle t_i \rangle = 0$, leading to self consistent determination of Σ_0 . For binary disorder where ϵ_i can be ϵ_A with probability x and ϵ_B with probability $(1-x)$ and $\epsilon_A - \epsilon_B = W$ one has

$$\Sigma_0 = \Sigma_0(G_{eff}) = \frac{xW}{1 - (W - \Sigma) G_{eff}}$$

Such a mean field approach restores the periodicity of the solid and enables one to apply usual \vec{k} -space band structure techniques.

The CPA in conjunction with first principles electronic structure calculations like KKR and LMTO has been employed widely for description of disordered alloys.

- (i) **KKR-CPA** (Stocks *et. al.* , 1977) – In the KKR-CPA the one electron random potentials which for simplicity is taken to be of non-overlapping muffin tin form are characterized at energy E by the partial wave scattering amplitudes $f_{\alpha,L}(E)$ where α refers to species and L stands for the angular momentum indices ℓ and m . $f_{\alpha,L}(E)$'s are taken to be configuration independent , although for a self consistent calculation they do depend on the concentration . The reference medium is described within the single site CPA by an ordered array of effective scattering amplitudes $\tilde{f}_L(E)$ which are obtained as the solutions of the equation

$$\sum_{\alpha} x^{\alpha} X^{\alpha} = 0 \quad (3.4)$$

where x^{α} is the concentration of the atoms of type α in the alloy and

$$X^{\alpha} = \Delta m^{\alpha} (1 - \tilde{\tau}^{00} \Delta m^{\alpha})^{-1} \quad (3.5)$$

m^{α} [= $(t^{\alpha})^{-1}$] is the inverse of the scattering matrix, corresponding to atom of type α in the alloy with $t^{\alpha} = -f_{\alpha} / \sqrt{E}$, Δm^{α} is the fluctuation of m^{α} above the mean value and $\tilde{\tau}^{00}$ is the site diagonal element of scattering path operator .

In general, various quantities in equations (3.4) and (3.5) are matrices which possess non-vanishing matrix element between different angular momentum states. However for symmetric muffin tin potentials and calculations carried out to $\ell \leq 2$, the various matrices become diagonal , a feature which greatly facilitates the performance of numerical calculations . The self-consistent nature of the KKR-CPA is clearly displayed in the observation that

$$\Delta m^{\alpha} = \bar{m} - m^{\alpha}$$

and

$$\bar{\tau} = 1/(2\pi)^{3/2} \int_{BZ} d^3k [\bar{m} - S(k)]^{-1}$$

where $S(k)$ denotes the KKR structure constants of the underlying lattice and the integral extends over the first Brillouin zone of the reciprocal lattice.

- (ii) **LMTO-CPA** (Kudrnovský and Drchal, 1990) – In LMTO-CPA one starts from the tight-binding LMTO Hamiltonian, the energy linearized version of KKR , in orthogonalized γ -representation given by

$$H_{RL,R'L'}^{\gamma} = C_{RL}^{\gamma} \delta_{RR'} \delta_{LL'} + (\Delta^{\gamma})_{1/2} S_{RL,R'L'}^{\gamma} (\Delta^{\gamma})_{R'L'}^{1/2} \quad (3.6)$$

R, R' denote atomic positions and L, L' denote collective angular momentum indices for (ℓ, m) and (ℓ', m') . The scattering properties the potential are characterized by the potential parameters, $X_{RL} = C_{RL}^\gamma, \Delta_{RL}^\gamma$ and γ_{RL} .

The Green function corresponding to the Hamiltonian (3.6) is

$$G_{RL,R'L'}(z) = (zI - H^\gamma)_{RL,R'L'}^{-1} = \Delta_{RL}^{\gamma^{-1/2}} [(P^\gamma(z) - S^\gamma)^{-1}]_{RL,R'L'} \Delta_{R'L'}^{\gamma^{-1/2}}$$

$P^\gamma(z) = (z - C^\gamma) / \Delta^\gamma$ being the potential function in the muffin tin orbital representation γ .

For random binary alloys $A_x B_{1-x}$ due to the random values of Δ_{RL} and γ_{RL} the Hamiltonian have a complicated off-diagonal randomness. Consequently the CPA which can treat only the site-diagonal disorder cannot be readily applied. To define a CPA Kudrnovský and Drchal who were the first to apply the LMTO-CPA technique to random alloy systems, re-expressed $G(z)$ in the general muffin tin orbital representation α in terms of site-diagonal random functions $\lambda_{RL}^\alpha(z)$ and $\mu_{RL}^\alpha(z)$ and an auxiliary Green function $g_{RL,R'L'}^\alpha$ as

$$G_{RL,R'L'} = \lambda_{RL}^\alpha(z) \delta_{RR'} \delta_{LL'} + \mu_{RL}^\alpha(z) g_{RL,R'L'}^\alpha(z) \mu_{R'L'}^\alpha(z)$$

$$g_{RL,R'L'}^\alpha = \{[P^\alpha(z) - S^\alpha]^{-1}\}_{RL,R'L'}$$

$$\lambda_{RL}^\alpha(z) = (\gamma_{RL} - \alpha_{RL}) \mu_{RL}^\alpha(z) / \Delta_{RL}^{\gamma^{1/2}}$$

$$\mu_{RL}^\alpha(z) = \Delta_{RL}^{\gamma^{1/2}} / [\Delta_{RL}^\gamma + (\gamma_{RL} - \alpha_{RL})(z - C_{RL}^\gamma)]$$

and choose the most tight-binding representation $\alpha_L = \beta_L$ so as to make the structure matrix $S_{RL,R'L'}^\beta$ non random.

The random quantities $P_{RL}^\beta(z)$, $\lambda_{RL}^\beta(z)$ and $\mu_{RL}^\beta(z)$ which enter the definition of $G(z)$ are all site-diagonal quantities. Their randomness can be expressed via occupation index η_R^Q , $Q = A, B$ so that

$$\langle G(z) \rangle = \sum_Q \lambda_L^{\beta,Q}(z) \langle \eta_R^Q \rangle \delta_{RR'} \delta_{LL'} + \sum_{Q,Q'} \mu_L^{\beta,Q}(z) \langle g_R^\beta(z) \rangle_{RL,R'L'}^{Q,Q'} \mu_{L'}^{\beta,Q'}(z)$$

The configuration averaged auxiliary Green function $\langle g^\beta(z) \rangle$ is given by

$$\{[\mathcal{P}^\beta(z) - S^\beta]^{-1}\}_{R'L'}$$

where , the coherent potential function $\mathcal{P}^\beta(z)$, which for cubic lattices is a site and angular momentum diagonal matrix with elements $\mathcal{P}_L^\beta(z)$ is determined from a set of coupled CPA equations:

$$\begin{aligned}\mathcal{P}_L^\beta(z) &= \langle P_L^\beta(z) \rangle + [P_L^{\beta,A}(z) - \mathcal{P}_L^\beta(z)] \Phi_L^\beta(z) \times [P_L^{\beta,B}(z) - \mathcal{P}_L^\beta(z)] \\ \Phi_L^\beta(z) &= 1/N \sum_k \left([\mathcal{P}^\beta(z) - S^\beta(k)]^{-1} \right)_{LL}\end{aligned}$$

Finally the configuration averaged Green function is written in terms of configuration average of the auxiliary Green function as

$$\langle G(z) \rangle_{RL,R'L'} = \Lambda_L^\beta(z) \delta_{RR'} \delta_{LL'} + M_L^\beta(z) \langle g^\beta(z) \rangle_{RL,R'L'} M_{L'}^\beta(z)$$

with

$$\Lambda_L^\beta(z) = \langle \lambda_L^\beta(z) \rangle + [\Delta \mu_L^\beta(z)]^2 [\langle P_L^\beta(z) \rangle - \mathcal{P}_L^\beta(z)] / [\Delta P_L^\beta(z)]^2$$

$$M_L^\beta(z) = \{ \mu_L^{\beta,A}(z) [P_L^{\beta,B}(z) - \mathcal{P}_L^\beta(z)] - \mu_L^{\beta,B}(z) [P_L^{\beta,A}(z) - \mathcal{P}_L^\beta(z)] \} / \Delta P_L^\beta(z)$$

CPA being a single site approximation has its own limitations . It has been pointed out time and again that it cannot take into account effects involving more than one site like the effect of clustering in split band alloys at low concentration limit , the problem of lattice relaxation leading to angular distortion of hopping integrals , the problem of alloys with short range order arising out of correlation between neighbouring sites. Futhermore the self-consistency involved in the solution of CPA equation is not trivial and one has to invoke subtle mathematical procedures to ensure proper convergence.

Off-diagonal Disorder Within The CPA

An approximate scheme of treating off-diagonal disorder within the single site approximation is given by Blackman , Esterling and Berk (1971) (BEB). While in the standard CPA the hopping integral is taken to be nonrandom , in the scheme of BEB the hopping integral depends upon the occupancy of the sites between which hopping will take place. As a consequence , while the self-energy corrections in standard CPA method are independent of the atomic species , reflecting the fact that both A and B atom see the same effective environment , the BEB scheme distinguishes the manner in which the electron diffuses away (and hence also the renormalisation effects) from atomic species.

The methodology developed in locator formalism (starting with atomistically localized electronic states and then introducing the overlap term) involves introduction of matrix locators g_i , Green function \underline{G}_{ij} and transfer integrals \underline{W}_{ij} given by

$$\underline{g}_i = \begin{pmatrix} \frac{n_i}{z - \epsilon_A} & 0 \\ 0 & \frac{m_i}{z - \epsilon_B} \end{pmatrix} = \begin{pmatrix} \frac{n_i}{g_A} & 0 \\ 0 & \frac{m_i}{g_B} \end{pmatrix}$$

$$\underline{G}_{ij} = \begin{pmatrix} n_i G_{ij} n_j & n_i G_{ij} m_j \\ m_i G_{ij} n_j & m_i G_{ij} m_j \end{pmatrix} = \begin{pmatrix} G_{ij}^{AA} & G_{ij}^{AB} \\ G_{ij}^{BA} & G_{ij}^{BB} \end{pmatrix}$$

$$\underline{W}_{ij} = \begin{pmatrix} \alpha_{ij} & \zeta_{ij} \\ \zeta_{ij} & \beta_{ij} \end{pmatrix}$$

where site diagonal energies ϵ_i take on the values ϵ_A or ϵ_B and the transfer integral W_{ij} describing the electron hopping between sites i and j can assume values $W_{ij}^{AA} = \alpha_{ij}$, $W_{ij}^{AB} = W_{ij}^{BA} = \zeta_{ij}$ or $W_{ij}^{BB} = \beta_{ij}$. n_i ($m_i = 1 - n_i$) is the projection operator equals unity (zero) when the site i is occupied by an A(B) atom.

The equation of motion satisfied by Green function matrix is then

$$\underline{G}_{ij} = \underline{g}_i (\delta_{ij} + \sum_k \underline{W}_{ik} \underline{G}_{kj})$$

By formally treating the second term on the right hand side as perturbation one finds the expression

$$\underline{G}_{ii} = (\underline{1} - \underline{g}_i \underline{\Delta}_i)^{-1} \underline{g}_i$$

where $\underline{\Delta}_i$ denotes the fully renormalized interactor.

Within the spirit of single site CPA, replacing bare locator \underline{g}_i by effective medium locator \underline{g} and introducing renormalized interactor $\underline{\Delta}$ in terms of \underline{g} one has

$$\underline{\bar{G}}_{ii} = (\underline{1} - \underline{g} \underline{\Delta})^{-1} \underline{g}$$

and the CPA self-consistency condition

$$\langle \underline{G}_{ii} \rangle_{ss} = \underline{\bar{G}}_{ii}$$

$\langle \dots \rangle_{ss}$ denotes the average over the occupation of a single site. This self-consistency equation for matrix Green function in turn leads to the determination of three independent elements of self-energy. Recently this formalism within TB-LMTO framework has been employed by Sluiter and Singh (1994). This takes into account the effect of off-diagonal disorder as registered by

a single impurity atom and provides an approximate technique for dealing with off-diagonal disorder.

Augmented Space Formalism.

The augmented space formalism was introduced by Mookerjee in 1973 as an alternative exact averaging scheme. In this formalism, instead of looking at the system as electrons moving in a random array of disordered potentials, one considers electrons moving in periodic potentials in the presence of a *field* which describes the disorder. Effectively one extends the Hilbert space \mathcal{H} on which the random Hamiltonian is described by augmenting with it a configuration space describing different configurations of the disordered system.

The approximate methods based on this disorder field formalism have a different underlying philosophy. In the effective medium mean field theories the approximation precedes configuration averaging. The approximations made prior to configuration averaging may not preserve the analyticity of Green function after the averaging in all cases. On the other hand in the disorder field picture, the Hamiltonian constructed in the full augmented space, already contains the information of all possible configurations and introduction of approximations are expected to preserve the analytic properties of Green function. Further advantage of such a averaging scheme is that the formulation is an extremely general one, applicable to functions of any random variables obeying certain conditions. This allows one to apply this formalism not only for Green function but also for more complicated functions of the Hamiltonians.

The starting point is a set of random variables $\{n_i\}$ which we call a configuration. A certain probability density $P(\{n_i\})$ is associated with various values of the configuration. Assuming that different n_i are statistically independent, one have

$$P(\{n_i\}) = \prod_i p_i(n_i)$$

where $p_i(n_i)$ is the probability density of the individual variables. This assumption ignores short-range order due to chemical clustering effect which invariably leads to statistical correlation between the $\{n_i\}$'s.

It should be noted that probability density $p_i(n_i)$ satisfies the properties

$$\begin{aligned} p_i(n_i) &\geq 0 \\ \int_{-\infty}^{\infty} p_i(n_i) dn_i &= 1 \end{aligned}$$

These properties are specific to the imaginary part of the resolvent of a self-adjoint operator in a certain Hilbert space. The formalism now introduces a Hilbert space ϕ_i and a orthonormal basis set $\{|f_n^i\rangle\}$ such that $p_i(n_i)$ corresponds to the imaginary part of the resolvent of a suitably chosen operator M_i in ϕ_i . If $|f_0^i\rangle$ is a specially chosen member of the orthonormal basis $\{|f_n^i\rangle\}$ in ϕ_i then

$$p_i(n_i) = -1/\pi \text{Im} \langle f_0^i | (n_i I - M_i)^{-1} | f_0^i \rangle \tag{3.7}$$

A prescription for construction of a suitable M_i for a given $p_i(n_i)$ is as follows:

For a given $p_i(n_i)$ if one could find a convergent continued fraction of the kind,

$$p_i(n_i) = -1/\pi \text{Im} \frac{1}{n_i^+ - a_1 - \frac{b_1^2}{n_i^+ - a_2 - \frac{b_2^2}{\dots}}}$$

where $n_i^+ = n_i + i0^+$

then a representation of the operator M_i is the tridiagonal matrix with a_1, a_2, \dots etc along the diagonal and b_1, b_2, \dots etc along the off-diagonal positions in some basis $\{|f_n^i\rangle\}$

Of course one has to restrict to probability distributions all of whose moments are finite, otherwise a convergent continued fraction expansion is not possible. Most of the physically valid probability distributions are of this kind, the only exception being the Lorentzian. A critical look at the construction procedure reveals that it is actually the inverse of the recursion method. For a random binary $A_x B_{1-x}$ alloy one has a bimodal probability distribution given by

$$p_i(n_i) = x\delta(n_i - 1) + (1 - x)\delta(n_i)$$

where

$$n_i = \begin{cases} 1 & \text{for } i = A \\ 0 & \text{for } i = B \end{cases}$$

For $p_i(n_i)$ as defined M_i is a tridiagonal matrix in the space ϕ_i of rank 2 with a representation

$$M_i = \begin{pmatrix} x & \sqrt{x(1-x)} \\ \sqrt{x(1-x)} & (1-x) \end{pmatrix}$$

in the basis $|f_0^i\rangle$ and $|f_1^i\rangle$

We now revert to the problem of configuration averaging. To start with let us consider an average of the form

$$\begin{aligned} \langle F \rangle &= \int_{-\infty}^{\infty} F(n_i) p_i(n_i) dn_i \\ &= \int_{-\infty}^{\infty} F(n_i) \{-1/\pi \text{Im} \langle f_0^i | (n_i I - M_i)^{-1} | f_0^i \rangle\} dn_i \end{aligned}$$

$$\begin{aligned}
 &= -1/\pi I m \sum_{mn} \int_{-\infty}^{\infty} dn_i F(n_i) \langle f_0^i | m \rangle \langle m | (n_i I - M_i)^{-1} | n \rangle \langle n | f_0^i \rangle \\
 &= -1/\pi I m \sum_m \int_{-\infty}^{\infty} dn_i F(n_i) \langle f_0^i | m \rangle (n_i I - m)^{-1} \langle m | f_0^i \rangle \\
 &= \sum_m \int_{-\infty}^{\infty} dn_i F(n_i) \langle f_0^i | m \rangle \delta(n_i I - m) \langle m | f_0^i \rangle \\
 &= \sum_m \langle f_0^i | m \rangle F(m) \langle m | f_0^i \rangle \\
 &= \langle f_0^i | \tilde{F}(M_i) | f_0^i \rangle
 \end{aligned} \tag{3.8}$$

The first step makes use of equation (3.7) , the second step is obtained by introducing complete set of eigenvectors of operator M_i and the third step follows from the orthogonality of eigenvectors.

$\sum_m |m\rangle F(m) \langle m| = \tilde{F}(M_i)$ is the same operator function of M_i as F was of n_i .

The generalization to a function of several variables $\{n_i\}$ is a straightforward one. To each variable n_i one has associated a Hilbert space ϕ_i , a basis set $\{|f_n^i\rangle\}$ and a representation of a self-adjoint operator M_i in this basis related to the probability density of the variable n_i . ϕ_i with its basis and operator M_i contains all possible information about the configurations of the variable n_i . The product space $\Phi = \prod_i^{\otimes} \phi_i$ can now be constructed which contains all possible states of the set $\{n_i\}$ i. e. all configurations of the disordered system. It is called the configuration space or disorder space. The basis in the product space is defined as

$$\{|f\rangle\} = \{|f^1\rangle\} \otimes \{|f^2\rangle\} \otimes \dots$$

while the operator $\tilde{M}^{(i)}$ in the product space is given by

$$\tilde{M}^{(i)} = I \otimes I \otimes \dots M_i \otimes I \dots$$

Once $\{|f\rangle\}$ and $\tilde{M}^{(i)}$ is defined one can define the operator functional $F(\tilde{M}^{(1)}, \tilde{M}^{(2)}, \dots, \tilde{M}^{(i)}, \dots)$ in Φ and the configuration averaging of the function F which is a function of multiple random variables $\{n_i\}$ is given by augmented space theorem

$$\langle F \rangle = \langle f_0 | F(\tilde{M}^{(1)}, \tilde{M}^{(2)}, \dots, \tilde{M}^{(i)}, \dots) | f_0 \rangle$$

where

$$|f_0\rangle = |f_0^1\rangle \otimes |f_0^2\rangle \otimes \dots$$

is the representative state against which configuration fluctuations are described.

The calculation of $\langle F \rangle$ thus reduces to obtaining a particular matrix element in augmented space. For electronic structure calculation in a disordered system F is chosen to be the matrix

element of the Green function $(zI - H)^{-1}$, where H describes the random Hamiltonian of the system and random variables in this case $\{n_i\}$ are the site occupation variables.

Cluster Coherent Potential Approximation

Among the various attempts for cluster generalization of CPA, the method based on augmented space formalism (Mookerjee, 1987) has been found to retain the correct analytic form of Green function. As discussed, in augmented space formalism the configuration averaging is achieved by expanding the usual Hilbert space \mathcal{H} to include the disorder space Φ in which the configuration fluctuations are described and then obtaining the ground state matrix element of operator functional of the random function in the enlarged augmented space.

The principal steps of cluster coherent potential approximation based on augmented space formalism goes on as follows:

- (i) The full augmented space $\Psi = \mathcal{H} \otimes \Phi$ is partitioned into a subspace Ψ_1 spanned by the cluster C and its configurations and the rest. If the cluster C is of size N then the rank of the subspace Ψ_1 is $N \otimes 2^N$. The Hamiltonian in the rest of the augmented space is replaced by an effective, non-random, translationally symmetric Hamiltonian H_{eff} .
- (ii) The Green function in the subspace Ψ_1 is obtained by the partition theorem into this subspace. The partition theorem tells that

$$G_1^0 = (zI_1 - H_1 - H_{12}G_2H_{12}^\dagger)^{-P_1}$$

$$\text{with } G_2 = (zI_2 - H_{eff})^{-P_2}$$

where X^{-P_j} is the inverse of the operator X in the subspace labelled by j alone, H_1 denotes the Hamiltonian in the subspace Ψ_1 , H_2 is the Hamiltonian in Ψ/Ψ_1 and H_{12} is the off-diagonal term between Ψ_1 and Ψ/Ψ_1 .

- (iii) The subspace Ψ_1 is again partitioned into a subspace spanned by the vectors $|R, f_0\rangle$ where $R \in C$ and the rest. The Green function in this subspace is obtained again by applying partition theorem.
- (iv) The augmented space theorem then tells that the configuration averaged Green function $\langle G_{RR'} \rangle$ is given by

$$\langle Rf_0 | (EI - \tilde{H})^{-1} | R'f_0 \rangle$$

where \tilde{H} is the operator functional in the extended augmented space.

- (v) The effective Hamiltonian H_{eff} is chosen such that the Green function for the effective medium, $G_{RR'}^{eff} = \langle G_{RR'} \rangle$, giving the self-consistency conditions for the CCPA.

Though the cluster coherent potential approximation, based on the augmented space formalism has been implemented within the framework of KKR and LMTO (Razee *et. al.*, 1990; Datta *et. al.*, 1993), to date its application has been limited to model systems like one with a s-band alone and extensions to realistic alloy systems with simultaneous solution of more than one self-consistency condition poses a difficult numerical problem, particularly if the size of the cluster is large.

Augmented Space Recursion Within The Framework Of TB-LMTO (TB-LMTO-ASR)

The recursion method (Haydock *et. al.*, 1972) provides a general numerical technique for calculating projected densities of states of one electron Hamiltonians expressed in a local orbital basis set. Because it is based on real space operations it has wide applicability in disordered materials, defect structures and surfaces. It can also be used to describe translationally invariant systems. For complex materials with large number of local orbitals in the basis set of each unit cell, recursion method may be proved to be more advantageous than the Brillouin-zone integration technique.

In recursion method, one exploits the sparseness of the local orbital representation of Hamiltonian H and performs a unitary transformation on the local orbital basis to produce a tridiagonal representation of the Hamiltonian. New basis functions are defined iteratively so as to guarantee that each new member interacts only with its preceding and following member. Let us denote the starting state of the recursion method by $|u_0\rangle$. The vector $H|u_0\rangle$ is an unrenormalized combination of the orbitals with which $|u_0\rangle$ interacts and the relative contributions of the orbitals are proportional to the strength of interactions. This combination is made orthogonal to $|u_0\rangle$ by removing the contribution $\langle u_0|H|u_0\rangle|u_0\rangle = a_0|u_0\rangle$ from $H|u_0\rangle$. a_0 defines the self-energy of $|u_0\rangle$. This vector is then normalized to give an orbital $|u_1\rangle$ with the normalization constant b_1 defining a measure of the strength of the interaction between $|u_0\rangle$ and $|u_1\rangle$. The vector $|u_1\rangle$ contains the first neighbour environment of $|u_0\rangle$.

In general the recursion procedure defines the new set of orthonormalized orbitals and the representation of the Hamiltonian in the new basis (the a_n and b_n) by the three term recurrence relation

$$b_{n+1}|u_{n+1}\rangle = (H - a_n)|u_n\rangle - b_n|u_{n-1}\rangle$$

The representation of H in the new basis is tridiagonal and is given by $H_{nn} = a_n$, $H_{n,n+1} = H_{n+1,n}^* = b_n$, $H_{mn} = 0$ for $|m - n| > 1$. The states $|u_n\rangle$ are localized on shell of orbitals, n hops away from the orbitals of the starting state $|u_0\rangle$. The parameters a_n and b_n describe the coupling of each environment to itself and its neighbours. This leads to a continued fraction representation for the Green function matrix element, $\langle u_0|G|u_0\rangle$ related to the projected density of states on $|u_0\rangle$ as

$$n(E) = -1/\pi \text{Im}\langle u_0|G|u_0\rangle$$

with the continued fraction expansion given by

$$\langle u_0 | G | u_0 \rangle = \frac{1}{z - a_1 - \frac{b_1^2}{z - a_2 - \frac{b_2^2}{\dots}}}$$

The recursion method is a moment preserving transformation: the weighted sum of closed paths on the original lattice and the effective chain are the same. $\{a_n, b_n\}$ contain information about the irreducible paths of lengths $(2n + 1)$ and $2n$ respectively i. e. those closed paths that do not return to the initial orbital at any stage. If the recursion algorithm is stopped after n steps, n exact levels of the continued fraction are obtained. The matrix element after n levels contains the exact contributions from all closed paths of n steps starting and ending at the central orbital. Thus if one tries to model an infinitely extended system, the recursion algorithm after n steps contains contributions only from a central cluster of $O(n^3)$ atoms. For numerical purposes this limits the number of atoms that can be modelled and also implies that one is always studying a finite system. In order to reduce the necessary amount of computer storage it is possible to make use of symmetry of lattice and orbitals, a point that will be pursued in following section. For finite cluster one obtains a terminating continued fraction yielding a number of isolated bound states. For most purposes this is an unphysical approximation and finite size effects are eliminated by embedding the cluster in an infinite medium. Mathematically this means that a terminator must be appended to the continued fraction expansion so as to obtain a Green function with a branch cut rather than a set of poles. The problem of finding a terminator $\tau(E)$ that gives an optimal surrounding medium has been studied in literature (Haydock and Nex, 1984; Lucini and Nex, 1987). In all terminating schemes one substitutes for $\tau(E)$ an Herglotz function so that the approximate Green function has the same singularities as that of the Green function of the system. The computation scheme is closely related to the theory of orthogonal polynomials, a fact that is exploited in the development of stable and efficient computer codes.

For a system described by a disordered Hamiltonian, the recursion method defined on the augmented space enables one to calculate the configuration averaged Green function directly. The advantage of the method is that it does not involve single site approximations and solutions of self-consistent equations as required in the CPA or its generalizations. Further, one can treat both diagonal and off-diagonal disorder on equal footing.

The starting point for the TB-LMTO augmented space recursion, is the most localized sparse tight-binding Hamiltonian derived systematically from the LMTO-ASA theory and generalized to substitutionally disordered random binary alloys:

$$H_{RL,R'L'}^\beta = \hat{C}_{RL} \delta_{RR'} \delta_{LL'} + \hat{\Delta}_{RL}^{1/2} S_{RL,R'L'}^\beta \hat{\Delta}_{R'L'}^{1/2}$$

$$\hat{C}_{RL} = C_{RL}^A n_R + C_{RL}^B (1 - n_R)$$

$$\hat{\Delta}_{RL}^{1/2} = (\Delta_{RL}^{1/2})^A n_R + (\Delta_{RL}^{1/2})^B (1 - n_R)$$

Here R denotes the lattice sites and $L=(\ell m)$ are the orbital indices (for transition metal $\ell < 2$) C_{RL}^A , C_{RL}^B and Δ_{RL}^A , Δ_{RL}^B are the potential parameters of the constituents A and B of the alloy in the most tight-binding representation β . n_R are the local site occupation variables which randomly take values 1 and 0 according to whether the site is occupied by an A atom or not. The representation of the Hamiltonian in the augmented space \tilde{H} consists of replacing the local site occupation variables $\{n_R\}$ by $\{\tilde{M}^R\}$, and is given by:

$$\begin{aligned} \tilde{H} = & \sum_{RL} \left(C_{RL}^B \tilde{I} + \delta C_{RL} \tilde{M}^R \right) \otimes a_R^\dagger a_R + \dots \\ & + \sum_{RL} \sum_{R'L'} \left(\Delta_{RL}^{1/2^B} \tilde{I} + \delta \Delta_{RL}^{1/2} \tilde{M}^R \right) S_{RL,R'L'}^\beta \left(\Delta_{R'L'}^{1/2^B} \tilde{I} + \delta \Delta_{R'L'}^{1/2} \tilde{M}^{R'} \right) \otimes a_R^\dagger a_{R'} \end{aligned}$$

where,

$$\begin{aligned} \delta C_{RL} &= (C_{RL}^A - C_{RL}^B) \\ \delta \Delta_{RL}^{1/2} &= (\Delta_{RL}^{1/2^A} - \Delta_{RL}^{1/2^B}) \end{aligned}$$

\tilde{I} is the identity operator defined in the augmented space while other parameters have their usual meaning. The operator \tilde{M}^R for binary probability distribution in the second quantized notation is given by:

$$\tilde{M}^R = x b_{R0}^\dagger b_{R0} + (1-x) b_{R1}^\dagger b_{R1} + \sqrt{x(1-x)} (b_{R0}^\dagger b_{R1} + b_{R1}^\dagger b_{R0}) \quad (3.9)$$

(b_{R0}^\dagger, b_{R0}) and (b_{R1}^\dagger, b_{R1}) are the creation and annihilation operators in the augmented space, where each site is characterized by two states $(0, 1)$.

The Hamiltonian is now an operator in a much enlarged space $\Phi = \mathcal{H} \otimes \prod \phi^R$ (the augmented space), where \mathcal{H} is the *Hilbert space* spanned by the countable basis set $\{|R\rangle\}$. The enlarged Hamiltonian does not involve any random variables but incorporates within itself the full information about the random occupation variables. If we substitute eq (3.9) for \tilde{M}^R , then with the aid of little algebra we can show that the augmented space Hamiltonian contains operators of the following types as discussed in (Datta and Mookerjee, 1992).

(a) $a_R^\dagger a_{R'}$ with $R=R'$ and $R \neq R'$ terms. The operators acting on a vector in the augmented space changes only the real space label, but keeps the configuration part unchanged.

(b) $a_R^\dagger a_{R'} b_{k\lambda}^\dagger b_{k\mu}$ with $R = R'$ and $R \neq R'$ terms. k is R or R' , while, λ and μ may take value 0 and 1. These operators acting on an augmented space vector may change the real

space label (if $R \neq R'$). In addition , they may also change the configuration at the site R or R' (if $\lambda \neq \mu$).

(c) $a_R^\dagger a_{R'} b_{R\lambda}^\dagger b_{R\mu} b_{R'\nu}^\dagger b_{R'\xi}$ with λ, μ, ν, ξ taking values 0 and 1. The operators may change the real space label (if $R \neq R'$), as well as the configuration either at R or R' or both.

Once we have identified the operators in the augmented space , it is worth mentioning how we represent the basis in the real space and in the configuration space. A basis $|m\rangle$ in the Hilbert space \mathcal{H} is represented by a column vector K_m with zeros everywhere except at the m -th position . The inner products are defined as

$$\begin{aligned}\langle m | \odot | n \rangle &= K_m^T K_n \\ a_m^\dagger a_n K_p &= \delta_{np} K_m\end{aligned}$$

A member of the basis in $\prod^\otimes \phi_R$ has the form

$$|f_{\lambda_1}^1 \otimes f_{\lambda_2}^2 \otimes \dots\rangle$$

where each λ_i may be either 0 or 1 .

In the usual terminology of ASF the number of 1's define the cardinality C of the basis and the sequence of positions where one has 1's is called the cardinality sequence $\{S_C\}$ and that labels the basis. Thus a binary sequence $B [C , \{ S_C \}]$ is a representation of the member of the basis in the configuration space . The dot product between the basis members is then

$$B[C, \{S_C\}] \odot B[C', \{S_{C'}\}] = \delta_{CC'} \delta_{\{S_C S_{C'}\}}$$

Having defined the Hamiltonian and its operation in augmented space , the recursion method defined on the augmented space , gives the configuration averaged Green function directly. For determination of configuration averaged Green function $\langle G_{RL,RL}(z) \rangle$ in augmented space recursive method one choses as starting state of recursion

$$|\xi_1\rangle = |R, L\rangle \otimes |f_0\rangle$$

The successive states $|\xi_n\rangle$ and recursion co-efficients $\alpha_n^{(L)}$ and $\beta_n^{(L)}$ are generated recursively from

$$\beta_{n+1}^\dagger |\xi_{n+1}\rangle = \tilde{H} |\xi_n\rangle - \alpha_n^L |\xi_n\rangle - \beta_n^L |\xi_{n-1}\rangle$$

where

$$\alpha_n^L = \langle \xi_n | \odot \tilde{H} | \xi_n \rangle$$

and

$$\beta_n^L = \langle \xi_{n-1} | \odot \hat{H} | \xi_n \rangle$$

Haydock (1972) has mapped the contribution to the continued fraction coefficients to self-avoiding walks on the underlying space . He has shown that the dominant contribution comes from walks that wind round the initial starting state . This allows one to work only on a finite part of the augmented space . Depending upon the accuracy required and computational power , one generate upto $n_1 = N - 1$ recursion coefficients .

The method of processing the Green function from the finite number of generated coefficients is achieved by appending a suitable terminator , as discussed earlier. The procedure , briefly , is as follows .

We generate orthogonal ploynomials of the first and second kinds $P_n (z)$ and $Q_n (z)$ which are solutions of :

$$P_{n+1}(z) = (z - \alpha_n)P_n(z) - \beta_n^2 P_{n-1}(z)$$

$$Q_{n+1}(z) = (z - \alpha_n)Q_n(z) - \beta_n^2 Q_{n-1}(z)$$

with $P_{-1} = 0 = Q_{-1}$, $P_0 = 1 = Q_0$.

The next step is to locate , from the generated continued fraction coefficients $n < n_1$, the lower band edge a , the band width r and the band weight w . From this we construct a model Herglotz function :

$$F(z) = 8w[z - (a + r/2) - \sqrt{(z - a)(z - a - r)}]/r^2$$

The *Termination Coefficients* , which are the coefficients of the continued fraction expansion of $F(z)$, are $\alpha_t = a + r/2$ and $\beta_t = r/4$. According to the scheme of Lucini and Nex (1987) , one now interpolate between the computed coefficients and those of the analytic terminator :

$$\bar{\alpha}_n = \begin{cases} \alpha_n & n < n_1 \\ 1/2(\{1 - \sin\{\delta(n + \phi)\}\}\alpha_n + \{1 + \sin\{\delta(n + \phi)\}\}\alpha_n^t) & n_1 < n < n_2 \\ \alpha_n^t & n_2 < n \end{cases}$$

The method is analogous to splicing as opposed to butt-joining pieces of wood. The result of this procedure is that the terminator is appended in a fairly smooth way , avoiding the formation of semi-localized states at the interface . The reflection from the potential barrier represented by the terminator interfere destructively decreasing the oscillations in the local density of states.

We now run the recursion again with \tilde{H} replaced by z , the state vectors by polynomials and the inner product by a union of Gauss-Chebyshev quadrature :

$$\langle f(z) \otimes g(z) \rangle = \sum_{i=1}^b w_i f(\alpha'_i) g(\alpha'_i)$$

where,

$$w_i = \frac{\pi w}{n+1} \sin^2 \theta_i$$

$$\alpha'_i = \alpha_i + (1 - \cos \theta_i) r/2$$

$$\theta_i = \pi \frac{i}{n+1}$$

This will generate a set of recursion coefficients $\{ \gamma_n, \delta_n \}$ and a set of mutually orthogonal polynomials $\{ R_n(z) \}$ and $\{ S_n(z) \}$.

The terminator is given by ,

$$\tau(z) = \frac{S_{n_2-2}(z) - F(z)R_{n_2-1}(z)}{\delta_{n_2-1}^2 [S_{n_2-3}(z) - F(z)R_{n_2-2}(z)]}$$

From the fact that R_n and S_n are polynomials of order n and $F(z)$ is a Herglotz function , it follows immediately that the terminator is itself Herglotz.

The Green function is given by ,

$$G(z) = \frac{Q_{n_2-2}(z) - \beta_{n_2-1}^2 \tau(z) Q_{n_2-3}(z)}{P_{n_2-1}(z) - \beta_{n_2}^2 \tau(z) P_{n_2-2}(z)}$$

The advantage of such a termination procedure is that the approximate resolvent retains the Herglotz properties. It is interesting to compare this with the fact that in the cluster generalizations of CPA one goes to great length to ensure Herglotz properties of the Green function and these approximations cannot maintain the accuracy in the band widths. The termination approximation preserves the first $2(N-1)$ moments of density of states exactly . This represents the effect of a cluster at a distance $(N-1)$ from the starting state . It also maintains the correct band-widths , band-weights and the correct singularities and estimates the higher moments with controlled accuracy .

The configuration averaged density of states is given by

$$n(E) = -\frac{1}{\pi} \text{Im} \sum_L \langle G_{RL,RL}(E + i0) \rangle$$

3.3 SYMMETRY REDUCTION OF AUGMENTED SPACE RECURSION

Discussion of the previous sections reveal that the most versatile and general way for handling the problem of disordered alloys would be to consider the augmented space formalism . Since the augmented space involves $N \times 2^N$ basis functions , the standard method for implementing this on a computer would require handling an impossibly large $(N \times 2^N) \times (N \times 2^N)$ matrix Hamiltonian . Even for a fcc cluster with first nearest neighbour shell , the simplest one can imagine , this would require 13×2^{13} basis functions . Because of this huge number of degrees of freedom of the full augmented space , in spite of its immense potential , the method could not be used successfully .

A number of attempts have been made for practical implementation of this formalism . One of the developments among these , is the travelling cluster approximation (Gray and Kaplan , 1976 ; 1977) , where a small number of classes of selected excitations in augmented space are preserved . In spite of the drastic simplification so introduced , the resulting equations are still so formidable to discourage further investigations after early attempts . In the cluster CPA (Mookerjee,1987) (in which one retains the disorder fluctuations only from a chosen cluster and replaces the rest of the system by an effective medium) as already discussed and pointed out, one is restricted by the limitation of solving number of self-consistent equations , numbers increasing with the size of chosen cluster .

In the present approach , on the other hand , one treats the full large augmented space Hamiltonian matrix with recursion method . The conceptual advantages in augmented space formalism include apart from analyticity , translational and rotational invariance automatically built-in in the augmented space Hamiltonian . This allows one to invoke the idea of utilising symmetry operations present in configuration space in addition to usual Hilbert space , in the context of recursion method , reducing the rank of the Hamiltonian drastically and making the implementation of augmented space formalism feasible . In the present section we devote ourself to symmetry consideration of recursion method in augmented space as well as in real space . Since the augmented space recursion essentially retains all the properties of real space recursion but described in an much enlarged space , it will be useful to consider symmetry operations in real space recursion first and then to consider that in augmented space recursion.

3.3.1 Real Space Recursion Invoking Symmetry

Recursion method discussed in great detail previously provides an algorithm for determining the resolvent of Hamiltonian as continued fraction expansion . The number of continued fraction to be calculated is limited by the size of the cluster of atoms and for a large number of recursion level on a small cluster , the higher order continued fraction co-efficients reflect the boundary effect , which manifests itself as the splitting of the degenerate t_{2g} and e_g orbitals . However , the choice of size of cluster is restricted by computer storage and time . Use of symmetry

operations in recursion method may prove to be an amicable solution of this , where one can obtain same resolution and accuracy but with much less computer storage and time .

It has been shown by Gallagher (1978) that if the starting state of the recursion belongs to an irreducible representation of the Hamiltonian , then the states belonging to different irreducible representation or different rows of the same irreducible representation do not mix in the process of recursion . So that one can restrict oneself to irreducible portion of the lattice .

The philosophy of utilising symmetry in recursion method , operationally , is as follows :

Basis vectors , defined iteratively in recursion procedure , carry information of more and more distant environment of the starting state $|u_0\rangle$. The vector $H|u_0\rangle$ is combination of states with which $|u_0\rangle$ interact and the relative contribution of a state $|u_n\rangle$ in $H|u_0\rangle$ is proportional to the strength of interaction between $|u_n\rangle$ and $|u_0\rangle$. The orbitals sitting at lattice sites which are connected by point group symmetry operations to each other have identical coupling to u_0 . If T is a unitary representation of a symmetry operation , then the states generated by unitary transformations , $T|u_n\rangle$'s carry the same information as that of $|u_n\rangle$. Hence it is useful to consider among the states coupled to $|u_0\rangle$, only those belonging to the irreducible of the Hamiltonian and redefine the Hamiltonian operation so as to reduce the computer storage and time.

Let $|I\rangle$ be an orbital on lattice site coupled to $|J\rangle$, both belonging to irreducible representation of the Hamiltonian and let $|I_1\rangle \dots |I_{N_1}\rangle$ be the distinct orbitals on sites obtained by operating $|I\rangle$ by symmetry operations T 's . They are called the orbitals equivalent to $|I\rangle$ $|J_1\rangle \dots |J_{N_2}\rangle$ be the corresponding equivalent orbitals for $|J\rangle$. Then the redefined Hamiltonian operation for recursion procedure confined to irreducible portion of the lattice will be given by

$$\langle I|H|J\rangle_{mod} = \sqrt{\frac{W_J}{W_I}} \langle I|H|J\rangle$$

where W_α is the number of distinct orbitals equivalent to $|\alpha\rangle$ (e.g. $W_I = N_1$ and $W_J = N_2$).

Having redefined the Hamiltonian operation , the recursion method is given by the usual three term recurrence relations as

$$b_{n+1}|n+1\rangle = H|n\rangle - a_n|n\rangle - b_n|n-1\rangle$$

with

$$a_n = \langle n|H|n\rangle$$

and

$$b_n = \langle n-1|H|n\rangle$$

LAT-TICE	N_{sh}	N_f	N_r	M	τ_f	τ_r
SQUARE	5	25	6	5	1.291	.558
	10	145	25	10	1.504	.742
	15	365	56	15	1.748	.930
	20	685	100	20	2.041	1.070
FCC	5	147	9	5	19.850	.468
	10	2057	71	10	22.910	.539
	11	2869	93	11	24.000	.570
SC	5	63	7	5	2.414	.410
	10	833	41	10	2.760	.600
	11	1159	53	11	2.850	.625

Table 3.1: Comparison in system size and time taken in recursion for square , face centered cubic and simple cubic lattices decribed by model tight-binding Hamiltonian with only s-orbital invoking and not invoking symmetry for fixed number of shells (N_{sh}) and fixed number of recursion steps (M). N_f and N_r are the number of sites in the full and symmetry reduced maps. τ_f and τ_r are the corresponing CPU times in seconds on a HP 9000/300 machine .

N_{sh}	N_f	N_r	M	τ_f	τ_r
5	147	29	-	-	-
7	561	95	-	-	-
10	2057	315	10	19.1	1.1

Table 3.2: Comparison in system size and time taken in recursion for face centered cubic lattices decribed by LMTO Hamiltonian with s-p-d orbital invoking and not invoking symmetry for fixed number of shell and fixed recursion step. Time quoted are CPU time in minutes in a HP 9000/300 machine . All table headings have the same meaning as in Table 3.1

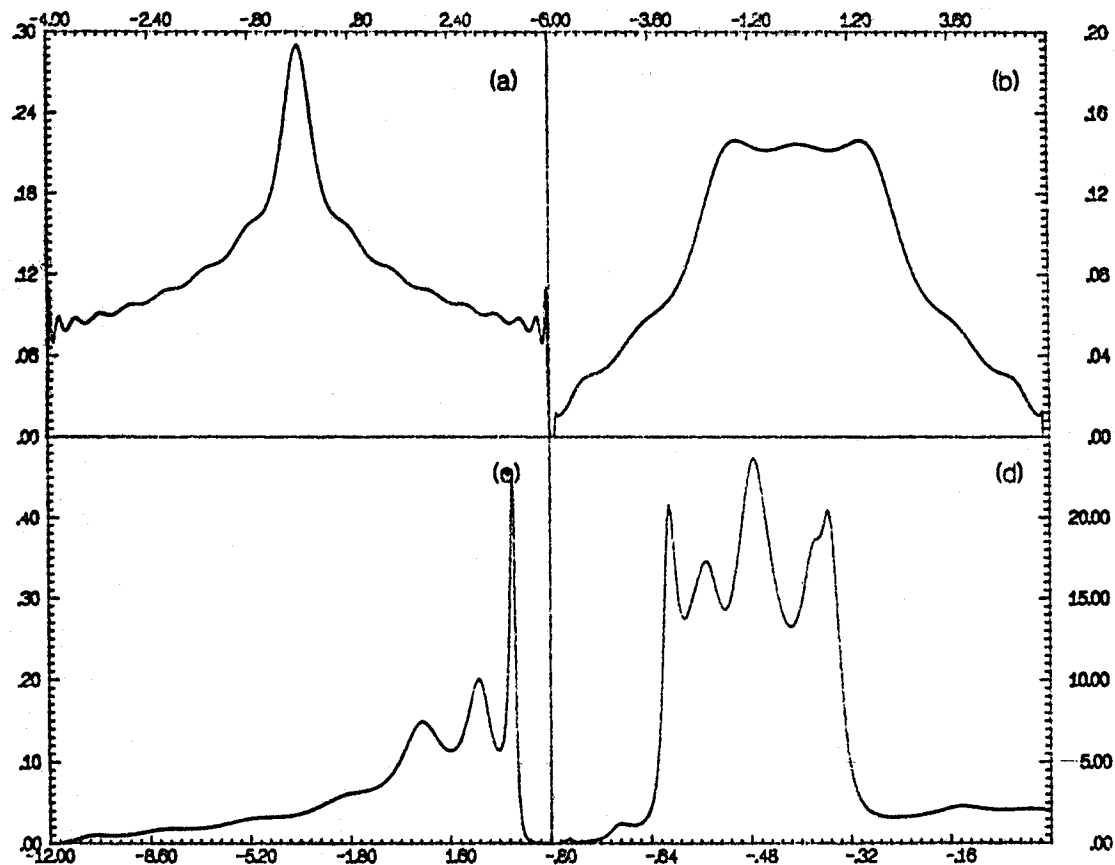


Figure 3.1: (a)-(c) Density of states for square ,simple cubic and fcc lattice described by tight binding Hamiltonian (on-site term $\epsilon = 0.$ and transfer term $V = -1.0$) obtained by recursion on symmetry reduced maps (d) density of states for fcc based Ag metal described by LMTO Hamiltonian on symmetry reduced map

where the orbitals $\{ |n\rangle \}$ are orbitals restricted to irreducible portion of the lattice and

$$H|n\rangle = \sum_m \langle n|H|m\rangle_{mod}|m\rangle$$

the summation running over the states coupled to $|n\rangle$ belonging to irreducible zone .

The above prescription reflects the symmetry of the underlying lattice only and holds good for recursion with s-like orbitals , having the full spherical symmetry . Inclusion of the p-orbitals introduces preferred x , y or z direction and breaks the symmetry between x , y and z axis , thus the point group symmetry operations which interchange between x , y and z co-ordinates are prohibited . Futhermore the effective irreducible basis , which is linear combination of the old basis sets , reflects the symmetry of the orbital itself and it is the symmetry of the orbitals which prohibits the overlap at a particular site position . We call these positions , symmetry positions with respect to overlapping orbitals .

Within the above frame-work of redefining Hamiltonian operation , the modified Hamiltonian operation , in presence of hybridization between orbitals not having spherical symmetry may be defined as

$$\langle I, L|H|J, L'\rangle_{mod} = \sqrt{\frac{W_J}{W_I}} \langle I, L|H|J, L'\rangle \beta_J(L, L')$$

The additional factor $\beta_J(L, L')$ (0 or 1) determines whether the position occupied by the site J is a symmtry position with respect to the orbitals L and L' or not .

In Table 3.1 - 3.2 we compare the number of sites and the CPU time needed for recursion , making use of symmetry and those obtained without invoking symmetry for square , simple cubic and fcc lattice. Figure. 3.1 shows density of states obtained by recursion on symmetry reduced maps.

3.3.2 Augmented Space Recursion Invoking Symmetry

The elegance of the augmented space formalism lies in its built-in translational and rotational invariance . The nonrandom augmented space Hamiltonian , containing the full information about the distribution of random variable bear the translational and rotational symmetry analogous to a nonrandom Hilbert space Hamiltonian . It is the homogeneity of disorder that gives rise to symmetry in configuration space . Considering the case of random binary alloys $A_x B_{1-x}$, for a site occupied by A atom , all the Z configurations with its (Z-1) neighbours occupied by A and one by B atom are equivalent . The augmented space is essentially an extended space , made out of direct product of two disjoint subspaces , the usual Hilbert space and the configuration space , giving information about the real space sites where there is deviation from uniform background of pure element . This allows one to extend all the symmetry consideration of real space recursion to augmented space recursion , carried out in an enlarged space .

A general basis in augmented space is the direct product of the Hilbert space basis and the configuration space basis

$$|\xi\rangle = |i\rangle \otimes B[\gamma, S\{\gamma\}]$$

$$B[\gamma, S\{\gamma\}] = |f_{\sigma_1, \sigma_2, \dots, \sigma_\gamma}\rangle$$

as discussed earlier , are uniquely specified by the set of points $\{ \sigma \}$ at which there are excitations .

The augmented space Hamiltonian commutes with all the symmetry operations of the Hilbert space . The transformation of basis orbitals under point group symmetry operation is given by

$$T\{|i\rangle \otimes |f_{\sigma_1, \sigma_2, \dots, \sigma_\gamma}\rangle\} = T|i\rangle \otimes |f_{T\sigma_1, T\sigma_2, \dots, T\sigma_\gamma}\rangle = |i'\rangle \otimes |f_{\sigma'}\rangle$$

Thus the equivalent states corresponding to $|\xi\rangle$ is obtained by applying symmetry operations independently to Hilbert space part and configuration part and picking up the distinct ones

The operation of the augmented space Hamiltonian redefined for confinement of recursion procedure to irreducible portion of Hamiltonian , for orbitals with spherical symmetry , is given by

$$\langle \xi_I | \tilde{H} | \xi_J \rangle_{mod} = \sum_I \langle \xi_I | \otimes \tilde{H} | \xi_J \rangle \sqrt{\frac{W_J}{W_I}}$$

where W_J and W_I denote the number of equivalent states corresponding to ξ_J and ξ_I .

N_{sh}	N_f	N_r	M	τ_f	τ_r
5	70	17	5	4.73	1.69
7	610	103	7	5.62	1.73
9	4838	691	9	6.87	1.77

Table 3.3: Comparison in system size and time taken in augmented space recursion for a model 50-50 alloy system described by tight-binding s-orbital Hamiltonian (on-site term for components A and B , $\epsilon_A = 2.0$, $\epsilon_B = -2.0$ and non-random off-diagonal term $V = -1.0$.) in a square lattice , invoking and not invoking symmetry for fixed number of shell and fixed recursion step. Time quoted are CPU time in seconds on a HP 9000/300 machine . All table headings have the same meaning as in Tables 3.1 and 3.2.

N_{sh}	N_f	N_r	M	τ_f	τ_r
1	1	1	-	-	-
2	25	7	-	-	-
3	385	70	8	43.	23.
4	5273	765	-	-	-
5	69877	9287	-	-	-

Table 3.4: Comparison in system size and time taken in augmented space recursion for the fcc based AgPd alloy system at 50-50 concentration described by TB-LMTO Hamiltonian , invoking and not invoking symmetry for fixed number of shell and fixed recursion step. Time quoted are CPU time in minutes in a HP 9000/300 machine . All table headings have the same meaning as in Tables 3.1-3.3.

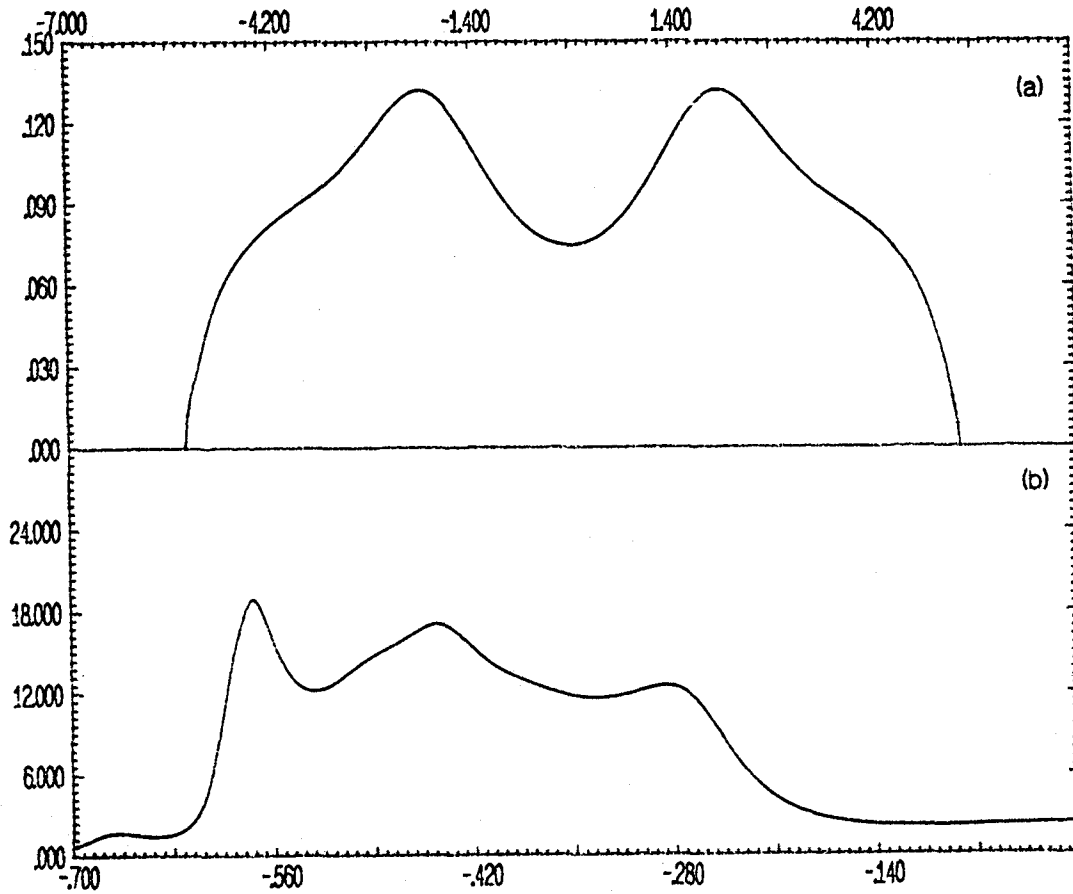


Figure 3.2: (a) Density of states for a model 50-50 alloy based on square lattice described by tight binding Hamiltonian (on-site terms $\epsilon_A = 2.0$; $\epsilon_B = -2.0$ and transfer term $V = -1.0$) obtained by recursion on symmetry reduced map . (b) density of states for fcc based 50-50 AgPd alloy described by LMTO Hamiltonian obtained by recursion on symmetry reduced map

Introduction of orbitals without spherical symmetry, introduces another factor of $\beta_{\xi_I}(L, L')$ determining whether the state ξ_I is a symmetric state with respect to orbitals L and L' , so that the redefined Hamiltonian operation becomes

$$\langle \xi_I | \tilde{H} | \xi_J \rangle_{mod} = \sum_I \langle \xi_I | \otimes \tilde{H} | \xi_J \rangle \sqrt{\frac{W_J}{W_I}} \beta_{\xi_I}(L, L')$$

A given site in augmented space is symmetric site with respect to orbitals L and L' , if the real space site i and the sites $\{ \sigma \}$ at which there are excitations satisfy the condition of being symmetric site with respect to orbitals L and L' , in the sense defined in the context of real space recursion

In Table 3.3 - 3.4 we compare the number of sites and the CPU time needed for augmented space recursion, making use of symmetry and those obtained without invoking symmetry for square and fcc lattice. Figure. 3.2 shows corresponding density of states obtained.

3.4 COMPUTATIONAL DETAILS.

We now mention some details concerning the numerical part of the problem. Total energy density functional calculations were performed for the elements. The Kohn-Sham equations were solved in the local density approximation (LDA). The LDA was treated within the context of the method of linear muffin tin orbitals in the atomic sphere approximation. The computation were performed semi relativistically and the exchange correlation potential of von Barth and Hedin (1972) was used. The basis set composed of $\ell = 0,1,2$ orbitals so that the occurring matrices are of order 9. The elemental potential parameters appropriate to the alloy radius was used to parametrize the alloy Hamiltonian. This essentially takes into account charge self consistency, as explained latter, in an approximate yet accurate way. For the purpose of augmented space recursion, a four shell augmented space map was generated from a cluster of 400 sites, with interaction upto first nearest neighbour for the most closed packed fcc based structures. For the pure metallic cases we have gone upto fifteen levels in the continued fraction to reproduce the sharp structure. For the alloys we have gone upto seven recursion levels. This is sufficient, since disorder smears out the fine structures in the density of states.

3.4.1 Charge Self Consistency

We describe here a way to account for charge self-consistency proposed by Kudrnovský and Drchal (1990). Their idea was an extension to disordered alloys of the method described by Andersen *et. al.* (1987) for ordered intermetallics.

The flexibility in the choice of the atomic sphere radii allows one to include the effects of charge self consistency approximately yet accurately without the need for full self consistency.

For this one needs the information of potential parameters and their volume derivatives of elements. The essential idea is the charge neutrality of the component spheres. LMTO-ASA offers the option to choose different radii for the host and the impurity atom and one can vary them with the restriction that overlap between spheres measured by

$$\frac{s^R + s^{R'} - |R - R'|}{s^R}$$

do not exceed 30% of s^R (s^R being the radius of the sphere at site R). Thus one can vary the sphere radii about the pure component values to obtain charge neutral spheres. For binary A_xB_{1-x} alloys with volume V^{alloy} per atom, the atomic volumes of the constituents, V^Q , ($Q = A, B$) should satisfy the volume constraint

$$xV^A + (1-x)V^B = V^{alloy} \quad (3.10)$$

The assumption of a linear pressure volume relation yields

$$\frac{(V^A - V_o^A)}{V_o^A} : \frac{(V^B - V_o^B)}{V_o^B} = B_o^B : B_o^A \quad (3.11)$$

where V_o^Q ($Q = A, B$) are the atomic volumes of the components at normal pressure and B_o^Q ($Q = A, B$) are the corresponding bulk moduli.

The solutions to equations (3.10) and (3.11) are

$$V^A = \frac{B_o^B V^{alloy} + (1-x)V_o^B(B_o^A - B_o^B)}{xV_o^A B_o^B + (1-x)V_o^B B_o^A} V_o^A$$

$$V^B = \frac{B_o^A V^{alloy} + xV_o^A(B_o^B - B_o^A)}{xV_o^A B_o^B + (1-x)V_o^B B_o^A} V_o^B$$

For alloys obeying Vegard's law where the volume per atom in the alloy is simply the concentration weighted average of the normal pressure atomic volumes of the constituents *i. e.*

$$V^{alloy} = xV_o^A + (1-x)V_o^B$$

the solution is trivial, $V^Q = V_o^Q$ ($Q = A, B$), that is, atomic volumes of the elements should be taken at normal pressure. The potential parameters in the alloy for the component Q ($Q=A, B$) should be calculated at new radius $s^Q = (3V^Q / 4\pi)^{1/3}$. For large differences between s^Q and s_o^Q [$= (3V_o^Q / 4\pi)^{1/3}$] it is important not to interpolate linearly in s^Q . The suggestion is to use logarithmic interpolation given by

$$\begin{aligned}
C_L^Q &= C_{oL}^Q + \frac{dC_L^Q}{d \ln s^Q} \ln(s^Q/s_o^Q) \\
\gamma_L^Q &= \gamma_{oL}^Q + \frac{d\gamma_L^Q}{d \ln s^Q} \ln(s^Q/s_o^Q) \\
\Delta_L^Q &= \Delta_{oL}^Q \left[\frac{s^Q}{s_o^Q} \right]^{\frac{d\Delta_L^Q}{d \ln s^Q}}
\end{aligned}$$

The potential parameters of elemental metals for normal pressure as well as their radial derivatives obtained via self consistent LMTO-ASA calculations are tabulated in the review article by Andersen *et. al.*(1985) . To correct for the fact that alloy Wigner-Seitz radius w_{alloy} differs from the radii s^Q which affects only two of the parameters Δ and γ , one has to multiply them by $(s^Q/w_{alloy})^{2l+1}$. This scheme of calculation provides one with the species potential of neutral spheres which are related to a common zero of the energy within ASA and thus rules out the calculation of a Madelung potential. The Madelung term due to charge transfer effect gives rise to a constant shift in potential parameter values. Calculation with neutral spheres with no Madelung term present has been shown to be accurate enough for metallic alloys , involving small charge transfers and consequently a small Madelung shift .

Our work is based on this prescription of charge self consistency scheme. It is worth mentioning at this point that in principle , one can also carry out the full charge self-consistency for the disordered alloys . Such a charge-self-consistent calculation involves self-consistency for the average component atom .

From the average component atom projected density of states one can calculate the energy moments , hence the charge density in the average component spheres by :

$$n_R(r) = 1/4\pi \sum \{m_{RL}^{(0)}\phi_{RL}^2(r) + 2m_{RL}^{(1)}\phi_{RL}(r)\dot{\phi}_{RL}(r) + m_{RL}^{(2)}(\dot{\phi}_{RL}^2(r) + \phi_{RL}(r)\ddot{\phi}(r)_{RL})\}$$

where

$$m_{RL}^{(q)} = \int_{-\infty}^{E_F} dE n_{RL}(E)(E - E_{\nu,RL})^q \quad (3.12)$$

$n_{RL}(E)$ is the orbital projected partial density of states . $\phi_{RL}(r)$ and $\dot{\phi}_{RL}(r)$ are the solution of the Schrödinger equation in a sphere. From the charge density one can calculate the potential by solving the Poisson equation and the exchange-correlation part by the density functional formalism . The Schrödinger equation is then solved to obtain a new set of potential parameters for components and the calculation is repeated until the input and output charge densities (or potentials) are identical within a preassigned error limit . However such a full-fledged self-consistent calculation is time-consuming and furthermore unlike the ordered intermetallics there is no unique prescription for calculation of the Madelung potential due to

charge transfer between various spheres and at this point one has to make one or the other approximate definition.

This full-fledged charge self-consistency scheme has been reserved for future work beyond this thesis.

3.4.2 The MultiSpin Coding Technique

We have discussed in section 3.3, how the symmetry reduction of augmented space Hamiltonian can be utilised for practical implementation of the augmented space recursion. We now discuss of the computational scheme that has been used in conjunction with symmetry reduction for a fast and space-saving implementation of the augmented space recursion.

Each basis in configuration space, carrying information about the occupation variable at every site, is nothing but strings of 0's and 1's. We may thus represent the basis vectors by a collection of binary words. In a M -bit machine, each M -bit word can represent upto $(M - 1)$ terms as a sequence of 0's and 1's and for the configuration of a lattice having size N , $N/(M - 1)$ words are necessary. This enables us to store configuration states efficiently and provides large scale saving of computer disk space.

The 0's and 1's characterizing the two states of a given site, may be identified with the up and down states of an Ising system and the operations of the augmented space Hamiltonian, which project out or change the configuration state at a given site are identical with the spin projection and spin flip operations of the Ising Hamiltonian. This allows us to use the computational techniques, used in the numerical work with the Ising model (Chowdhury *et al.*, 1987), extensively.

The operations on the configuration part of the augmented space Hamiltonian can be represented as

$$b_{i\lambda}^\dagger b_{i\mu} B[C, \{S_C\}] = B'[C', \{S_{C'}\}]$$

$b_{i\lambda}^\dagger$, $b_{i\mu}$ are creation and annihilation operators of excitations caused by the disorder fluctuation at the site i . $B[C, \{S_C\}]$ represents the binary sequence representation of a configuration space basis member with cardinality C and cardinality sequence $\{S_C\}$ and similarly $B'[C', \{S_{C'}\}]$ represents that with cardinality C' and cardinality sequence $\{S_{C'}\}$.

If $\lambda = \mu$, then we have the projection operation, so that $C = C'$ with $\{S_{C'}\} = \{S_C\}$. If $\lambda \neq \mu$ then we have the spin flip operation. There can be two possibilities, either i belongs to the cardinality sequence $\{S_C\}$ or it does not. If $i \in \{S_C\}$, since the flip operation changes the variable at site i from 1 to 0, we have $C' = C - 1$ and $\{S_{C'}\} = \{S_C\} \ominus i$. Alternatively, for $i \notin \{S_C\}$ we have $C' = C + 1$ with $\{S_{C'}\} = \{S_C\} \oplus i$. These can be achieved with the help of predefined logical operations in any programming language; *e.g.* IBITS, IBSET and

IBCLR in fortran77. IBITS tests the bit type (whether it is 0 or 1) at a given site , IBSET sets bit type at a given site to be 1 while IBCLR sets bit type at a given site to be 0 .

Thus for the flip process ,

$$B'[C', \{S_{C'}\}] = (\mathcal{L})IBCLR(i)B[C, \{S_C\}] + (1 - \mathcal{L})IBSET(i)B[C, \{S_C\}]$$

with

$$\mathcal{L} = IBITS(i)B[C, S_C]$$

Configuration corresponding to i-th site stored in m-th position of n-th word

where

$$n = \frac{(i - 1)}{M - 1} + 1$$

$$m = (i - 1) - (n - 1)(M - 1)$$

The binary word representation on one hand saves the computer storage enormously . On the other the use of logical operations with bit manipulation techniques makes the action of the augmented space Hamiltonian computationally very fast , avoiding the repetitive use of branching IF statements .

3.5 APPLICATIONS

3.5.1 AgPd Alloys : A Test Case

The AgPd alloy series is one of the test cases among binary systems . This is in part due to its simple metallurgical properties , namely , that the two constituents form continuous solid solutions with no change in crystal structure. It has the advantage that the centres of the d bands of the two constituents are appreciably separated , so that the effects caused by changing the composition can be resolved. X-ray photoemission spectra result (Hünfer *et. al.* , 1973) for wide range of alloy composition is available for AgPd . XPS density of states reveals that the centers of the bands are almost independent of concentration for Ag as well as for Pd .

This ,in turn , indicates that the local potentials at the sites of Ag and Pd are roughly independent of concentration , an assumption which underlies the CPA description of the binary alloy systems , as well. A comparison between XPS density of states and CPA density of states show that the over all prediction of the CPA is verified in AgPd system , an alloy system that

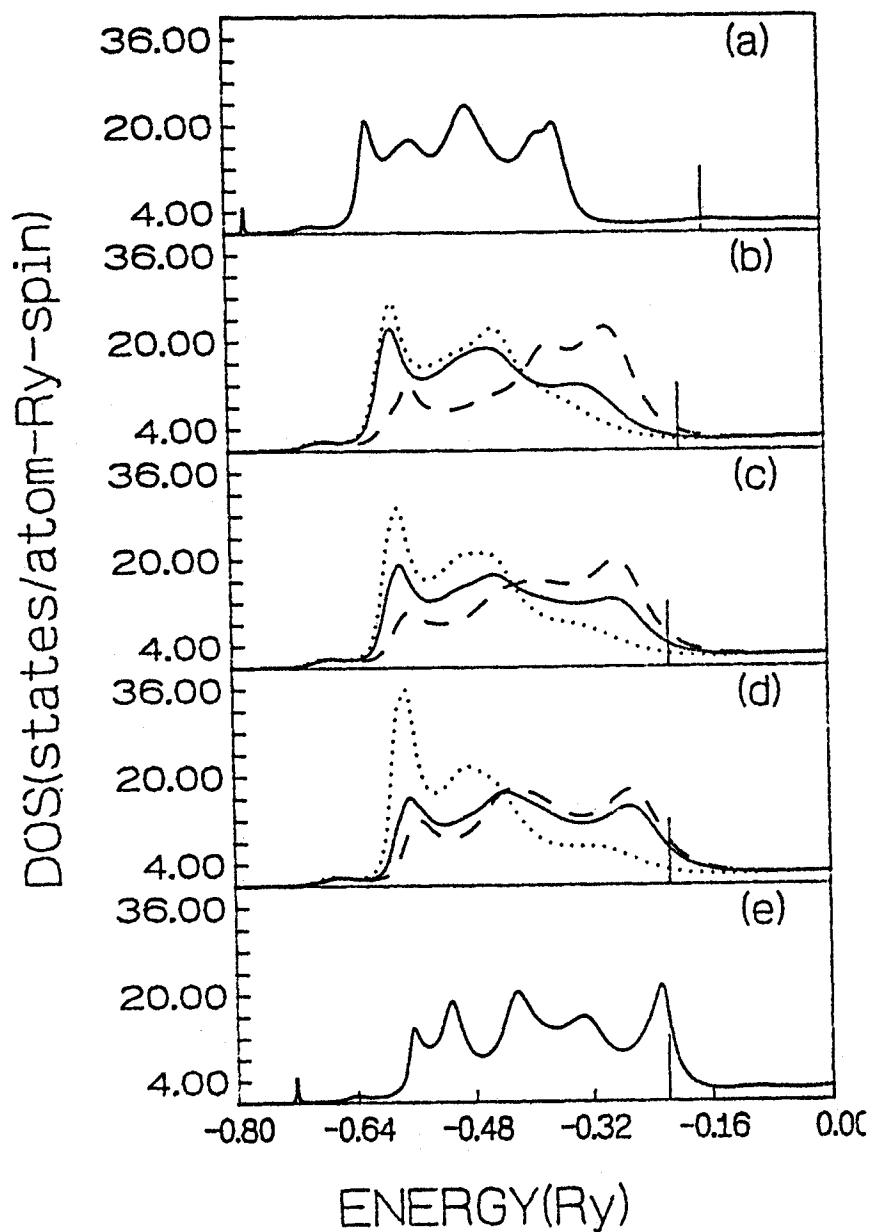


Figure 3.3: The total(solid) and partial densities of states on Ag(dotted) and Pd(dashed) in Ag_xPd_{1-x} alloys for (a) $x=1.0$ (b) 0.75 (c) 0.5 (d) 0.25 (e) 0.0 as obtained in TB-LMTO-ASR calculation . The vertical lines show the position of the Fermi level.

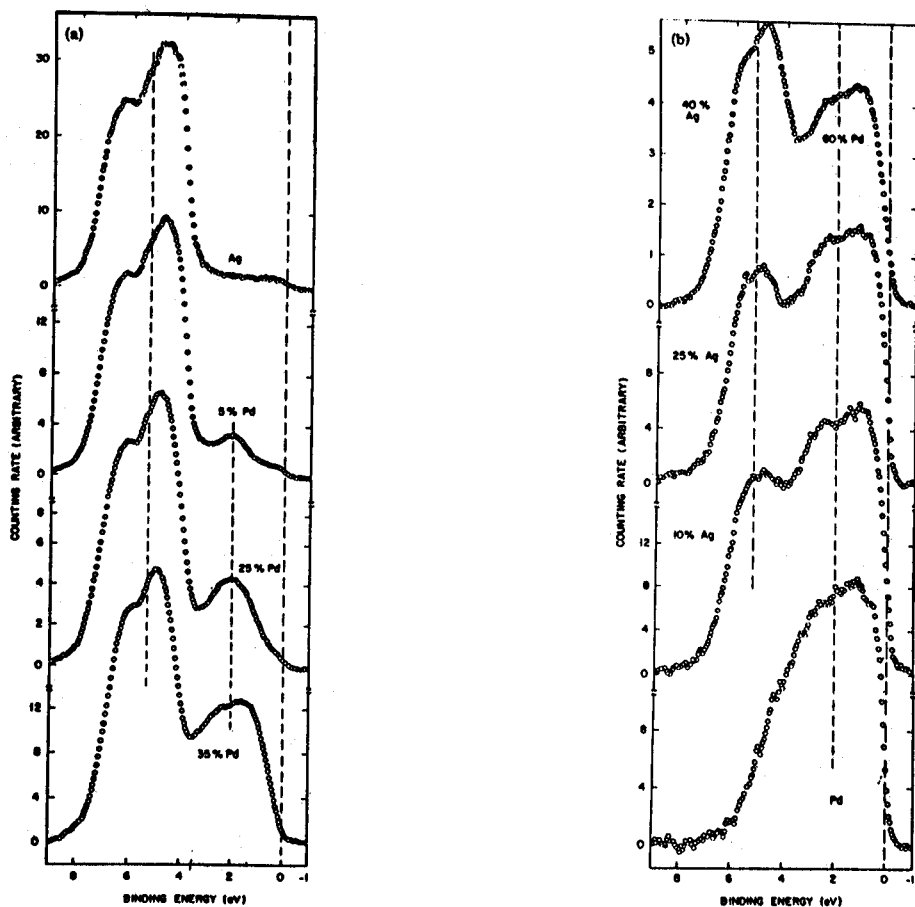


Figure 3.4: The XPS density of states for Ag_xPd_{1-x} alloys (Hüfner *et. al.*, 1973).

falls into the split-band regime with dominating diagonal disorder, weak off-diagonal disorder and small mismatch in the atomic sizes of the constituents, as they come from the same row of the periodic table.

Both charge self-consistent and charge non-self consistent calculation has been done in the KKR-CPA framework (Winter and Stocks , 1983) . LMTO-CPA calculations for AgPd alloys have been done by Kudrnovský and Drchal (1990).

While the charge non-self consistent implementation of the KKR method suffers from the mismatch of the energy scales , the approximate way of performing charge self-consistency within LMTO-ASA frame-work provides proper positioning of constituent bands on the energy axis , avoiding the necessity of performing time-consuming charge self-consistent calculations. The emperical TB-CPA result (Laufer and Papaconstantopoulos , 1987) for AgPd alloys with proper description of diagonal disorder and alignment of crystal Fermi levels to determine relative position of Ag and Pd bands on the energy scale also provides a reasonable electronic structure description of the AgPd alloy system. We have deliberately chosen AgPd as a testing case of theory , since our aim is to go beyond CPA , we will have to first prove the theory to cases where CPA works satisfactorily. In Figure. 3.3 we present our result for Ag_xPd_{1-x} for $x = 1.0 , 0.75 , 0.5, 0.25$ and 0.0 .XPS results for AgPd alloys are shown in Figure. 3.4. Our result agree reasonably well with impurity peak due to Pd for the Ag rich alloys . The general shape of the density of states of the constituents , the position of the Fermi energy and the dominant peaks have been reproduced.

It should be mentioned that the Pd based impurity peak for Ag-rich AgPd alloys and Ag based impurity peak for Pd-rich AgPd alloys, obtained in KKR method are more pronounced and the detail shapes are in better agreement with experiment than those obtained using LMTO methods (LMTO-CPA and TB-LMTO-ASR). However the agreement for the impurity peak positions (0.14 Ryd measured from Fermi energy for Pd impurity peak in $Ag_{75}Pd_{25}$ alloys and 0.4 Ryd measured from Fermi energy for Ag impurity peak in $Ag_{25}Pd_{75}$ alloys) is good enough. The reason may probably be attributed to the use of less accurate electronic structure description of LMTO in LMTO-CPA and in LMTO-ASR compared to that in KKR-CPA .

3.5.2 CuPd Alloys

Copper and Palladium form random alloys of fcc structure at temperatures above 600° K throughout the concentration range . This structure persists to low temperatures except for palladium concentrations between about 10 % and 25 % , where transformation into the Cu_3Au structure and long period ordered structure occur, and between 30 % and 50 % , where transformation into the CsCl structure occur.

However using rapid quenching techniques it is possible to maintain the disordered fcc phase at low temperature throughout the concentration range .

In spite of the propensity of these alloys to establish some degree of short-range order , as

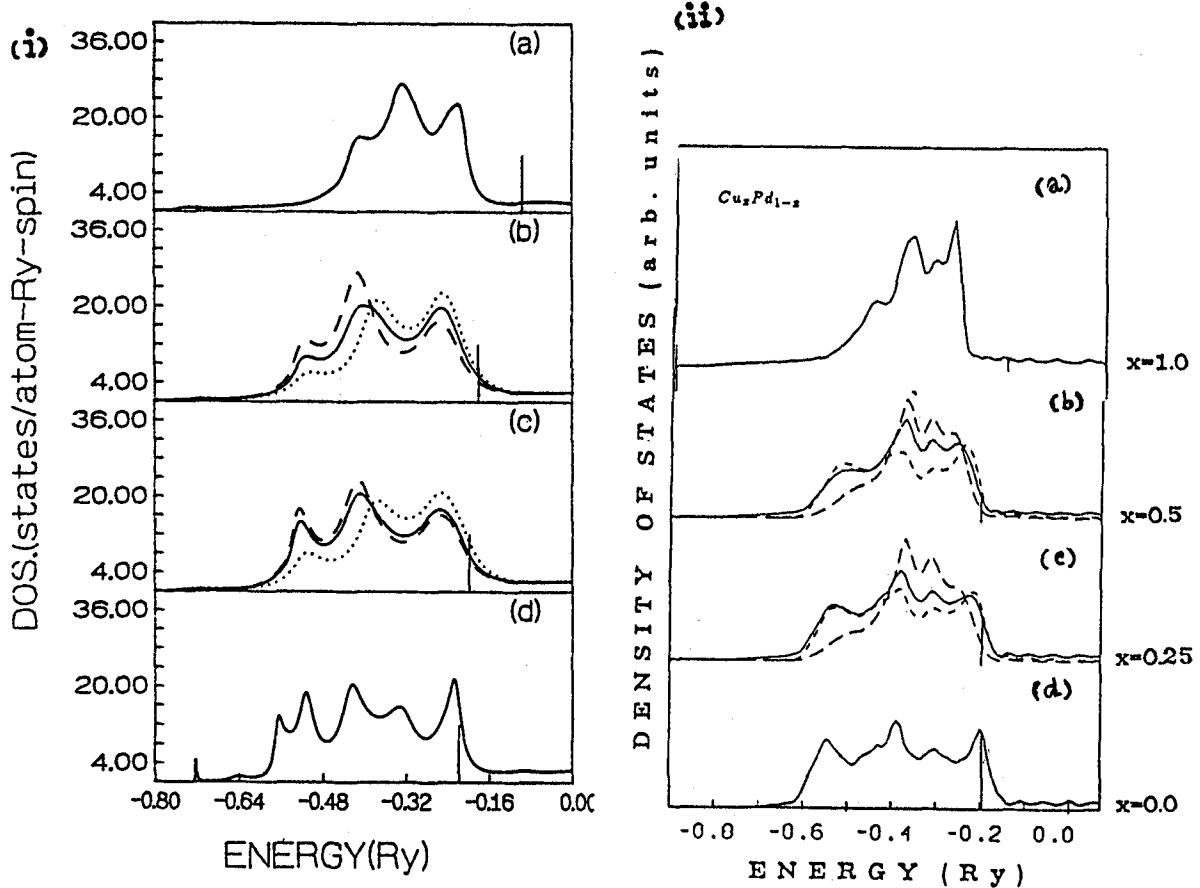


Figure 3.5: The total and partial densities of states on Cu and Pd sites in Cu_xPd_{1-x} alloys for (a) $x=1.0$ (b) 0.5 (c) 0.25 (d) 0.0 as obtained in (i) TB-LMTO-ASR calculation and (ii) LMTO-CPA calculation . Solid lines represent total densities of states , dotted(dashed) and dashed(long-dashed) lines represent partial densities of states in Cu and Pd for figures (i) ((ii)). Vertical lines mark the positions of Fermi-levels.

has been demonstrated by diffuse electron scattering work (Ohshima and Watanabe, 1973), it seems reasonable as a first step to calculate the electronic structure of CuPd alloys under the assumption of complete randomness. Even if the physical quantity in question depends non negligibly on ordering or clustering effects, the results for the random case are needed as the starting point for taking into account such effects.

The trends in the electronic structure of the CuPd alloys are quite different from those of AgPd. In tight-binding terms we characterize CuPd as a system in which off diagonal disorder dominates diagonal disorder. As a result a number of novel features appear in the density of states. The most important effect is that there is a common d band at all concentrations and no palladium virtual bound state, rendering the split band picture of the alloy theory totally invalid.

Furthermore, the pure Cu and Pd d band widths are very different, being respectively 3.3 eV and 5.5 eV. This non-isochoricity leads to effect like lattice relaxation, leading to perturbation in the fcc structure of the alloy, dominant in the Cu-rich regimes of the alloy. Treatment of such effects need extension beyond CPA and attempt to take into account such effects within the present frame-work has been dealt in the next section. In the present section we present the result for $\text{Cu}_x\text{Pd}_{1-x}$ with $x = 1.0, 0.5, 0.25$ and 0.0 and defer the result for Cu-rich alloys $\text{Cu}_{75}\text{Pd}_{25}$ for the next section. Since this is an alloy with predominant off-diagonal disorder, the inability of the empirical TB-CPA method to treat properly the off-diagonal disorder and to determine the relative positions of alloy constituents on the energy scale, give result (Laufer and Papaconstantopoulos, 1987) that disagrees in the details of the density of states. Same is true for the non charge self-consistent KKR-CPA (Rao *et. al.*, 1984). LMTO-CPA calculation (Kudrnovský and Drchal, 1990) in which the disorder in the multiplicative factors Δ 's of the off-diagonal element is taken into account via a mapping of the Hamiltonian with only diagonal disorder compares well with our result (shown in Figure. 3.5(i)-(ii)).

3.6 LATTICE RELAXATION

Alloys with constituents coming from different rows of periodic table (like CuPd, CuAu, CuBe, CuRh) are characterized by large differences in pure component band-widths, reflected as strong off-diagonal disorder. The single-site CPA combined with simple-minded virtual band treatment of off-diagonal disorder by linear scaling of the valence band does not work in these cases and one has to use more sophisticated theories of CPA, like KKR-CPA (Stocks *et. al.*, 1977) with disorder in scattering t matrices or properly generalized off-diagonal treatments like BEB (Blackman *et. al.*, 1971) within CPA or the approach of Kudrnovský and Drchal (1990) of mapping the off-diagonal disorder problem onto an equivalent diagonal disorder problem.

For alloys with components from different rows, there is also an associated size effect due to different atomic radii of components. In most alloy theories developed, this size effect is usually overlooked and atoms are placed on a regular lattice with fixed lattice constant all

over the lattice . In such a model , namely the virtual crystal structure model (Mašek and Kudrnovský , 1986) , the lattice cannot accommodate the differential expansion (contraction) around the larger (smaller) component and the lattice remains locally strained . For dilute alloys with low concentration of larger (smaller) radii components , such deviation from ideal lattice structure becomes appreciable and may lead to significant changes in electronic density of states . This lattice relaxation effect has been suggested as one of the possible candidate for explaining the discrepancy between the photoemission studies (Wright *et. al* , 1987) and the theoretical calculations of KKR-CPA (Winter *et. al.* , 1986) on Cu rich CuPd alloys.

Such non-isochoric alloys with their associated relaxation effects are important for various other reasons . Various phenomenological theories of alloying , such as Hume-Rothery rules, state that size effects are significant with regard to phase stability . The problem of size effect in the context of the Li-Al phase diagram has been considered approximately by Sluiter *et. al.* (1990). Furthermore , lattice relaxation has been found to have significant effect on local magnetic moments of dilute alloys . In general , the moment decreases (increases) with a local lattice compression (expansion) (Stefanou *et. al.* , 1987a) .

The TB-LMTO-ASR is capable of treating off-diagonal disorder on an equal footing to diagonal disorder . Since in augmented space recursion method , the form of the Hamiltonian is kept intact with both diagonal and off-diagonal disorder , the problem of lattice relaxation which brings about disorder in structure matrix describing the geometry of the lattice can be dealt with ease.

3.6.1 Approaches for the study of Lattice Relaxation

Previous approaches

(i) The KKR-Green function method (Stefanou *et. al.* , 1987b)

KKR-Green function calculations including lattice relaxation effect has been carried out for a Pd impurity in Cu host . In this calculation , first the Green function of the pure Cu host was obtained from a self-consistent band structure calculation . By inserting the Pd impurity , the Pd potential as well as the potential of the neighbouring Cu atoms were allowed to be perturbed . The effect of lattice relaxation is taken into account by allowing the outward relaxation of the first shell of Cu atoms . The multiple scattering within this cluster embedded in the pure host was then calculated exactly and the potential are determined self-consistently by iteration . However , proper extension of a such a scheme to concentrated alloys requires a more sophisticated theory than the KKR-CPA.

(ii) LMTO-CPA approach (Kudrnovský and Drchal,1989)

The different sizes of atoms cause structural deformations in random alloys and the structure constant arising in LMTO Hamiltonian $S_{RL,R'L'}^0$ becomes dependent on the occupancy of sites R and R' by A or B type of atom . It leads to a trimodal distribution

of structure constant (S^{AA} , S^{AB} or S^{BA} and S^{BB}) assuming the perturbation due to structural deformation to be restricted between connecting pair of atoms . Single sited CPA theory cannot account for the exact inclusion of this structural disorder in $S_{RL,R'L'}^0$ and they are accounted approximately by setting

$$(S_{RL,R'L'}^0)_{relaxed}^{QQ'} = (S_{RL,R'L'}^0)_{unrelaxed} \left(\frac{w_{alloy}}{\sqrt{s^Q s^{Q'}}} \right)^{l+l'+1}$$

Q , Q' can be A or B type.

where w_{alloy} , s^Q and $s^{Q'}$ denote Wigner-Seitz radius for the alloy and the pure components Q , Q' respectively. This is based on the scaling relation of the structure factor matrix given by

$$S_{RL,R'L'}^0 \propto \left(\frac{1}{d} \right)^{l+l'+1}$$

where $d = |R - R'|$ and the approximation of relaxed distance $d^{QQ'}$ between two sites R and R' occupied by atoms Q and Q' , in terms of the distance d_0 between the same sites in the unrelaxed lattice as

$$d^{QQ'} \approx d_0 \frac{(s^Q + s^{Q'})}{2w_{alloy}} \approx d_0 \frac{(s^Q s^{Q'})^{1/2}}{w_{alloy}}$$

Thus disorder in structure factor , essentially , modifies the multiplicative factors $(\Delta_L^Q)^{1/2}$ and $(\Delta_L^{Q'})^{1/2}$. Furthermore the factors introduced in Δ 's due to approximate treatment of charge self-consistency (discussed in section 3.4.1) exactly cancel out that coming from $(S_{RL,R'L'}^0)_{relaxed}$ and the simple prescription is to use pure component potential parameters for alloy calculations .

This simplified scheme of calculation takes into account the disorder in interatomic distances approximately without consideration of angular distortion of bonds arising due to size effect and gives us the experience of the consequence of lattice relaxation effects in alloys.

(iii) Supercell Approach (Lu *et. al.*,1991a;1992)

Lu *et. al.* (1991a;1992) applied the *special quasirandom structures* construction to non-isochoric alloys in the context of local-density total-energy minimisation , finding a distribution of A-A , A-B and B-B bond lengths deviating from single , unrelaxed values . They applied LAPW band structure techniques to repeated supercell where they created a distribution of distinct environments , average corresponding to the random medium

For concentration $x = 0.25$, the special quasi-random structure was constructed by

A_3B_2 layers stacked along [2 0 1] direction . Their calculation of lattice expansion in dilute limit for CuPd alloys gave 2 % expansion around Pd atom , which agree well with EXAFS experimental data .

However their calculation being based on supercell technique has its own limitation , as an example , being restricted to concentration $x = 0.25$, 0.5 and 0.75 .

Present Approach

TB-LMTO-ASR With Structural Disorder

The random Hamiltonian for binary AB alloys described under the framework of tight-binding LMTO basis is given by

$$H_{RL,R'L'}^\beta = \sum \{C_{RL}^A n_R + C_{RL}^B (1 - n_R)\} + \sum \sum \{(\Delta_{RL}^{1/2})^A n_R + (\Delta_{RL}^{1/2})^B (1 - n_R)\} \dots S_{RL,R'L'}^\beta \{(\Delta_{R'L'}^{1/2})^A n_{R'} + (\Delta_{R'L'}^{1/2})^B (1 - n_{R'})\}$$

where the potential parameters C and $\Delta^{1/2}$ at site R in the most localized β representation can be of A type or B type depending upon whether n_R is 0 or 1 i.e. , whether it is occupied by an A atom or a B atom . In absence of any positional disorder , the structure matrix which characterizes the underlying lattice structure is independent of the component atom type and one expects it to be non-random . However for non-isochoric alloys , the minority component introduced in the matrix of the majority component gets shifted from the unrelaxed lattice positions . In other words where such a minority component sits, the lattice locally deviates from that of a regular lattice.

The effect of lattice distortion depends on the local environments as the structure matrix essentially vanishes beyond the second nearest neighbour for most of the closed structures. As an example , on a fcc lattice we can identify the smallest tetrahedral units of nearest neighbour atoms. The possible combinations of A and B atoms occupying the corners of the unit can be of type AAAA,AABB,ABBB,ABBB,BBBB (shown in fig 3.6).

The configurations obtained by rotation from another configuration have same contribution to the structure matrix. Thus the structure matrix element between two points occurring in the unit will be given by

$$S_{R_i L, R_j L'}^\alpha = S_{R_i L, R_j L'}^{\alpha(AAAA)} n_{R_i} n_{R_j} n_{R_k} n_{R_m} + S_{R_i L, R_j L'}^{\alpha(AAAB)} [n_{R_i} n_{R_j} n_{R_k} (1 - n_{R_m}) + \dots + (1 - n_{R_i}) n_{R_j} n_{R_k} n_{R_m} + n_{R_i} (1 - n_{R_j}) n_{R_k} n_{R_m} + n_{R_i} n_{R_j} (1 - n_{R_k}) n_{R_m}] + S_{R_i L, R_j L'}^{\alpha(AABB)}$$

$$\begin{aligned}
& [n_{R_i}n_{R_j}(1-n_{R_k})(1-n_{R_m}) + (1-n_{R_i})n_{R_j}(1-n_{R_k})n_{R_m} + \\
& (1-n_{R_i})(1-n_{R_j})n_{R_k}n_{R_m} + (1-n_{R_i})n_{R_j}n_{R_k}(1-n_{R_m}) \\
& + n_{R_i}(1-n_{R_j})(1-n_{R_k})n_{R_m} + n_{R_i}(1-n_{R_j})n_{R_k}(1-n_{R_m})] + S_{R_iL,R_jL'}^{\alpha(BBBA)} \\
& [n_{R_i}(1-n_{R_j})(1-n_{R_k})(1-n_{R_m}) + (1-n_{R_i})n_{R_j}(1-n_{R_k})(1-n_{R_m}) \\
& + (1-n_{R_i})(1-n_{R_j})n_{R_k}(1-n_{R_m}) + (1-n_{R_i})(1-n_{R_j})(1-n_{R_k})n_{R_m}] + \\
& S_{R_iL,R_jL'}^{\alpha(BBBB)}(1-n_{R_i})(1-n_{R_j})(1-n_{R_k})(1-n_{R_m})
\end{aligned}$$

where n_{R_k} and n_{R_m} describes the influence of the local environment on the structure matrix element connecting points R_i and R_j . This description takes into account both the effect of distortions of the distance between R_i and R_j and the angular distortion of the square as we go from one configuration to another. For the fcc lattice with structure matrix practically vanishing beyond the first nearest neighbour shell, number of such inequivalent configurations considering all the nearest neighbours will be 144. Consideration of all these configurations will lead to an exact treatment of the distortion effect. However since the computational effort becomes very quickly prohibitive with increase in the possible values assumed by the S-matrix, we will assume that the influence of other nearest neighbours on the structure matrix element connecting each atom with its particular neighbour to be small. This is the *terminal point approximation*. In this approximation all terms involving n_{R_k} and n_{R_m} in the example are replaced by the averages and the effect of angular distortions are only taken in an average sense. Invoking the terminal point approximation the number of inequivalent configurations become three, making the distribution of structure matrix to be a tri-modal one. Since all CPA calculations involving single-site approximation cannot deal with off-diagonal disorder with tri-modal probability distribution, one has to make further approximations at this point. The augmented space recursion, being free from such limitations can deal with this off-diagonal disorder exactly.

Since $n_{R_i}^2 = n_{R_i}$, an examination of the above Hamiltonian reveals that it involves four possible terms, one describing the uniform background against which the fluctuations are measured, a term describing fluctuation at the site R_i , a term describing fluctuation at the site R_j , neighbouring site of R_i and finally a term describing joint fluctuations at both the sites R_i and R_j . The effective Hamiltonian in the augmented space is then constructed by replacing the site occupation variable n_R by operator \tilde{M}^R defined in the configuration space.

The degree of lattice relaxation is however a delicate problem which calls for the first-principle treatment including total energy calculation. The corresponding calculations should provide both displacement of atoms and the electronic structure in the relaxed lattice. Since such a self-consistent is not possible to carry out, at least at present time we shall assume that the lattice relaxes in such a way so as to keep the nearest neighbour distance equal to the sum of the corresponding atomic radii, namely the rigid ion structure model (RIS) (Mašek and Kudrnovský, 1986). It should be mentioned that total energy calculations with respect to the degree of lattice relaxation have been done using super-cell LAPW method by Lu *et. al.* (1991a;1992) which has been discussed earlier.

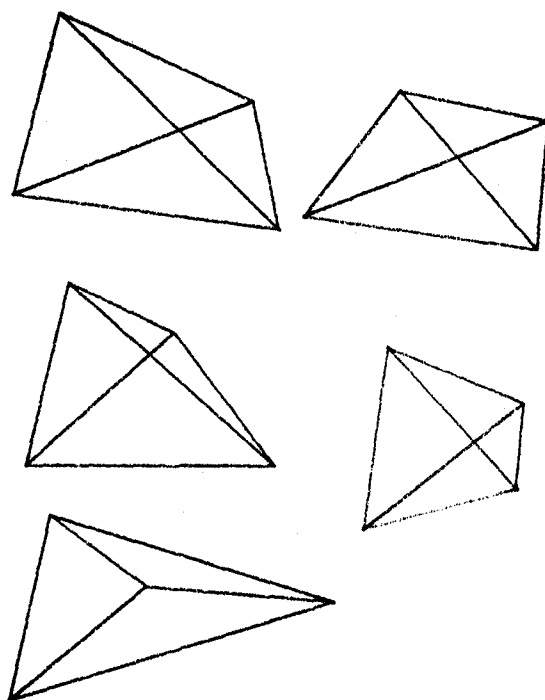


Figure 3.6: Structure of a tetrahedron fcc cluster for various possible occupations of vertices by A and B atoms

3.6.2 Application to Cu-rich CuPd and CuBe alloys

Cu-rich CuPd Alloys :

As already discussed unlike other transition metal alloys for example $\text{Ag}_x\text{Pd}_{1-x}$, $\text{Cu}_x\text{Ni}_{1-x}$ and $\text{Cu}_x\text{Pd}_{1-x}$ alloys consist of atoms belonging to different series in the periodic table and thus differing significantly in atomic number. Since the Pd 4d-wavefunctions are much more extended than the Cu 3d-wavefunctions, making Pd 4d-bandwidth two times greater than that of Cu, the electronic structure of CuPd alloys dilute in Pd does not show the virtual-bound state which is characteristic of CuNi and AgPd.

The electronic structure of non-isochoric Cu-rich CuPd alloys have recently attracted a considerable attention because of the controversial issue of experimental result contradicting the theoretical analysis based on charge self-consistent KKR-CPA calculation. The disagreement between theories like KKR-based CPA (Winter *et. al.*, 1986) and experiments (Wright *et. al.*, 1987) lie in considerable suppression of low energy peak and in the narrowing of Pd local density of states in the experimental data. The former effect comes from use of same Wigner-Seitz radii for Pd and Cu atom, leading to overscreening at the Pd site. This makes the Pd site more attractive, producing a low energy peak. Since LMTO calculations offer one the advantage of working with different atomic sphere radii for Pd and Cu, the calculated density of states under the LMTO framework does show suppression of low energy peak. Secondly the narrowing of Pd local density of states is caused by the lattice expansion around the impurity atom. The actual Cu-Pd distance is underestimated in the single muffin-tin model. Consequently both the Cu-Pd and Pd-Pd hopping and the Pd band-widths are overestimated. We have carried out calculation for $\text{Cu}_{95}\text{Pd}_5$ and $\text{Cu}_{75}\text{Pd}_{25}$ alloys. In Figure. 3.7(i) and 3.7(ii) we present the Pd local density of states for $\text{Cu}_{95}\text{Pd}_5$ and $\text{Cu}_{75}\text{Pd}_{25}$ alloys with and without lattice relaxation effect which show agreement with this expectation. In Figure. 3.8(i) and 3.8(ii) we present the same for Cu local density of states.

Calculation for Pd local density of states taking into account lattice relaxation effect has been carried out using single impurity calculation of KKR-Green function (Stefanou *et. al.*, 1987b), LMTO-CPA (Kudrnovský and Drchal, 1989) and LAPW-supercell method (Lu *et. al.*, 1991a). The single impurity result has been convoluted (the width 0.1 eV) by Kudrnovský and Drchal (1989) to simulate finite concentration alloys so as to make the result comparable with that of the $\text{Cu}_{95}\text{Pd}_5$ alloy.

Bose *et. al.* (1992) have applied LMTO-recursion method for calculating the density of states for the disordered $\text{Cu}_{75}\text{Pd}_{25}$ alloy in which configuration averaging was done by direct averaging of LDOS for 50 configurations. This, as they rightly pointed out, cannot efficiently sample all the possible environment.

If we compare our result with that of Bose *et. al.*'s result, we find that the ours result better reproduce the relative heights of the peaks for Pd local density of states as obtained in CPA calculation and in the experiment of Wright *et. al.* (1987) [shown in Figure. 3.9] where they obtained empirical results for Cu and Pd partial density of states by taking the advantage

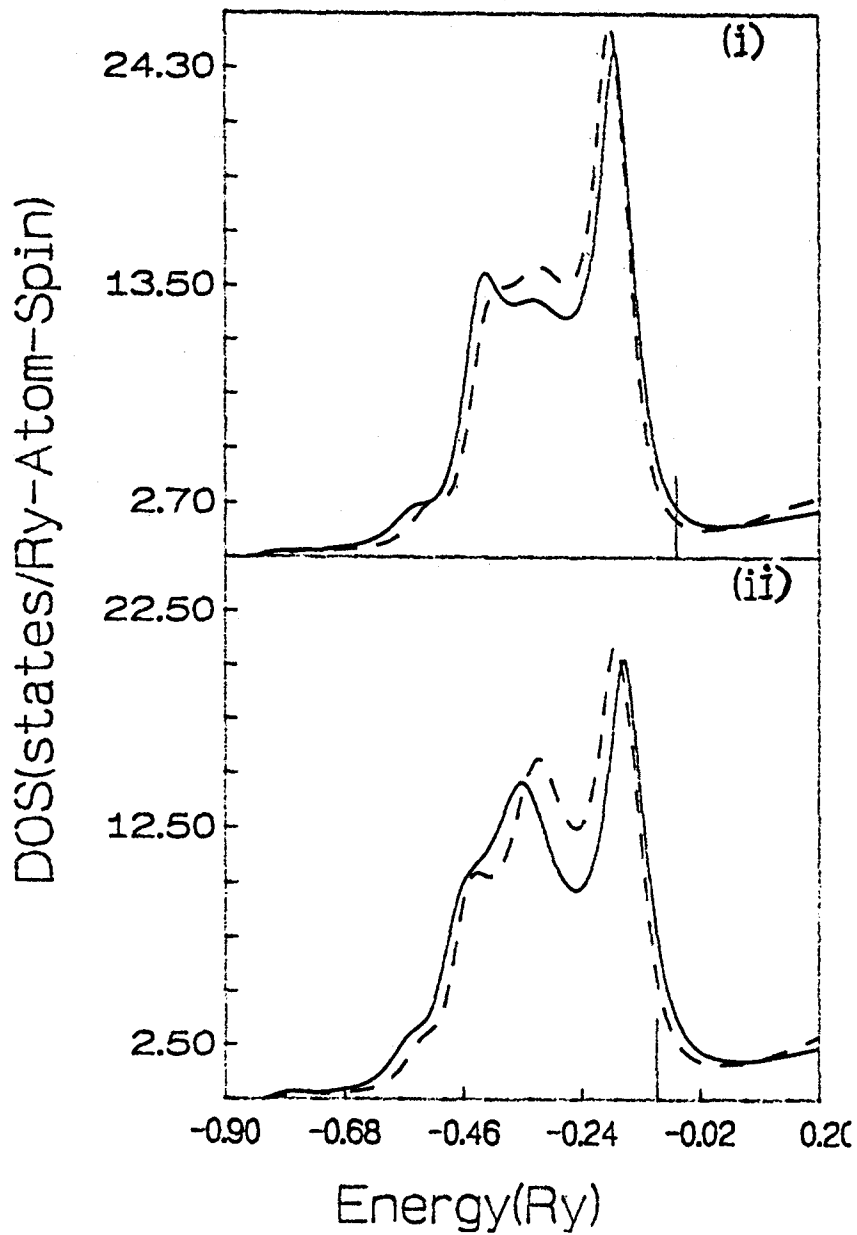


Figure 3.7: The local densities of states on Pd site in (i) $\text{Cu}_{95}\text{Pd}_5$ and (ii) $\text{Cu}_{75}\text{Pd}_{25}$ alloys. The solid one represents result without lattice relaxation and the dashed one with lattice relaxation effect. The vertical lines show the position of the Fermi Energy.

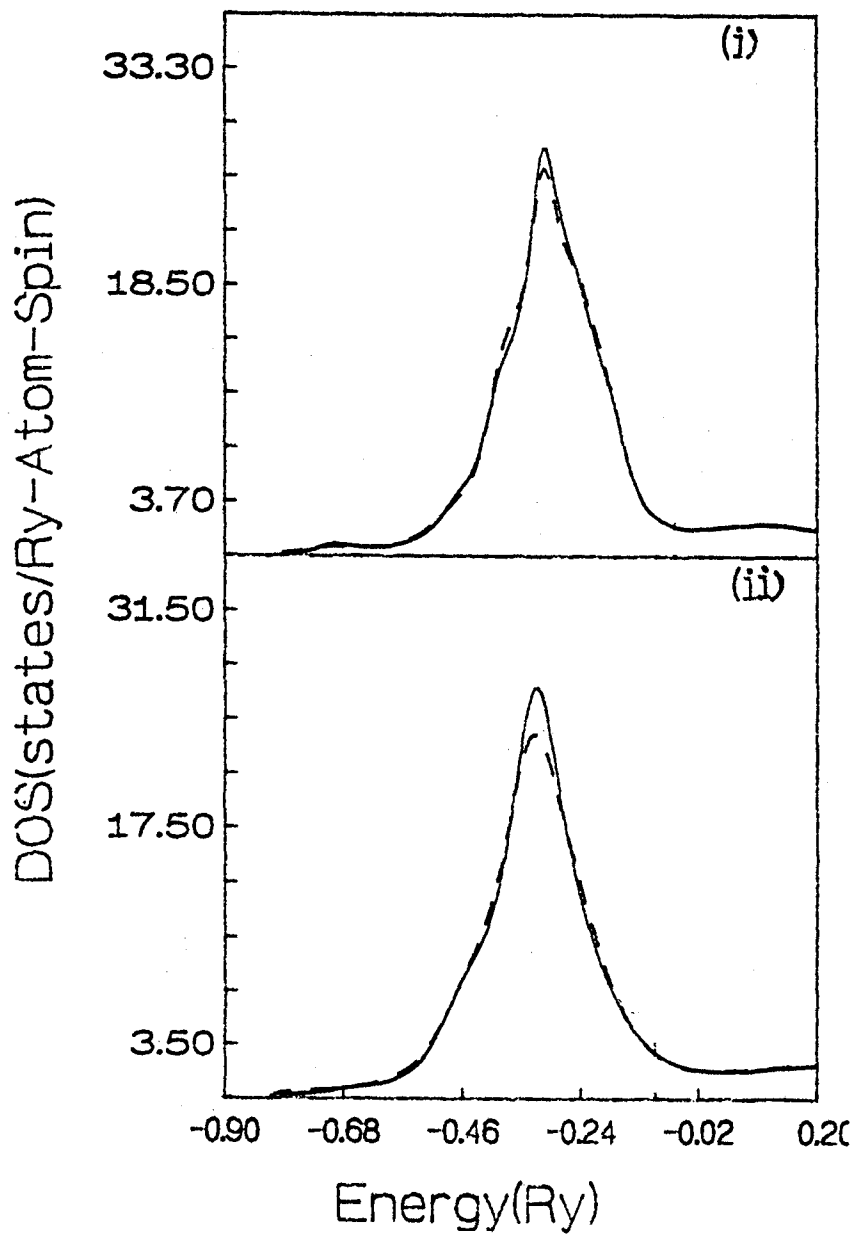


Figure 3.8: The local densities of states on Cu site in (i) $\text{Cu}_{95}\text{Pd}_5$ and (ii) $\text{Cu}_{75}\text{Pd}_{25}$ alloys. The solid one represents result without lattice relaxation and the dashed one with lattice relaxation effect. The vertical lines show the position of the Fermi Energy.

Peak position and relative peak heights	LMTO-CPA	LMTO-Recursion	LAPW-Supercell	LMTO-ASR
Peak I	-0.09	-0.08	-0.073	-0.075
Peak II	-0.24	-0.26	-0.21	-0.22
Peak III	-0.34	-0.35	-0.33	-0.39
ρ_I / ρ_{II}	1.36	1.0	1.56	1.3
ρ_I / ρ_{III}	1.36	1.0	1.4	2.0

Table 3.5: Peak positions and relative peak heights of Pd local density of states (relaxed calculation) in the $\text{Cu}_{75}\text{Pd}_{25}$ alloy . Values quoted for LMTO-CPA and LMTO-recursion are taken from figures of Bose *et. al.* (1992) and the results for LAPW-supercell are taken from Lu *et. al* (1992). Peak I , Peak II , Peak III denote the positions of three successive peaks in LDOS of Pd positioned from higher to lower energy .Peak positions are measured in Ryd from Fermi levels . ρ_I , ρ_{II} , ρ_{III} denote density of states at corresponding positions .

Peak position and relative peak heights	LMTO-CPA	LMTO-ASR	KKR-Green Function
Peak I	-0.11	-0.12	-0.11
Peak II	-0.26	-0.25	-0.27
Peak III	-0.35	-0.34	-0.38
ρ_I / ρ_{II}	1.2	1.7	1.5
ρ_I / ρ_{III}	1.2	1.7	1.5

Table 3.6: Peak positions and relative peak heights of Pd local density of states (relaxed calculation) in the $\text{Cu}_{95}\text{Pd}_5$ alloy . Values quoted for LMTO-CPA and KKR-Green function method are taken from figures of Kudrnovský and Drachal (1989) . Peak I , Peak II , Peak III denote the positions of three successive peaks in LDOS of Pd positioned from higher to lower energy .Peak positions are measured in Ryd from Fermi levels . ρ_I , ρ_{II} , ρ_{III} denote density of states at corresponding positions .

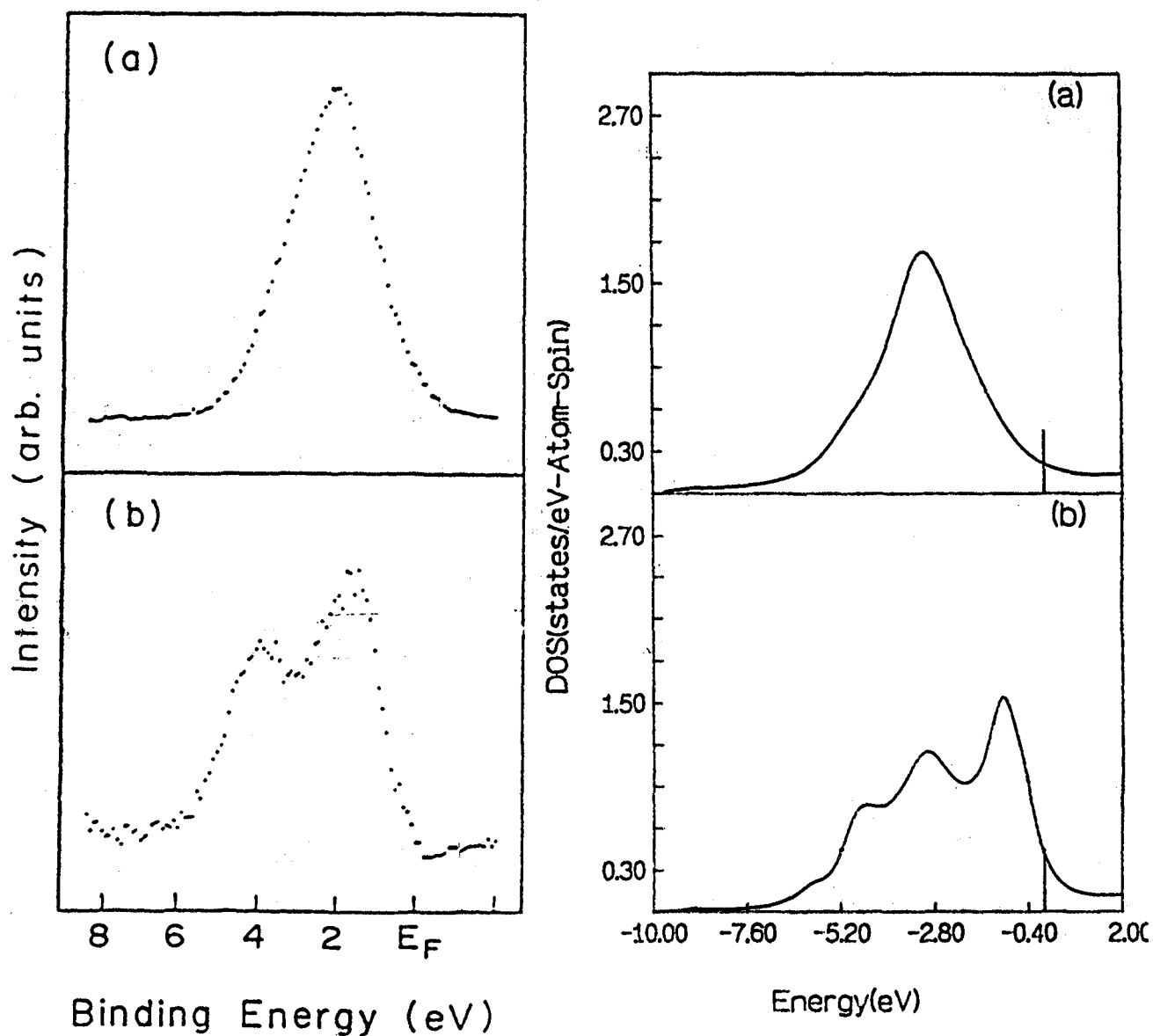


Figure 3.9: (a) Cu and (b) Pd LDOS's obtained from the valence-band photoelectron spectra in $Cu_{75}Pd_{25}$ of Wright et. al.(1987) . Results of relaxed TB-LMTO-ASR calculation are also shown by plotting data in the same scale as that of experiment for comparison . Fermi energy has been adjusted at 0 eV.

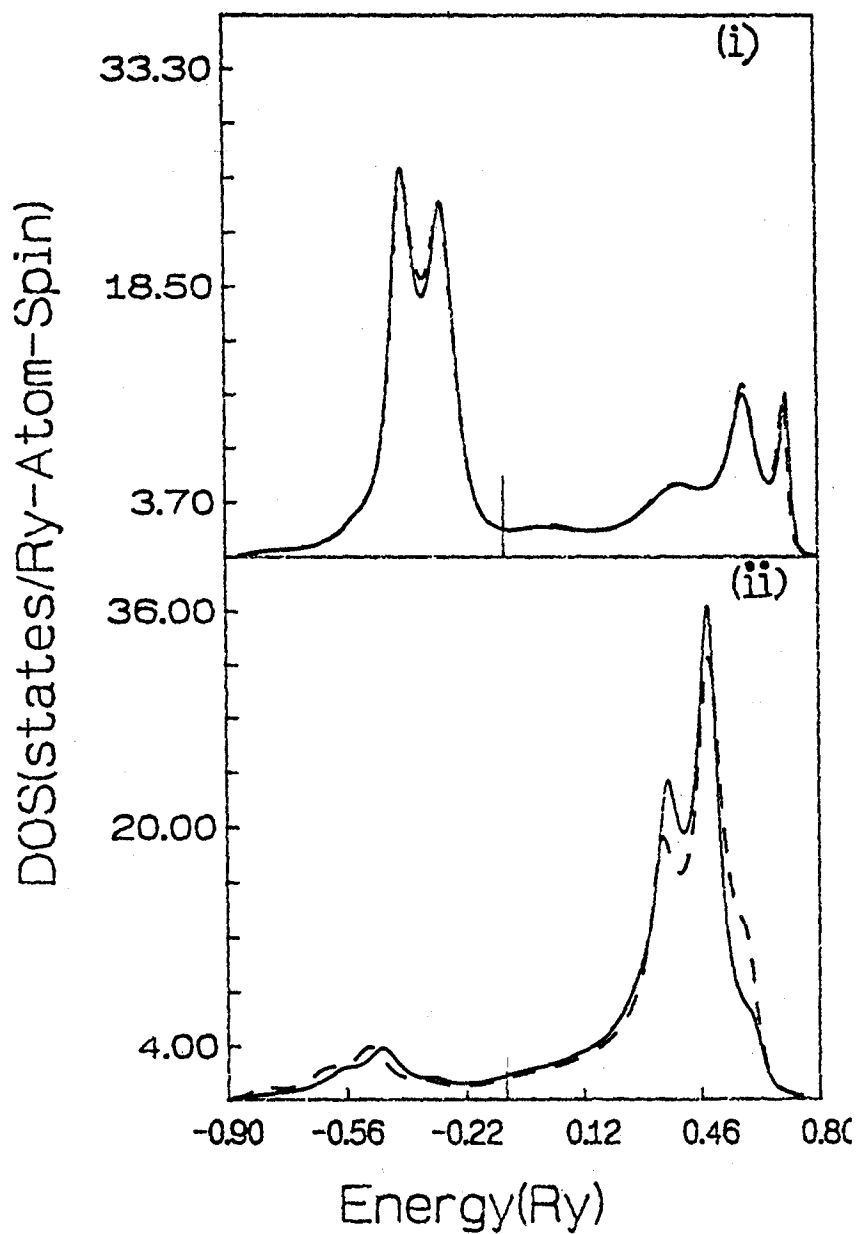


Figure 3.10: (i) The local densities of states on Cu site in $\text{Cu}_{90}\text{Be}_{10}$ alloys. The solid one represents result without lattice relaxation and the dashed one with lattice relaxation effect. The vertical lines show the position of the Fermi Energy. (ii) Same as (i) but for local densities of states on Be site .

of the copper minimum in the Pd photo- electron cross-section.

For Cu local density of states , we donot observe three sharp peaks , which are obserbed in CPA calculations based on KKR method as well as LMTO method. However this is in agreement with the experimental result of Wright *et. al.*(1987) . A comparative study of the characteristic quantities of component resolved density of states obtained in lattice relaxed calculation of various theoretical methods has been made in Table (3.5)and (3.6) for Pd local density of states in $\text{Cu}_{75}\text{Pd}_{25}$ and $\text{Cu}_{95}\text{Pd}_5$ alloys.

Cu-rich CuBe Alloys :

Cu alloyed with small amounts of Be increases the material strength of the pure metal considerably. It has been argued (Askeland , 1990) that the slip dislocations get pinned by strong local lattice distortions (arising out of size mismatch of constituents) giving rise to high strength-to-weight ratio.

Be atom is smaller in radius as compared to Cu atom. The size mismatch between Cu and Be radii is about 10 % , larger compared to that of Cu and Pd which is about 7 % . Since Be atom is smaller in radius the lattice around Be site instead of being expanded gets contracted and use of same hopping underestimates Be-Cu , Be-Be hopping and Be band width . In Figure. 3.10. we have plotted Cu LDOS and Be LDOS for the $\text{Cu}_{90}\text{Be}_{10}$ alloy , with and without lattice relaxation effect . While Cu LDOS remains essentially unchanged under lattice relaxation effect with minor effect as in CuPd alloys the Be LDOS shows a broadening effect with the centre of gravity shifted towards lower energy .

3.7 SUMMARY

In summary , the proposed methodology of augmented space recursion in conjunction with TB-LMTO method proves to be a simple , accurate and computationally efficient method for the first principle calculation of electronic structure of disordered alloy systems . The method provides a systematic way for extending beyond single site coherent potential approximation . It has been shown to be capable of taking into account the effect of lattice relaxation within a prescribed form . The use of recursion technique with suitable terminating scheme on the augmented space , so constructed , makes sure of the fact that TB-LMTO-ASR Green functions retain the essential Herglotz properties.

Chapter 4

STUDY OF PHASE FORMATION AND PHASE TRANSITIONS IN BINARY ALLOY SYSTEM *

4.1 INTRODUCTION.

As mentioned in the previous chapter, alloys are multiphase systems and it is of great interest to the condensed matter theorist to find out , when and under what conditions a particular phase becomes favourable for a particular alloy system . Such studies involve determination of the ground states (*i.e.* stable phases at 0° K) as a function of the composition and then use of the ground states to construct a temperature-composition phase diagram which indicates the regions of concentration and temperature within which the alloy will exist in a particular phase after it has been allowed to reach thermodynamic equilibrium.

The phase diagrams of transition metal alloys show a wide variety of ordered structures stable at low temperature. One can distinguish namely the following types of ordered structures: coherent structures which are built on a b.c.c, f.c.c , h.c.p...lattice, A15 structures, long period ordered structures , laves or even more complicated phases. Several attempts to classify the ordered crystal structures of binary alloys A_xB_{1-x} according to the values of the various semi-empirical parameters have been reported previously (Ducastelle,1991). The simplest parameters are the average number of electrons per atom $\bar{N} = x N_A + (1-x) N_B$ and the valence difference $\Delta N = N_A - N_B$. For the sake of good scientific progress it is now important to obtain a microscopic understanding . Such an understanding should encompass fundamental concepts such as configurational energy, heats of mixing *etc.* and should lead to the construction of alloy phase diagrams with *ab-initio* , parametrization free quantum mechanical methods. It would

¹ * Part of this chapter has been accepted for publication in Phys.Rev.B (October,1994)

then hold the promise of providing a predictive capability of material properties leading to the design of materials with novel properties compatible with specific engineering applications.

Models are often formulated in terms of effective multi-site interactions which can be used to represent the configurational energy of the system under study. These interactions can either be inferred experimentally, determined within phenomenological theories or obtained as the result of fitting procedures in specific statistical models. Such determinations have been employed in most applications in the past. During the last few years a first principle calculation of these interactions on the basis of the electronic structure of substitutionally disordered alloys has been possible as a step towards unifying the theoretical metallurgy and the basic physics of condensed matter. The difference between the configurational energies between two ordered structures giving the relative stability energy is then obtained as a linear combination of various effective interactions. To have an idea of the magnitude of energy that has to be handled for this, we quote the energies with different orders of magnitude, namely, the cohesive energy (a few eV per atom), the formation energy (a few 10^{-1} eV per atom), the ordering energy (about 10^{-1} eV per atom) and the relative stability energy (about 10^{-2} eV per atom). In view of such order of magnitudes, it is obvious that before any physical prediction about stability can be made, energies have to be computed very accurately. In literature several such methods exist which have been briefly reviewed in subsection 4.2.1. Our work as a contribution in this direction addresses the calculation of ordering energies in terms of uniquely defined, concentration-dependent effective cluster interactions in substitutional binary alloys, use of cluster interactions for study of phase stability and determination of instability temperature in phase-separating alloy systems by making use of cluster interactions in conjunction with statistical model.

4.2 THE FREE ENERGY MODEL

Discussion of the introductory section reveal that the study of phase formation and stability of solid solutions can be undertaken on the knowledge of accurate approximations to the configurational energy and on the use of statistical models.

The configurational partition function can be written as

$$Z = \sum_{states} \exp\{-E(state)/K_B T\} = \sum_{\{n\}} g\{n\} \exp\{-E(\{n\})/K_B T\} \quad (4.1)$$

where $g\{n\}$ is the statistical weight of the configuration defined by the set $\{n\}$ of occupation variables (takes value 1 if a state is occupied by A type of atom or 0 if it is occupied by B atom for binary alloy systems)

Equation (4.1) can be rewritten as

$$Z = \sum_{\{n\}} \exp\{-F(\{n\})/K_B T\}$$

with the nonequilibrium free energy function F defined by

$$F\{n\} = E\{n\} - TS\{n\}$$

and the configurational entropy given by

$$S\{n\} = K_B \ln g\{n\}$$

The equilibrium free energy is then obtained approximately by minimising the non-equilibrium free energy function (i.e., replacing the sum in the partition function formula by its maximum term so that fluctuations about the most probable states are neglected) as

$$F_{eq} \cong \min_{\{n\}} F\{n\}$$

4.3 ENERGY CALCULATION : MODEL IN TERMS OF EFFECTIVE CLUSTER INTERACTIONS

4.3.1 Previous Approaches

Traditionally there has been two different approaches of obtaining the effective cluster interactions. The first approach is to start with the electronic structure calculation and total energy determination of ordered super-structures of the alloy and to invert these total energies to get the effective cluster interactions namely, the Connolly-Williams method (Connolly and Williams, 1983). The other approach is to start with the disordered phase, set up a perturbation in the form of concentration fluctuations associated with an ordered phase and study whether the alloy can sustain such a perturbation. This approach includes the generalized perturbation method (GPM) (Ducastelle and Gautier, 1976), the embedded cluster method (ECM) (Gonis *et. al.*, 1984) and the concentration wave approach (Gyorffy and Stocks, 1983). All the latter three work are based on calculation within the frame-work of coherent potential approximation. Recently there has been attempt (Dreyssé *et. al.*, 1989) to obtain effective pair interaction for each individual random configuration of the disordered alloy using recursion technique and then to obtain the configuration averaged pair interaction by direct configurational averaging (DCA). We give brief descriptions of all these methodologies.

(1) The Method Of Connolly And Williams.

In the approach proposed by Connolly and Williams, the total energy for a given binary alloy configuration J , is written in the form

$$E^{(J)} = \sum_p V_p \xi_p^J$$

where V_p and ξ_p^J denote, respectively the concentration independent effective cluster interaction (ECI)'s associated with clusters of p -sites and the p -site correlation function and the summation runs over all cluster types including the empty lattice on a fixed lattice structure. The correlation functions are given explicitly by the expression

$$\xi_p^J = \frac{1}{N_p} \sum_{\{m_i\}} n_{m_1} n_{m_2} \dots n_{m_p}$$

where N_p is the number of sites in cluster p and $\{n\}$ are the occupation variable at each site included in the cluster and the sum runs over all p -th order clusters of a given type. The correlation functions can be found, essentially by inspection, for any ordered alloy configuration. The corresponding energies $E^{(J)}$ can be obtained from a calculation of the electronic structure of the ordered material. A simple matrix inversion then allows the identification of ECI's. In spite of its recent applications, this method is restricted by conceptual difficulties. The most important among these is the uniqueness of the interactions. These parameters can be strongly dependent on the set of ordered structures used in the fit. Such a configurational dependence of ECI's can lead to significant differences in calculated thermodynamic properties.

(2) The Method Of Concentration Waves.

The method of concentration waves in the study of the tendencies towards ordering and phase separation in binary alloys was originally proposed by Khachaturyan and co-workers (Khachaturyan, 1983). Perhaps the most outstanding accomplishment of the concentration wave approach to ordering phenomena is the ability to predict the structure of the ordered phase. Such predictions are based on the knowledge, heretofore obtainable from experimental studies (e. g. X-ray, electron and neutron diffraction), of the characteristic function $S^{(2)}(\mathbf{k})$. This function is essentially the lattice fourier transform of the pair correlation function.

The method of concentration wave allows the calculation of $S^{(2)}(\mathbf{k})$ from a knowledge of the electronic structure of an alloy, thus obviating the need for obtaining correlation functions experimentally. The calculations involve introduction of an inhomogeneous CPA. In the inhomogeneous CPA, it is assumed that each site in the alloy is characterized by a concentration x_i , scattering matrix t_i and self-energy Σ_i . The site dependent self-energy is determined through the condition

$$\langle t_i \rangle = x_i t_i = 0$$

If environmental effects can be considered as being small in some sense, the thermodynamic

function of the alloy Ω can be expanded in powers of $\delta x_i = x_i - x$, where x is the concentration of the solute.

$$\Omega = \Omega_0 + \sum_i S_i^{(1)} \delta x_i + 1/2 \sum_{ij} S_{ij}^{(2)} \delta x_i \delta x_j$$

where

$$S_{i_1, i_2, \dots, i_n}^{(n)} = \left(\frac{\delta^{(n)} \Omega}{\delta x_{i_1} \dots \delta x_{i_n}} \right)_{x_i = x}$$

is the expansion coefficient calculated for $x_i = x$ and Ω_0 is the concentration dependent but configuration independent contribution of the homogeneous CPA medium. This method then yields the two particle correlation function on sites $i \neq j$ as a direct fourier transform

$$S_{ij} = \frac{2}{\pi} \text{Im} \int_{-\infty}^{E_F} \sum_k S(k) \exp(-ik \cdot R_{ij}) dE$$

where

$$S(k) = (\delta t)^2 X(k) \{1 - x(1-x)(\delta t)^2 X(k)\}^{-1}$$

with

$$X(k) = \frac{1}{N} \sum_{n \neq m} (\bar{G}_{nm})^2 \exp(ik \cdot R_{nm})$$

and

$$\delta t = t_A - t_B$$

for binary AB alloy. \bar{G} denotes the Green function of the homogeneous CPA medium. Although, in principle, the method of concentration wave is exact within the context of linear response theory, its implementation requires the use of a mean field approach to ordering. It cannot take into account the non-linear effects of local statistical fluctuations.

(3) Generalized Perturbation Method.

The thermodynamic potential for an electron system is given by

$$\Omega(T, \mu) = U - TS - \mu N$$

where T, S, μ and N refer to the temperature, electronic entropy, chemical potential and number of particles respectively. Considering the band structure contribution to Ω :

$$\Omega_e(\mu) = - \int_{-\infty}^{\infty} d\epsilon \theta(\epsilon - \mu) N(\epsilon, \mu)$$

where $N(\epsilon, \mu)$ stands for the configurationally averaged integrated density of states. For a particular configuration of a substitutional binary alloy, fully specified by the set of occupation numbers $\{n_i^\alpha\}$ ($n_i^\alpha = 1$ if site i is occupied by an α species, 0 otherwise), the band energy $\Omega_e(\{n_i^\alpha\}, \mu)$ can be written, by considering the expression of the integrated density of states as a sum of two terms: (i) the concentration dependent energy $\Omega_e(\{x^\alpha\}, \mu)$ of the CPA reference medium which is configuration independent and (ii) a configuration dependent energy $\Omega'_e(\{n_i^\alpha\}, \mu)$ given by,

$$\Omega'_e(\{n_i^\alpha\}, \mu) = - \frac{1}{\pi N} \text{Im} \int_{-\infty}^{\infty} d\epsilon \theta(\epsilon - \mu) \text{Tr} \log(1 - \mathbf{X}\tau^x)$$

where the trace is taken over the site and angular momentum space. \mathbf{X} is the scattering matrix operator which is site diagonal and has the form $\mathbf{X} = \sum_i \sum_{uv} n_i^\alpha t_i^{\alpha, uv} |u, i\rangle \langle v, i|$, $t_i^{\alpha, uv}$ being the scattering matrix for orbitals u, v characterizing an atom of type α at site i embedded in the CPA medium. The quantity τ^x is the strictly off-diagonal part of the homogeneous CPA Green function. Expanding the logarithm, making use of the CPA condition for the case of binary alloys $A_{1-x}B_x$ and the condition

$$\Delta \mathbf{X} = \mathbf{X}^B - \mathbf{X}^A$$

we obtain

$$\Omega'_e(\{n_i^\alpha\}, \mu) = \sum_2 \frac{1}{k} V_{i_1, i_2, \dots, i_k}^{(k)} \delta x_{i_1} \dots \delta x_{i_k}$$

where $\delta x_{i_k} = n_{i_k}^B - x^2$ and the k -th order effective cluster interaction involving sites i_1, \dots, i_k is given by

$$V_{i_1, \dots, i_k}^{(k)} = - \frac{1}{\pi N} \text{Im} \int_{-\infty}^{\infty} d\epsilon \theta(\epsilon - \mu) \text{Tr}(\Delta X_{i_1} \tau^{x, i_1 i_2} \Delta X_{i_2} \dots \Delta X_{i_k} \tau^{x, i_1 i_k})$$

Then quantity Ω'_e commonly called the ordering energy is then given by to lowest order in the perturbation

$$\Omega'_e = 1/2 \sum_s V_{o_s}^{(2)} \delta x_o \delta x_s$$

²The choice of δx_i is quite different in the concentration wave approach and the GPM and ECM. In the concentration wave method the choice is $\delta x_i = x_i - x$. On the other hand in GPM and ECM (to be discussed later) one has $\delta x_i = n_i^B - x$.

where V_{os} is the effective pair interaction between sites o and s :

$$V_{os} = V_{os}^{AA} + V_{os}^{BB} - V_{os}^{AB} - V_{os}^{BA}$$

$V_{os}^{\alpha\beta}$ indicates that all sites other than o and s are CPA medium sites and the sites o and s can be occupied by A or B atom in four possible combination .

The positive (negative) sign of V_{os} indicating a tendency towards ordering (segregation). In the CPA-GPM pair -interactions obtained are not usually renormalized in the sense that they do not include corrections from the self-retracing paths and higher order interactions , both of which Bieber and Gautier (1984) have shown can be important.

(4) Embedded Cluster Method.

In the embedded cluster method one starts from the configurational energy expressed in the form

$$\Omega(\{n_i\}) = E^{(0)} + \sum_{i=1}^N E_i^{(1)} \delta x_i + 1/2 \sum_{ij} E_{ij}^{(2)} \delta x_i \delta x_j + \dots \quad (4.2)$$

where $n_i = x + \delta x_i$ and the coefficients $E_{i_1, \dots, i_p}^{(p)}$ occurring in the expansion are interchange energies associated with clusters C_p of p sites. An p -site interchange energy for a given configuration J_{C_p} outside cluster C_p is defined as

$$E_{i_1, \dots, i_p}^{(p)}(J_{C_p}) = \prod_{j=1}^p (1 - Q_{i_j}^{AB}) E_{i_1, \dots, i_p}^{(AA \dots A)}(J_{C_p})$$

where $Q_{i_j}^{AB}$ changes an A atom to a B atom on site i_j and $E_{i_1, \dots, i_p}^{(AA \dots A)}(J_{C_p})$ denotes the configurational energy associated with A atoms on sites i_1, i_2, \dots, i_p . The expansion coefficients in (4.2) are given as the averages of $E_{i_1, \dots, i_p}^{(p)}(J_{C_p})$ over all configurations J_{C_p} of the medium surrounding the cluster C_p .

$$E_{i_1, \dots, i_p}^{(p)} = \langle E_{i_1, \dots, i_p}^{(p)}(J_{C_p}) \rangle = \sum_{J_{C_p}} E_{i_1, \dots, i_p}^{(p)}(J_{C_p}) P_{J_{C_p}}$$

$P_{J_{C_p}}$ is the probability of occurrence of J_{C_p} .

Thus one have

$$E^0 = \langle E \rangle = \sum_J P_J E^J$$

$$E^1 = \langle E_i^{(1)}(J_i) \rangle = \sum_{J_i} P_{J_i} (E_i^A(J_i) - E_i^B(J_i))$$

$$E_{ij}^{(2)} = \sum_{J_{ij}} P_{J_{ij}} (E_{ij}^{AA}(J_{ij}) - E_{ij}^{AB}(J_{ij}) - E_{ij}^{BA}(J_{ij}) + E_{ij}^{BB}(J_{ij})) \quad (4.3)$$

$E_i^A (J_i)$ ($E_i^B (J_i)$) is the configurational energy associated with single site cluster when the site is occupied by A(B) atom for a given configuration J_i outside the single site cluster . Similarly $E_{ij}^{\alpha\beta} (J_{ij})$ denotes the configuration energy associated with pair cluster [$\alpha, \beta = A, B$] for given configuration J_{ij} outside the cluster .

Equation (4.3) involving effective cluster interchange energies is formally exact and thus avoids the need of summing a series such as in case of GPM . In the CPA approximation , the configurational energy of an alloy is calculated within ECM as sum of irreducible , renormalized cluster interactions associated with cluster of atoms embedded in a CPA effective medium.

(5) Direct Configuration Averaging

The method of direct configurational averaging proposed by de Fontaine and his co-workers defines the generalized Ising model of a binary $A_x B_{1-x}$ alloy for a system of N lattice sites and N atoms . Each of the atoms is associated with a specific lattice site and the *spin variable* σ_q takes values $+1$ or -1 depending upon whether the atom associated with the site q is A or B . Any configuration of the system may uniquely be described by the N -dimensional vector $\sigma = (\sigma_{q_1}, \sigma_{q_2}, \dots, \sigma_{q_N})$. The Hamiltonian of the system may be written as

$$E(\sigma) = V_0 + V_q \bar{\sigma}_q + \sum_{p_\alpha \geq 2} m_\alpha V_\alpha \bar{\sigma}_\alpha$$

where p_α is the number of sites in the cluster α , $\bar{\sigma}_\alpha$ are given by the product of spin variables over all sites , $q_1 , q_2 , \dots , q_{p_\alpha}$ in α , averaged over all the equivalent clusters of lattice, m_α denotes the multiplicity of the cluster α . The coefficients in the expansion , ECI for a given cluster α is given by the normalized trace over all configurations of the α cluster function with

$$V_\alpha = \frac{1}{2^N} \sum_{\{\sigma\}} \sigma_\alpha E(\alpha)$$

For the case of α representing a pair of lattice sites q and q' one have

$$V_{qq'} = 1/4 (\{E_{AA}\} + \{E_{BB}\} - \{E_{AB}\} - \{E_{BA}\})$$

where $\{ E_{IJ} \}$ is the average energy of all possible configurations with I-J pair of atoms at sites q and q' .

In addition to the summation over all configurations (the *grand canonical version*) it is possible to define a complete , orthonormal basis of functions in the space of configurations at a given concentration (the *canonical version*). In the latter the cluster expansion co-efficients

have an explicit concentration dependence . Both schemes for defining ECI's have been used in the DCA and definite relationship exist (Asta *et. al.*,1991) between the concentration-independent and dependent ECI's , in the thermodynamic limit . The real space recursion method in conjunction with orbital peeling technique is used for determination of ECI at a given configuration . The random effective interactions are then configuration averaged by direct summing over 20-30 configurations where the configuration sum is a restricted one over all configuration with fixed concentration for concentration dependent ECI's and an unrestricted , unweighted one for concentration independent ECI's.

The method of direct configuration averaging is restricted by the fact that it is not possible to make sure that the true thermodynamic limit is achieved . It has been shown by Berera (1990) that the convergence of the numerical values of cluster interactions with the number of configurations becomes increasingly worse for effective interactions between more distant neighbours , reducing the accuracy .

4.3.2 Present Approach

The starting point of our calculation is the expansion of the configuration energy in terms of effective cluster interactions. The expansion for the configuration energy E for a binary alloy A_xB_{1-x} may be written as :

$$E(n_i) = E^{(0)} + \sum_{i=1}^N E_i^{(1)} \delta x_i + 1/2 \sum_{i,j=1}^N E_{ij}^{(2)} \delta x_i \delta x_j + \dots$$

δx_i is the concentration fluctuation given by $n_i - x$, where $x = \langle n_i \rangle$. The coefficients $E^{(0)}$, $E^{(1)}$... are the effective renormalized cluster interactions (renormalized in the sense that all possible scattering off from a cluster of definite size embedded in an average medium are included). $E^{(0)}$ is the energy of the averaged disordered medium, $E_i^{(1)}$ is the interchange energy for the species A and B, and it defines the single body interaction resulting from the interchange of a B atom with an A atom at site i in the alloy, $E_{ij}^{(2)}$ is the effective renormalized pair interaction which is the difference in the single body interaction at i , when sites j ($\neq i$) is occupied either by A or B atom.

The renormalized pair interactions express the correlation between two sites and are the most dominant quantities for the analysis of phase stability. The single-body interaction , though volume and concentration dependent are structure insensitive and should not be considered in stability analysis. We will retain terms up to pair interactions in the configuration energy expansion. Higher order interactions may be included for a more accurate and complete description.

At this point it is worth mentioning that our scheme of calculation of the renormalized pair interactions is similar to other methods based on embedding clusters in an effective medium. The calculation involves the determination of the electronic structure as well as averaging

over different configurations of the system. It is precisely in this averaging scheme that the different methods based on the embedding method differ from one another. In the CPA-ECM the averaging is done within the framework of the CPA. In the DCA the averaging is done directly by summing over different random configurations. Our scheme employs augmented space recursive method for obtaining configuration averaged Green function in conjunction with orbital peeling technique introduced by Burke (1976) which utilises the information about local properties provided by recursion method for calculating small energy differences avoiding numerical instability. We give below a detailed description of determination of effective pair interaction under this scheme.

Determination Of Effective Pair Interactions.

Often the most important effective cluster interaction of the concentration fluctuation expansion of the configurational free energy is the effective pair interaction (EPI) defined as

$$E_{ij} = V_{AA} + V_{BB} - V_{AB} - V_{BA} \quad (4.4)$$

It gives the interchange energy associated with two sites embedded in an otherwise average medium, being occupied by A or B type of atom. In the Hartree-Fock approximation, the total energy of a solid consists of two terms, an one electron band structure contribution V_{BS} and an electrostatic term V_{ES} which includes several contributions. These are coulomb repulsion of the ions and the correction for double counting the electron-electron and the exchange and correlation energy in V_{BS} . It is usually assumed that for differences like in (4.4), the electrostatic contributions approximately cancel out and one is left with solely the one-electron band-structure term. This assumption has been shown to be valid in a number of alloy systems. Thus what is needed is to calculate the one electron band structure contribution with fixed occupancy at sites i and j in an otherwise average medium.

$$V_{IJ} = \int_{-\infty}^{E_F^{IJ}} E n_{IJ}(E) dE$$

where E_F^{IJ} and $n_{IJ}(E)$ denote the Fermi-energy and electronic density of states for specific case with $(I, J = A, B)$.

Conservation of electrons imply that

$$\int_{-\infty}^{E_F^{AA}} n_{AA}(E) dE = \int_{-\infty}^{E_F^{AB}} n_{AB}(E) dE$$

and

$$\int_{-\infty}^{E_F^{BB}} n_{BB}(E) dE = \int_{-\infty}^{E_F^{BA}} n_{BA}(E) dE \quad (4.5)$$

Writing

$$\int_{-\infty}^{E_F^{IJ}} n_{IJ}(E) dE = \int_{-\infty}^{E_F} n_{IJ}(E) dE + \int_{E_F}^{E_F^{IJ}} n_{IJ}(E) dE \approx \int_{-\infty}^{E_F} n_{IJ}(E) dE - \Delta E_F^{IJ} n(E_F) \quad (4.6)$$

where E_F represents the Fermi energy of the averaged medium, $n(E_F)$ is the density of the states of the averaged medium at $E = E_F$ and $\Delta E_F^{IJ} = E_F - E_F^{IJ}$, one has from eqn (4.5)

$$\int_{-\infty}^{E_F} \{n_{AA}(E) + n_{BB}(E) - n_{AB}(E) - n_{BA}(E)\} dE \approx \{\Delta E_F^{AA} + \Delta E_F^{BB} - \Delta E_F^{BA} - \Delta E_F^{AB}\} n(E_F)$$

Expressing effective pair interaction in terms of band structure contributions one have

$$E_{ij} = \int_{-\infty}^{E_F^{AA}} E n_{AA}(E) dE - \int_{-\infty}^{E_F^{AB}} E n_{AB}(E) dE + \int_{-\infty}^{E_F^{AA}} E n_{BB}(E) dE - \int_{-\infty}^{E_F^{AB}} E n_{BA}(E) dE$$

Using

$$\int_{-\infty}^{E_F^{IJ}} E n_{IJ}(E) dE \approx \int_{-\infty}^{E_F} E n_{IJ}(E) dE - E_F \Delta E_F^{IJ} n(E_F)$$

and eqn (4.4) this leads to

$$E_{ij} = \int_{-\infty}^{E_F} (E - E_F) \Delta n(E) dE$$

with $\Delta n(E) = n_{AA}(E) + n_{BB}(E) - n_{AB}(E) - n_{BA}(E)$

According to Einstein and Schriffer (1973) for an Hamiltonian H with eigenvalues E_k

$$\begin{aligned} \det(EI - H) &= \prod_k (E - E_k) \\ -\frac{1}{\pi} \text{Im} \frac{d}{dE} \log \det(EI - H) &= \sum_k \delta(E - E_k) \\ &= n(E) \end{aligned}$$

Here $E = E + i0$. So that

$$\begin{aligned} \Delta n(E) &= (-1/\pi) \text{Im} \frac{d}{dE} \log \frac{\det((EI - H^{AA})) \det((EI - H^{BB}))}{\det((EI - H^{AB})) \det((EI - H^{BA}))} \\ &= \frac{d}{dE} \eta(E) \end{aligned}$$

where $\eta(E)$ the generalized phase shift is defined as

$$\eta(E) = (-1/\pi) \text{Im} \log \sum_{IJ} \det \langle \mathcal{G}^{IJ} \rangle \xi_{IJ}$$

with

$$\xi_{IJ} = \begin{cases} -1 & \text{for } I = J \\ +1 & \text{for } I \neq J \end{cases}$$

and

$$\langle \mathcal{G}^{IJ} \rangle = \langle (EI - H^{IJ})^{-1} \rangle$$

(...) denoting averaging over all sites except i and j .

The operation involved in the definition of EPI is an exchange of atoms on sites i and j . Since this is a localized perturbation the size of the determinant is finite. The Hamiltonian for an A atom at site i and a B atom at site j for example could be written in block form as

$$H^{AB} = \begin{pmatrix} \mathcal{H}_A^i & \mathcal{H}_{AB} & \mathcal{H}_{A0} \\ \mathcal{H}_{BA} & \mathcal{H}_B^j & \mathcal{H}_{B0} \\ \mathcal{H}_{0A} & \mathcal{H}_{0B} & \mathcal{H}_0 \end{pmatrix}$$

where \mathcal{H}_A^i (\mathcal{H}_B^j) are the Hamiltonian submatrices describing the A(B) atoms at site $i(j)$, \mathcal{H}_0 is the Hamiltonian submatrix for the host and the other matrices couple the different submatrices. Since the subblock of the Hamiltonian relative to all atoms except those at sites i and j is unaltered under the exchange procedure involved in the definition of EPI, the orbital peeling method provides an efficient means for obtaining the generalized phase shifts. It provides accurate computation of differences of integrated quantities involving density of states when the difference of the integrated quantities are smaller than the absolute error in the integrals, avoiding a large subtractive cancellation procedure.

From the block representation of H^{AB} one finds that $(EI - H^{AB})$ has $(EI - \mathcal{H}_0)$ as a submatrix and from the properties of a partitioned matrix (Burke, 1976) it follows that

$$\det(EI - H^{IJ}) = \det G_{IJ}^{-1} \det(EI - \mathcal{H}_0)$$

where G_{IJ} denote the upper IJ block of the Green function \mathcal{G}^{IJ} .

Hence one has the generalized phase shift

$$\eta(E) = (-1/\pi) \text{Im} \log \frac{\det \langle G_{AB} \rangle \det \langle G_{BA} \rangle}{\det \langle G_{AA} \rangle \det \langle G_{BB} \rangle}$$

Orbital Peeling Technique

For the case of Hamiltonian described by m -orbital basis set, G_{IJ} 's become matrices of size $2m \times 2m$ and one has to find the determinant of matrices having rank $2m$. A useful feature of orbital peeling method is that one needs to calculate only the diagonal matrix element of a specific Hamiltonian. The basic philosophy lies in removing the embedded atoms orbital by orbital. Mathematically this is a convenient method, since this turns the term $\log \det$ into sum over separate logarithms of individual matrix elements. Using repetitive use of partitioning properties of G matrices, Burke demonstrated that

$$\det G_\alpha = \sum_k \bar{G}_{\alpha k}$$

with

$$\bar{G}_{\alpha k} = \{EI - H_k^\alpha\}^{-1}$$

where H_k^α is the matrix formed by deleting the first $(k-1)$ rows and columns of H^α . It seems that for each pair $\{IJ\}$ two atoms are to be peeled, but because of the symmetry in the definition of EPI one needs only one atom to be peeled. Among the pairs (AA) and (BA) the difference lies in the occupancy of the site i which is occupied by the A atom in one case and B in the other while the site j is occupied by A type of atom in both the cases. If one peels off the site i then what remains is an A type of atom at site j and the remaining host. Since the contribution of pairs (AA) and (BA) are of opposite sign, the contribution of pairs (AA) and (BA) with i -th site peeled off cancel out. Similar argument holds good for pairs (BB) and (AB). Thus in computing the phase shift one requires peeling only on the atom at position i for each of the four possible configurations.

Once the phase shift is obtained, one is left out with performing the integration. The integration by parts lead to

$$E_{ij} = - \int_{-\infty}^{E_F} \eta(E) dE$$

The behaviour of this function quite complicated and hence integration by standard routines (e. g. Simpson's rule or Chebyshev polynomials) is difficult, involving many iterations before convergence is achieved. Furthermore the integrand is multivalued, being simply the phase of $\det \sum_{IJ} (G_{IJ}) \xi_{IJ}$. The way out for this suggested by Burke is rooted in the fact that

$$\frac{d}{dE} \log G = \sum_{\gamma=1}^{p-1} \frac{1}{E - Z_\gamma} - \sum_{\gamma=1}^p \frac{1}{E - P_\gamma}$$

where Z_γ (P_γ)'s are the zeroes (poles) of G expressed as continued fraction expansion evaluated upto p levels.

Substituting this in the definition of EPI one have a series of unit residue poles on the real axis enabling one to obtain EPI as sum of terms involving zeroes and poles of $\langle \tilde{G}_{IJ,k} \rangle$:

$$2 \left(\sum_{\gamma} Z_{\gamma} - \sum_{\gamma} P_{\gamma} + (N_P - N_Z) E_F \right)$$

where N_P (N_Z) is the number of poles(zeroes) below E_F . The factor 2 accounts for the spin degeneracy. This technique referred to as method of poles and zeros enables to carry out integration avoiding the problem of multivaluedness.

Calculation Of Peeled Averaged Green Function

Thus the determination of effective pair interaction reduces in determination of zeros and poles of peeled off Green functions with pair $\{IJ\}$ embedded in an average medium. We shall employ the augmented space recursion coupled with the tight-binding linearized muffin tin orbital method (TB-LMTO-ASR) for a first principle determination of configuration averaged peeled off Green functions $\langle \tilde{G}_{AA,k} \rangle$, $\langle \tilde{G}_{AB,k} \rangle$, $\langle \tilde{G}_{BA,k} \rangle$, $\langle \tilde{G}_{BB,k} \rangle$. The configuration averaged peeled off Green function $\langle \tilde{G}_{IJ,k}(z) \rangle$ is $\langle (zI - H_k^{IJ})^{-1} \rangle$, H_k^{IJ} representing the random Hamiltonian with sites i and j occupied by I and J type of atoms and (k-1) row and columns deleted from the Hamiltonian matrix element involving the site i . Thus H_k^{IJ} in the most localized sparse tight binding representation derived systematically from the LMTO-ASA theory and generalized to random alloys has the following form:

$$\begin{aligned}
 H_k^{IJ} = & \sum_{\ell=k}^9 C_{i,\ell}^I a_i^\dagger a_i + \sum_{\ell=1}^9 C_{j,\ell}^J a_j^\dagger a_j + \dots \\
 & + \sum_{m \neq i, j} \sum_{\ell=1}^9 (C_{m,\ell}^B + \delta C_{\ell} n_m) a_m^\dagger a_m + \dots \\
 & + \sum_{m \neq i} \sum_{\ell=k}^9 \sum_{\ell'=1}^9 \Delta_{i,\ell}^{1/2,I} S_{i\ell,m\ell'}^\beta (\Delta_{m,\ell'}^{1/2,B} + \delta \Delta_{\ell'}^{1/2} n_m) a_i^\dagger a_m \dots \\
 & + \sum_{m \neq j} \sum_{\ell=1}^9 \sum_{\ell'=1}^9 \Delta_{j,\ell}^{1/2,I} S_{j\ell,m\ell'}^\beta (\Delta_{m,\ell'}^{1/2,B} + \delta \Delta_{\ell'}^{1/2} n_m) a_j^\dagger a_m \dots \\
 & + \sum_{m \neq j} \sum_{\ell=1}^9 \sum_{\ell'=k}^9 (\Delta_{m,\ell}^{1/2,B} + \delta \Delta_{\ell}^{1/2} n_m) S_{m\ell,i\ell'}^\beta \Delta_{p,\ell'}^{1/2,I} a_m^\dagger a_i \dots \\
 & + \sum_{m \neq i} \sum_{\ell=1}^9 \sum_{\ell'=1}^9 (\Delta_{m,\ell}^{1/2,B} + \delta \Delta_{\ell}^{1/2} n_m) S_{m\ell,j\ell'}^\beta \Delta_{q,\ell'}^{1/2,I} a_m^\dagger a_j \dots \\
 & + \sum_{m \neq i, j} \sum_{n \neq i, j} \sum_{\ell=1}^9 \sum_{\ell'=1}^9 (\Delta_{m,\ell}^{1/2,B} + \delta \Delta_{\ell}^{1/2} n_m) S_{m\ell,n\ell'}^\beta (\Delta_{n,\ell'}^{1/2,B} + \delta \Delta_{\ell'}^{1/2} n_n) \\
 & (a_m^\dagger a_m + a_n^\dagger a_n)
 \end{aligned} \tag{4.7}$$

We note that the Hamiltonian has both diagonal and off diagonal disorder characteristic of LMTO Hamiltonian of a random alloy. We shall retain this form of Hamiltonian as was done in case of the density of states calculations and shall use this for the augmented space recursion. The essential idea of augmented space recursion discussed in great detail in chapter 3 involves the replacement of random occupation variables $\{n_m\}$ by operators $\{\tilde{M}^{(m)}\}$ constructed in configuration space from the continued fraction expansion of the probability density of variables n_m , so as to define an effective, nonrandom Hamiltonian in augmented space and to perform the recursion with this effective augmented space Hamiltonian in order to get the continued fraction coefficients of configuration averaged Green functions. We have already demonstrated the application of this methodology in connection with the determination of density of states for random alloys. We note that the difference lies in the form of Hamiltonian. Instead of being completely random is now a *peeled* one with fixed occupancy at two given sites. This prohibits the operations arising due to configuration fluctuations at sites i and j . Furthermore the potential and structure factor matrices at site i instead of being (9×9) matrices are now reduced matrices of rank $(9 - k + 1) \times (9 - k + 1)$, k being the orbital which is to be peeled off.

With these changes kept in mind, the Hamiltonian operations in real space and in configuration space goes on identically as in case of a completely random alloy with efficient storage of configuration states in binary words and use of logical operations for the action of Hamiltonian in the configuration space. With the occupancy of the two sites fixed, the local symmetry of the augmented space is lowered and one has to carry out the recursion in a suitably reduced subspace. However cutting off fluctuations at sites i and j reduces the rank of augmented space Hamiltonian considerably, enabling us to do recursion in the augmented space without employing any symmetry reduction.

We obtain continued fraction expansion coefficients of configuration averaged Green functions for four possible occupancies of i and j , AA, AB, BA, BB, in each case the orbitals from $(1 - 9)$ being peeled off one after another. The poles and zeros of these Green functions are obtained from computed N number of continued fraction expansion coefficients. The poles and zeros being the eigenvalues of symmetric tridiagonal matrices of rank N and $(N-1)$ are obtained by the method of bisection based on the Sturm sequence property followed by Newton's method for isolated roots. Thus augmented space recursion coupled with orbital peeling allows us to compute pair-potentials directly, without resorting to any direct averaging over several configurations.

4.3.3 Comparison With Previous Approaches

As mentioned earlier, a number of methodologies exist in literature for the study of phase stability and thermodynamic properties of substitutionally disordered alloys. The common characteristic of these methods is that all of them rely on the first-principle calculation of the electronic structure of judiciously chosen systems so as to extract sets of parameters relevant for

studying phase formation which can be used in conjunction with statistical models to calculate thermodynamic properties . Among the existing methodologies, in the KKR-GPM (Turchi *et. al.* , 1988) and TB-LMTO-DCA (Wolverton *et. al.* , 1993a ; 1993b) approaches , one obtains the real space pair interactions starting from the information of disordered phase , thus making these methodologies directly comparable to our TB-LMTO-ASR . Also both of these methodologies have been applied successfully to a number of alloy systems including the two in which our methodology will be applied . On the other hand , the method of Connolly-Williams is based on calculation of ordered structures (Lu *et. al.* , 1991b) while in the method of concentration waves one obtains the pair correlation functions directly in reciprocal space (Staunton *et. al.* ,1991). These methods cannot be directly compared with our approach.

Determination of pair interactions in the three methodologies namely KKR-GPM , TB-LMTO-DCA and TB-LMTO-ASR involves the determination of electronic structure as well as averaging over sets of configurations , both of which are achieved in distinct ways in the three methodologies . Pair-interactions being quantities of milli-Rydberg order depend sensitively on the description of the alloy Hamiltonian and the averaging scheme invoked . Therefore, before we present our result , we wish to make a comparison of our methodology with the two others , pointing out the similarities and dissimilarities.

The TB-LMTO-DCA shares most of the features of our TB-LMTO-ASR :

- (i) Both methods employ the TB-LMTO for the description of electronic structure. Both use the first order Hamiltonian.
- (ii) In both methods, calculations are carried out in real space, without resorting to any single site approximation.
- (iii) Both methods use the orbital peeling method to obtain the effective renormalized pair interactions.

In spite of all these similarities they also have a number of differences which may be shown to cause differences in numerical values of the pair interactions . Regarding the description of electronic structure , though both of them use the first order TB-LMTO Hamiltonian $H^{(1)}$, they differ in some of the important details :

- (i) For the input to alloy calculations, the TBLMTO-DCA assumes an alloy volume which is obtained either by Vegard's law or by energy minimization with respect to the lattice constant. The potential parameters for constituent elements are then calculated at the common Wigner-Seitz radius of the alloy. In our calculations we have taken unequal Wigner-Seitz radii for components, which takes into account charge self-consistency approximately, yet accurately and consistently (discussed in chapter 3).
- (ii) The TBLMTO-DCA uses the prescription of Shiba (1971) to obtain the off-diagonal matrix element between unlike atoms. In TB-LMTO-ASR defined on the augmented

space, one builds up the off-diagonal matrix element from the potential parameters Δ_i^A and Δ_j^B and the structure matrix S_{ij}^β , and one does not have to resort to Shiba's prescription.

- (iii) In the TB-LMTO-DCA the charge neutrality is achieved by shifting the on-site energy of a constituent with respect to the other, such that each configurationally averaged atom is locally charge neutral. On the other hand, as emphasized, in the present scheme, charge neutrality is achieved by exploiting the flexibility of atomic radii of constituents.

The method of carrying out the configuration averaging involved in the definition of the pair interaction differs significantly in two methodologies. In the TB-LMTO-DCA the pair interactions are obtained for several configurations randomly generated (consistent with all possible concentration for the grand canonical version and consistent with a particular concentration for the canonical version) and the averaging is done directly as a weighted sum. Because the pair interactions are integrated quantities, they are expected to converge fast with the number of configurations sampled. However in principle such a method cannot sample all possible realizations or in other words there is no surity that the thermodynamic limit has been achieved. On the contrary, in the TB-LMTO-ASR the configuration averaging is done using the augmented space theorem. The subsequent termination of the recursive generation of the continued fraction co-efficients of the configuration averaged Green function can be carefully controlled.

The KKR-GPM method is distinct from TB-LMTO-DCA and TB-LMTO-ASR. The main features of this method are :

- (i) KKR is used for the description of the electronic structure. Since there is no linearization involved, the KKR method is certainly more accurate than the TB-LMTO.
- (ii) The single site CPA is used for the configuration averaging. CPA with restored periodicity, in a mean field manner, facilitates the calculations to be carried out in \vec{k} -space.
- (iii) In the GPM method, effective cluster interactions are defined perturbatively order by order, through self-retraced paths. In the most CPA-GPM calculations, the EPI does not include corrections from the self-retraced paths and higher order interactions, both of which, as shown by Bieber and Gautier (1984), may be important. On the other hand TB-LMTO-DCA and TB-LMTO-ASR, both being based on embedding cluster type of approach are non-perturbative and include all possible scatterings from pair of atoms embedded in a random medium.

In subsequent sections we present our calculations for PdV and PdRh and we make direct comparison between the numerical values of pair interactions evaluated in all the three methods.

4.3.4 Phase Stability in PdV Alloys

The stability properties of the Pd-V system is well studied both experimentally as well as by theoretical methods like KKR-CPA coupled with generalized perturbation method (Turchi *et. al.*, 1988) and by LMTO coupled with direct configurational averaging (Wolverton *et. al.*, 1993a). Our choice of the Pd-V alloys is motivated by the fact, that in transition metal alloys (apart from few exceptions) the d band arguments show that the most strongly ordered alloys will have an average band filling near the middle of the d-band, or somewhere near five d-electrons, whereas alloys with band filling close to completely empty or full d level will tend towards phase separation. Pd-V alloys, with constituents on opposite ends of the transition metal series, will order according to the above prescription. Furthermore being a well studied alloy, we have results available for comparison so that the reliability of our methodology can be demonstrated.

Figure 4.1 shows the total density of states for Pd-V alloys, for various concentrations with the positions of the Fermi level shown. In order to maintain accuracy the Fermi energy E_F has been calculated from the $H^{(1)} - h o h$ Hamiltonian. For the calculation of the pair interaction we followed the same methodology coupled with orbital peeling discussed in detail earlier with first order Hamiltonian. We found that since pair potentials are differences of integrated quantities, there seems to be no appreciable difference in doing the calculation with the $H^{(1)}$ and $H^{(1)} - h o h$ Hamiltonians.

In Figure 4.2 and 4.3 we have plotted the nearest neighbour effective pair interactions, as functions of band filling and energy, at three different concentrations for the Pd-V alloy. The relation between the two figures can be understood by looking at the variation of the number of states per spin with energy. This is shown in Figure. 4.4. The shape of the curves is in agreement with those obtained by other methodologies (Gonis *et. al.*, 1987), consisting of a phase separating region at the band edges and an ordering region near the centre. The magnitude of the effective pair interaction decreases with distance with increasing number of nodes. In Figure 4.5 we have plotted V_2, V_3 and V_4 ³ for $x = 0.5$ as a function of band filling to demonstrate this point. This in turn indicates the rapidly convergent properties of the configuration energy expanded in terms of effective cluster interactions. We find that $|V_1| \gg |V_2, V_3 \text{ or } V_4|$, so that the ordered structures appear only when $V_1 > 0$.

In Table 4.1 we present the results for the pair interactions upto the fourth nearest neighbours obtained from different methods for comparison with our calculation. The calculation in TB-LMTO-DCA has been done under the grand canonical scheme resulting in concentration independent pair interactions. Formally the concentration independent pair interactions described under the grand canonical scheme and concentration dependent pair interactions under the canonical scheme can be directly compared only at concentration $x = 0.5$. It is for this reason in table 4.1 we present results for the 50-50 PdV alloy.

³ $V_n = E_{ij}^2$, $|r_i - r_j| = na$ where a is the lattice constant

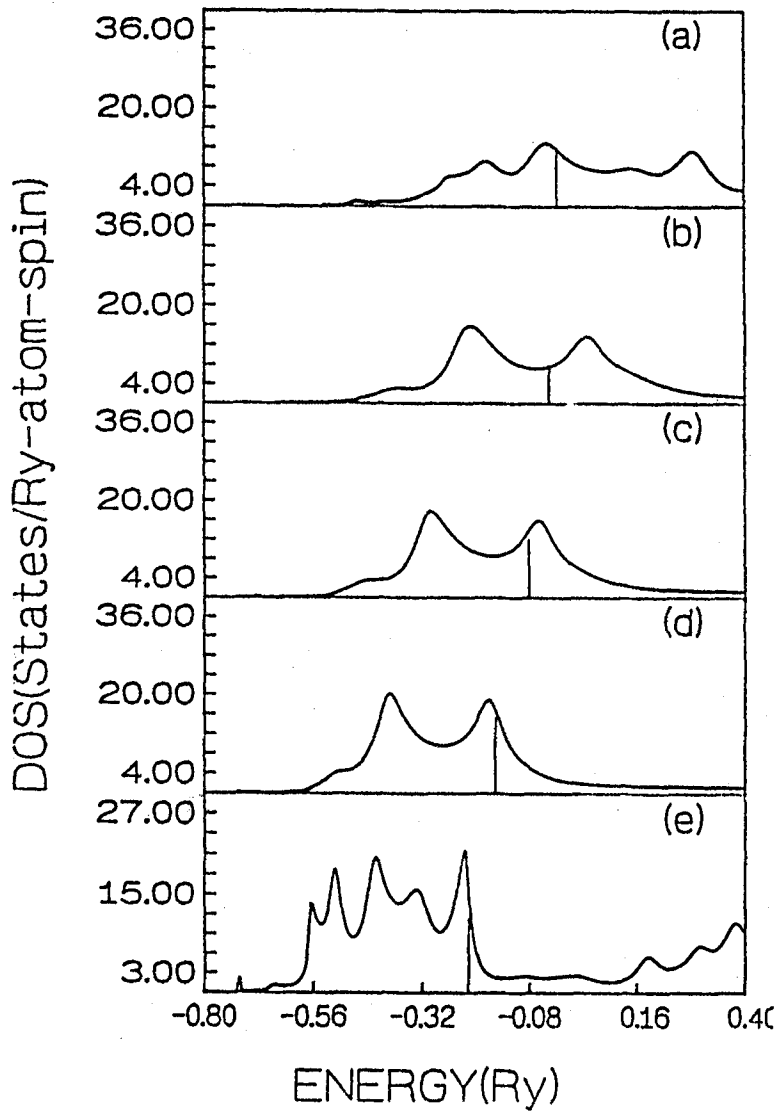


Figure 4.1: Density of states vs Energy for Pd_xV_{1-x} alloys. (a) $x=0.0$ (b) $x=0.25$ (c) $x=0.5$ (d) $x=0.75$ (e) $x=1.0$. The vertical lines mark the positions of the Fermi energies.

PAIR INT.	TBLMTO-DCA	KKR-GPM	TBLMTO-ASR
V_1	4.2	2.0	4.3
V_2	-1.1	-0.8	-0.1
V_3	0.3	0.5	0.1
V_4	0.2	0.1	-0.2

Table 4.1: Effective Pair-Potentials in mRyd/atom for various distances between the pairs for a 50-50 PdV alloy. TBLMTO-DCA values are taken from (Wolverton *et. al.*,1993a) and KKR-GPM from (Turchi *et. al.*,1988).

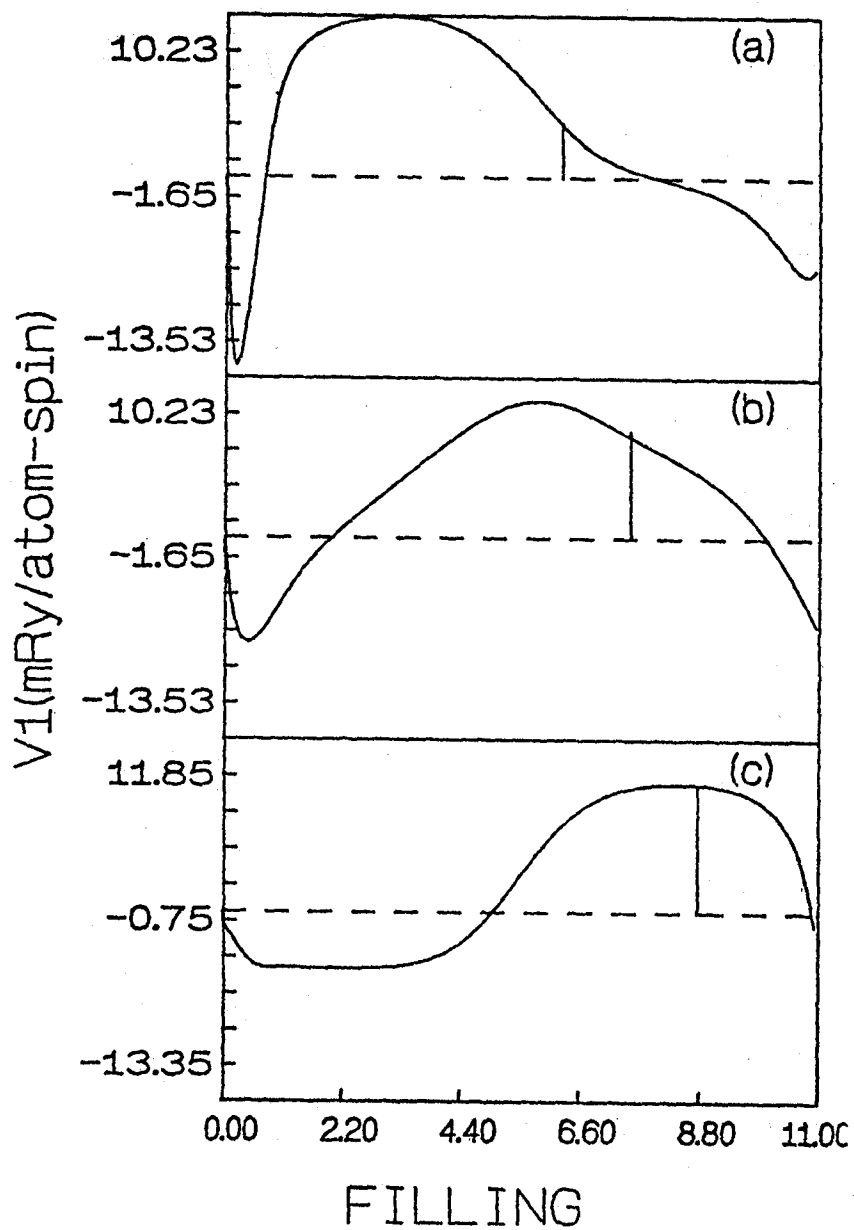


Figure 4.2: The nearest neighbour pair interaction V_1 vs band filling for $\text{Pd}_x\text{V}_{1-x}$ alloys : from top to bottom $x=0.25$, $x = 0.5$ and $x = 0.75$. Vertical lines mark the band filling in the three different concentrations.

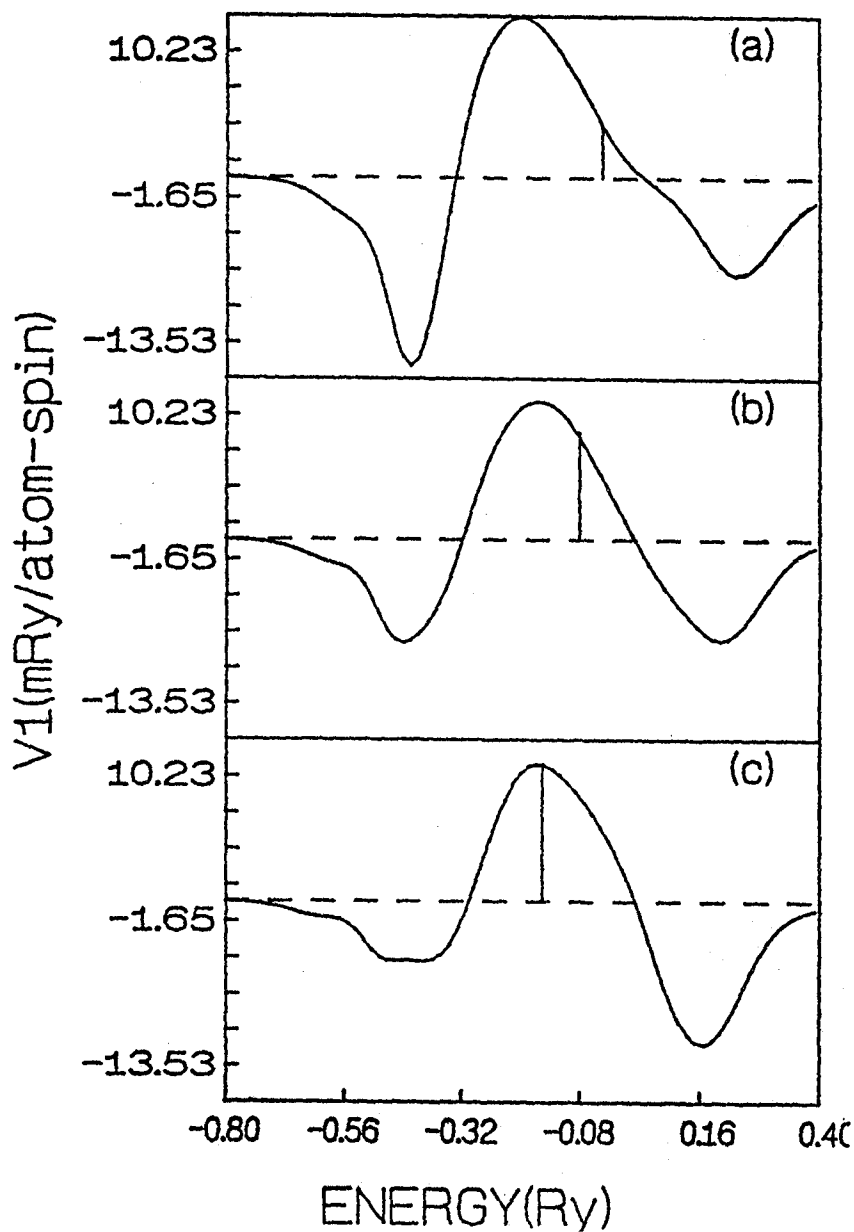


Figure 4.3: The nearest neighbour pair interaction V_1 vs energy for $\text{Pd}_x\text{V}_{1-x}$ alloys : from top to bottom $x=0.25$, $x = 0.5$ and $x = 0.75$.Vertical lines mark the Fermi energies.

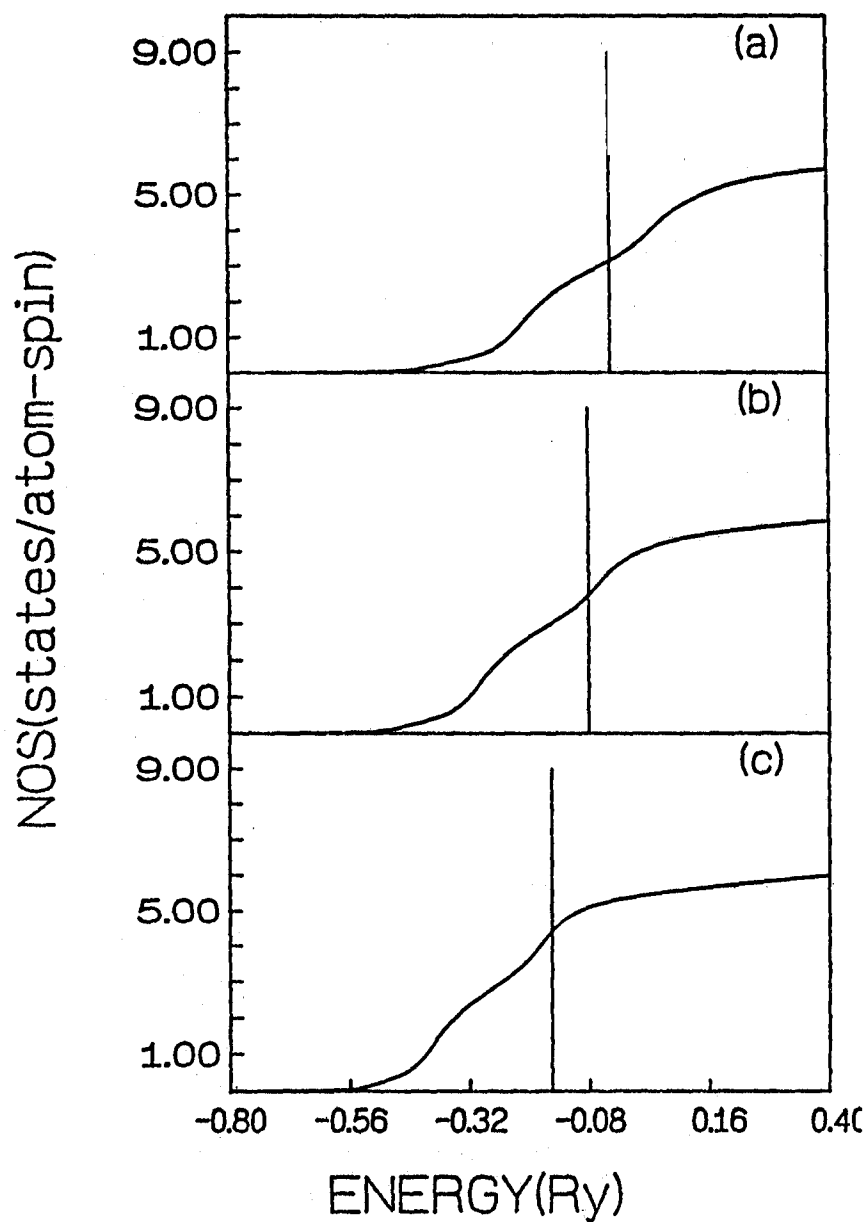


Figure 4.4: The number of states per atom as functions of energy for the three alloys mentioned in Figure. 4.2-4.3. The vertical lines mark the Fermi energies.

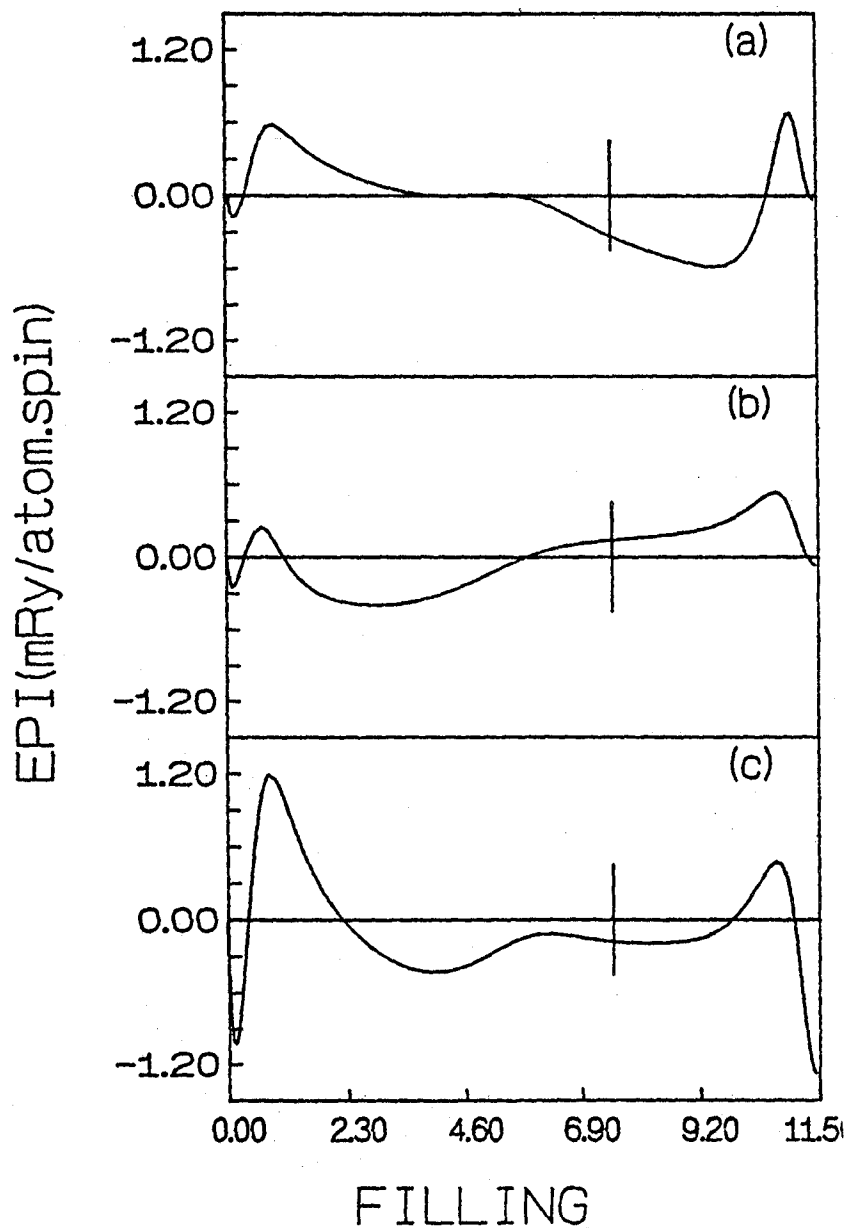


Figure 4.5: The n^{th} neighbour pair interactions vs band filling for $x=0.5$, from top to bottom $n=2$, $n=3$ and $n=4$. Vertical lines mark the band filling in the three different concentrations.

It is clear from the table⁴ that agreement in the dominant interaction V_1 is better between the TBLMTO-DCA and the present work, while there is some mismatch between the values of V_2 , V_3 and V_4 . The reason may be attributed to the differences in description of electronic structure and in the averaging scheme involved in the three methodologies, as pointed out previously. The sign of V_4 in our work is opposite to that of TB-LMTO-DCA and KKR-GPM. However negative sign of V_4 is in agreement with recent work of Singh and Gonis (1993) where they obtained negative value of V_4 within the frame-work of KKR-ASA-GPM.

Once we have obtained the effective pair interactions, they can be used to calculate the ordering energy, hence the relative stability of various ordered phases at a given concentration. They involve calculating the energies of several structures suspected of being ground states and then simply choosing the ones with lowest energies. This approach suffers from the obvious deficiency that it crucially depends on one's ability to suspect the true minimum-energy states. In other words with this simple model, it is possible (indeed, very likely) that one could miss the correct ground state.

Predicting, for a given binary system, which intermetallic structures will have lowest energy for all compositions at 0° K, is an important task. Fortunately, most intermetallics of interest are superstructures of either fcc, bcc or hcp. Then the problem of determining the lowest energy superstructures of a given lattice is a simpler one.

We will follow the method given by Kanamori and Kakehashi (1977) of geometrical inequalities. The authors consider the energy of three dimensional Ising like model

$$E = \sum_k V_k p_k$$

where V_k is the interaction constant of k-th nearest neighbour interaction and p_k is the total number of k-th neighbouring pairs of particles in a given configuration. The particles correspond to atoms of minority component of binary alloys, since the concentration x is confined to the range $x \leq 0.5$ and V_k is given by

$$V_k = V_k^{AA} + V_k^{BB} - V_k^{AB} - V_k^{BA}$$

When the interaction is of finite range, the ground state E_g follows a broken line as function of concentration x , changing the slope dE_g/dx at several characteristic values of x . At the inflection point the ground state is an ordered structure, while it is generally two-phase mixture of ordered structures corresponding to near-by inflection points at an intermediate value of x . This E_g vs x relation was derived rigorously by them for fcc lattice including interactions upto

⁴While comparing different results one should be careful about the units used. In the KKR-GPM and our work the effective interactions are quoted in mRyd/atom-spin, whereas in TBLMTO-DCA they are quoted as meV/atom. In addition in the KKR-GPM and our work the energy expansion is in terms of concentration fluctuations, whereas in the TBLMTO-DCA the expansion is in terms of site-spin variables. This introduces a factor of 1/4 in the definition of the effective interactions.

COMPO - SITION	ORDERED STRUCTURES	KKR -GPM	TBLMTO -ASR	TBLMTO -DCA
PdV ₃	DO ₂₂ -L1 ₂	4.3	4.0	-
PdV	A ₂ B ₂ -L1 ₀	4.5	2.02	3.16
Pd ₃ V	DO ₂₂ -L1 ₂	-0.4	-0.31	-

Table 4.2: Antiphase boundary energies in mRy/atom-spin for PdV at different atomic compositions. The antiphase boundary energies for the KKR-GPM has been taken from Figure. 1 of (Turchi *et. al.* , 1988) while the value for TBLMTO-DCA has been calculated from pair interactions quoted in table 3 of (Wolverton *et. al.* ,1993a)

COMPO - SITION	ORDERED STRUCTURE	TBLMTO -DCA	KKR -GPM	TBLMTO -ASR
PdV ₃	L1 ₂	-8.58	-6.67	-7.98
PdV	L1 ₀	-11.02	-7.40	-10.53
Pd ₃ V	DO ₂₂	-9.8	-2.31	-8.54

Table 4.3: Ordering energies in mRy/atom for PdV at different atomic compositions.

four-th nearest neighbour by method of geometrical inequalities satisfied by the correlation functions p_k 's . Under the minimum p_1 condition $x = 0.25$ and $x = 0.5$ are always the inflection points . Defining ξ by

$$\xi = V_2 - 4V_3 + 4V_4$$

the authors proved rigorously that DO₂₂ structure and A₂B₂ are the corresponding structures at $x = 0.25$ and $x = 0.5$ for $\xi > 0$ and L1₂ and L1₀ are the corresponding ones at $x = 0.25$ and $x = 0.5$ for $\xi < 0$. In Figure. (4.6) we present the superstructures DO₂₂ , L1₂ , L1₀ and A₂B₂ . It indicates that ξ gives the energy associated with $1/2$ a (1 1 0) (a is the lattice constant) between every two (0 0 1) planes . It is for this reason it is named as the antiphase boundary energy.

In Figure 4.7 we have plotted the negative of anti-phase boundary energy $\epsilon = -\xi$ as a function of band filling for Pd-V with $x = 0.25, 0.5$ and 0.75 . The number of zeros is in agreement with the arguments based on moments (there has to be at least four zeros) (Ducastelle,1991) .

We find from Figure 4.5 that $\epsilon < 0$ at $E = E_F$ for $x = 0.75$ suggesting that at this concentration DO₂₂ structure is stable. A similar analysis shows that $\epsilon > 0$ for $x = 0.25$ at $E = E_F$ and here the L1₂ structure is stable. This is further supported by the fact that an exchange of stability between L1₂ and DO₂₂ occurs for large electron number. For $x = 0.5$, among the possible ground state configurations are L1₀ and A₂B₂ , we find L1₀ to be stable one with $\epsilon > 0$.

In table 4.2 we quote the antiphase boundary results for three different alloy compositions

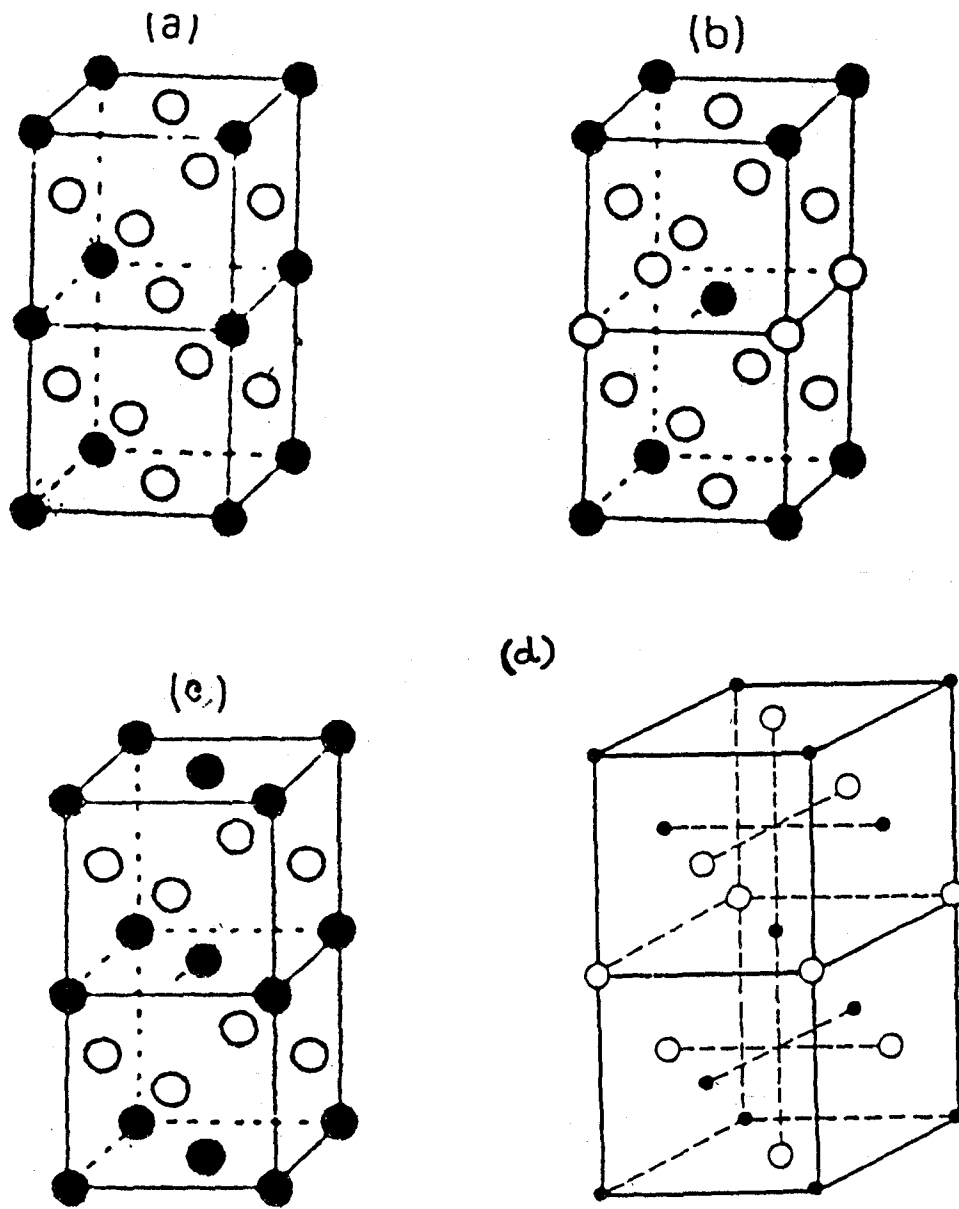


Figure 4.6: The superstructures (a) $L1_2$, (b) DO_{22} , (c) $L1_0$ and (d) A_2B_2 . Two unit cells have been represented for $L1_0$ and $L1_2$ for a comparison.

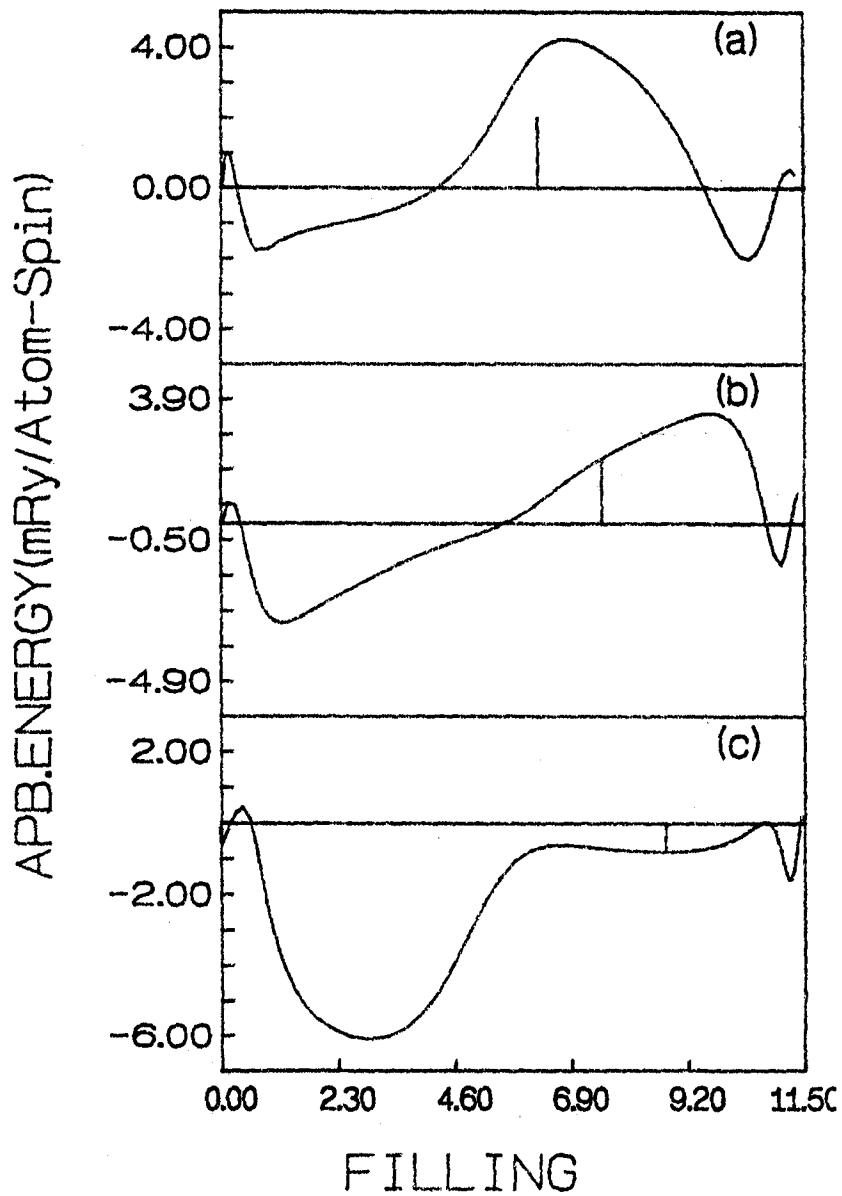


Figure 4.7: The antiphase boundary energies for $x =$ (a) 0.25 (b) 0.5 and (c) 0.75. Vertical lines mark the band filling in the three different concentrations.

of PdV in three different methodologies . The TB-LMTO-DCA using grand canonical version of pair interaction can be compared with only the 50-50 alloy case.

Ordering energy ⁵ gives a quantitative estimate of the energy difference involved in a order-disorder transition and is the most critical test of the formalism, because it is much smaller (typically of the order of 0.1eV or smaller) than other quantities relevant to alloying, such as the formation energy of the random state which is five or more times larger. Ordering energy being the difference between the energy of an ordered structure and the corresponding random phase is expressed in terms of effective pair interactions V_k as

$$\Omega_{or} = 1/2 \sum_k V_k \delta x_0 \delta x_k$$

δx_0 , δx_k denoting the concentration fluctuation at site 0 and k respectively while V_k is the effective pair interaction between sites 0 and k . In order to complete comparison with other works , we quote in table 4.3 ordering energies also .

In particular, the ordering energy of the DO₂₂ structure is rather small in the KKR-GPM as compared to the TBLMTO-DCA and our work. We should mention here that the TBLMTO-DCA includes higher order interactions (upto quadruplets). For PdV alloys with associated asymmetry about x = 0.5, inclusion of these higher order interactions may prove to be important (Wolverton *et. al.* 1992)

It is interesting to note that the prediction of the stable ordered ground states for all the three concentrations is the same in all the three methods discussed.

4.4 ENTROPY CONTRIBUTION : THE BRAGG-WILLIAMS MODEL

The central problem of the entropy calculation is that of calculating approximate expressions for the number of configurations of crystal lattice having definite distributions of clusters of lattice points which may be , in general , occupied by any one of a given set of atomic species . The Bragg-Williams model is derived from a state-of-order description based on single- site averaging *i. e.*, on the *point* cluster .

In order to derive Bragg-Williams model (BW) it is required to define non-trivial single site averages which can be obtained by sublattice averaging as follows:

One considers an ensemble of M systems { sublattices in the Bragg-Williams sense } , each system containing N number of lattice points . Initially all systems are assumed to have identical distribution n_i and after that exchange of defect atoms between sublattice systems are allowed

⁵figures for the TBLMTO-DCA have been read from Figure. 2(d) of the reference (Wolverton *et. al.*,1993a), while those for the KKR-GPM is taken from Table 1 of (Turchi *et. al.* , 1988)

to take place conserving the internal energy . This procedure automatically ensures long-range correlations between the sublattice systems so that the microcanonical ensemble average gives

$$x_i = \langle n_i \rangle_0 = 1/M \sum_{\text{sublattices}} n_i$$

Now one seeks the number of ways g_M of distributing x_i M number of A atoms and $(1-x_i)$ number of B atoms over the M sublattices in such a way that A and B atoms have correct fractional distribution of x_i and $(1-x_i)$. The result is the familiar one

$$g_M(i) = \frac{M}{(x_i M)!(1-x_i)M!}$$

Similar expressions are obtained for all other of N points of the sample lattice so that the total weight factor per sublattice system of the ensemble g is given by M-th root of the product over all N points

$$g = \left[\prod_i g_M(i) \right]^{1/M}$$

Using the expression of configurational entropy $S = K_B \ln g$, the entropy expression under Bragg-Williams approximation will be given by

$$S = K_B \left[\sum_i x_i \ln x_i + \sum_i (1-x_i) \ln(1-x_i) \right]$$

where the Stirling's approximation has been used for the logarithm of the factorials .

4.4.1 Phase-separation And Calculation Of The Instability Temperatures In Pd-Rh Alloys

The Pd-Rh alloys provide a convenient test case for application of the methodology because of its particularly simple phase diagram , which consists of only liquid and fcc solid solution phases . It is one of the few alloy systems that does not show polymorphism and there is relatively little transfer of charge or size disparity between the atoms . Application of d-band like argument for Pd-Rh alloys with almost filled d-band give clustering tendency at low temperature.

Figure (4.8) shows the plot of nearest neighbour effective pair interaction for $\text{Pd}_{75}\text{Rh}_{25}$, $\text{Pd}_{50}\text{Rh}_{50}$ and $\text{Pd}_{25}\text{Rh}_{75}$ alloys as a function of band filling energy .

We note that unlike the Pd-V alloy case , the plot is dominated by negative value of the pair interaction. In Figure. (4.9) we plot the effective pair interactions upto sixth nearest

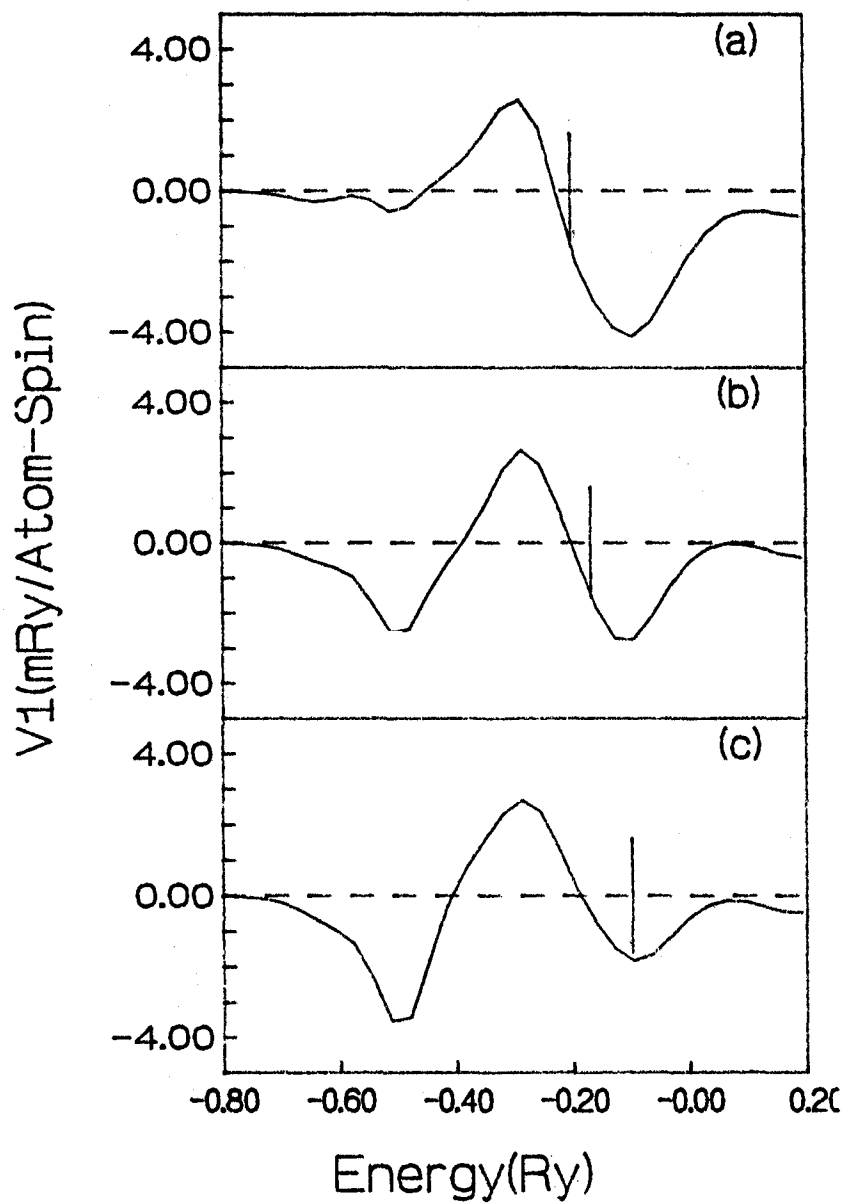


Figure 4.8: The nearest neighbour pair interaction V_1 vs energy for $\text{Pd}_x\text{Rh}_{1-x}$ alloys : from top to bottom $x=0.75$, $x = 0.5$ and $x = 0.25$. Vertical lines mark the Fermi energies.

PAIR INT.	TBLMTO-DCA	KKR-GPM	TBLMTO-ASR
V_1	-0.764	-0.85	-0.80
V_2	≈ 0	-0.05	-0.02
V_3	≈ 0	-0.12	0.02
V_4	≈ 0	≈ 0	≈ 0

Table 4.4: Effective Pair Potentials in mRyd/atom for various distances between the pairs for a 50-50 PdPh alloy. TBLMTO-DCA values are taken from (Wolverton *et. al.*, 1993b) and KKR-GPM from (Turchi *et. al.*,1988) . In order to make our and KKR-GPM result comparable to that of TB-LMTO-ASR , effective pair interactions have been multiplied by factor of 1/4 as in table 4.1.

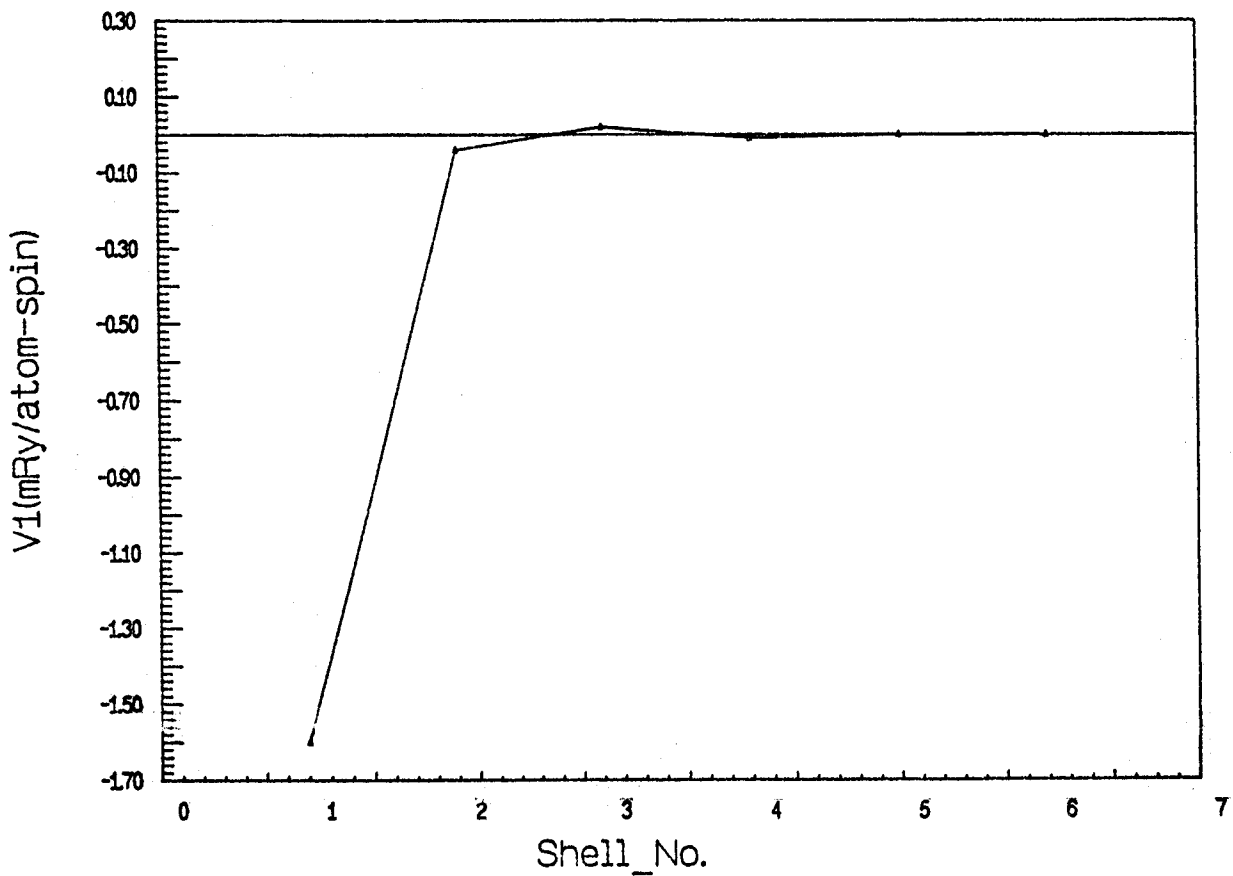


Figure 4.9: V_n as a function of n for the $Pd_{50}Rh_{50}$ alloy .

neighbours for the $\text{Pd}_x \text{Rh}_{1-x}$ alloy with $x = 0.5$. It shows that pair interactions in the Pd-Rh alloys decay very rapidly as a function of neighbour distance and the dominant interaction V_1 is always negative. In magnetic analogy this would correspond to a ferromagnetic interaction. In an alloy, this means that the constituent atoms prefer to be surrounded with atoms of their own kind. In other words, the alloy will tend to phase separate and will exist as a mixture of two phases, one phase is palladium-rich substitutional alloy and the other is rhodium-rich.

In table (4.4) we quote the numerical values of pair interactions upto four-th nearest neighbours as obtained by KKR-CPA-GPM (Turchi *et. al.* 1988), in grand-canonical DCA (Wolverton *et. al.* 1993b) and in the present methodology. We note that the agreement of numerical values between different methodologies is much better compared to that of the PdV alloy case. This may be attributed to the fact that Pd-Rh being a much simpler system compared to PdV, in the context of much smaller charge transfer and the amount of disorder present between the constituents, the difference between different methodologies may not have significant contributions. A systematic study of the effect of various alloy Hamiltonians on the numerical value of effective pair interactions for the Pd-Rh alloy system has been made by Wolverton *et. al.* (1993b). As already emphasized that the alloy Hamiltonian used in the present case is parametrized by constituent's TB-LMTO potential parameters, made consistent with the alloy Wigner-Seitz radius by volume derivative correction. Thus the potential parameters contain the information of the concentration which will be found to be important for desired asymmetry of the spinodal curve (to be discussed later on). The nearest neighbour pair interaction for the alloy Hamiltonian parametrized with TB-LMTO calculations in which Pd and Rh is each at its own equilibrium lattice constant has also been carried out. In such a scheme potential parameters of the alloy Hamiltonian do not bear the concentration dependence. For, each concentration, it has been found to have a larger negative value compared to that of earlier scheme. For $\text{Pd}_{50}\text{Rh}_{50}$ alloy calculation in latter scheme with concentration independent potential parameters give the value of V_1 to be -2.71 mRy per atom per spin which agree well with the value -2.6 mRy per atom per spin obtained in systematic study of Wolverton *et. al.* (1993b) This in turn proves the reliability of the averaging scheme invoked in the present methodology.

Calculation Of The Instability Temperatures

We now undertake the calculation of instability temperatures in \vec{k} -space. The process of ordering and segregation in binary alloys may be interpreted as the loss of stability of a disordered solution with respect to the static concentration waves. The fourier transform of the concentration deviations at each site from the uniform background of disordered solid solution represent concentration plane waves or static concentration waves, a term coined by Khachaturyan (1983). As already mentioned the study of phase formation requires accurate approximations to the configurational energy as well as use of statistical models to obtain the configurational entropy. Thus minimization of the free energy F will be accomplished when the configurational energy E reaches its minimum allowable value. The configurational energy under the approximation of pair interaction can be represented in fourier space as product of

fourier transform of effective pair interaction $V(k)$ and that of pair correlation function $Q(k)$

$$E = N/2 \sum_k V(k)Q(k)$$

N being the number of lattice points .

Thus minimization of E will naturally occur for states of order characterized by maxima in the $Q(k)$ pair correlation spectrum located in the regions of the absolute minima of $V(k)$. Consequently much can be predicted about the types of ordering reactions to be expected from a study of the shape of the $V(k)$ function , in particular , from a search of its absolute minima .

The necessary condition for point (h^0) to be at a minimum of $V(k)$ is given by the set of equations

$$\frac{\delta V}{\delta h_\alpha^0} = 0 \quad (4.8)$$

($\alpha = 1, 2, 3$).

The wave vector is defined as $\vec{k} = \sum_1^3 h_\alpha b_\alpha$.

$$h_\alpha = \frac{m_\alpha}{N}$$

($m_\alpha = 0, \pm 1, \pm 2, \dots$) for N number of real space lattice sites. b_α 's are the primitive translational vectors of the reciprocal lattice .

The function $V(k)$ possesses in addition to translational symmetry , the point group symmetry of the reciprocal lattice . Thus if a solution of equation (4.8) is found at some $\vec{k}(h^0)$, other extrema of the same type must exist at all other points belonging to the star of the vector \vec{k} , the star of a wave-vector consisting of all those vectors which transform into one another by the operations of symmetry of the space group of the reciprocal lattice . If a symmetry element (rotation , rotation-inversion or mirror plane) of the space group in \vec{k} -space is located at the point (h) the vector representing the gradient $\nabla_h V(h)$ of an arbitrary potential energy function $V(h)$ at that point must lie along or within the symmetry element . If two or more symmetry elements intersect at (h) , one must necessarily have

$$|\nabla_h V(h)| = 0$$

since a finite magnitude vector cannot lie simultaneously in intersecting straight lines having only a point in common . At these so called special points eqn (4.8) is satisfied by symmetry requirements alone . This universal character of the special points was pointed out by Lifshitz (1942) and by Khachaturyan (1963) and different types of ordered structures can be related directly to the minima of $V(h)$.

In other words given the knowledge of concentration wave vector , one can readily predict the most stable ordered structure of the system at low temperature , comparable with the knowledge derived from experimental studies like x-ray , electron and neutron diffraction . A peak at $\vec{k} = (0 0 0)$ indicates phase separation while a peak at $\vec{k} = (1 0 0)$ in a fcc material suggests ordering in the Cu_3Au or CuAu ordered structure. Peaks away from the special points may correspond to the formation of long period superstructures , a well-known example being provided by CuPd alloys . We have calculated the quantity $V(\mathbf{k})$ by inverse fourier transform , by summing V_n upto six shell of neighbours . This method favourably contrasts with the evaluation of $V(\mathbf{k})$ directly in \mathbf{k} -space and is justified by the fast convergence of V_n with the shell number as shown in Figure. (4.9) . Similar method of obtaining $V(\mathbf{k})$ by inverse fourier transformation have been adopted previously by Kudrnovský et.al. (1992) in the context of surface alloys using TB-LMTO-CPA-GPM technique. In Figure. (4.10) we plot the $V(\mathbf{h})$ surface for the $\text{Pd}_{50}\text{Rh}_{50}$ alloy at $h_3 = 0$ plane . The minimum is at $(0,0,0)$ indicating $\langle 0 0 0 \rangle$ type of instability with associated clustering effect.

The stability limit of the concentration wave , that is , the temperature , at which the instability of the disordered solid solution with respect to static concentration wave first sets in is determined by the vanishing of the second derivative of the free energy . The concept of the stability limit coincident with the critical point in higher-order transitions is generally extended into metastable regions (below first order transition lines) , defining the so-called ordering spinodal . For phase separating system like Pd-Rh , it defines the region in the temperature-concentration plane below which the alloy is unstable and separates into palladium-rich and rhodium-rich solutions . In the region just outside the spinodal , the alloy is metastable , given sufficient diffusion , the alloy will phase separate . The region of metastability continues to the phase boundary beyond which the solid solution exhibits clustering type short-range order but will not phase separate.

Estimating the configurational entropy in simple point approximation of Bragg-Williams the stability limit T_0 can be obtained in the following way.

The expectation value of the configurational energy is

$$\langle E \rangle_0 = \sum V_{ij}^{(2)} \langle \delta x_i \delta x_j \rangle_0$$

considering only the pair interaction term . The symbol (0) denoting microcanonical averaging . Adding to this the configurational entropy part free energy takes the form

$$F = \sum V_{ij} \gamma_i^0 \gamma_j^0 + K_B T \sum_i [x_i \ln x_i + (1 - x_i) \ln(1 - x_i)] + NVx(1 - x)$$

with

$$\gamma_i^0 = \langle \delta x_i \rangle_0 = x_i - x$$

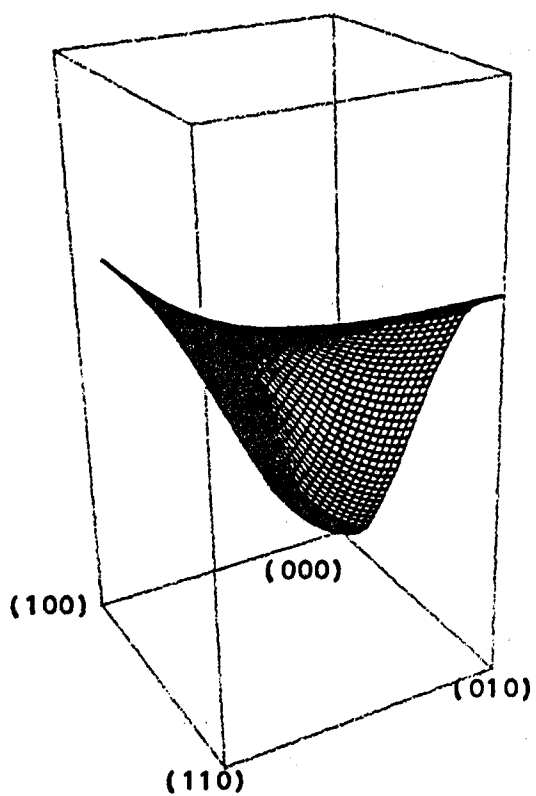


Figure 4.10: $V(h)$ surface for the $\text{Pd}_{50}\text{Rh}_{50}$ alloy at $h_3 = 0$ plane.

and the self-term $V = V_{ij}$ for $i = j$. In keeping with the point cluster approximation, the average of the product $\langle \delta x_i \delta x_j \rangle_0$ has been replaced by the product of averages γ_i^0 .

The second derivative of free energy with respect to γ_i^0 is given by the harmonic term $F^{(2)}$ of the Taylor's expansion of the above mean field free energy F in powers of the configuration variables γ_i^0 . As mentioned, it is the relevant one for the stability analysis. For that purpose, it is convenient to simplify it by Fourier transform \mathcal{F} .

$$F^{(2)} = N/2 \sum_h \Gamma(h) F(h) \Gamma(h)$$

where $\Gamma(h) = \mathcal{F}\gamma_i^0$ and $F(h) = K_B T + V(h) x(1-x)$

The stability of a solid solution with respect to a small amplitude concentration wave of given wave vector $\vec{k}(h)$ is guaranteed as long as $F(h)$ is positive definite. Instability sets in when $F(h)$ vanishes *i. e.*

$$F(h) = K_B T_0 + V(h) x(1-x)$$

T_0 being the temperature at which instability sets in for the concentration wave considered.

Thus it appears that according to BW model, the stability limit or spinodal is always represented in the phase diagram (T, x) by a parabola, symmetric about $x = 0.5$. It is the concentration dependence of effective pair interaction which brings about the asymmetry. In Figure. (4.11) we plot the stability limit temperatures for $x = 0.1, 0.25, 0.5, 0.75, 0.9$.

The points outline a roughly parabolic curve, the spinodal. We note that temperature $x = 0.25$ is larger than that of $x = 0.75$. This is in agreement with the experimental observation of nature of miscibility gap giving phase boundary between the solid solution phase and phase separating phase. In terms of ECI's, the physical reason for the observed asymmetry can be understood in the following way. Pure Rh has a smaller equilibrium volume than Pd. The potential parameters parametrizing the Hamiltonian which contain information of concentration, is consistent with an alloy Wigner-Seitz radius which decreases linearly from Pd-rich side to Rh-rich side. Thus the Pd-Rh distance is estimated to be larger in Pd-rich side compared to that in Rh-rich side, making the nearest neighbour interaction (the dominant one in determination of stability limit) more attractive in Rh-rich side.

The maximum point of the spinodal curve which corresponds to maximum temperature of the miscibility gap comes out to be 1350° K which is 160° K higher than the experimentally predicted one (Shield and Williams, 1987). The overestimation is contributed by the entropy estimate which in simple Bragg-William approximation gives an elevated estimate to transition temperature. Furthermore neglect of phononic contribution to entropy part also leads to a rise in calculated temperature. The agreement between the experiment and the results obtained by Wolverton *et. al.* (1993b) using Cluster Variation method for entropy estimation and that of Wang *et. al.* (1993) using Monte Carlo method is more closer.

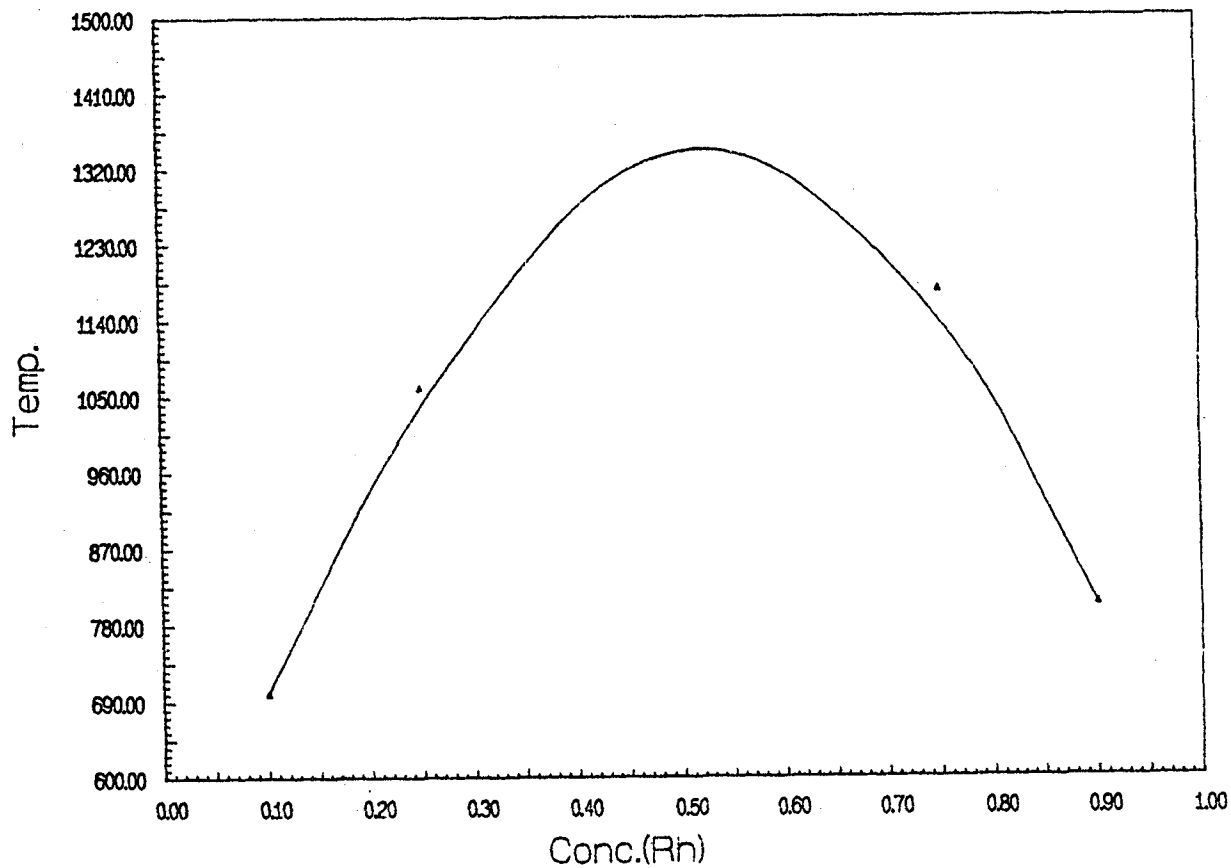


Figure 4.11: Spinodal curve for PdRh alloys . The points indicate calculated points while the solid line is the cubic spline fit through points.

4.5 SUMMARY.

Our results demonstrate that augmented space recursion and orbital peeling in conjunction with LMTO formalism, constitute a viable and computationally feasible approach to the calculation of phase stability in binary substitutionally disordered alloys. The estimated values of pair interactions for the systems studied are in general agreement with that obtained by other existing theoretical methods, along with some discrepancies, the reasons for which have been pointed out. The transition temperatures calculated for PdRh alloys within the framework of Bragg-Williams model of entropy calculation, gives somewhat overestimated values, which is expected for point cluster approximation of entropy calculation.

Chapter 5

CONFIGURATION AVERAGING OF THERMODYNAMIC POTENTIAL IN DISORDERED ALLOYS *

5.1 INTRODUCTION.

The concept of configuration averaging is considered to be a central to the understanding of the properties of disordered systems. Introduction of disorder causes lack of sufficient information about the sample. A particular configuration is defined by the set of random numbers characterizing a set of atomic sites. While each local environment of a sample is necessarily a microscopic realization of randomness, the physical properties measured by an experimentalist is a macroscopic one, containing information about all possible statistical description of the system. In the asymptotic limit therefore, averaging over all possible local environments amounts to averaging over all possible configurations. This in turn introduces the concept of spatial ergodicity, where in analogy with time ergodicity, the spatial averaging (in contrast to time averaging) is replaced by configuration averaging, configurations being born out of disorder fluctuations rather than by thermal fluctuations.

Now it may happen that in a physical system at finite temperature, some degrees of freedom are in thermal equilibrium, but some others are not. This is the situation encountered in some magnetic alloys (*e. g.* in spin glasses). The atoms carry magnetic moments that are assumed to be in thermal equilibrium, but frequently the alloy itself is quenched so that the atoms are frozen at some fixed positions, determined by the quenching treatment. The measured

¹ * The contents of this chapter has been published in J.Phys.Condens.Matter 6 1529 (1994)

thermodynamic potential (or the free energy) at a particular temperature then has to be obtained by performing an average over all atomic configurations using the thermodynamic distribution of that temperature as the statistical distribution .Such an averaging procedure , namely the quenched averaging differs from the usual annealed avergaing . In a random system we have two time scales : one τ_{th} associated with thermal fluctuations and other τ_{dis} associated with disorder configurational fluctuations . For quenched averaging $\tau_{dis} \gg \tau_{th}$, while for annealed averaging $\tau_{dis} \approx \tau_{th}$.In mathematical language , in annealed averaging , disorder averaging is done on the grand potential before the logarithm is taken to yield the thermodynamic potential (free energy) . In constrast , in quenched averaging , the disorder averaging is carried out on the thermodynamic potential itself , *i.e.* after taking the logarithm of the grand potential . As already mentioned , the power of augmented spcae formalism for disorder configuration averaging lies in the fact that it is not restricted to averaging of Green function only , but is a general one , applicable to any random function with randomness prescribed by a probability distribution with finite moments.

We make use of this formalism to obtain quenched and annealed averaged thermodynamic potentials of a disordered binary alloy described by tight-binding Hamiltonian with on-site disorder . We will follow the fermionic field-theoretic approach of the augmented space formalism leading to scattering diagrams for thermodynamic potential in the extended augmented space . We will study , in addition , the difference between annealed and quenched averaging from the scattering diagrammatic approach , to obtain insight into the difference between the two processes.

5.2 THE AUGMENTED SPACE FORMALISM AND FERMION FIELD THEORY.

We start with disordered lattice problem with random site energies ϵ_i 's . The initial random Hamiltonian is given by:

$$H = \sum_i \epsilon_i P_i + \sum_i \sum_j V_{ij} T_{ij}.$$

P_i and T_{ij} are projection and transfer operators corresponding to a countable basis $\{|i\rangle\}$ spanning the Hilbert space \mathcal{H} . The overlap matrix element V_{ij} may be assumed to be non-random. According to the augmented space theorem (Mookerjee, 1973), discussed earlier , the configurationally averaged quantity $\langle F \rangle$ which is some function of the random Hamiltonian will then be given by ground state average of the operator \tilde{F} which is now the same function of an effective Hamiltonian \tilde{H} defined in the augmented space $\Psi = \mathcal{H} \otimes \Phi$

$$\tilde{H} = \sum_i \tilde{M}^{(i)} \otimes P_i + \sum_i \sum_j V_{ij} I \otimes T_{ij}.$$

The effective Hamiltonian \tilde{H} contains complete information about the quantum behaviour of the system described in \mathcal{H} and its statistical behaviour described in Φ .

The effect of disorder is to cause scattering. This scattering event can be pictured as interaction between the electron and pseudo-particles describing configuration fluctuations at each site against the reference state. If the disorder on each site is binary, then the statistics of these pseudo-particles should be fermionic because no two pseudo-particles can occupy the same site. The effective Hamiltonian \tilde{H} can now be written in second quantized form (Mookerjee, 1974) in both spatial and disorder part giving

$$\tilde{H} = \sum_i \epsilon_B a_i^\dagger a_i + \sum_i \sum_k \sum_{k'} M_{i,kk'} a_i^\dagger a_i b_{ik}^\dagger b_{ik'} + \sum_i \sum_j V_{ij} a_i^\dagger a_j.$$

b_{ik}^\dagger and b_{ik} create and annihilate pseudo-fermions at the i -th site. k, k' are additional quantum numbers specifying the orthogonal basis states in ϕ_i . It specifies distinct values or configurations assumed by ϵ_i . Rank of the matrix M_i is given by the number of orthogonal basis states in ϕ_i , i.e. by the number of k 's.

5.2.1 Calculation Of The Quenched Averaged Thermodynamic Potential And Scattering Diagrams

Since the effective Hamiltonian \tilde{H} in augmented space has now been recast in second quantized form characterizing the disorder scattering as an interaction between electron and pseudo-fermion present at the scattering site, the usual tools of diagrammatic field-theoretic techniques can be applied.

The quenched thermodynamic potential of a disordered alloy at temperature T can be written as

$$\langle \Omega \rangle_{av} = -\frac{1}{\beta} \langle f_0 | \ln \text{Tr} \exp[\beta(H - \mu N)] | f_0 \rangle.$$

$\beta = 1/K_B T$, μ is the chemical potential of the system, N is the operator giving number of electrons. $|f_0\rangle = \prod_i^\otimes |f_0^i\rangle$ is the vacuum state of the field space. It is the state in disorder space which has no fluctuation, i.e. all the sites are assumed to be filled with pseudo-fermions of one specific field quantum number. As usual in the interaction picture formalism we define quantity $U(\beta)$ through

$$\exp[-\beta(H_0 - \mu N + H')] = \exp[-\beta(H_0 - \mu N)] U(\beta)$$

H_0 is the unperturbed and H' the interaction Hamiltonian. $U(\beta)$ satisfies the equation :

$$\frac{\partial U(\beta)}{\partial \beta} = -H'(\beta)U(\beta)$$

with $H'(\beta) = \exp(\beta H_0) H' \exp(-\beta H_0)$ and $U(0) = 1$. Solution of $U(\beta)$ in terms of the Dyson ordering operator is

$$U(\beta) = 1 + \sum_{n=1}^{\infty} \frac{(-1)^n}{n!} \int \dots \int d\tau_1 \dots d\tau_n P[H'(\tau_1) \dots H'(\tau_n)]. \quad (5.1)$$

Let us now consider the specific problem of AB an alloy with impurity concentration x of A atoms. The effective Hamiltonian H can be split up into two parts: (i) the unperturbed Hamiltonian of the host B atom

$$H_0 = \sum_i \epsilon_B a_i^\dagger a_i + \sum_i \sum_j V_{ij} a_i^\dagger a_j$$

and (ii) the interaction Hamiltonian

$$H' = \sum_i \sum_k \sum_{k'} M_{i,kk'} a_i^\dagger a_i b_{ik}^\dagger b_{ik'}$$

The matrix M_i takes into account fluctuation of i -th site energy ϵ_i against ϵ_B . Thus this fluctuation $\eta = \epsilon_i - \epsilon_B$ can be either 0 with probability $(1-x)$ or can be $W = (\epsilon_A - \epsilon_B)$ with probability x . So, $p(\eta) = (1-x)\delta(\eta) + x\delta(\eta - W)$

The M_i matrix appropriate to this probability distribution is, as introduced earlier

$$M_i = W \begin{pmatrix} x & \sqrt{x(1-x)} \\ \sqrt{x(1-x)} & 1-x \end{pmatrix}$$

The disorder quantum number k takes two values $k = 0$ and $k = 1$. For simplicity let us define $B_{i0}^\dagger = \sqrt{x} b_{i0}^\dagger$ and $B_{i0} = \sqrt{x} b_{i0}$, $B_{i1} = \sqrt{1-x} b_{i1}^\dagger$ and $B_{i1} = \sqrt{1-x} b_{i1}$

Now

$$\begin{aligned} H'(\tau) &= \exp(\tau H_0) H' \exp(-\tau H_0) \\ &= W \sum_i \sum_k \sum_{k'} a_i^\dagger(\tau) a_i(\tau) B_{ik}^\dagger(\tau) B_{ik'}(\tau) \end{aligned}$$

Further, defining $W_{ij}(\tau, \tau') = W \delta_{ij} \delta(\tau - \tau')$, the above equation may be written as :

$$H'(\tau) = \int d\tau' \sum_i \sum_j \sum_k \sum_{k'} W_{ij}(\tau, \tau') a_i^\dagger(\tau) a_i(\tau) B_{jk}^\dagger(\tau') B_{jk'}(\tau')$$

Written in terms of $U(\beta)$, expression for the quenched thermodynamic potential becomes

$$\langle \Omega \rangle_{av} = \Omega_0 - \frac{1}{\beta} \langle f_0 | \ln Tr \exp[\beta(\Omega_0 - H_0 + \mu N)] U(\beta) | f_0 \rangle.$$

where Ω_0 is the thermodynamic potential for the unperturbed system characterized by the Hamiltonian H_0 . In order to visualize how the scattering diagrams are generated in the augmented space, let us examine in detail the first-order term in the perturbation series expansion of(5.1) :

$$\Omega_1 = -\frac{1}{\beta} \int d\tau \langle f_0 | [Tr (\exp(\beta(\Omega_0 - H_0 + \mu N)) H'(\tau))]_{con} | f_0 \rangle. \tag{5.2}$$

The subscript *con* refers to the fact that only connected diagrams in the Hilbert space \mathcal{H} are to be considered, since it is straightforward to show that the effect of taking the logarithm is to eliminate the contribution of all *unconnected* diagrams.

Let us now define,

$$Tr \left[\exp(\beta(\Omega_0 - H_0 + \mu N)) a_i^\dagger(\tau_1) a_j(\tau_2) \right] = \begin{cases} -G_{ij}^0(\tau_1, \tau_2) & \text{for } \tau_1 \geq \tau_2 \\ G_{ij}^0(\tau_1, \tau_2) & \text{otherwise} \end{cases}$$

G^0 is the finite temperature Green function corresponding to the ordered system . The corresponding Green function in the disorder field space is defined through

$$\langle f_0 | B_{ik_n}^\dagger(\tau_1) B_{ik_m}(\tau_2) | f_0 \rangle = g_{ik_n, ik_m}(\tau_1, \tau_2) = \gamma_n \delta_{nm} \delta_{ij} \theta(\tau_1 - \tau_2).$$

where $\gamma_0 = -x$ and $\gamma_1 = (1 - x)$

Above definitions follow from choice of the *vacuum state* as $|f_0\rangle$ in the disorder field space Φ which is a state in which all sites are described by quantum number $k = 0$. Thus $b_0^\dagger |f_0\rangle = 0$ and $b_1 |f_0\rangle = 0$.

Applying Wick's theorem to both the configuration and the spatial part of (5.2) and employing the definition of G^0 and g we get an expression for the first-order correction as

$$\Omega_1 = -\frac{1}{\beta} \sum_i \sum_j \int d\tau_1 d\tau_2 G_{ii}^0(\tau_1, \tau_1^+) W_{ij}(\tau_1, \tau_2) g_{j_0, j_0}(\tau_2^+, \tau_2).$$

The corresponding scattering diagram is shown in Figure 5.1 .

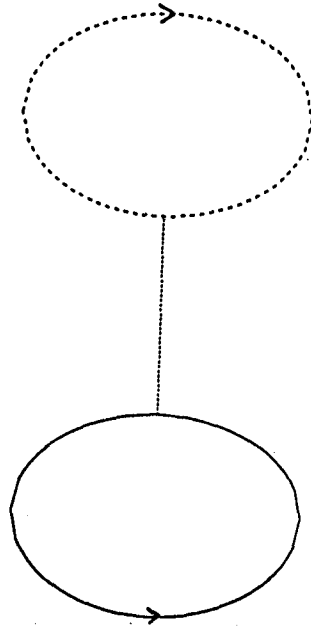


Figure 5.1: The first order scattering diagram for the thermodynamic potential. Full lines indicate electron propagators, the dashed lines indicate the disorder propagators and the dotted line the interaction W_{ij}

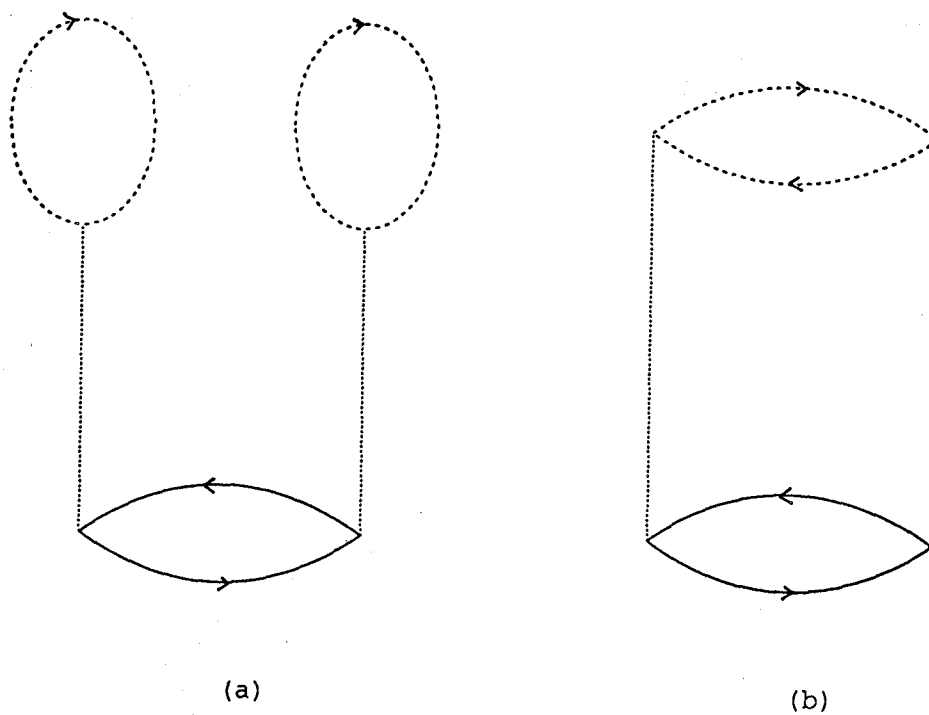


Figure 5.2: Two second order scattering diagrams for the thermodynamic potential.

The solid lines represent the ordered Green function G^0 , the dotted lines represent disorder field Green function g while the dashed lines represent interaction $W_{ij}(\tau_1, \tau_2)$. Using the expressions for the Green functions we obtain :

$$\Omega_1 = -\frac{xW}{\beta} \sum_i \int d\tau_1 G_{ii}^0(\tau_1, \tau_1^+)$$

Expressing in terms of Matsubara frequencies $\omega_n = i(2n+1)\pi\beta + \mu$ with $n = 0, \pm 1, \pm 2, \dots, \pm\infty$ and going over to momentum space we have

$$\Omega_1 = -\frac{xW}{\beta} \lim_{\tau \rightarrow 0} \int \frac{d^3p}{8\pi^3} \sum_{\omega_n} G^0(p, \omega_n) \exp(-i\omega_n\tau).$$

Similarly the contributions in second order coming from scattering diagrams shown in Figs.5.2(a) and 5.2(b) will be

$$-x^2 \frac{W^2}{\beta} \int \int \frac{d^3p_1}{8\pi^3} \frac{d^3p_2}{8\pi^3} \sum_{\omega_n} G^0(p_1, \omega_n) G^0(p_2, \omega_n).$$

and

$$x(1-x) \frac{W^2}{\beta} \int \int \frac{d^3p_1}{8\pi^3} \frac{d^3p_2}{8\pi^3} \sum_{\omega_n} G^0(p_1, \omega_n) G^0(p_2, \omega_n).$$

5.2.2 Summation Of The Perturbation Series For The Thermodynamic Potential

In order to sum up the perturbation series of averaged thermodynamic potential it is not sufficient to consider only skeleton diagrams and to add the self-energy parts to the ordered state Green function G^0 because it leads to over-counting difficulties. To get a summed up expression for $\langle \Omega \rangle$ we notice that if we open up any of the n closed solid line loops of any the n -th order diagram for the thermodynamic potential, we obtain a possible n -th order diagram for the configurationally averaged finite temperature Green function. This is seen if we compare Fig 5.3 with Fig5.1.

Configurationally averaged finite-temperature Green function can be introduced as

$$\langle G_{RR'}(\tau_R, \tau_{R'}) \rangle = \langle f_0 | \frac{\langle a_R(\tau_R) a_{R'}^\dagger(\tau_{R'}) U(\beta) \rangle}{\langle U(\beta) \rangle} | f_0 \rangle.$$

where $\langle .. \rangle$ indicates thermal and $\langle f_0 | \dots | f_0 \rangle$ indicates configurational averaging. Expanding $U(\beta)$ as a perturbation series and considering only connected diagrams in the Hilbert space \mathcal{H}

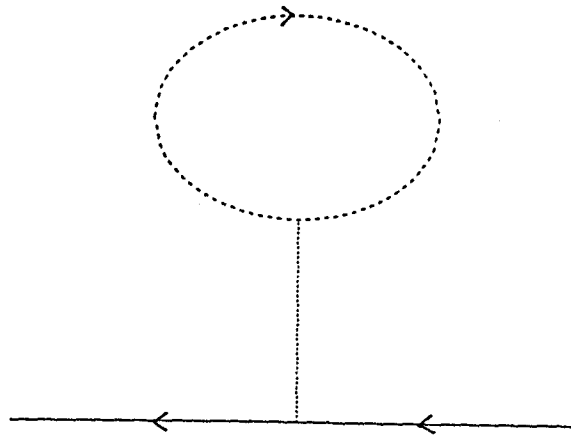


Figure 5.3: The scattering diagram obtained by opening up one of the closed electron loops in the diagram for thermodynamic potential in Figure 5.1. This belongs to the scattering diagram set for the averaged electron propagator.

so as to cancel $\langle U(\beta) \rangle$ in the denominator the first-order contribution to the perturbation series will be

$$\begin{aligned} & \sum_i \sum_j \int \int d\tau_1 d\tau_2 \sum_k \sum_{k'} W_{ij}(\tau_1, \tau_2) a_{R_i}(\tau_R) a_{R'}^\dagger(\tau_{R'}) a_i^\dagger(\tau_1) a_i(\tau_1) B_{j_k}^\dagger(\tau_2) B_{j_{k'}}(\tau_2) \\ &= \sum_i \sum_j \int \int d\tau_1 d\tau_2 W_{ij}(\tau_1, \tau_2) G_{R_i}^0(\tau_R, \tau_1) G_{i_{R'}}^0(\tau_1, \tau_{R'}) g_{j_0, j_0}(\tau_2^\dagger, \tau_2) \\ &= -xW \sum_i \int d\tau_1 G_{R_i}^0(\tau_R, \tau_1) G_{i_{R'}}^0(\tau_1, \tau_{R'}) \end{aligned}$$

Changing over to momentum and frequency space above contribution becomes $-xW [G^0(p, \omega_n)]^2$. Similarly second-order contributions corresponding to Fig 5.4(a) and Fig 5.4(b) are

$$x(1-x)W^2 [G^0(p, \omega_n)]^2 \int \frac{d^3 p_1}{8\pi^3} G^0(p_1, \omega_n)$$

and

$$-x^2 W^2 [G^0(p, \omega_n)]^2 \int \frac{d^3 p_1}{8\pi^3} G^0(p_1, \omega_n)$$

If $\Sigma'_{(n)}(p, \omega_n)$ denotes total self-energy part of the n-th order diagrams, proper or improper then n-th order contribution to quenched thermodynamic potential will be

$$\Omega_n = \frac{1}{n\beta} \int \frac{d^3 p}{8\pi^3} \sum_{\omega_n} G^0(p, \omega_n) \Sigma'_{(n)}(p, \omega_n)$$

$$\langle \Omega \rangle = \sum_{n=0}^{\infty} \Omega_n$$

the factor $1/n$ arises due to the over counting difficulty mentioned earlier. The difficulty of carrying out summation with factor $1/n$ can be overcome by using a mathematical trick. We may consider the coupling parameter W to be varying and integrate over different values of this parameter keeping the chemical potential μ fixed.

$$\langle \Omega \rangle = \Omega_0 + \frac{1}{\beta} \int \frac{d^3 p}{8\pi^3} \sum_{\omega_n} \int \frac{dW'}{W'} G^0(p, \omega_n) \Sigma'_{W'}(p, \omega_n)$$

where $\Sigma'(p, \omega_n)$ is the sum of all possible self-energy parts, proper or improper.

Expressing in terms of the proper self-energy :

$$\Sigma' = \Sigma + \Sigma G^0 \Sigma + \dots$$

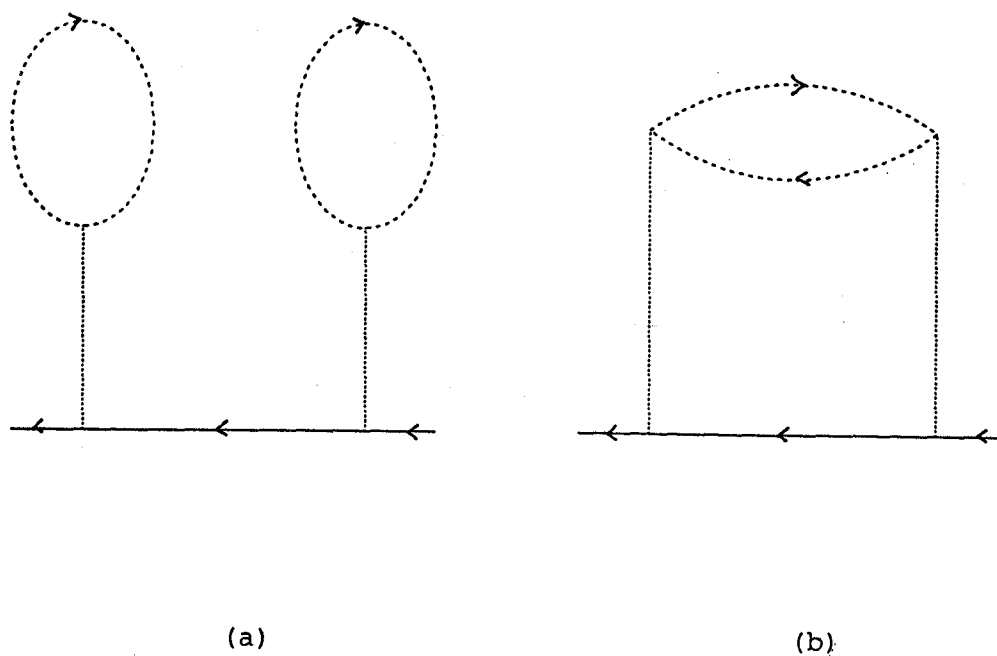


Figure 5.4: The scattering diagrams obtained by opening up one of the closed electron loops in the second order scattering diagrams for the thermodynamic potential in Figure 5.2

we have an expression

$$\langle \Omega \rangle = \Omega_0 + \frac{1}{\beta} \int \frac{d^3 p}{8\pi^3} \sum_{\omega_n} \int \frac{dW'}{W'} \frac{\Sigma_{W'}(p, \omega_n)}{[G^0(p, \omega_n)]^{-1} - \Sigma_{W'}(p, \omega_n)}. \quad (5.3)$$

The Chemical potential μ can be determined from this by solving :

$$N = -\frac{\partial \langle \Omega \rangle}{\partial \mu}$$

N is mean number of electrons present . From equation (5.3) one has

$$N = -\frac{\partial \Omega_0}{\partial \mu} - \frac{1}{\beta} \sum_m \sum_{\omega_n} \int \frac{d^3 p}{8\pi^3} \Sigma'_{(m)}(p, \omega_n) \partial / \partial \mu [G^0(p, \omega_n)].$$

The ordered free energy is given by

$$\Omega_0 = -\frac{1}{\beta} \int \frac{d^3 p}{8\pi^3} \ln[1 + \exp(-\beta(E_p - \mu))].$$

E_p being the energy corresponding to the host Hamiltonian H_0 with momentum p .

Using this expression of the ordered free energy and the fact that differentiating any n -th order diagram is equivalent to differentiating any of its n solid lines, it follows that

$$N = \int \frac{d^3 p}{8\pi^3} \sum_{\omega_n} \frac{1}{\omega_n - E_p - \Sigma(p, \omega_n)}.$$

Equation (5.3) relates the quenched thermodynamic potential to the self-energy part of the configurationally averaged finite temperature Green function . The self energy Σ can be determined by summing up the irreducible scattering diagrams as shown in Figure 5.5.

Summing up various infinite sets of scattering diagrams leads to various approximations . If we take into account correlated scattering from all sites within a cluster C exactly but ignore all scattering diagrams involving correlated scattering between sites within and without the cluster , the resulting approximation is a C - cluster coherent potential approximation (CCPA). The diagram for one such correlated scattering involving two sites is shown in Figure 5.6 . The simplest of these approximations is the single-site coherent potential approximation (CPA). In this approximation only uncorrelated scatterings are taken in account . In diagrammatic language it amounts to considering only diagrams with non-overlapping pseudo-fermion loops associated with more than one site . Mookerjee(1974) has shown that the summed up series for the scattering diagrams in augmented space in this case is identical to that of the algebraic approach of CPA . Using the correspondence between scattering diagrams and graphical techniques of

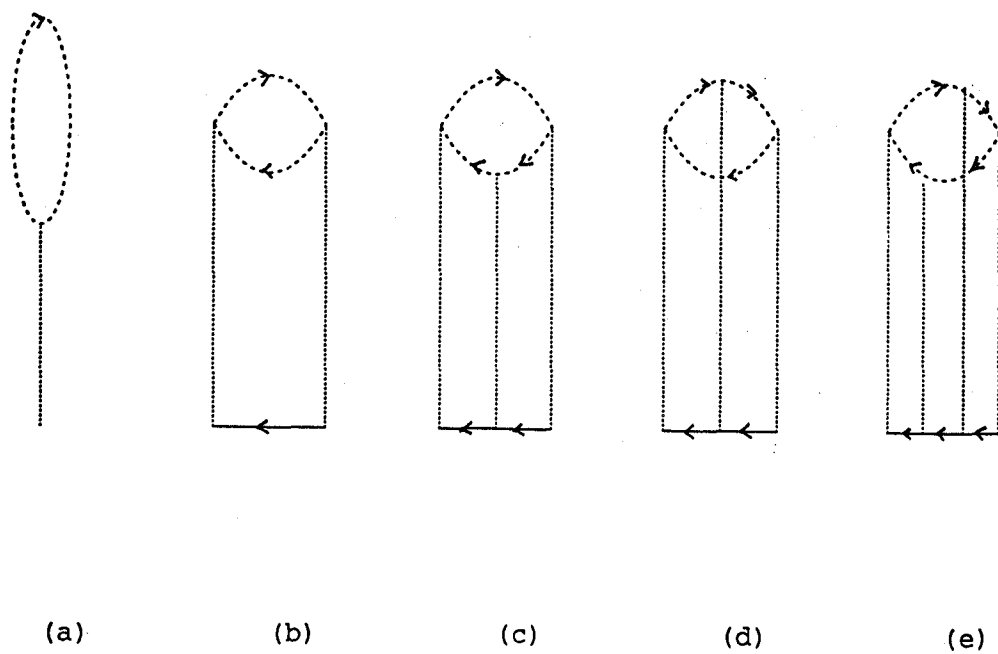


Figure 5.5: Irreducible scattering diagrams for the self-energy for the averaged electron propagator

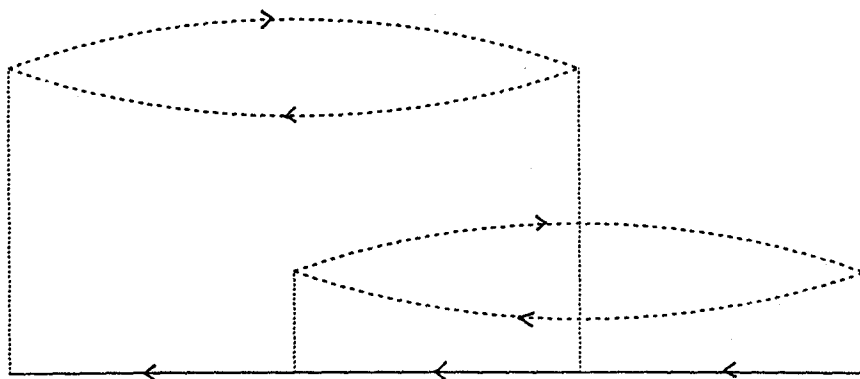


Figure 5.6: A scattering diagram for correlated scattering from two sites .Such diagrams are neglected in the single site coherent potential approximation

Haydock (1972) and the direct relation between the algebraic and the graphical techniques, he has argued that a identical relationship holds for the summation of scattering diagrams for the correlated scattering from clusters and the algebraic, partitioning method for the CCPA. The averaged Green function and the self-energy as discussed earlier can be obtained by applying the ideas of the recursion method directly on the augmented space . The equivalence of scattering diagram summation and the algebraic method will allow us to use the above ideas to obtain the averaged thermodynamic potential in a generalized cluster-approximation.

5.2.3 Annealed Averaging Of The Thermodynamic Potential

The essential difference between quenched and annealed averaging of the thermodynamic potential is whether configuration averaging is done before or after taking the logarithm of the grand-potential . In diagrammatic language, before a matrix element is taken in the configuration space, each vertex has two arrows as shown in Figure 5.7(a). The operation of taking the matrix element between $|f_0\rangle$ in configuration space, *i.e.* configuration averaging, amounts to joining these arrows in pairs to form disorder propagators. The same procedure is true for the trace operation in the real Hilbert space. Moreover, taking the logarithm amounts to discarding the unconnected diagrams. In quenched averaging, since we take the trace first, followed by the logarithm, a diagram like Figure. 5.7(b) will be considered as an unconnected diagram and hence discarded. On the other hand, for the annealed averaging, since we take the matrix element in configuration space after taking the trace, the same unconnected diagram now becomes connected in the full augmented space and hence when the subsequent logarithm is taken its contribution is not zero. Such diagrams in the full augmented space constitute the difference between the two different averaging procedures.

Inspecting diagrams of various orders of the interaction parameter , it is straight forward to identify diagrams which , though unconnected in the real space, are connected in the full augmented space via the disorder propagator . Some of these diagrams are shown in Figure. 5.8. Physically it is understandable why the annealed averaging should have extra scattering diagrams and why these should lead to a renormalization of the disorder propagator. In quenched averaging, the disorder fluctuations are frozen. Thermal fluctuations have no effect on disorder propagators. Once a system is in a disorder configuration, it always remains so. The picture of disorder propagators as *propagators* is a mathematical artifact, as was clearly understood in the scattering picture of the CPA earlier by Leath *et. al.* (1974). The delta function time dependence of the disorder propagator is a reflection of this fact. In annealed averaging, however, thermal fluctuations and fluctuations in disorder configurations take place on the same footing. It is therefore not surprising that we have to consider extra scattering diagrams which express these fluctuations and we do expect thermal fluctuations to renormalize the disorder propagators and vice-versa.

Summing up of the perturbation series of annealed thermodynamic potential needs introduction of a new type of configurationally averaged finite temperature Green function . Let us call this

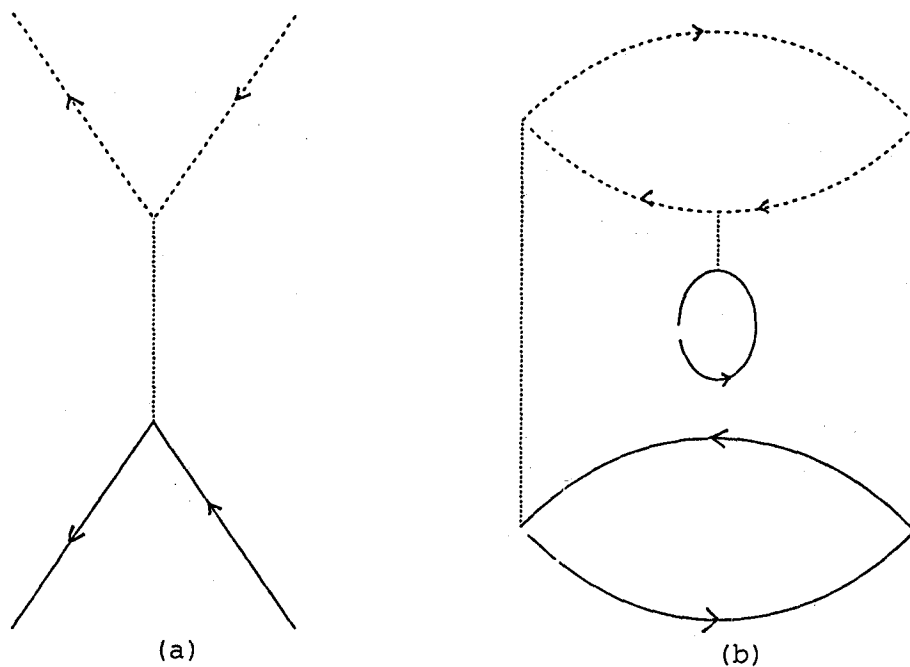


Figure 5.7: (a) A scattering vertex in augmented space. (b) A new scattering diagram for the annealed average. Note that for annealed average electron propagators renormalize the disorder propagator.

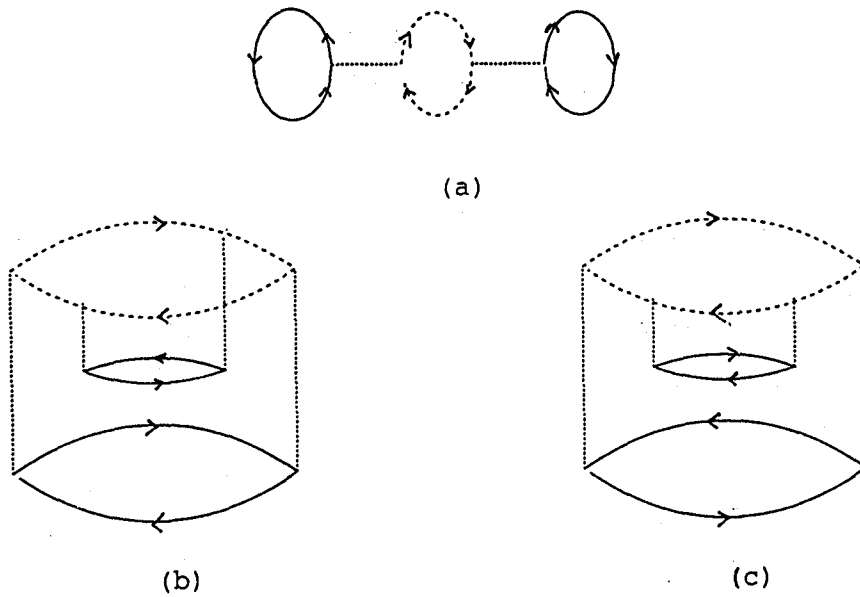


Figure 5.8: Scattering diagrams which arise in annealed averaging of the thermodynamic potential but not its quenched average.

the annealed averaged Green function G^A in order to distinguish it from configurationally averaged Green function introduced in section 5.2.2 . Scattering diagrams for the annealed averaged Green functions are obtained by breaking open solid lines of the diagrams for the annealed thermodynamic potential are shown in Figure. 5.9 . Considering specific case of Figure. 5.9(c) , its contribution to averaged Green function can easily be obtained by using previously mentioned rules for dotted , dashed and solid lines as

$$\sum_{i_1} \dots \sum_{i_8} \int \dots \int d\tau_1 \dots d\tau_8 W_{i_1, i_2}(\tau_1, \tau_2) W_{i_3, i_4}(\tau_3, \tau_4) \dots W_{i_7, i_8}(\tau_7, \tau_8) \dots$$

$$G_{R, i_1}(\tau_R, \tau_1) G_{i_1, i_7}(\tau_1, \tau_7) G_{i_7, R'}(\tau_7, \tau_{R'}) G_{i_3, i_5}(\tau_3, \tau_5) G_{i_5, i_3}(\tau_5, \tau_3) \dots$$

$$g_{\uparrow\uparrow}(i_2\tau_2, i_8\tau_8) g_{\downarrow\downarrow}(i_8\tau_8, i_6\tau_6) g_{\downarrow\downarrow}(i_6, \tau_6, i_4\tau_4) g_{\downarrow\downarrow}(i_4\tau_4, i_2\tau_2)$$

For convenience we denote the quantum number $k = 0$ by \uparrow and $k = 1$ by \downarrow . Expressing in terms of Matsubara frequencies, contribution of above diagram to the self-energy will be

$$x(1-x)W^2 G_{i_1, i_1}(\omega_n) \sum_{\omega_m} (1-x)^2 W^4 G_{i_1, i_1}(\omega_m) G_{i_1, i_1}(\omega_m)$$

Thus we notice that the effect of unconnected electronic Green function in the Hilbert space is to renormalize the right-going and left-going disorder propagators. If we denote the contribution of the right-going disorder propagator by g_r instead of $(-x)$ and that of left-going disorder propagator by g_l instead of $(1-x)$ then the summed up self-energy diagrams including all connected diagrams in the full augmented space, connected either via the electronic propagator or via disorder propagator and containing only single propagator loops can be written as

$$\Sigma^A(\omega_n) = -W \sum_{n=0}^{\infty} \sum_{s+t=n} \gamma_r^s \gamma_l^t (1 + \sigma_{\uparrow\downarrow}) [G_{i_1, i_1}(\omega_n) W]^{s+t-1} N_{s,t}$$

$$+ \sum_{\omega_n} \sum_{n=0}^{\infty} \sum_{s+t=n} W \gamma_r^s \gamma_l^t (1 + \sigma_{\uparrow\downarrow}) [G_{i_1, i_1}(\omega_n) W]^{s+t-1} N_{s,t} - W \gamma_r \quad (5.4)$$

where γ_r and γ_l give the renormalized contribution of right-going and left-going disorder propagator ; $\sigma_{\uparrow\downarrow}$ represents the contribution from the disconnected portions of the electronic propagator in the Hilbert space which simultaneously renormalizes a left-going and a right-going disorder propagator , an example of this being Fig.5.9(b) ; $N_{s,t}$ represents the number of diagrams containing s right-going and t left-going propagators.

It is easy to check that $N_{s,t} = sN_{s-1,t} + tN_{s,t-1}$ with $N_{s,0} = \delta_{s,1}$ and $N_{0,t} = 0$ The second term in the above expression for $\Sigma_A(\omega_n)$ represents the correction from self-energy diagrams independent of ω_n , an example of this being Figure. 5.9(a) .

The Dyson equation corresponding to the right-going and the left-going disorder propagators can be written as (with α denoting either right (r) or left(l) propagators)

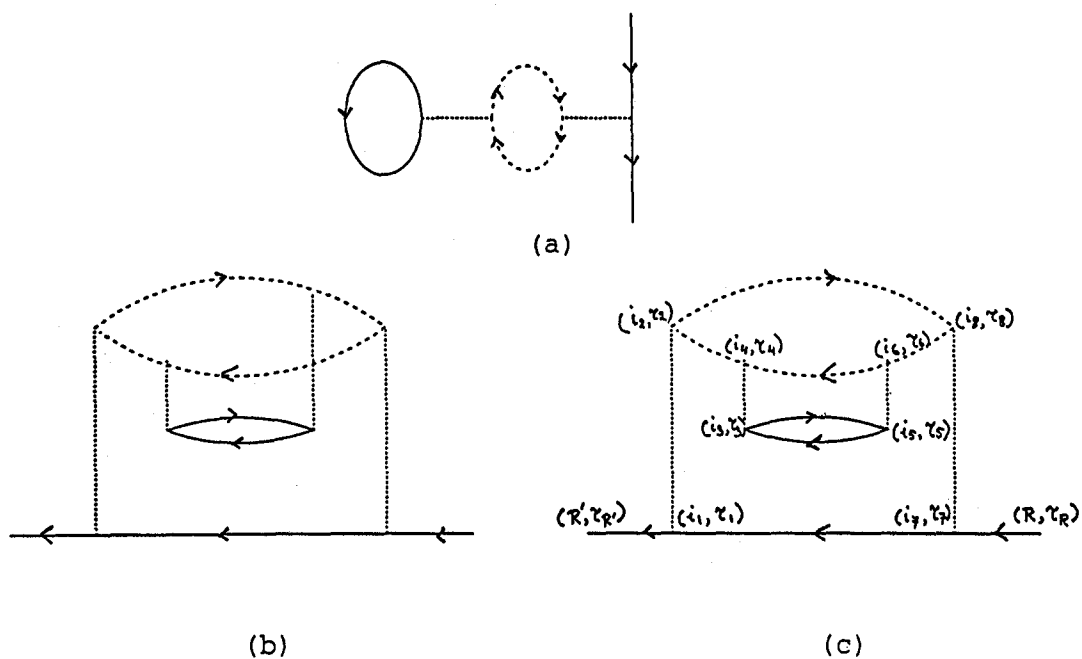


Figure 5.9: Scattering diagrams for an *annealed* propagator obtained by opening up one of the electron loops in the scattering diagrams shown in Figure 5.8

$$\gamma_\alpha = g_\alpha + g_\alpha \sigma_\alpha \gamma_\alpha$$

with the self-energies σ_r and σ_ℓ given by

$$\sigma_\alpha = - \sum_{\omega_n} \sum_{n=0}^{\infty} \sum_{s+t=n} W^{s+t} [G_{i_1, i_1}(\omega_n)]^{s+t} \gamma_\alpha^{s+t-1} N_{s,t}. \quad (5.5)$$

Contribution of $\sigma_{\uparrow\downarrow}$ is given by

$$\begin{aligned} \sigma_{\uparrow\downarrow} = & - \sum_{\omega_n} \sum_{n=0}^{\infty} \sum_{s+t=n} \sum_{s'+t'=n} \gamma_r^s \gamma_\ell^t W^n [G_{i_1, i_1}(\omega_n)]^{s'+t'} N_{s,t} N_{s',t'} \\ & \dots\dots + W \gamma_r G_{x_1, x_1}(\omega_n). \end{aligned} \quad (5.6)$$

The last term in equation (5.6) is included in order not to double count a factor already included in $\sigma_{\uparrow\downarrow} \gamma_r$.

Thus the evaluation of the summed up expression for the self-energy requires the knowledge of σ_r, σ_ℓ and $\sigma_{\uparrow\downarrow}$. Inspecting equations 5.5 it appears that, apart from the summation over Matsubara frequencies, the formally summed up expression is similar to that of the quenched self-energy under the single-loop approximation, in which the roles of the electronic propagators and the disorder propagators have been interchanged. Hence, in order to perform the double summation over various orders of interaction and over the number of distinct ways of arranging s number of right-going and t number of left going electronic propagators in equation 5.5 let us define analogous to Schultz and Shapero(1973), generating functions for σ_r, σ_ℓ .

$$\Gamma_1(u, v) = \sum_{s=1}^{\infty} u^s f_s(v)$$

$$\text{with } f_s(v) = \sum_{t=0}^{\infty} v^t N_{s,t}$$

It satisfies the recursion relation

$$f_s(v) = \frac{v}{1-v} f'_{s-1}(v)$$

where

$$f' = df/dv \text{ along with the initial condition } f_0 = \ln v.$$

Utilizing the recursion relation of $f_s(v)$, the partial differential equation satisfied by generating function Γ_1 can be given by

$$\left(\frac{1}{vu} - \frac{\partial}{\partial u} \right) \Gamma_1(u, v) = \frac{1}{v} + \partial \Gamma_1(u, v) / \partial v$$

changing variables to $\xi = (u + v)/2$ and $\eta = (v - u)/2$ leads to the canonical form

$$\frac{\partial \Gamma_1}{\partial \xi} = \frac{\Gamma_1}{(\xi^2 - \eta^2)} - \frac{1}{(\xi + \eta)}. \quad (5.7)$$

writing $\sigma_\alpha = \sum \sigma_\alpha(\omega_n)$ where α can either be r or ℓ , one may has

$$\sigma_\alpha(\omega_n) = -\frac{1}{\gamma_\alpha} \Gamma_1(WG_{i_1, i_1}(\omega_n)\gamma_\alpha, WG_{i_1, i_1}(\omega_n)\gamma_\alpha)$$

Inserting this in equation (5.7) leads to the first order ordinary differential equation

$$\gamma_\alpha \frac{d\sigma_\alpha(\omega_n)}{d\xi} = \gamma_\alpha \frac{\sigma_\alpha(\omega_n)}{\xi^2} + \frac{1}{\xi}. \quad (5.8)$$

along with the boundary condition $\sigma_\alpha \rightarrow 0$ as $\xi \rightarrow 0$

In order to perform the summations in equation (5.6) apart from sum over Matsubara frequencies ω_n , we rewrite the formal representation of $\sigma_{\uparrow\downarrow}$ in the following way :

$$\sigma_{\uparrow\downarrow} = \sum_{\omega_n} \sigma_{\uparrow\downarrow}(\omega_n) + W\gamma_r G_{i_1, i_1}(\omega_n)$$

with

$$\sigma_{\uparrow\downarrow} = -\sum_{n=1}^{\infty} [WG_{i_1, i_1}(\omega_n)\gamma_\ell]^n \sum_{s=0}^n \gamma_r^s \gamma_\ell^{-s} N_{s, n-s} \sum_{s_1+t_1=n} N_{s_1, t_1}$$

We notice that

$$\sum_{s_1+t_1=n} N_{s_1, t_1} = (n-1)!$$

We now define another generating function $\Gamma_2(v, u) = \sum_{n=1}^{\infty} (n-1)! v^n f_n(u)$ where the function

$f_n(u) = \sum_{r=0}^n u N_{r, n-r}$. The recursion relation satisfied by $f_n(u)$ can be obtained easily as

$$f_n(u) = u(1-u)f'_{n-1}(u) + (n-1)uf_{n-1}(u)$$

with initial condition $f_1(u) = u$

The generating function $\Gamma_2(v, u)$ can be shown to satisfy the the second -order partial differential equation

$$v \frac{\partial^2 \Gamma_2(v, u)}{\partial v^2} - u \frac{\partial^2 \Gamma_2(v, u)}{\partial v \partial u} = \frac{\Gamma_2(v, u)}{(1-u)v^2} - \frac{1}{v} - \frac{\partial \Gamma_2}{\partial v}$$

By changing the variables u and v to $\xi = v$ and $\eta = \ln v - \ln u$, the above second order partial differential equation can be reduced to the canonical form of a linear, inhomogeneous hyperbolic equation of the second order

$$\frac{\partial^2 \Gamma_2}{\partial \xi \partial \eta} = F(\xi, \eta, \partial \Gamma_2 / \partial \xi, \partial \Gamma_2 / \partial \eta, \Gamma_2). \tag{5.9}$$

where

$$F(\xi, \eta, \partial \Gamma_2 / \partial \xi, \partial \Gamma_2 / \partial \eta, \Gamma_2) = \frac{\Gamma_2}{\xi} (1 - \xi / \exp(\eta)) - \frac{1}{\xi}$$

In terms of this generating function we obtain

$$\sigma_{\uparrow\downarrow} = -\Gamma_2(WG_{i_1, i_1}(\omega_n) \gamma_\ell, \gamma_r / \gamma_\ell).$$

We have to solve the equation along the curves defined by $\xi = WG_{i_1, i_1}(\omega_n) \gamma_\ell$ and $\eta = \ln(WG_{i_1, i_1}(\omega_n) \gamma_\ell^2 / \gamma_r)$ in conjunction with the boundary conditions $\xi \rightarrow 0, \Gamma_2 \rightarrow 0, \partial \Gamma_2 / \partial \xi \rightarrow 0$

The solution of such hyperbolic linear partial differential equations with given sufficient boundary conditions is known exactly in terms of its Green function (see e.g. Sneddon, 1980). Once we have solved the equations 5.8 and 5.9, the summation over Matsubara frequencies can be done in a trivial way by performing the contour integration

$$\sum_{\omega_n} F(\omega_n) = \oint_C \frac{F(z) dz}{1 + \exp[\beta(z - \mu)]}$$

where the contour is taken to encircle the zeros of the denominator.

As regards the summation in equation 5.4 the first and second term are identical apart from summation over Matsubara frequencies and a change of sign in case of second term. We introduce a third generating function

$$\Gamma_3(v, u) = \sum_{n=1}^{\infty} u^n f_n(v)$$

with $f_n(v) = \sum_{r=0}^{\infty} v^r N_{r, n-r}$

It is easy to check that this generating function satisfies the first order partial differential equation

$$u \frac{\partial \Gamma_3}{\partial u} - v \frac{\partial \Gamma_3}{\partial v} = \Gamma_3 \left[1 + \frac{1}{(1-v)u} \right].$$

Along with the boundary conditions $u \rightarrow 0, \Gamma_3 \rightarrow 0$ for all values of v and $v \rightarrow 0, \Gamma_3 \rightarrow 0$ for all values of u . The solution of this equation with the given boundary conditions leads to obtaining Σ^A as

$$\begin{aligned} \Sigma^A(\omega_n) &= -\frac{1}{G_{i_1, i_1}(\omega_n)} (1 + \sigma_{\uparrow, \downarrow}) \Gamma_3(W G_{i_1, i_1}(\omega_n) \gamma_\ell, \gamma_r / \gamma_\ell) \\ &+ \sum_{\omega_n} \frac{1}{G_{i_1, i_1}(\omega_n)} (1 + \sigma_{\uparrow, \downarrow}) \Gamma_3(W G_{i_1, i_1}(\omega_n) \gamma_\ell, \gamma_r / \gamma_\ell) - W \gamma_r. \end{aligned}$$

Finally since annealed Green function is obtained from scattering diagrams of annealed thermodynamic potential by breaking open electronic propagator part annealed averaged thermodynamic potential will be given by an equation identical to that of equation (5.3) where Σ has to be replaced by Σ^A . The form of Σ^A under single-loop approximation can be obtained in the above prescribed manner. The advantage of this formalism is since it treats the quantum as well as statistical part in a unified way, whatever approximation is made applies equally to both part.

5.3 SUMMARY.

The fermion field theoretic approach to the augmented space formalism has been applied for obtaining thermodynamic potential of disordered alloys. Standard diagrammatic technique has been employed for both types of averaging of thermodynamic potential - quenched as well as annealed with the following results :

- (i) Quenched thermodynamic potential of disordered alloys has been obtained in this formalism in a general way .
- (ii) Difference between quenched and annealed averaging of thermodynamic potential appears in considering certain additional classes of scattering diagrams in latter case. These are such that although they are disconnected in the real Hilbert space and would have no contribution if the logarithm were taken prior to averaging, become connected in full augmented space via disorder propagators. Thus they contribute to annealed and not to quenched averages.

- (iii) This difference between quenched and annealed averaging is manifested in summed up self-energy Σ which in turn is related to thermodynamic potential . Considering additional contributions to self-energy Σ^A for annealed case , the effect of disconnected portion of diagrams in Hilbert space is to renormalize the disorder propagators .
- (iv) Under the single-loop approximation , two types of disorder self-energies σ_l and σ_r ,renormalizing either left-going or right-going disorder propagator and another $\sigma_{\uparrow\downarrow}$, renormalizing both of them simultaneously may be obtained from generating functions which appear as solutions of first-order differential equations and linear hyperbolic partial differential equation of second order followed by summations over Matsubara frequencies. Given the boundary conditions these differential equations have solutions whose formal expressions are available.

REFERENCES

1. Abrahams E. , Anderson P. W. , Licciardello D. C. and Ramakrishnan T. V. (1979), *Phys. Rev. Lett* **42** 673
2. Askeland Donald R. (1990), *The Science and Engineering Of Material* , Brooks /Cole Engeneering Divison.
3. Andersen O.K. (1975) , *Phys. Rev.* **B12** 3060
4. Andersen O. K. and Jepsen O. (1984) , *Phys. Rev. Lett.* **53** 2571
5. Andersen O.K.,Jepsen O. and Glötzel D. (1985) ,in *Highlights of Condensed Matter Theory* ed. Bassani F. , Fumi F. and Tosi M.P. (North Holland, Amsterdam) 59
6. Andersen O. K. , Jepsen O. and Sob M (1987), in *Electronic Band Structure and its Applications* ed. M. Yussouff (Springer Lecture Notes) **281** 1
7. Anderson P. W. (1958) , *Phys. Rev.* **109** 1492
8. Asta M. , Wolverton C. , de Fontaine D and Dreyssé H (1991) , *Phys. Rev* **B44** 4907
9. Azbel M. Ya. (1983) , *Phys. Rev* **B28** 4106
10. Basu C. , Mookerjee A. , Sen A. K. and Thakur P. K. (1991) , *J. Phys. Condens Matter* **3** 9055
11. Berera A (1990) , *Phys. Rev.* **B42** 4311
12. Blackman J. A. , Esterling D. M. and Berk N. F. (1971) , *Phys. Rev* **B4** 2412
13. Bloch F. (1928) , *Z. Physik* **52** 55
14. Bieber A. and Gautier A. (1984), *J. Phys. Soc. Japn* **53** 2061
15. Bose S.K., Kudronovský J., Jepsen O. and Andersen O.K. (1992) , *Phys. Rev.* **B45** 8272
16. Burke N. R. (1976), *Surf. Sci* **58** 349
17. Callaway J. (1964), *Energy Band Theory* Academic Press , New York , London
18. Chhabra A. and Jensen V. R. (1989), *Phys. Rev. Lett.* **62** 1327
19. Chowdhury D. , Gawlinski E. T. and Gunton J. D. (1987) , *Comp. Phys. Commun.* **43** 329
20. Connolly J. W. D. and Williams A. R. (1983) , *Phys. Rev. B* **27** 5169

21. Datta A. and Mookerjee A. (1992) , Int. J. Mod. Phys. **B6** 3295
22. Datta A. , Thakur P. K. and Mookerjee A. (1993) , Phys. Rev. **B 48** 8567
23. Das G. P. (1992) , Pramana , **38** 545
24. Dreysse H. , Berera A. , Wille L. T. and de Fontaine D. (1989) Phys. Rev. **B39** 2442
25. Ducastelle F. and Gautier F. (1976), J. Phys. **F6** 2039
26. Ducastelle F. (1991) , *Electron Theory In Alloy Design* ed. by Pettifor D. G. and Cottrell A. H. , Vol 534 , North Holland
27. Einstein T. L. and Shrieffer J. R. (1973) Phys. Rev. **B7** 3629
28. Gallagher J. (1978) , *Ph. D. Thesis*, University of Cambridge, U. K.
29. Godin T. J. and Haydock R. (1988), Phys. Rev. **B38** 5237
30. Godin T. J. and Haydock R. (1991) , Europhys. Lett. , 14(2) 137
31. Gonis A. , Stocks G. M. , Butler W. H. and Winter H. (1984) , Phys. Rev. **B29** 555
32. Gonis A. , Zhang X. G. , Freeman A. J. , Turchi P., Stocks G. M. and Nicholson D. M. (1987) , Phys. Rev. **B36** 4630
33. Gray L.J. and Kaplan T. (1976) , J.Phys. **C9** L303, L483
34. Gray L. J. and Kaplan T. (1977), Phys. Rev. **B15** 3260, 6005
35. Gyorffy B. L. and Stocks G. M. (1983) , Phys. Rev. Lett. **50** 374
36. Halsey T. C. , Meakin P. and Procaccia I. (1986) , Phys. Rev. Lett **56** 854
37. Haydock R. (1972) , *Ph.D. Thesis*, University of Cambridge, U.K.
38. Haydock R. (1980) *Solid State Physics* **35** Academic Press
39. Haydock R. (1981), Philos. Mag. **B43** 203
40. Haydock R. and Nex C. M. M. (1984), J. Phys. *Solid State* **17** 4783
41. Haydock R. (1986) , Philos. Mag. **53** 554
42. Haydock R. (1989) , Comput. Math. Commun. **53** 133
43. Haydock R. , Heine V. and Kelly M. J. (1972) J.Phys. **C 5** 2845
44. Hohenberg P. C. and Kohn W. (1964) , Phys. Rev. **136** 864

45. Hünfer S. , Wertheim G. K. and Wernick J. H. (1973) , Phys. Rev. **B8** 4511
46. Imry Y. (1986) , *Directions In Condensed Matter Physic* 1 ed. Grinstein G. and Mazenko G. (Singapore ; World Scientific) 101
47. Kanamori J. and Kakehashi Y. (1977) , J. Phys.(Paris) Colloq **38** C7-274
48. Khachaturyan A. G. (1963) , Sov. Phys. Solid State (Eng. Transl.) **5** 16 and 548
49. Khachaturyan A. G. (1983) , *Theory Of Structural Transformations In Solids* , Willey , New York
50. Khmel'nitskii D. E. (1984), Physica **126** B+C 235
51. Kirkpatrick S. and Eggarter T. P. (1972), Phys. Rev **B6** 3598
52. Kohn W. and Rostocker N. (1954), Phys. Rev. **94** 1111
53. Kohn W. and Sham L. J. (1965) , Phys. Rev. **140** 1133
54. Korringa J. (1947) ,Physica **13** 392
55. Kudrnovský J. and Drchal V. (1989) , Solid State Commun. **70** 577
56. Kudrnovský J. and Drchal V. (1990) , Phys. Rev. **B 41** 7515
57. Kudrnovsky J. , Bose S. K. and Drchal V. (1992) , Phys. Rev. Lett. **69** 308
58. Laufer P. M. and Papaconstantopoulos D. A. (1987) , Phys. Rev. **B35** 9019
59. Leath P.L., Elliot R.J. and Krummhanl J.A. (1974), Phys.Rev. **46** 465
60. Lifshitz E. M. (1942) ,J. Phys. (Moscow) **7** 61 and 251
61. Liu Y and Chao K. A. (1986), Phys Rev **B34** 5247
62. Lu. Z. W. , Wei S. H. and Zunger Alex (1991a) , Phys. Rev. **B44** 3387
63. Lu. Z. W. , Wei S. H. and Zunger Alex (1991b) , Phys. Rev. Lett. **66** 1753
64. Lu. Z. W. , Wei S. H. and Zunger Alex (1992) , Phys. Rev. **B45** 10314
65. Lucini M. U. and Nex C. M. M. (1987) , J Phys **C20** 3125
66. Mašek J. and Kudrnovský J. (1986) , Solid State Commun. **58** 67
67. McKinnon A. and Kramer B. (1981), Phys. Rev. Lett. **147** 1546
68. Mookerjee A. (1973) , J. Phys. **C 6** 1340

69. Mookerjee A. (1974), *J Phys C : Solid State Phys* 7 3432
70. Mookerjee A. (1987) , *J. Phys.* C17 1511
71. Mookerjee A. , Chakrabarti B. K. , Dasgupta I. and Saha T. (1992), *Physica* A186 258
72. Mott N. F. and Jones H. (1958) , *The Theory Of Metals and Alloys* Dover , NY
73. Mott N. F. (1968), *J. Non-Cryt. Solid*, 1 1
74. Mott N. F. (1974),*Metal-Insulator Transitions* , Taylor and Francis , London
75. Nordheim L (1931) , *Ann Phys (Lipz)* 9 607
76. Nowak H.J., Andersen O.K., Fujiwara T.,Jepsen O. and Vargas P. (1991) , *Phys. Rev.* B44 3577
77. Ohshima K and Watanabe D. (1973) , *Acta. Crystallogr. Sect.* A29 520
78. Pastawski H. M. , Weisz J. F. and Albornoz S. (1983), *Phys. Rev.* B28 6896
79. Pendry J. B. (1987), *J. Phys.* C20 733
80. Pettifor D. (1992) , *Electron Theory in Alloy Design* ed. Pettifor D. and Cottrell A (London : The Institute of Materials) p 81
81. Picard J. L. and Sarma G. (1981), *J. Phys.* C14 L127,L617
82. Popovic D. , Fowler A. B. and Washburn S. (1991), *Phys. Rev. Lett* 67 2870
83. Rao R. S. , Bansil A. , Asonen H and Pessa M (1984) , *Phys. Rev.* B29 1713
84. Razee S.S. A., Rajput S.S. , Prasad R. and Mookerjee A. (1990) , *Phys. Rev.* B42 9391
85. Shiba H. (1971) , *Prog. Theor. Physics (Japan)* 46 77
86. Shield J. E. and Williams R. K. (1987) ,*Scr. Metall* 21 1475
87. Shultz T.D. and Shapero D. (1973), *Phys.Rev.* B7 5090
88. Singh P. P. and Gonis A. (1993) , *Phys. Rev.* B47 6744
89. Slater J. C. (1937) , *Phys. Rev* 51 846
90. Sluiter M. and Singh P. P. (1994) , (preprint)
91. Sluiter M. , de Fontaine D. , Guo X. Q. , Podloucky R. and Freeman A. J.(1990) , *Phys.Rev.* B42 10460
92. Sneddon F. (1980), *Elements of Partial Differential Equations* (McGraw-Hill) 119

93. Soven P. (1967) , Phys. Rev. **156** 809
94. Stauton J. B. , Gyorffy B. L. , Johnson D. D. , Pinski F. J. and Stocks G. M. (1989) , in *Alloy Phase Stability* , ed.Stocks G. M. and Gonis A. , NATO ASI series E , **163** (Kluwer , Dordrecht)
95. Stauffer D. (1979), Phys. Rep **54** 1
96. Stefanou N. Braspenning P.J.,Zeller R. and Dederichs P. H. (1987a) ,Phys. Rev. **B36** 6372
97. Stefanou N., Zeller R. and Dederichs P. H. (1987b) ,Solid State Commun. **62** 735
98. Stocks G. M. , Gyorffy B. L. , E. S. Giuliano and Ruggeri R. (1977) , J. Phys. **F7** 1859
99. Taylor D. W. (1967) , Phys. Rev. **156** 1017.
100. Thakur P. K. , Brouers F. and Ananthakrishnan G. (1989), *unpublished*
101. Thouless D. J. (1974), Phys. Rep. **13** 93
102. Turchi P. E. A. , Stocks G. M. , Butler W. H. , Nicholson D. M. and Gonis A. (1988) , Phys Rev **B37** 5982
103. von Barth U. and Hedin L. (1972) , J Phys **C5** 1629
104. Wang Yang , Faulkner J. S. and Stocks G. M. (1993) , Phys. Rev. Lett. **70** 3287
105. Weightman P.,Wright H. , Waddington S.D., Marel D. vander Sawatzky G. A. , Diakun G.P. and Norman D. (1987) , Phys. Rev **B36** 9098
106. Winter H. and Stocks G.M. (1983) , Phys. Rev. **B27** 882
107. Winter H., Durham P. J., Temmerman W. M. and Stocks G. M. (1986) , Phys.Rev. **B33** 2370
108. Wolverton C. , Ceder G. , de Fontaine D. and Dreyssé H. (1992), Phys. Rev **B45** 13105
109. Wolverton C. , Ceder G. , de Fontaine D. and Dreyssé H. (1993a) , Phys. Rev **B48** 5766
110. Wolverton C., Ceder G. , de Fontaine D. and Dreyssé H (1993b) , Phys. Rev. **B48** 726
111. Wright H., Weightman P. , Andrews P. T., Folkerts W., Flipse C. F. J. , Sawatzky G. A. , Norman D. and Padmore H. (1987) , Phys. Rev. B **B35** 519
112. Xue W. and Lee P. A. (1988), Phys. Rev **B38** 3913
113. Zhang Z. Q. and Sheng P. (1991), Phys. Rev **B44** 3304